"DEVELOPMENT OF SAW DEVICES FOR APPLICATION IN POLYMER NANOCOMPOSITE BASED GAS SENSORS"

A THESIS SUBMITTED TO THE

SAVITRIBAI PHULE PUNE UNIVERSITY

FOR THE AWARD OF DEGREE OF

DOCTOR OF PHILOSOPHY

(ELECTRONIC SCIENCE)

BY

PRABHAKAR S. VARADE

UNDER THE GUIDANCE OF

Prof. Dr. A. D. SHALIGRAM

DEPARTMENT OF ELECTRONIC SCIENCE

SAVITRIBAI PHULE PUNE UNIVERSITY

PUNE- 411 007

JULY 2018

DEDICATED TO

My Gurus and My family

CERTIFICATE

Certified that the work incorporated in this thesis, **"DEVELOPMENT OF SAW DEVICES FOR APPLICATION IN POLYMER NANOCOMPOSITE BASED GAS SENSORS"** submitted by Mr. Prabhakar S. Varade was carried out by the candidate under my supervision. Such material as has been obtained from other sources has been duly acknowledged in this thesis.

Place: PUNE
Date: 17/07/2018

Dr. A. D. Shaligram
Research Guide
Professor and Head,
Department of Electronic Science,
Savitribai Phule Pune University,
Pune-411007

D E C L A R A T I O N

I hereby declare that the dissertation entitled "DEVELOPMENT OF SAW DEVICES FOR APPLICATION IN POLYMER NANOCOMPOSITE BASED GAS SENSORS" completed and written by me has not previously formed the thesis for the award of any Degree or similar title of this or any other University or examining body.

Place: PUNE

Date: 17/07/2018

Prabhakar S. Varade

Research Student

ACKNOWLEDGEMENTS

I am fortunate to have this opportunity to express my sincere thanks to my mentors whose collective and intellectual advice, support and encouragement made this research work possible. I would like to thank you for encouraging my research and for allowing me to grow as a researcher. Your advice on both research as well as on my career have been priceless.

It gives me immense pleasure to express my deep sense of gratitude and indebtedness towards my guide **Prof. A. D. Shaligram** and my earlier guide **Dr. Mrs. S. A. Gangal** for their valuable guidance, detailed and insightful comments, critical assessment, endless encouragement, and moral support throughout the progress of this research work.

I am very grateful to **Dr. Gajanan Ekbote,** Chairman, Progressive Education Society, for allowing me to do this research work. I am gently indebted to **Dr. Rajendra Zunjarrao**, Principal, Modern College of Arts, Science and Commerce, Shivajinagar, Pune, India, **Prof Shamkant Deshmukh**, Secretary, Progressive Education Society and **Dr. Prakash Dixit**, Deputy Director of Progressive Education Society, for their continuous encouragement and moral support. My special thanks to my teachers **Dr. A. V. Patil, Dr. Ratan. Borse, Prof. Halwar, Prof. Garde and Prof. Mrs. Tiwari** who encouraged me throughout my career.

suggestions during the research work. I would like to extent my thanks to **Mr. Sunil Garve, Mr. Minanath Kolpe, Mr. Nitin Shenavi, Mr. Bhalekar, Mrs. Savita, Mr. Kalekar, Mr. Deore, Mr. Pore, Mr. Laddad** and **Mr. Shinde, Mr. Walimbe** (Department of Physics, SPPU), **Mr. Lokhande, Mr. Deshpande,** who have been a great support for the technical facilities throughout the experimentation. I would like to express my sincere thanks to the office Staff- **Mrs. Sushama Sawant, Mrs. Sangita Konda, Mrs. Madhavi, Mrs. Rajshree Patil** of Department of Electronic Science, SPPU, for all their support during my research work.

A special thanks to my family members including my brothers **Deepak** and **Sandip** and sisters **Jyoti** and **Manisha**, my niece **Tejal** and nephews **Shantanu** and **Divyesh**, my sister-in laws **Vaishali** for their support to strive towards my goals.

A special acknowledgement goes to my friends of many years **Prof. Milind Gajbhiye, Mr. Deepak Soanawane, Dr.Shivaji Pacharne, Dr. Mrs. Savita Kulkarni, Mr. Nitin Gaikwad, Mrs. Savita Itkarkar, Dr. Bhagwan Mali**, for their unconditional support and encouragement has been precious all these years.

A special thanks also goes to **Late. Prof. R. N. Karekar,   Prof. P. S. Chirputkar, Dr. Pande, Dr. Paranjape** whose fatherly support has been a big

driving force for my research work. I would like to thank all who directly or indirectly have supported me during this research work.

Last but not the least, I would like to thank my beloved parents **Shri. Shivdas Varade** (Father) and **Mrs. Ratna S. Varade** (Mother) , my wife **Mrs. Renuka** and my dear daughter **Miss. Purva** and my dear son **Mast. Shivam** for their patient support and encouragement throughout my research work. Because of their sacrifice and adjustments during this period I could focus on my research work. My feelings for them are beyond expression.

Prabhakar S. Varade

CONTENTS

Chapter 1 : Introduction

Chapter 2 : Literature Review

Chapter 3 : Design, Simulation and Development of Surface Acoustic Wave Sensors

3.1 Introduction
3.2 Design of SAW Devices
3.3 Modelling and Simulation
  3.3.1 Modelling of SAW delay line using Matlab
  3.3.2 MATLAB Simulation results for equivalent circuit model
  3.3.3 Transmission matrix modelling for the SAW delay line device
  3.3.4 MATLAB simulation results for transmission matrix method
    3.3.4.1 Input and output information in FEM
    3.3.4.2 Finite element formulation
  3.3.5 SAW device Simulation using FEM
  3.3.6 FEM simulation of a SAW delay line using COMSOL Multiphysics
    3.3.6.1 The mathematical model for a SAW delay line
    3.3.6.2 Simulation Methodology
    3.3.6.3 Results and discussions on FEM simulation of SAW delay line
3.4 Fabrication of SAW devices
  3.4.1 Problems faced during SAW device fabrication
  3.4.2 Dimensions of Fabricated SAW delay line devices
  3.4.3 SAW Device Characterization
3.5 Development of Chemiresistors for Gas Sensing Application
3.6 Conclusion
References

Chapter 4: Synthesis And Characterization of Polyaniline And Polyaniline –Nanocomposites

4.1 Introduction
4.2 Polyaniline and Its Synthesis
  4.2.1 Polyaniline preparation Methods
  4.2.2Distillation of Aniline
  4.2.3 Polymerization of Aniline using Potassium Dichromate
  4.2.4 Structural and morphological characterization of polyaniline
4.3 Results And Discussions
  4.3.1 XRD of Polyaniline
  4.3.2 Fourier Transform -Infrared Spectroscopy (FT-IR) of Polyaniline
  4.3.3 TGA-DTA of Polyaniline
  4.3.4 Preparation of Polyaniline pellets and resistance measurement
  4.3.5 Electrical Properties
4.4 PANI Preparation and Characterisation (Sample 2)
  4.4.1 Structural and Morphological Characterisation of Polyaniline (Sample 2)
  4.4.2 Results and Discussion
    4.4.2.1 FT-IR Analysis
    4.4.2.2 XRD Studies
    4.4.2.3 SEM Studies
    4.4.2.4 Electrical properties
  4.4.3 Conclusion
4.5 Synthesis of Polymer Nanocomposites

Chapter 5 : Experimental Studies on Polyaniline and Polyaniline - Nanocomposites Based Gas Sensors

Acoustic Wave (SAW) Devices
5.5.8 Conclusion
References

6.1 Introduction
6.2 Summary and conclusions
6.3 Future Scope

Index to Figures

Index to Tables

Index to Tables

CHAPTER 1

INTRODUCTION

Introduction

In recent years, many attempts were made by the researchers on the development of various types of the gas sensors, including metal oxide, metal oxide semiconductors, IR sensors, electrochemical sensors etc. These sensors have some issues such as they needs to operate at higher temperatures, are incompatible with measuring system, lack of sensitivity and selectivity. These issues can be resolved by using a new class of sensor called as 'Surface Acoustic Wave (SAW) sensor'. These sensors offer high sensitivity, selectivity, robustness and ready to operate at room temperature. So, in the present work, development of SAW delay line sensor along with polyaniline nanocmposite material as a sensing material for ammonia and VOCs detection has been done. The work have been carried out in different steps: Synthesis of sensing material, Sensor development, testing of sensing layer performance using SAW device for ammonia and VOCs, result analysis and conclusion.

The following sections of the chapter address the research background followed by motivation of the research and objectives, overview of the research work and organization of the thesis.

1.1 Background and Motivation

Sensors play important role in every field of daily life, so there is need to employ suitable sensors according to the requirement [1]. Sensor converts energy from one form to another form. Different types transduction method used in sensors are: Electrical, Mechanical, Chemical, Thermal, Magnetic and Radiant. The sensor possesses some important characteristics such as, sensitivity, selectivity, repeatability, linearity, hysteresis, range and span. The selection of sensors for particular application mainly depends on its characteristics such as sensitivity, selectivity and repeatability.

Sensors can be used in different industrial uses and in our day-to-day activities. Sensors provide us with real-time information that helps us to take important decisions in various industrial applications. It becomes very easy to make smart electronic control systems due to better sensors available for each physical parameter. They increase the safety in every field and lower the overall cost. .

Due to versatility and reliability are preferred in many electronic applications. There is a big requirement of sensors for processing physical, chemical and biological parameters. The development of smart sensors can be very useful to the agriculture development, energy industries, and the military and other industrial organizations [2,3].To facilitate sensing in such hostile or inaccessible environments, the sensor system must be self-contained and preferably accessed using wireless communication techniques. Designing reliable, cost effective, and small sized wireless sensors creates significant challenges to the scientific community. Advanced concepts and techniques exist that can address this challenge.

A) Need of Gas Sensors

The environmental pollution is increasing day by due to various hazardous gases get added due to use of modern appliances and beauty products. Also due to some industrial byproducts from various processes. Many gases are also used in various processing plants; therefore the hazardous gas concentration is increasing. To identify the percentage of the pollutant gases and to take measures for their control, again to maintain the proper percentage of useful gases such as oxygen, nitrogen. There is need of the devices which will provide this information appropriately and automatically. This is possible with use of gas sensors or smart sensors.

B) SAW Gas Sensors

New generations of micro sensors based on SAW technologies are available to provide information of a broad range of different parameters, including humidity,

temperature, pressure, gas percentages, etc. using wireless communications. SAW devices were discovered many years ago, and since then researchers have investigated their properties and application.
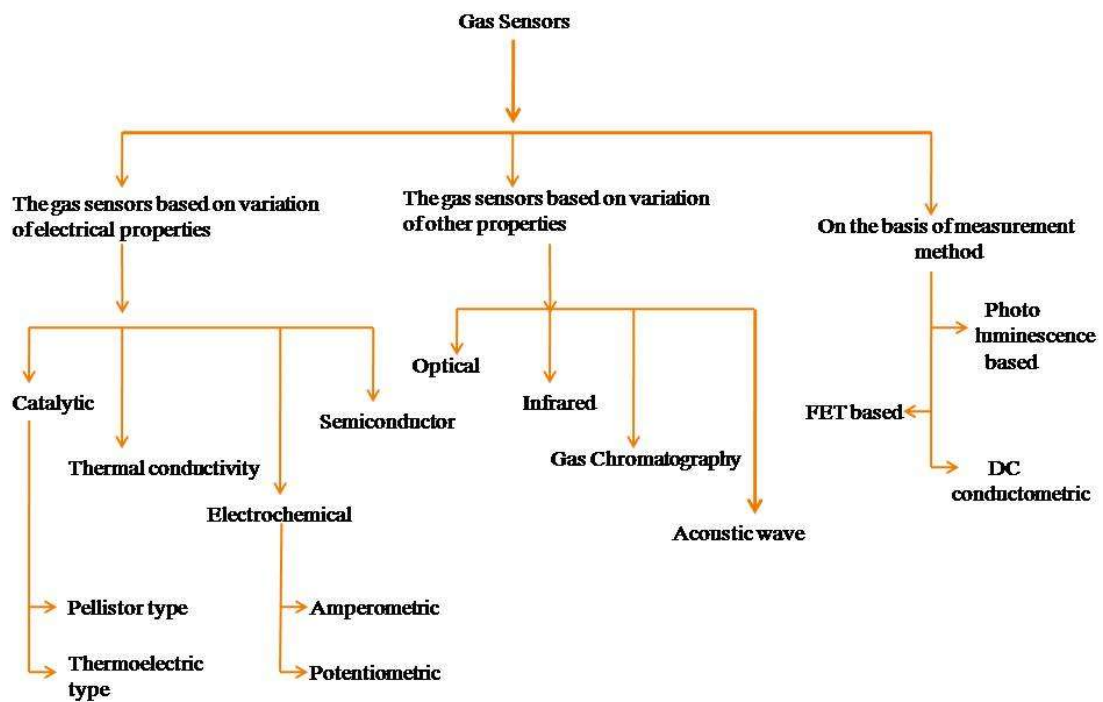
Fig. 1.1 Types of gas sensors.
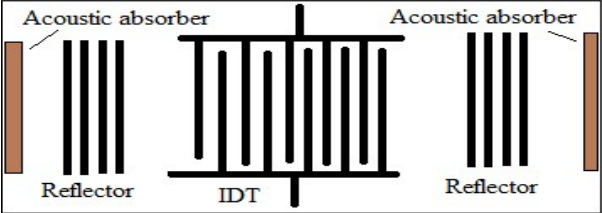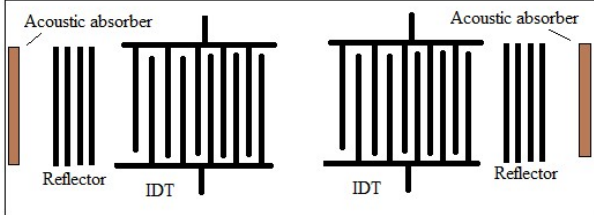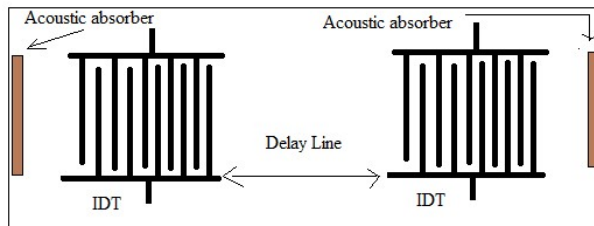
They use the concept of piezoelectricity for transduction and sensing mechanism uses mass loading and acoustoelectric effect. SAW devises are tiny in size and are compatible with ICs, therefore are used in various analog and digital communication and sensing applications [6]. Thus, they are used commercially from few many years. Basic principle used in SAW device is depends on the modulation in propagation of a acoustic wave along the device surface. The main advantage of using SAW devices as sensors is that, the velocity of these waves is five orders of magnitude less than EM waves. Therefore, SAW sensors are much smaller in size when compared to their electromagnetic counterpart. Due to their lower velocity, the propagation path can be used for detection of analytes. The substrate is piezoelectric such as quartz, $LiNb0_3$, $LiTaO_3$ and Langasite [7]. When
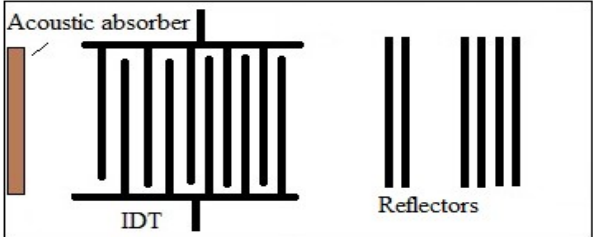
a varying voltage waveform is imposed on a transducer, a surface wave is propagated on and within SAW devices. The resulting waveform has been modified based on the physical property chosen to be measured, and this change in waveform can be used to quantify the measurand, thereby providing a useful measurement. The small size, flexible measurement capability and mass reducibility of SAW devices provides a fantastic encouragement for developing a range of small, low-power sensors for a broad range of applications. The other applications of applications of SAW devices includes used as filters, duplexers and oscillators [6, 7]. SAW devices offers higher sensitivity to minute changes in mass loading and surface conductivity and therefore widely used in gas sensing applications. [8-10].

The SAW devices are quite versatile and have a capability to work remotely and to withstand in harsh environment. Keeping in mind these advantages of SAW devices, we aimed to develop a SAW delay line device which can be easy to use as gas sensor with respect to the kind of sensing material used. It is feasible to deposit appropriate sensing material by the user on the delay line area of this device. Since the SAW devices are readily available in market but it is difficult to use them as gas/vapor sensor because the assembly is closed with tight packaging. Further, the area available for material deposition is very small with necked eye it is very difficult to identify and deposit the sensing material. There is big possibility of breaking the contact wires in it. Even there is chance of shorting the IDTs if the sensing material is good conducting. To avoid this possibilities and to improve sensing parameters we have made an attempt to develop the SAW delay line device using 128^0 YX cut single side polished $LiNbO_3$ which have quite higher propagation velocity(3992 m/s) and coefficient of coupling (K^2= 5.56)[8].Table below lists the different configurations of SAW device used for sensing applications[11].

Figure 1.2 below illustrates the idea of SAW delay line as a gas sensor. This is most commonly used because it avoids the possibility electrical short between input and output IDTs when conducting films are used as sensing layer. To avoid the loss of acoustic energy, acoustic absorbers of suitable material such as polyimide can be formed on input IDT side as well as output IDT side.

Table 1.1: SAW device configurations and their applications

SAW configurations	Applications
SAW one port resonator 	SAW resonators are used to provide stable frequency oscilations.
SAW two port resonator 	Two port SAW resonators can also be used as chemical and bio-sensors.
SAW reflective delay line device 	SAW delay line devices are used for producing delay in television and other such electronic circuits. They are widely used as chemical and bio-sensors.

SAW configurations	Applications
SAW reflective delay line	Are mostly used as SAW ID tags and in passive wireless SAW sensing systems.
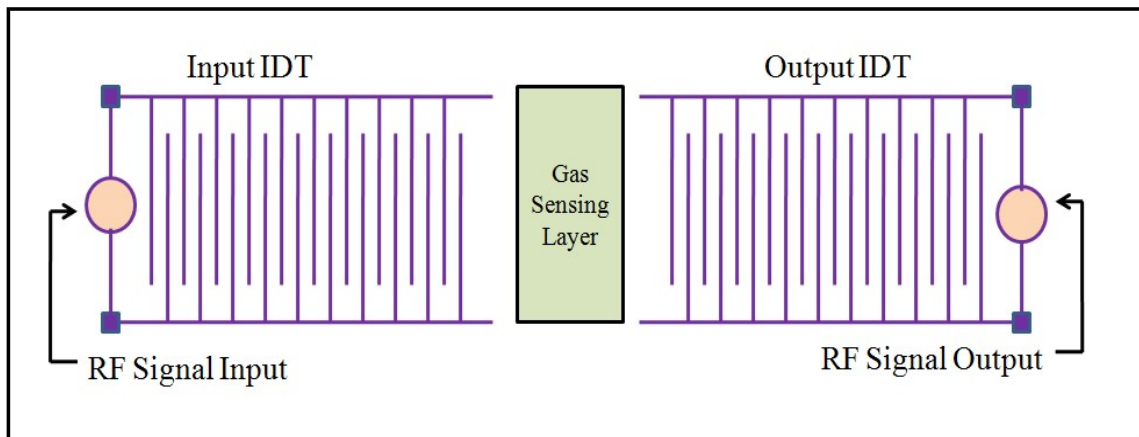
Fig.1.2 SAW delay line as a gas sensor

The gas to be detected, when passes over the delay line then the gas particles get adsorbed on the gas sensing layer. These adsorbed particles add the mass in the delay line area or changes the film conductivity. This causes the velocity / amplitude change of resultant SAW wave at the output IDT. This change can be interpreted as frequency change or insertion loss change. Thus, the presence of gas is detected. To reduce signal interference caused by mechanical waves moving in the direction opposite the output IDT and other reflected waves, acoustic absorbers can be applied to the surface of the piezoelectric substrate. Materials such as silicon or polyimide may be deposited on both the horizontal edges of the SAW device. These are the consistent materials for acoustic absorbance. Wax and epoxies are also used as an absorber at high frequencies.

1.2 Aim and Objectives

Aim: Design, fabrication and testing of SAW device using piezoelectric substrate for the application in ammonia and volatile organic compounds detection.

The **objectives** of the work are as follows:

- To carry out literature survey of SAW device performance in gas sensor applications
- To design and simulate behavior of SAW device using MATLAB /COMSOL multiphysics.
- To fabricate and test the SAW devices.
- To prepare and deposit polymer nano-composite material on SAW sensor for gas detection
- To Measure performance parameters of developed sensor and develop prototype SAW device for gas detction
- To study dependence of performance on PANI- SnO_2 composite.
- To discuss the factors governing the quality of developed sensors.

1.3 Overview of present Research work

In the thesis work, development of surface acoustic wave devices for application in polymer nanocomposite based gas sensors is concluded**.** A range of sensors are available based on different working principles such as catalytic gas sensors, thermal conductivity gas sensor electrochemical sensors, gas chromatography based sensors, semiconductor sensors, optical gas sensors, infrared gas sensors and acoustic sensors. The catalytic sensor need heating elements for their operation as an extra hardware; they also need signal conditioning circuits to produce the output in useable form. The thermal conductivity type sensors have limitation that gases with thermal conductivities less than air are difficult to detect using this method due to interference, for example, carbon dioxide and butane.

The electrodes used in electrochemical sensor are quite costly. Out of these, metal oxide sensors are more preferred in gas detection applications due to their greater material sensitivity and relatively fast response times. But these sensors have one main drawback that, they should operate at elevated temperatures. This problem of operating at elevated temperatures can be resolved with maintaining other advantages as it is possible by selection of surface acoustic wave sensors. These sensors are based on piezoelectric effect therefore developed using suitable piezoelectric substrate and basically execute the mass loading and acoustoelectric effect. Table below gives idea about the most commonly used piezoelectric substrates in SAW devices with their advantages and disadvantages. The SAW sensors are quite robust, possess high sensitivity, compact in size, do not need power supply for operation, can be operated remotely and in harsh environment. These sensors are now commonly used for chemical and biosensing applications.

These can be used for any sensing applications by selecting appropriate sensing material for the target gas. The most commonly used SAW device configurations in gas sensing applications are the delay line and two port resonator. For SAW based gas sensors, thin film of suitable polymers, metal oxide, or polymer nanocomposites are commonly used. These polymers and polymer nanocomposites are easily synthesized with chemical or electrochemical method and deposited by various methods. The most suitable deposition methods are spin coat, dip-coating and drop casting. We used drop cast method for present study.

Table 1.2: Commonly used piezoelectric substrates for SAW [12-13]

Piezoelectric substrate	Merits	Demerits
Quartz	Less acoustic attenuation, Temperature stabilization is simple, High temperature (573 ^{0}C) operation is possible.	Weak EM coupling, Phase change occurs.
$LiNbO_3$	Large electromechanical coupling coefficient and high acoustic velocity.	High temperature coefficient, Lithium loss.
$LiTaO_3$	High electromechanical coupling coefficient	High temperature coefficient.
ZnO	High electromechanical coupling coefficient.	High dielectric loss.
$GaPO_4$	Maximum operating temperature-970 ^{0}C.	Phase transformation occurs.
Langasite	Highest operating temperature-1470^{0}C, Easy temperature compensation	Low acoustic velocity and low coupling coefficient.

In this research work with rigorous review, we proposed to develop the low cost high sensitivity SAW delay line device useful for gas sensing application at room temperature. 128^0 YX cut lithium niobate is used as substrate material because it has high electromechanical coupling coefficient and high acoustic velocity as reported in table 1 which helps to increase the device sensitivity. Due to the sensitivity of SAW devices to small changes in mass loading and surface conductivity, SAW devices have been extensively studied as gas sensors [6-8].

The SAW delay line device was designed for three different resonant frequencies between 10-20MHz ranges. The modeling and simulation for the device with wavelength of 360 µm is carried out with equivalent circuit method and transmission matrix method using MATLAB9.0. Finite element method based simulation for the same device is also carried out using COMSOL multiphysics 5.0. By using these simulations, we estimated the parameters of the proposed sensors and their responses to the target gas in terms of frequency and amplitude change.

The designed SAW delay line devices are fabricated using conventional photolithography and the problems faced during lithography are reported in the thesis. The developed devices are tested using arbitrary function generator, digital storage oscilloscope (DSO) and network analyzer. The results are discussed in the Thesis. The possible causes of variation in developed device responses are also discussed.

For the selected target gases, the polyaniline (PANI) material is used as sensing layer and prepared by chemical method. It is characterized by using analytical techniques such as XRD, FTIR, TGA- DTA and SEM. From this characterization the material formation is confirmed and discussed about it nature. Further to improve sensing performance nanocomposite is used as sensing material. The SnO_2 nanoparticles are prepared by sol-gel method and characterized by SEM.

The nanocomposite of PANI and SnO_2 materials is prepared by following two different methods namely in-situ and chemical route [14, 15]. Both the materials are further characterized by following XRD, FTIR, SEM and FE-SEM. The results obtained proved that the SnO_2 nanoparticles are mixed with PANI matrix and hence the nanocomposite is formed. The response of PANI- SnO_2 composite to ammonia and volatile organic compounds (VOCs) are first tested using chemiresistors on electrometer. The chemiresistors were prepared on glass epoxy substrate as well as on glass substrates. Their electrical characterization is done

on LCR meter. The films of the composite are deposited on delay line of SAW device by drop cast method. The response of PANI-SnO$_2$ composite to ammonia and VOCs (acetone, ethanol, methanol, and toluene) at room temperature is tested for different concentrations on network analyzer. The same process is also applied for SAW IC (SIPAT LB 211DS 01) and the results of both types of devices are discussed in the thesis. The analysis of SAW sensors is done on the basis of results obtained.

1.4 Organization of Thesis

The outcome of present research work is documented in this thesis. The thesis comprises of six chapters.

Chapter 1, provides background of the present work; aim and objectives are then presented. Overview of the research work is given in brief. Organization of the thesis is also included in this chapter.

Chapter 2,presents literature survey with a main focus on SAW working principle, device fabrication and its use as a gas sensor. The first part of this chapter explains the brief idea of sensors in general, sensor characteristics and types. In sensor types more emphasis is given on gas sensors. The detailed theory of SAW including piezoelectric effect, mass loading, acoustoelectric effect and important characteristics of piezoelectric materials are also elaborated. Different techniques of SAW generation and types of surface acoustic waves (Rayleigh wave, shear horizontal wave, love wave, acoustic plate mode wave) are explained with their applications. Types of SAW devices such as one port SAW resonator, two port SAW resonator and SAW delay line device are explained with reference to their use in gas sensing application.

Sensor characteristics, second order effects in SAW response, IDT characterization, and layered SAW also reviewed. A brief review of SAW sensor including its principle, type of wave, sensing material used and corresponding gas sensed is reported in tabular form.

In chapter 3, the details of SAW device, design, fabrication and its simulation is explained. In design of SAW device the important parameters such as frequency of operation (Resonance frequency), bandwidth, and device physical size are discussed. Other important aspects such as selection of piezoelectric substrate, types and materials of interdigital transducer and role of acoustic absorber are explained here. The actual design of SAW delay line device with its physical parameters and substrate type is emphasized. After device design different simulation techniques available for SAW devices are elaborated. Modeling and Simulation of SAW delay line device based on equivalent circuit method and finite element method (FEM) using MATLAB and COMSOL multiphysics respectively are discussed in this chapter. The second half of this chapter explains the actual fabrication steps of SAW device starting from preparation of mask layout to contact leads. Different issues faced during SAW device fabrication and are also discussed in this chapter. The characteristics of developed SAW device without sensing layer are also discussed in this chapter. The fabrication of resistive type interdigital transducer (IDT) with different finger width and finger pairs is also presented in this chapter.

In chapter 4, the synthesis and characterization of polyaniline (PANI) material, along with its characterization (XRD, FTIR, and TGA) is discussed. The polyaniline thin film, a pellet preparation is also reported here. In later part of this chapter, synthesis of SnO_2 nanoparticles and polyaniline - SnO_2 nanocomposite is discussed. In characterization -XRD, FTIR, SEM and FESEM results of both the materials are analyzed.

In Chapter 5, the performance testing of IDT sensor with sensing material (polyaniline, polyaniline- SnO_2 nanocomposite) for volatile organic compounds and ammonia gas is discussed. Also, the performance testing of developed SAW delay line device and SAW IC (SIPAT LBS 201101) for VOCs and ammonia with sensing layer is discussed.

Finally, chapter 6 summarizes of all the findings, contributions and conclusions along with statement of future scope.

Next chapter presents, the exhaustive literature review on principle and development of SAW sensors, different types of SAW sensors, configurations, advances in SAW sensors and their application as gas sensors.

References

[1] A.D. Shaligram, "Sensors and transducers", Chittan publication India, 2014.

[2]Jared Kirschner, Surface Acoustic Wave Sensors (SAWS):Design for Application,Surface Acoustic Wave Sensors (Saws): Design For Fabrication. Microelectromechanical Systems. December 6, 2010.

[3] Jagannath Devkota , Paul R. Ohodnicki , and David W. Greve ,"SAW Sensors for Chemical Vapors and Gases",Sensors2017, *17*, 801.

[4] Simon, I., Barsan, N. & Bauer, M. 2001 Micromachined metal oxide gas sensors: opportunitiesto improve sensor performance. Sens. Actuat. *B* **73**, 1–26.

[5]] Xiao Liu , Sitian Cheng , Hong Liu , Sha Hu, Daqiang Zhang and Huansheng Ning,"A Survey on Gas Sensing Technology",*Sensors* 2012, *12*, 9635-9665.

[6]Ruyen Ro, Shi-Yuan Chang, Rey-Chue Hwang, And Dale Huipin Lee, *Identification of Ionic Solutions Using a* SAW Liquid Sensor,Proc. Natl. Sci. Counc. ROC(A) Vol. 23, No. 6, 1999. pp. 810-815.

[7] D. S. Ballantine, Jr., Robert M. White, S. J. Martin, Antonio J. Ricco, E. T. Zellers, G. C. Frye, H. Wohltjen, Moises Levy, Richard Stern, *Acoustic Wave Sensors, Theory, Design, and Physico-Chemical Applications,* New York: Academic Press limited.,1996.

[8] A. D' Amico, APalma and E. Verona,"Surface Acoustic wave hydrogen sensor", Sensors and Actuators, Vol-3, pp-31-39, 1982.

[9] Y.J.Lee, H.B.Kim, Y.R.Roh, H.M. Cho and S. Baik, "Development of SAW gas sensor for monitoring SO_2 gas", Sensors and Actuators A: Physical, Vol-64, No.2, pp 173-178, 1998.

[10] R.A. McGill, V.K Nguyen, R.Chung et.al, "The NRL-SAWRHINO a nose for toxic gases", Sensors and Actuators, B:Chemical, Vol-65, No-1,pp 10-13,2000.

[11] Reindl L., Scholl G., Ostertag T., Scherr H., W olff U. and Schmidt F., "Theory and Application of Passive SAW Radio Transponders as Sensors", IEEE Transactions on Ultrasoncis, Ferroelectrics and Frequency Control, Vol. 45, No. 5, pages 1281-1292, 1998.

[12] Mujahid, A.; Dickert, F.L.," SAW and Functional Polymers. In *Gas Sensing Fundamentals*; Kohl, C.-D.,Wagner, T., Eds.; Springer: Berlin/Heidelberg, Germany, 2014; pp. 213–245.

[13] Chin, Matthew L. "A Fabrication Study of a Surface Acoustic Wave Device for Magnetic Field Detection." Thesis, Oregon State University, 2006. *Scholars Archive at OSU*.Oregon State University, 5 June 2006. Web. 5 Dec. 2010.

[14] Kondawar SB, et al.,"Conductive polyaniline-tin oxide nanocomposite for ammonia sensor", *Adv. Mat. Lett.* 2012, 3(5):393-398.

[15] Matnishyan AA et. al,"Synthesis and investigation of polyaniline-tin oxide nanocomposite",Journal of Contemporary Physics, 2010, 45(5):246–250.

CHAPTER 2

LITERATURE REVIEW

2.1 Introduction

Microelectromechanical systems (MEMS) are very much in demand due to their versatile characteristics and wide applications in precise instrumentation. Surface acoustic wave (SAW) devices form an important part of MEMS family. A SAW is an acoustic wave travelling along the surface of a material exhibiting elasticity, the amplitude of these waves is higher at the surface and decreases exponentially along the depth of the substrate. The basic principle behind SAW generation and detection is the piezoelectricity. In piezoelectric materials, electrical charge is produced when mechanically strained and vice versa. The SAW devices exhibit a frequency response according to the properties of surface acoustic wave propagating over their substrate.

SAW devices are one of the major components in many communication systems such as radio frequency identification (RFID), mobile phones, television sets, remote controlled units, satellite receivers, keyless entry systems, etc. SAW devices are also used as micro actuators such as SAW micro pumps, nano stepping motors. Sensors based on SAWs find many diverse applications such as gas and vapor detection, biosensors, strain and pressure sensors. Remote data sensing is done by connecting on board antennas to the SAW devices [1]. *There is always a need for superior* SAW sensors that has better sensitivity, selectivity and fabrication techniques. There has been research carried out on use of SAW devices as gas sensor for detecting verity of gases using different sensing materials. The present chapter describes the working principle of SAW sensor, types of SAW sensors, different piezoelectric substrates used for SAW sensor design and its characteristics, specific design parameters.

2.2 Acoustic wave sensors

These sensors are classified according to the various acoustic wave propagation modes determined by factors including substrate material, crystal cut, direction of particle displacement relative to the direction of wave propagation and the sensing surface. The electrode structure used to facilitate the acoustic wave propagation is also an important factor. The popular AW sensors includes Thickness Shear Mode (TSM) SAW, Shear Horizontal Surface Acoustic Wave (SH-SAW), SH-Acoustic Plate Mode (SH-APM), Lamb wave, Love wave mode and surface skimming bulk wave. In principle, the waves may travel through the bulk of the substrate , near the surface of substrate or guided by reflections from multiple surfaces [2]. Depending on the type of acoustic wave, they can be used in liquid or gaseous media or both. Before the discussion on these devices, we will briefly explain the important term which is the backbone of all SAW devices and known as 'piezoelectricity.'

2.2.1 Rayleigh mode based SAW sensor

Fundamentally, the acoustic wave devices use Interdigital transducers (IDTs) to convert acoustic wave into electric and vice-versa. The Figure 2.1 shows Rayleigh mode SAW delay line device structure. The particle displacement in such sensor contains two fundamental modes, one of which is parallel to the direction of wave propagation and the other normal to the sensing surface. Therefore, the particles in Rayleigh mode SAW devices execute elliptical paths. Practically the energy of the Rayleigh waves is limited within 1-2 wavelengths depth of the substrate.

The velocity of these devices depends on kind of piezoelectric substrate used and its orientation. The frequency of operation depends on the IDT finger width and gaps. The main limitation of Rayleigh wave devices is that they are not suitable for liquid media sensing because they get attenuated in liquids [3,4]. Thus, the application of these devices is restricted in sensing gaseous media.
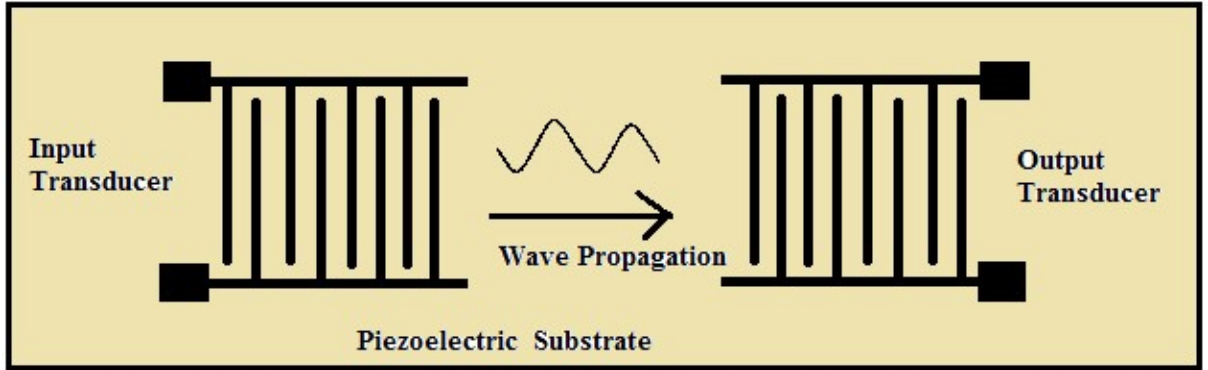
Fig 2.1 Rayleigh mode SAW delay line device structure

The literature survey shows that the Rayleigh wave based SAW devices can be useful in detecting the parameters such as temperature, pressure, electrical conductivity and mass [5-7].

2.2.2 SAW Wave Equation

Generally, a description of the mechanism of elastic wave propagation in a piezoelectric medium would require an evaluation of both the mechanical equations of motion as well as the electromagnetic ones governed by Maxwell's equations. Since the mechanical propagation of SAW wave velocities in the order of 10^5 is less than the velocity of light, however, it may be determined that the mechanical solution will dominate such wave transport processes. The wave solutions for the mechanical wave propagation of the surface wave are indeed complex. It transpires, however, that the electrical potential ϕ that they induce at the surface of the piezoelectric may be modeled to a high degree of accuracy as a travelling wave of potential ϕ (in Volts) such that

$$\phi = \phi\,(x,t) = |\phi|e^{j(\omega t - \beta x)}e^{-\beta|y|} \qquad\qquad (1)$$
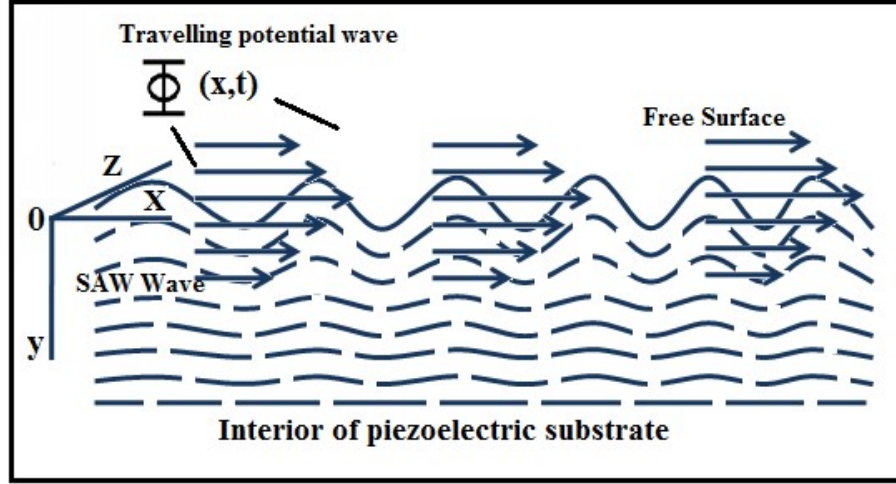
Fig. 2.2 Traveling wave of potential propagates at the SAW velocity.

Here $\omega = 2\pi f$ = angular frequency (rad/s) of the applied signal, while β = phase constant (rad/m) such that $\beta\lambda = 2\pi$ and $\lambda = v/f$ is the acoustic wavelength at SAW velocity v.

The first term $e^{j(\omega t - \beta x)}$ in Eq. (1) relates the travelling wave distribution of potential (with magnitude ($|\phi|$) along the SAW propagation axis at the surface of the piezoelectric $(y = 0)$. This potential is not just confined to the piezoelectric surface, or to the region of the acoustic travelling wave. It also extends above it by a distance on the order of one acoustic wavelength. Because of the complex nature of the potential and field distributions along the y-axis, this variation contained in the second term $e^{-\beta|y|}$ of Eq. (1) is at best a very approximate one. The relative amplitude of potential ϕ away from the free surface is then reduced by a factor of $1/e$ when $\beta = |y|$ where distance y above the surface is negative in the co-ordinate notation used.

The spatial variations of ϕ at the piezoelectric surface will produce electric fields of intensity $E(V/m)$. Along the SAW propagation axis, the longitudinal component E_x of electric field will be given by $E_x = -\partial\phi/\partial x$ for the co-ordinate axis notation of Fig.2.2. There will also be a complex variation of the electric field intensity E_y

$=\partial\phi/\partial y$ extending above and below the free surface as depicted in Fig. 2.3. The distribution of E_y above the free surface has significance in the design of silicon-based SAW convolers.

It is often convenient to relate electric circuit processes in terms of an equivalent circuit model. Its accuracy depends on the degree to which circuit and boundary conditions have been accurately represented. For example, travelling waves on transmission lines are commonly modeled in terms of either lumped or distributed inductance-capacitance (L-C) equivalent circuits. In such modeling, it is assumed that the propagating electromagnetic wave is in a purely transverse electromagnetic mode.
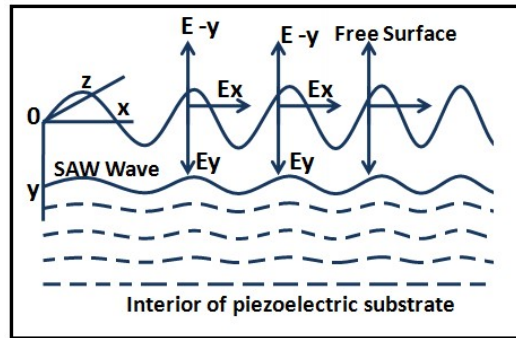
Fig 2.3 Travelling wave electric field with its potential.
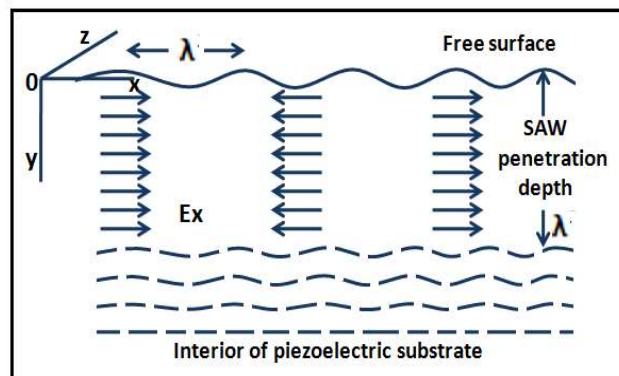
Fig. 2.4 Transmission line model of SAW.

For modeling, some SAW transmission and reflection processes, it is also suitable to use equivalent transmission line circuit models and concepts. As with the electrical transmission line considered above, the accuracy of each model will be given by the assumed boundary and transmission conditions. Thus, for example, if the piezoelectric surface stresses associated with surface wave transmission are assumed to be mainly compressional, the electric field associated with potential ϕ can be modeled as $E = E_x$(and $E_y = 0$) at the surface. If we assume here E_x is consistent within a defined penetration depth at the surface, then the SAW propagation can be modeled in terms of a uniform travelling wave E_x with the SAW acoustic velocity v on an equivalent transmission line as shown Fig.2.4, where this particular simplification is used in the development of the *in-line Mason equivalent circuit* for relating SAW propagation in terms of equivalent electrical parameters.

Familiar electrical transmission line parameters such as characteristic impedance, given by $Z_0 = \sqrt{L/C}$, where L is distributed inductance and capacitance C, can then be reformulated in terms of piezoelectric parameters for an equivalent SAW transmission line model, within the constraints imposed by the assumed boundary conditions.

2.3 Design of SAW Devices

In the design of a surface acoustic wave sensors there are many factors which are to be taken into consideration. Further, the factors such as size, efficiency, and sensitivity can be optimized by considering the proposed application. The structure of the sensor depends on the mode (wired and wireless) of operation which is application specific.

2.3.1 Parametric Determinations

While designing SAW sensors, the important characteristics of the device must be specified as discussed above. frequency, impulse response, and frequency

response of the device. Commonly considered parameters are explained as follows [8].

1) Resonant Frequency f_r

The resonant frequency f_r of the device is the frequency f of the generated surface acoustic wave in a normal environment. In most cases the absence of input is the ambient environment condition..

The important parameters in determining the synchronous frequency of the device is the finger width, and finger gap of the IDT, which decides the pitch. The dimension of finger pitch is four times the width of the finger when the finger widths and finger gaps are equal, this is also equal to the lambada (λ). The following equation then describes the resonant frequency of the device

$$f_{r=}\frac{v}{\lambda} \qquad (2)$$

Where v is the acoustic velocity of a wave in the substrate and which substrate dependent is. To achieve the proposed resonant frequency, the accuracy and precision of the mask and of the photolithography must be high.

2) *Bandwidth (B)*

The bandwidth is the range of the acoustic wave frequency generated by the input IDT. The bandwidth of the SAW device can be increased by decreasing the number of finger pairs in the IDT. According to Hirst et. al. [10], the bandwidth of the device can be mathematically described as follows:

$$B = \frac{2f_0}{Np} \qquad (3)$$

By substituting Equation 4 into Equation 5, we gain new insight into the expression for BW:

$$B= \frac{2}{Np} v = 2 \frac{v}{l_{IDT}} \qquad (4)$$

Where lIDT is the total length of the IDT, The amplitude of synchronous frequency relative to nearby frequencies can be increased by lowering the bandwidth. Thus, a smaller bandwidth gives higher resolution for the sensor.

3) Physical Size: This parameter is application specific and must be considered on the basis of material availability. The minimum dimensions of the device are determined by the dimensions of the of IDTs, the delay line, and any absorbers between the IDTs and the edge of the substrate. To specify the length in terms of pitch and fundamental frequency, following mathematic expression is used

$$l_{IDT} = pN = \frac{N}{f_0} v \qquad (5)$$

The equations 2, 3and 5 puts some limitations on the operating frequency of a SAW sensor. At the lower side of the frequency range, the necessary pitch of the IDT would be large. To maintain a sufficiently low bandwidth a very large sensor would be required. At the higher end of the frequency range, the necessary pitch of the IDT would be quite small and therefore SAW is limited to the band 10MHz to 3GHz.cny , limited by the minimum feature size of current photolithography techniques.

2.3.2 Material Selection

While designing surface acoustic wave devices the important components to be considered are choice of substrate material, selection of conducting material for IDT and material for acoustic absorbers. The following section details about the selection of materials for SAW device. In addition, to material selection the packaging of SAW is also discussed in the following section.

1) Piezoelectric Substrate

 Selecting a piezoelectric substrate involves choosing both a material and a crystal orientation which yields the desired set of properties. The important properties to be considered in design includes the coefficient of thermal expansion, electromechanical coupling factor, wave propagation velocity, compatibility with standard microelectronic fabrication techniques, and cost [12].

Table 2.1 shows the relevant material properties of common piezoelectric materials for SAW sensor design.

2) *Interdigitated Transducers*

The important properties to be considered while selecting a IDT material are substrate adhesion, boiling point, resistivity, and cost [12]. To achieve better coupling between the IDT and the piezoelectric substrate, good surface adhesion is to be achieved. That depends on substrate boiling point and temperature. So a material with low boiling is good. Table 2.2 shows relevant properties for common interdigitated transducer metals.

3) *SAW device Packaging*

For low temperature application basically ceramic packaging is commonly used for SAW devices. But for higher temperatures more than 500 ^{0}C commercially available SMT packages of metal and ceramic are not suitable. In 2001, Joachim W. Mrosket al.[13] illustrated by the pictures shown in Fig.2.5 Consequently, except for laboratory experiments, one must come up with an assembly and interconnect strategy that avoids commercial packages. One approach is to stick a crystal lid onto the SAW substrate chip with the help of a ceramic adhesive. The

substrate and the lid should consist of the same material (e.g., langasite) and the adhesive is chosen such that its thermal expansion coefficient matches that of the crystals. Unfortunately, unlike the adhesive, the piezoelectric crystals are anisotropic; hence, a perfect matching of the thermal expansion coefficients can only be achieved in one direction, and the layered system, substrate–adhesive–lid, will necessarily suffer from thermal stresses at high temperatures. However, preliminary tests showed the feasibility of this packaging technique. From literature survey it is found that until (May 2018) it is not clear whether langasite can be direct bonded like silicon (a well-known standard process) or LiNbO$_3$. So there is need to carry the research on the same.

(a)   **(b)**
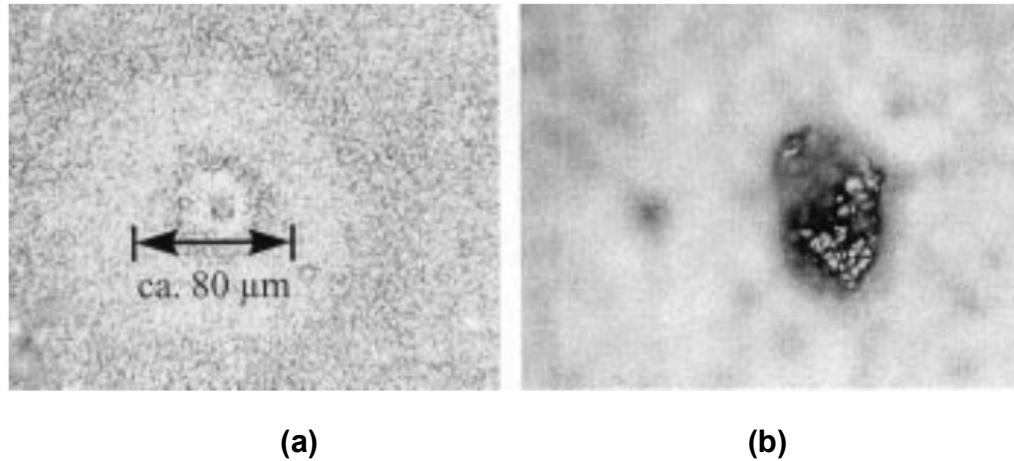
Fig. 2.5 Defects in the W/Ni/Au ground metallization of a commercial SMT package after 60 min at (a) 500 C and (b) 700 C.[13]

Table 2.1: Common piezoelectric substrate properties. [12]

Material Name	Orientation (Axis)	Velocity (m/s)	Temperature coefficient (ppm/^{0} C)	Coupling Coefficient (%)	Cost (Qualitative)
Quartz	Y,X	3159	-24	0	Low
Quartz	Y ST, X	3159	0	0.16	Low
Lithium tantalite	Y,Z	3230	35	0.74	Medium

Lithium tantalite	167 Y,X	3394	64	NA	Medium
Lithium niobate	Y,Z	3488	94	4.6	High
Lithium niobate	128^0 Y,X	3992	75	5.6	High
Langasite	Y, X	2330	38	0.37	High

Table 2.2: Relevant properties for common interdigitated transducer metals. [12]

Metal	Boiling point (K)	Electrical Resistivity (μΩ-cm)	Substrate Adherence (Qualitative)	Cost (Qualitative)
Gold	3129	2.2	Poor	High
Copper	3200	1.7	Good	Low
Aluminum	2792	2.65	Good	Low
Titanium	3560	50	Good	Medium
Tungsten	5858	5.0	Average	Medium

2.3.3 SAW Substrate Crystal Cuts and IDT alignment

In general, SAW piezoelectric substrates are anisotropic. i.e. their SAW propagation characteristics are not constant in all directions. Unless avoided, this can lead to an undesirable second-order effect known as *beam steering,* which can degrade the response of a SAW device filter. Avoidance of beam steering requires the use of piezoelectric substrates with crystal cuts such that the SAW velocity is either a maximum or a minimum, along that particular cut. Inappropriate alignment of an IDT with the required crystal cut can also result in beam steering, to a degree dependent on the anisotropy characteristics of the substrate material used.

2.3.4 Generation of surface acoustic waves (SAW)

Through survey conducted it is reported that various types of transducers are used to generate SAW over non-piezoelectric substrate. The following Figure 2.6(a)

shows a wedge shaped longitudinal bulk wave transducer that generates unidirectional Rayleigh wave. These transducers are popularly used for non-destructive testing of flaws in non-piezoelectric materials. Similarly, a shear wave transducer as shown in Figure 2.6(c) can also be employed to generate Rayleigh waves. The depth of the wave generated is in the order of width of the transducer. The common method to excite and receive surface wave in SAW devices is to fabricate comb like metallic electrode over piezoelectric substrate which is shown in the Figure 2.6(b). The IDT performs the function of conversion of electrical energy to mechanical energy, and vice versa. A voltage applied to the finger structure cause spatial periodic fringing field at the substrate, accordingly due to piezoelectric coupling a strain field is generated. The stress developed with the strain will propagate as SAW in both left and right sides of the transducer. The waves add constructively and reach maximum if the distance between two adjacent fingers is half or quarter a SAW wavelength. The frequency of operation of the IDT depends on the period (P) of the IDT. The frequency of operation f_o for the IDT structure as shown in figure 2.5 (c) and is given by

$$f_o = \frac{v}{\lambda} \qquad (6)$$

$$\text{and } \lambda = 2p \qquad (7)$$

where v is the velocity of the SAW , which is constant for a material , λ is the wavelength of the wave , p is the pitch of the IDT, The IDTs can be fabricated on piezoelectric substrate using lithography technique.

(a)   (b)

(c)
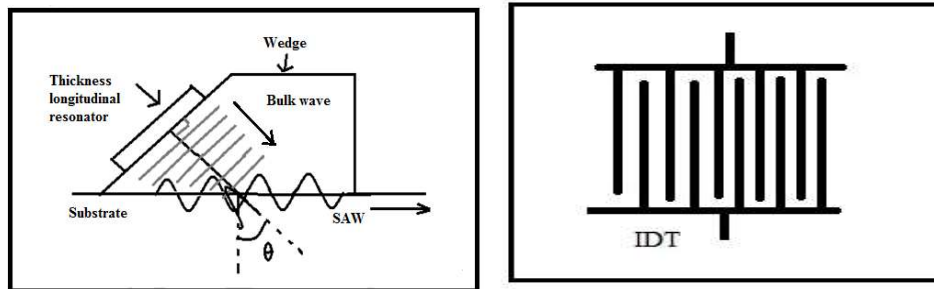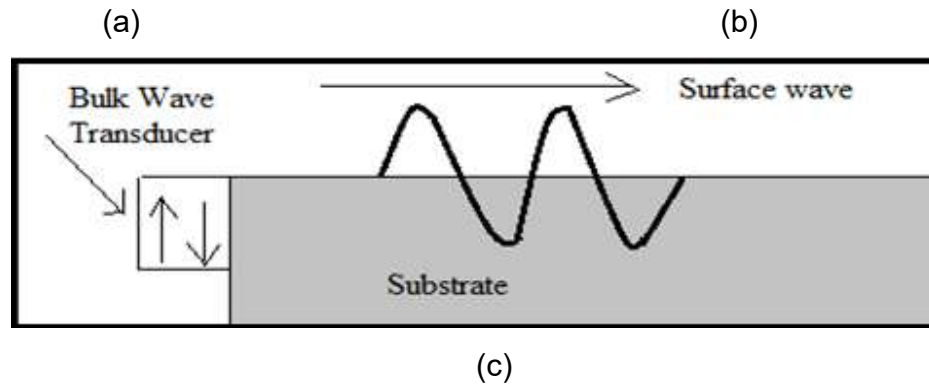
Fig.2.6 Various transducers employed to excite SAW over piezoelectric substrates (a) Wedge transducer (b) Interdigital transducer (c) Edge Transducer [14-15]

2.3.5 SAW device Configurations

SAW devices are usually developed on piezoelectric substrates such as lithium niobate, lithium tantalite, langasite, and quartz. Non piezoelectric materials such as silicon dioxide and diamond are usually coated with piezoelectric materials such aluminum nitride (AIN), lead zirconate-titanate (PZT), zinc oxide (ZnO), polymer-film piezoelectric, such as polyvinyildene fluoride (PVDF), etc. are used as SAW devices. Two basic configurations of SAW devices are SAW delay line model and SAW resonator model. The following section briefly explains both the configurations.

SAW Delay line device

A SAW delay line device consists of two IDTs on the surface of the piezoelectric substrate separated by a few wavelengths (delay line). In this configuration, one IDT acts as a transmitter and other acts as a receiver or vice -versa. The transmitter IDT launches and receiver IDT detects the SAW over the substrate. Table1 in chapter 1 shows the elements of a SAW delay line device.

The delay time, τ, can be calculated using the relation:

$$\tau = L/v \qquad (8)$$

where L is the center to center distance between the input and output IDTs and v is the SAW unperturbed velocity. The space in between the adjacent fingers is maintained at a $\lambda/4$ so the acoustic waves generated by the adjacent finger pairs add in phase. The important design parameters of the delay line device are number of finger pairs in the IDTs, acoustic aperture, IDT center-to-center distance and transducer periodicity. In designing a delay line for a specific application, the frequency response that is required is first converted to impulse response, which is then used to determine the relative weights of the IDT fingers [16]. Delay lines normally have a sine frequency response. IDT fingers are sometimes apodized to suppress the side lobe levels in the response of the delay line. Thus, the finger width, gap between the fingers and the acoustic aperture determine the frequency response of the delay line device [17].

SAW One Port Resonator

This device resonator consists of two sets of reflectors and are fabricated on the either side of the bidirectional IDTs as shown in Table1.1 Chapter first [18] . The reflectors could be made of shorted or open metal strips. At the Bragg frequency, such that the periodicity of reflector electrodes equals half the λ, reflection from the individual strips have the same phase, they add coherently, as in a single electrode of an IDT. This SAW resonator action can be achieved by single long IDT as shown in figure 2.6(b), where multiple reflections within the IDT lead to standing waves and resonate at a particular frequency.

SAW Two Port Resonator

It is explaind infirst chapter. Its construction is same as dealy line device with the addition of reflectors on both sides of the IDTs. The device is designed so that reflectors resonate at IDT resonance frequency. [19].The parameters that influence the response of two-port resonators are the number of IDT fingers, the separation between the grating and the IDT, the grating reflectivity, the metallization height, and the substrate properties [20].

2.3.6 Principle of operation of SAW-based gas sensor

Figure 2.7 shows the idea about its working principle; a thin sensing layer is created using suitable depositing method on a piezoelectric substrate where the surface wave is excited. If the sensor material can absorb gas molecules from the surrounding atmosphere, then the boundary conditions for the propagating surface wave are changed and consequently the velocity and attenuation of the wave undergo a change. These changes can be further measured using oscillators, frequency counter and network analyzer. The velocity of propagation of the surface wave depends on various factors, the most important of which are substrate and the layer characteristics. Particularly in the case of sensitive thin semiconductor layers the propagation of the waves is much perturbed due to adsorption of the particles of gases at the surface of the layer [21].
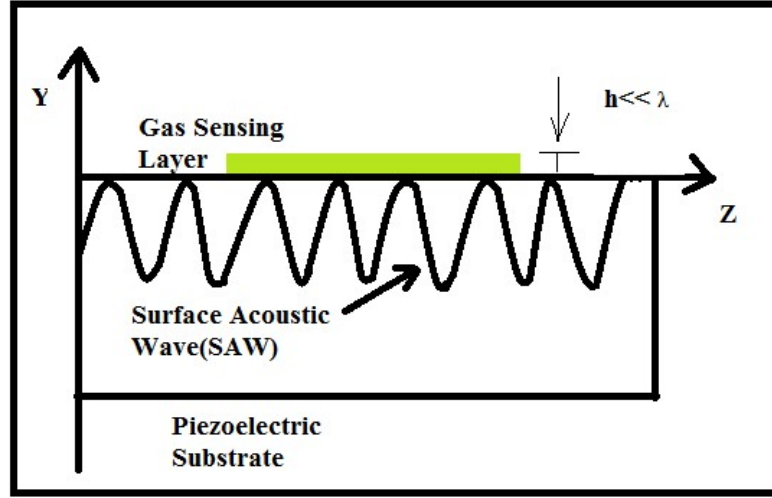
Fig. 2.7 Idea of SAW based gas sensor

2.3.7 Factors which perturb the propagation of the surface wave

The fundamental principle in acoustic wave sensors is the perturbation of the acoustic wave propagation characteristics by the measurand. This perturbation can be measured as a shift in the center frequency of the device or a change in the insertion loss. The various factors that can perturb the acoustic wave propagation characteristics namely mass (m), stiffness (c), conductivity (σ), dielectric coefficient (ε), temperature (T), pressure (p) is described by the following equation[22].

$$\frac{\Delta v}{v_0} = \frac{1}{v_0} \left(\frac{\partial v}{\partial m}\Delta m + \frac{\partial v}{\partial c}\Delta c + \frac{\partial v}{\partial \sigma}\Delta \sigma + \frac{\partial v}{\partial \epsilon}\Delta \epsilon + \frac{\partial v}{\partial T}\Delta T + \frac{\partial v}{\partial p}\Delta p + ... \right) \qquad (9)$$

Since a change in the velocity can be caused due to any of the above effects, it is necessary to consider the sensitivity to other parameters. Compensation for overlapping sensitivities is normally achieved using differential configuration where only one of the two devices are used as sensor and the other as reference.

The use of array sensors for the analysis of multi-component measurands is therefore essential for gaining a better understanding of the sensing mechanisms

[23-24]. Early investigations by groups including D 'Amico and Verona [5], Ballantine and Wohltjen [3], reported that the selectivity, sensitivity, and reproducibility of the overall sensing system may be improved by using an array of sensors, together with the careful selection of the type of sensor system implemented. It seen that the pattern recognition techniques are commonly used to enhance the information extraction of the sensor array through intelligent data processing [26-27]. Hoummady et. al. [25] explained in detail the SAW sensor structures and the results obtained for parameters like temperature, pressure, mass loading, viscoelasticity and conductivity. The following section briefs the most common parameters that are sensed using acoustic wave devices.

Temperature

The velocity of the acoustic wave is significantly affected by change in temperature which causes change in dimensional and mechanical properties of the substrate. In the temperature sensitive environment quartz is normally used to compensate the effects because the quartz has zero temperature coefficients. Alternatively, it can be also compensated by using materials with opposite temperature coefficients. Hauden et. al.[28], Bao et. al.[29], have presented an extensively studied report on SAW based temperature sensors.

Pressure

The Acoustic sensors basically sense the change in pressure caused by induced strain. Talbi et. al.[30], Schimetta et. al.[31] and Vlassov et. al.[32] have reported study on acoustic wave pressure sensors. The effect of other interfering parameters and pressure are compensated by using differential arrangement where one sensor acts as reference and hence compensates the effect of interfering parameters [33].

Mass loading

Acoustic wave devices are also used for monitoring the thickness of films, chemical and biosensing since they are sensitive to mass loading on the surface [2]. The mass sensitivity of SAW devices mainly depends on its resonant frequency, structure geometry, properties of piezoelectric substrate and the mode of acoustic wave. A mass sensitivity factor, C_m, can be mathematically expressed as [2]:

$$C_m = \lim_{\Delta m \to 0} \frac{\Delta v / v_0}{\Delta m} = \lim_{\Delta m \to 0} \frac{\Delta f / f_0}{\Delta m} \qquad (10)$$

where Δm is the uniformly distributed mass per unit area added to the surface of the device, v_0 and f_0 are the unperturbed acoustic wave velocity and device frequency and Δv and Δf are the changes in the acoustic wave velocity and hence the device frequency due to the mass loading.

Since the guiding layers in Love Wave and FPW devices effectively traps most of the acoustic wave energy at the top of the device [34-35] hence, these devices exhibit the highest mass sensitivities. The sensing mechanism can be formulated by carefully interpreting the acoustic sensor response to mass loading. By implementing SAW array sensors and smart sensor systems the problem of overlapping sensitivities to a number of parameters (such as temperature, pressure, viscosity, etc) in acoustic and biosensor can be resolved.

Viscoelasticity

The SAW device parameter such as insertion loss or a change in the phase [36-37] are used to measure the viscosity by adding single droplet of the liquid on acoustic wave sensors. For the viscosity measurement the precaution should be taken to maintain the liquid temperature same as that of substrate temperature because the phase change is quite sensitive to the change in temperature. Further, in viscosity measurement the dynamic range of sensor is limited beyond a certain

value of viscosity because the liquid relaxation time exceeds the acoustic wave period and saturates the insertion loss.

In SAW device viscosity change affects the propagation of acoustic wave in all applications involving liquid media. Hence, careful consideration should be given to applications where viscosity effects interfere with the desired sensing parameter under investigation. Viscosity measurement is commonly implemented by employing SH-APM and SH-SAW devices since here the surface normal component of the wave are absent and hence shear horizontal wave is not attenuated in liquid media.

Conductivity

The influence of electrical conductivity of a thin surface film on the surface wave velocity and attenuation can be mathematically expressed in terms of following equations [22].

$$\frac{\Delta v}{v_0} = - \frac{K^2 \sigma_S^2}{2\sigma_S^2 + (v_0 c_S)2} \tag{11}$$

$$\frac{\Delta \alpha}{k} = \frac{K^2 \sigma_S v_0 c_S}{2\sigma_S^2 + (v_0 c_S)2} \tag{14}$$

Where, K^2 is the electromechanical coupling coefficient of the substrate, σ_s is the sheet conductivity of the film and c_s is the capacitance per unit length of the surface. The acoustic wave sensors can be implemented to sense the gases that influence the conductivity of the deposited film.

From Equation 10 and Equation 11, it can be seen that the sensitivity of the conductivity based SAW sensors can be improved by using higher K^2 substrates. The Lithium Niobate substrate has high K^2 and lower mechanical coupling which eliminates the effects of mass changes. Therefore, it is commonly used in conductivity based gas sensors. In case of SAW conductivity sensors the

electrolytes and buffer solution used should have same viscosity and density for detecting electrolytes. Thus, the change in frequency is due to changes in conductivity. It is reported that both SH-SAW and SH-APM [38] devices have been used as conductivity sensors.

2.3.8 Change in SAW frequency due to sensing material coating

Wohltjen after Auld has reported an equation for the frequency shift produced by the deposition of a soft organic polymeric film onto a SAW device [39,40]:

$$\Delta f = (k_1 + k_2)f_0^2 h\rho' - k_2 f_0^2 h\left\{\frac{4\mu'(\lambda' + \mu')}{v_0^2(\lambda' + 2\mu')}\right\} \qquad (12)$$

Where Δf is the frequency shift, f_0 is the unperturbed oscillation frequency, k_1 and k_2 are material constants, h is the film thickness, ρ' is the film density and μ' and λ' are the film shear modulus and first Lamb constant, respectively. Wohltjen [41] has mentioned that for certain types of polymers the second term on the right-hand side of Equation 12 becomes negligible when the ratio $4\mu'/vo^2$ is less than 100, giving the simplified expression:

$$\Delta f = (k_1 + k_2)f_0^2 h\rho' \qquad (13)$$

Which shows a linear decrease in Δf with increasing mass per unit area. It should be taken in to account that the derivation of equations 12 and 13 assumes that the film is lossless, non-conducting, non-piezoelectric, isotropic, and thin relative to the acoustic wavelength λ (h < 0.2% λ).The above equations are valid for poly(methacrylate)films up to 2.1μm thick[41],Langmuir-Blodgett (LB) films of tetrakis-(cumylphenoxy) phthalocyanines up to 65 layers[39], and various other LB films up to 70 layers[42]. Other films, however, have not shown agreement over the same ranges [39], while for some films that showed a linear decrease in Δf with increasing thickness, the mass sensitivity was scientifically less than predicted. Other workers have also found deviation from Equations 12 and 1 including frequency shifts in the incorrect direction.[43] These results may be credited to changes in film viscoelastic properties, acoustic loss into the film, and sheet conductivity effects. In addition, it is important that the film properties should conform to the conditions assumed in the derivation of Equations 12 and 13; the

properties of the films used in the experiments reported above have not always been known.

The effect of vapor sorption into the film is noticeably important since the majority of SAW sensing applications described to date use this process. Vapor absorption will result in both film volume and modulus changes. Frye et. al.[44] have suggested that positive frequency shifts at low vapor concentrations for a methanol-polyimide system may be due to either film stiffening or changes in film thickness on swelling. They further recommended that at higher methanol vapor concentrations plasticizing effects could make a considerable contribution to the observed response. Martin and Frye subsequently employed a Maxwellian model to describe the effects of temperature and plasticization on response for such systems. Bartley and Dominguez [45] developed expressions to check the effects of film stiffness on sensor response. Their results showed that positive frequency shifts were unlikely to be caused by film stiffening effects since these should be considerably smaller than the mass loading effect.

Most recently Grate et. al.[46] explained a model based on partition coefficients to find effect of polymer mass loading and thermal expansion as a measure of polymer swelling. Their results shows that swelling effects can be significantly greater than mass-loading effects when the polymer and vapor densities are similar, and that this can be explained by polymer modulus changes.

Other factors affecting SAW sensor response have been acknowledged but little investigated since the effects are believed to be minor in comparison with those already mentioned. Among these latter effects is the influence of the dielectric constant of the contacting medium [39]. This can be easily proved since the dielectric constant is related to both the dipole moment and the polarizability through the Debye equation

$$N_V \left[\frac{(a+\mu_D^2)}{(3\epsilon_0 kT)} \right] = \frac{3(\epsilon_r - 1)}{(\epsilon_r + 2)} \qquad (14)$$

Where N_v = number of molecules per unit volume, α = polarizability, μ_D = dipole moment, ϵ_0 = permittivity of free space, k = Boltzmann constant, T = absolute temperature, and ε_r= relative permittivity (dielectric constant). There is the chance of coupling between a dielectric medium on the SAW device surface and the electric potential wave associated the SAW through the piezoelectric substrate through rearrangement of dipoles and/or induced dipoles with the changing electric field. This is possible since the time scale for molecular reorientations and polarization effects is on the picoseconds time scale, well within the frequency ranges typically used for SAW sensors. This is illustrated by the recent observation of Baer and Flory [47] that liquids with a high dielectric constant show significant attenuation of leaky SAW waves through electrical dissipation. This will produce some perturbation of the SAW velocity, although the size of this effect is probably very small in comparison to the effects described above.

2.3.9 Conducting Surface Layers

A SAW travelling through a piezoelectric medium is accompanied by an electric potential wave, which can be affected by an applied electric field or the properties of a conducting or semiconducting surface layer. A. J Ricco et. al.[22] studied the effect of film conductivity change on the performance of SAW based gas sensors .The author found that reaction with strongly oxidizing gases, in particular NO_2, increases the conductivity of the PbPc film. Acousto-electric coupling of the traveling electric potential wave associated with the SAW to charge carriers in the PbPC film slows the acoustic wave velocity altering the oscillation frequency of the circuit. This sensor is about 1000 times more sensitive, in terms of the number of NO_2 molecules that can be detected (10^{16} molecules/cm^3 of PbPc film), than an identical SAW sensor functioning via mass loading would be Sensitivity to a few ppm of NO_2 in N_2. Alder [48] described the effect of such a layer and reported that both amplification and attenuation of the SAW could result, depending on the charge carrier drift velocity in the conducting layer: If this is less than the phase

velocity of the acoustic wave then attenuation occurs; if it is greater, amplification occurs.

2.3.10 Rigid, Non-conducting Films.

It has been reported that sensors have employ insulating metal oxide and silica films. The latter were created by the sol-gel process, the SAW sensor being used as a microbalance to obtain nitrogen adsorption isotherms for the processed gel [49-50]. In this case, the response of the device was given by the equation:

$$\frac{\Delta f}{f_0} = \frac{k\Delta v}{v_0} = -kc_m f_0 m\delta \qquad (15)$$

Where δ is the number of adsorbed molecules per unit area, c_m is the mass sensitivity of the device (= 1.3 X 10^{-6} cm^2s/g for quartz), m is the mass of one molecule of the adsorbing species, and k = 1 if the complete surface area of the device is covered. This equation assumes that only the mass term in Equation 15 is significant under the conditions used. Equation 15 can be extended to the case of a rigid, thin non-piezoelectric non-conducting film by noting that the term mδ is the added mass per unit area and can be replaced by $h\rho'$ where h and ρ' are the film thickness and density respectively, i.e.

$$\Delta f = -kc_m f_0^2 h\rho' \qquad (16)$$

2.3.11 Contact with a Liquid Layer

Roederer and Bastiaans[51]first explained the use of a SAW sensor in contact with a liquid for a micro gravimetric immune sensor, though the type of the acoustic wave travelling under the conditions used has been disputed by Calabrese et al.[52].The nature of the interaction between the acoustic wave and the liquid layer will depend on the thickness of the layer relative to the acoustic wavelength. The attenuation of Rayleigh waves by liquid helium has been reported by Cheeke and Morisseau[53]. Rayleigh waves have both longitudinal and transverse components. For the case of a liquid in contact with the surface, the longitudinal component couples to the liquid through the liquid viscosity while the transverse component couples through an acoustic mismatch. The new mode of propagation

is known as a leaky Rayleigh wave. The comparative contributions of these two mechanisms depend on the liquid viscosity and the thickness of the liquid layer. If the layer is very thin the attenuation can be quite moderate and a Rayleigh wave can still propagate, but for liquid layers thicker than a few acoustic wavelengths the losses are large and can result in total attenuation of the Rayleigh wave [52].

2.4 Sensor Characteristics

The characteristics such as sensitivity, selectivity, response kinetics, detection limit, repeatability, and stability of a SAW chemical sensor depends upon the materials properties, device design, fabrication techniques, operating frequency, and environmental conditions [54-55]. Piezoelectric SAW transducers possess ultra-high sensitivity, fast response, suitable structure and size, and are compatible with other technologies. However, the sensitivity, selectivity, response times, and other factors determining the suitability of SAW sensors for an application depend critically on the properties of the sensing layers [55, 56].

SAW sensors can detect chemicals at very low concentrations (~ppb level). The sensitivity depends upon the IDT characteristics, the center frequency, the sensing layer properties such as, thickness, surface roughness, and temperature of operation [56]. It is reported that their mass sensitivity increases as the square of the operating frequency [57, 58]. For example, Dickert et. al.[59] experimentally showed a parabolic increase in sensor sensitivity and a linear increase in noise level with center frequency when going from 80 MHz to 1 GHz. Thickness of the sensing layers is also found to be a major factor to affect the sensitivity of SAW sensors [60]. In ideal cases, the sensitivity increases with thickness but changes in roughness, crystallinity, and hardness of a layer with thickness have potential impact in the sensitivity. For instance, an increased roughness attenuates the acoustic waves thereby decreasing the sensitivity of the sensors. The sensitivity is also greatly affected by the substrate temperature. Venema et. al.[60]. Fabricated LiNbO$_3$ SAW sensors of different operating frequencies, coated metal-free patholocynine films with three different thicknesses, and operated at two

temperatures for detection of NO_2 gas. For a given thickness of the sensing layer, they have observed higher sensitivity of the sensor operating at higher frequency. However, the sensor operated at lower frequency and containing thinner over layer was more sensitive than the one operated at higher frequency and containing thicker layer. Similarly, they have also observed higher detection sensitivity to NO_2 at higher temperature.

The selectivity of SAW chemical sensors is solely dependent upon the material properties of the sensing layer [61,64]. When a SAW sensor is exposed to a mixture of various gases, it sorbs or reacts with them differently so that the strength of the sensor output is different for each component. Venema et. al.[60] employed the patholocynine coated sensors for selective detection of NO_2 in a mixture of various gases and reported that the observed results shows that the SAW sensor coated with a proper material can be used for selective detection of analytes.

In addition to the selectivity, the reversibility and repeatability depend upon the materials properties of the sensing layer and its interaction type with the analytes. If the interaction is by physisorption, there is a high chance of a reversible and repeatable response provided sufficient time is allowed for equilibration but this type of interaction leads to a less selective detection. On the other hand, if the interaction is by chemisorptions, the absorption is relatively more selective but has relatively poor reversibility due to the formation and breaking of chemical bonds. The stability and hence the reproducibility of the sensors depends upon the stability of materials used and the compatibility between the sensing material and the piezoelectric substrate. If the mechanical adhesion between the substrate and the sensing layer is strong and the film does not deform, the sensor can last for longer time [63-64].

The rate of sensing layer-analyte interaction and hence the response time of a SAW sensor is affected by several factors. In the case of mass-based sensing

layers, the response and recovery times of a SAW sensor mainly depend upon the rate of diffusion of the adsorbed mass into the film and to the piezoelectric substrate and back to the film surface. The sensors with thinner sensing layers usually have faster response kinetics. With decreasing the thickness, the gas diffuses in and out of the film rapidly so that time required for reaching to the equilibrium decreases. Thin sensing layers thus result in rapid response to gases [60, 65]. In a frequency-dependent study, Dickert et. al.[59] have shown that the sensors with higher operational frequency can have shorter response time in addition to their improved sensitivity. They have attributed the reduction of the response time to the possibility of using thinner layers in the high frequency transducers. It has also been shown that the response time of a SAW chemical sensor varies with temperature [60, 66]. With increasing the temperature, the diffusion/dissociation rate of the analytes may increase thereby decreasing the response time.

2.5 Deviations from Ideal Phase Response in SAW Devices/Filters (Second Order Effects)

Practical SAW sensors/filters are not ideal devices. Various second-order effects perturb the ideal environment to some degree and degrade the filter response**.** Sources of SAW device/filter response degradation are as explained below:

1*. Electromagnetic feed through (crosstalk)*

It relates to the direct coupling of input signal from input to output IDTs in the form of electromagnetic radiation. Essentially, the two IDTs act as capacitor plates, which may be separated by only a few acoustic wavelengths. The amount of electromagnetic feed through, which increases with frequency as the capacitive reactance decreases, can be significant. This feed through is coupled to the output IDT at the velocity of light to interact with the SAW signal arriving there. The interaction gives rise to periodic ripples of amplitude and phase across the SAW filter pass-band at ripple frequency :

$$f_r = l \, / \, \tau \tag{17}$$

where, $\tau = L/u$

is the SAW propagation time between IDT phase centers separated by distance L. This can be one of the most troublesome sources of interference in SAW devices. (Others include parasitic due to packaging and bonding wires.)

2. *Triple-transit-interference (TTI)*

TTI is due to multiple SAW reflections between bidirectional input and output IDTs. This is normally due to regenerative effects caused by current flow in the IDTs. Some of the SAW power received by the output IDT is reradiated into the piezoelectric. That portion from the output IDT that arrives back at the input can lead to further regeneration of a SAW wave. As a result, the main voltage signal induced in the output IDT is corrupted by additional voltages due to these multiple SAW reflections. The path differences between the main and doubly reflected SAW signals result in amplitude and phase ripple across the SAW passband at a ripple frequency f_r = 1/2T.

3. *Electrode finger reflections*

The thin-metal film IDT fingers deposited on the piezoelectric crystal surface introduce impedance and mass-loading discontinuities so that a portion of the surface wave is reflected from both the front and back surface of each finger. If not cared for by appropriate design, this causes interference with the main surface wave. In addition, multiple SAW reflections can occur between input and output IDTs to form an additional source of TTI.

4. *Bulk wave interference*

Unlike SAW waves, bulk waves can propagate in any direction within the body of the substrate material. Those bulk wave components that arrive at the output IDT induce voltages that are additional to those induced by the surface wave. Over the SAW filter band-width, interference between the two voltage components will cause distortion of the desired amplitude, phase and group delay characteristics for the SAW response alone. This will corrupt the pass-band amplitude and phase response, as well as reduce the out-of-band amplitude rejection levels. It will also lead to increased filter insertion loss.

5. *Circuit factor loading*

This results from the finite source and load impedances that are external to the SAW filter. Both the input and output impedances of a SAW filter are frequency-dependent parameters. The consequence of this is that an input voltage will be divided between source resistance and filter input impedance in a frequency-dependent way, unless compensated. The same situation applies to the output transducer circuitry.

6. *Impedance mismatches*

In the input IDT circuitry, signal power is divided between the generator resistance and a fictitious resistance associated with SAW power radiation into the acoustic substrate medium. Maximum power transmission by the SAW wave only occurs when the two resistances are matched (i.e., equal).The same situation arises with the load resistance connected to the output IDT circuit. Source or load changes result in insertion loss increases or changes due to mismatching.

7.*Diffraction*

Diffraction occurs in SAW IDTs in much the same way as it does in optical systems. Ideally, the SAW emissions induced by, and travelling under, excited IDT electrodes should have "flat" wavefronts so that all parts of a wavefront launched by one IDT finger arrive at a receiving IDT finger after the same time delay. As in optics, however, the SAW wavefront will be spherical to a degree that is dependent on the aperture of the radiating source. This will corrupt the filter response. Anisotropy of the piezoelectric medium will also give rise to focusing or defocusing of the surface wave.

8.*Harmonic responses*

Excited IDT fingers can generate SAW waves at harmonic signal frequencies in addition to those generated at the fundamental signal frequency. (This may be a desirable or undesirable feature, depending on the application, and is listed in brackets as a result.) The levels of such harmonic frequencies will be dependent on the relative width of the metal fingers with respect to their separations. They will also depend on the overall IDT geometry used. This can lead to undesirable levels of harmonic response outside the pass-band of the fundamental signal. In some applications, however, the SAW filter is designed to operate at a desired harmonic frequency while suppressing the fundamental at the same time.

The task of the SAW designer is to ensure that these perturbations are reduced to acceptable levels. This requires knowledge of their sources as well as of circuit design techniques for dealing with them.

2.6 Advances in SAW Based Chemical sensors

In recent years, there have been notable advances in various aspects of SAW chemical sensors as reported in[67-68] even though early studies were focused in understanding the sensing mechanism and exploring the detection techniques [57, 69,70]. Major directions of the advancement include (i) the optimization of sensing layer properties and coupling of the layers with analytes and piezoelectric substrates ;(ii) the control of the undesired effects and drifts that can arise from the devices itself, the environment, and the measurement system [71]; (iii) application for detecting and monitoring a range of gases and VOCs, at different operating conditions [72]; and (iv) integration with electronics and improvement in signal analysis. Below, we discuss some of these advances.

2.6.1 Sensing Layer Considerations

The properties of the sensing layers and their coupling with the target analytes and piezoelectric substrates are important factors to consider for developing high performance sensors [73]. A good sensing material must be able to interact with the target gas selectively, strongly, and quickly while maintaining its stability over long time. Selective detection of gases can become challenging as a sensing material can interact with multiple gases as well as many sensing materials can interact with the same gas. However, fine-tuning the sensor response is possible by selecting proper materials or their derivatives for specific analytes types and targeted applications [74]. In addition, an ideal over layer has to have reversible and repeatable interaction with the analytes, strong mechanical adhesion with piezoelectric substrates, be tolerant to the measuring environment, and leave IDTs open electrically.

Many materials have been tested as the sensing layers for SAW-based gas sensing [74]. Most commonly used materials are conducting, non-conducting polymers and semi-conducting metal oxides [66]. Other widely used materials

include carbon nanostructures [75, 76] and grapheme oxide, metals, ceramics [68], and composite materials [77]. More recently, interest is in relatively new materials such as metal-organic-frameworks (MOFs) [78] and porous materials for their higher sorption capacity [79]. These materials are applied using different techniques such as sputtering, evaporation, spin coating, drop casting, spray coating, and Langmuir-Blodgett methods depending upon the properties of the materials [74]. To fulfill the requirement of particular sensing application, materials with suitable material characteristics and proper interaction type with analytes have to be selected as a sensing layer [79].Different types of conducting, non-conducting polymers and their derivatives have been used for developing room temperature chemical sensors for detection of various Volatile organic compounds (VOCs) such as alcohols, aromatic compounds, and some inorganic gases. Some widely used variants include pure polymers, functional organic polymers, molecularly imprinted polymers, self-assembled polymers, and polymer composites [74]. The sensors based on polymer films have usually short response and recovery times as they generally absorb the gases via physisorption. Redox reactions can be involved in case of conductive polymers, especially when they are doped to increase the conductivity. Another advantage of polymers comes from the ease of fabrication. They are solution processable and can be coated by simple techniques such as spin coating and drop casting. The selectivity of the sensors based on these materials is relatively poor even though it can be enhanced to some extent by some modification in their structure or by doping.

Metal-oxides, on the other hand, have been widely used to detect inorganic gases and some VOCs at high temperatures [72, 80]. Some popularly used metal oxides in SAW sensors include the films and nanostructures of Co_3O_4, WO_3, In_2O_3, ZnO, SnO_2, TiO_2 and TeO_2 [66 68]. Their high temperature suitability comes from the fact that they (i) possess high thermal stability; and (ii) mostly interact with gases at high temperatures. These materials interact with different oxidizing and reducing gases via chemisorptions or redox reaction depending upon the temperature [73].

This helps developing selective sensors using these materials. The sensitivity of these materials is weak at room temperature but can be tuned at higher temperatures depending upon the materials and target analytes. However, they possess very long recovery time due to the involvement of redox reactions that limit their use for real time gas monitoring and sensor array development .Other materials such as carbon-nanotubes [75], grapheme [81], and a variety of composite materials [77] metal-oxides [74]. For instance, carbon nanotubes have shown very high sensitivity to various VOCs and inorganic gases at room temperature. They have large surface-to-volume ratio, fast response time for many gases, and high adsorption capacity that make them promising materials for development of sensitive room temperature sensors [82]. They can also be decorated with other materials to improve the sensitivity and selectivity. Composites of semiconductors and metals have also shown improved sensitivity and response time. Ippolito et. al. developed H_2 SH-SAW sensors using pure and Au catalyzed WO_3 as sensing layers on $ZnO/LiTaO_3$ layered piezoelectric substrate [83]. They were able to detect 0.06% H_2 in air using the catalyzed sensors whereas 0.5% H_2 was the lowest limit for pure WO_3 sensor at different temperatures.

Recent reports have shown that using nanostructures (e.g., nanorods, nanofibers) rather than solid films can improve the sensing response of polymers and metal oxides as well [84]. As an example, Sadek et al. [85] fabricated a layered ZnO ,60^0 Y-X $LiNbO_3$ sensor, functionalized the surface with polyaniline/In_2O_3 nanofiber composite, and employed for detection of H_2, NO_2, and CO at room temperature. They have observed faster response and recovery times compared to those of a solid film-based otherwise identical sensor with a good repeatability. Similarly, Giffney et. al. [84] fabricated identical $LiNbO_3$ SAW sensors using nano-rods and spin-coated films of ZnO as the sensing layers and employed for ethanol vapor detection at 270 ^{0}C. They showed a large frequency shift (24 kHz) in the nano-rod based sensor against a shift of 9 kHz in the film-coated sensor when exposed to

the same concentration (2300 ppm) of ethanol vapor. Besides exploring various materials for sensing layer, there have been studies to optimize the physical parameters of the layer such as the thickness, uniformity, surface roughness, and its mechanical adhesion with substrate to improve the sensor response [80] . Venema et. al. [86] showed the highest sensitivity of a SAW sensor to NO_2 with the thickest patholocynine coating. However, later it became clear that there exists a critical thickness of the layer beyond which the sensitivity starts decreasing. For example, Luo et. al. [66] studied the effect of the film thickness (150 nm–382 nm) of SnO_2 film on the sensitivity and response time in detecting H_2S. They found the highest sensitivity and the shortest response time with the film thickness of 275 nm telling the importance of choosing an appropriate thickness for optimal sensor response. In 2010, Fisher et. al.[65] showed large changes in propagation loss of palladium-coated Y-Z $LiNbO_3$ SAW delay line depending upon the film thickness and suggested a need of further study in understanding the effect of film thickness on SAW gas sensing. Based on this report, Tasaltin et. al. showed that the main interaction mechanism between the ZnO nanostructured sensing layer and SAW waves can change from acoustoelectric to mass or elastic effect beyond a certain thickness [68].

Some researchers [83, 87] have reported a possibility of improving the sensitivity of SAW chemical sensors by designing metal - semiconductor layered sensing coatings instead of using a metal only or semiconductors only layer. As an example, Jakubik et. al.[87,88] developed $LiNbO_3$ SAW sensors for H_2 detection by coating copper patholocynine, Pd, WO_3, and their combinations to form metal-semiconductor layered structures. They have observed a much higher sensitivity to H_2 gas when using a metal semiconductor layered structure compared to the single metal or semiconductor sensing film. The improved sensitivity of the bilayer-based sensors over metal or semiconductor-only layer was attributed to an extended live conductivity regime of the layered structure. The metal layer alone shorts the electric field associated with the SAWs causing only mass-loading to be

effective as the interaction mechanism whereas the semiconductor only layer could result to a weak acoustoelectric coupling due to relatively small active regime of the conductivity. However, when metal semiconductor layered structure is formed, the active conductivity regime and hence the acoustoelectric coupling between the layers and surface waves can be extended to a higher sensitivity range. This leads to the detection of target gases with higher sensitivity. Selection of an appropriate technique to apply sensing layers on SAW transducers is another important factor to consider for improving the sensor performance. For instance, a polymer film obtained by dip coating or by layer by layer deposition can have well controlled thickness, smooth surface, and better adhesion with the substrate than the one obtained by spin coating or drop casting. McGill et. al. [89] has made a comparative study of various chemoselective polymers and different deposition techniques for optimal response of SAW chemical sensors. Similarly, Pestov et. al.[90] showed an improvement in stability of the sensing layers using photo-polymerization on SAW resonators.

2.6.2 Controlling the Interfering Factors

Though SAW offers high sensitivity to chemicals, SAW sensors may go through interferences from various internal and external factors so that the output may deviate from the expected one [91]. The internal factors that may cause false response include the viscoelastic properties of the sensing layers, wave reflections from the edges of the devices, impedance mismatch of the IDTs, and the temperature rise of the substrate materials during RF signal excitation. The external factors that may cause a deviation of the sensor response include the environmental factors such as temperature, pressure, humidity, and the presence of unwanted chemicals. Finally, measuring instruments and signal analysis could also introduce errors in the sensor output. Different techniques have been suggested and employed to minimize various possible drifts in these sensors [86,91]. The unexpected effect from the sensing layers such as the viscoelasticity, incompatibility, roughness, etc. can be controlled by selecting robust sensing

materials or using better deposition techniques [74, 89]. Similarly, the reflections from the edges of the devices and IDT impedance mismatch can also be addressed to some extent by using wave absorbers at the device edges or optimizing the IDT and reflector designs [92]. The temperature rise due to temperature dependence of the piezoelectric substrates, the sensing materials, or IDT materials can be addressed by using less temperature sensitive materials. The piezoelectric crystals with selective orientations have low TCF (e.g. quartz) that provides more stable sensor signal with reduced cross-sensitivity to temperature.

The environmental temperature variation can affect the material properties of the substrates and the sensing layers such as the dielectric constants, conductivity, and elasticity that have direct influence on the wave propagation. To compensate the temperature drift from the environment or from the piezoelectric substrates, researchers often use a reference device in the same substrate [22, 60, and 93]. Figure 2.8 shows such a schematic of a dual delay line oscillator (differential scheme) to compensate the temperature drift in which one delay line is coated with the sensing material of interest for gas exposure and the second delay line is left uncoated. The signal in the unloaded delay line can be subtracted from the loaded delay line signal to remove the thermal and other environmental drifts. This scheme has been useful in compensating the thermal drifts room the substrate itself or from the environment layer [94].
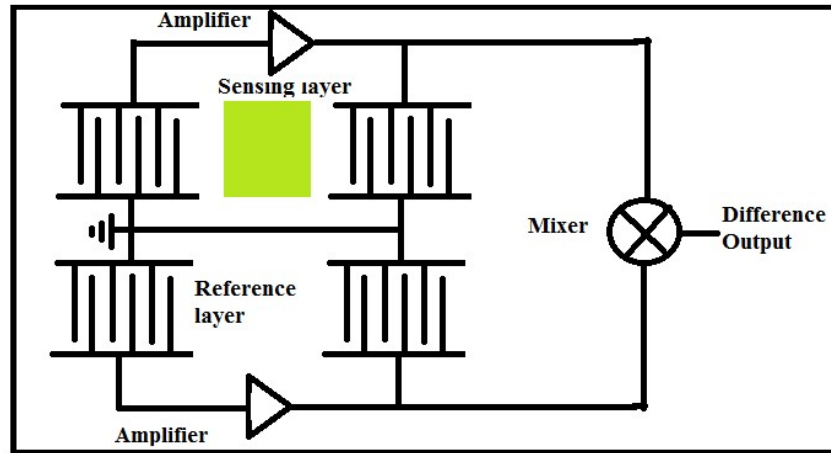
Fig. 2.8 Schematic of dual delay line SAW sensor for compensation of thermal drift [95].

An additional significant cause of the environmental drift is the humidity. Several studies have shown that humidity may cause an increase or decrease of the detection sensitivity depending upon the material characteristics [68,96]. In 1993, Rebikre et. al.[96] reported that a CuPc-coated NO_2 SAW sensor can have higher sensitivity in more humid environment. In a recent study by Tasaltin et. al.[68], the humidity was found to have both positive and negative effect to the sensitivity of a ZnO-coated SAW sensor. They have observed an increase in the sensitivity for acetone, chloroform, propanol and trichloroethylene vapors with humidity while a decrease for methanol and ethanol vapors. The effect of humidity on sensor response can be compensated by operating the sensors at higher temperatures [97]. Other than operating at higher temperatures, using a hydrophobic material as the sensing layer may be an effective approach to circumvent the humidity effect.

In addition, there can also be other sources of drifts including the measurement system itself and the residue of a previous measurement. The drifts from the measurement system can be addressed using high resolution instruments and careful integration of devices with the electronics. Similarly, one can eliminate the drift by designing a measurement system for complete removal of the residuals.

For instance, Muller et. al. [98] demonstrated a cyclic measurement technique to eliminate such drifts in detection of NO_2 using SAW sensor.

More recently, there has been effort to addressing various drifts collectively. For example, Wen et. al. [99] fabricated a dual-track SAW sensor with WO_3 coating that showed good response characteristics to small concentrations of NO_2 gas. They were able to detect up to 0.5 ppm of NO_2 gas with good reproducibility and stability. They claimed that this configuration could eliminate the external perturbations, suppress the bulk waves, and improve the side lobe rejection thereby improving the sensor response. On the other hand, there are needs to minimize the device cross-interferences to several parameters including temperature, strain, unwanted chemicals, and humidity for their efficient use as chemical sensors.

In the following sections, we review the electrical properties of the IDTs, particularly with respect to capacitance and its effect on the sensor performance.

2.7 Characterisation of an Interdigital Transducer (IDT)
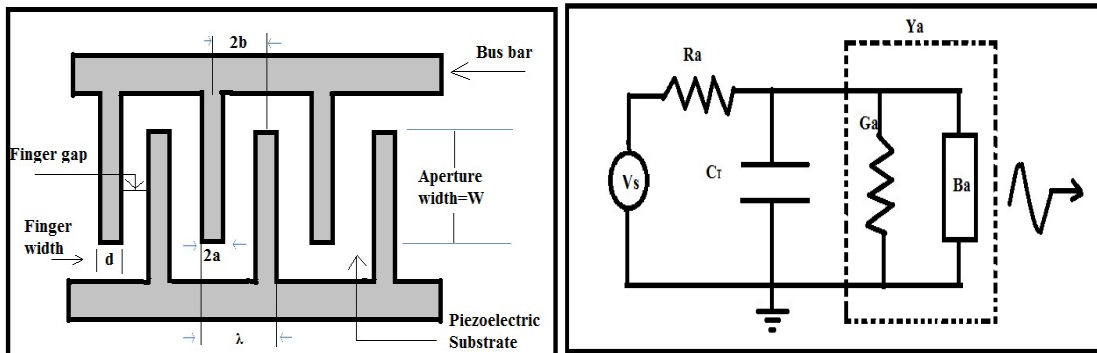
Fig.2.9 (a) Construction of an IDT.b) Equivalent circuit of an IDT as an acoustic transmitter.

The operation of SAW devices is the mainly depend on IDT. IDT can act as both a transmitter and a receiver. In characterizing the electrical properties and

operation of IDTs we therefore, have to take in account both the electrical and acoustic properties. These can be described either in terms of the impedance (Z) or the admittance (Y =1/Z), both of which are functions of frequency. Even though it is normal to measure impedance, it is often more convenient to consider the admittance in any explanation. This admittance is due to the ordinary capacitance of the IDT, which does not depend on the acoustic properties, and an acoustic admittance Y_a where the subscript "a" denotes its acoustic origin. This results from the interaction of the IDT with the acoustic waves generated by it; an alternating potential applied across the fingers of the IDT results in the generation of acoustic waves which, as they propagate away from the IDT, induce currents in the other electrodes. If the substrate on which the IDT was manufactured is non-piezoelectric, it would act exclusively as a capacitor. The electrical equivalent circuit representation of the IDT of Figure 2.9(a), when acting as a transmitter is shown in Figure 2.9(b). The acoustic admittance is complex, the real part being the radiation conductance G_a and the imaginary part being the radiation susceptance B_a. V_s and R, are the source voltage and resistance, respectively, and C_T is the capacitance of the IDT which gives rise to the electrical admittance $j2x/C_T$[95].

2.7.1 Calculation of Interdigital Capacitance

The calculation of the capacitance of an interdigital electrode array is of general importance in the field of microelectronic device fabrication as well as in the design of interdigital capacitive gas sensors. This can be achieved by taking in account the contributions from the surface charge on the electrode surface against (a) the crystal, (b) the medium in contact with the device surface, and (c) any second medium present between the electrode fingers. In general, for two parallel plate electrodes separated by a dielectric medium, capacitance increases with increasing dielectric constant and plate area and decreases with increasing separation; more polar substances have higher dielectric constants. This simple expression for capacitance has to be modified to take into account the elliptical

field lines resulting for the case of the parallel, coplanar electrodes forming an IDT. Scapple[39,96] described the calculation of the capacitance of an interdigital array based on the capacitance per unit length for two identical infinite coplanar parallel strips[97] with near edge distance 2(a)and far-edge distance 2(b) (in MKS units)

$$C_s = \epsilon \frac{K[(1-r^2)^{1/2}]}{K[r]} \tag{18}$$

Where if the substrate has a dielectric constant ϵ_1 and the medium above it has dielectric constant ϵ_2 then $\epsilon = (\epsilon_1 + \epsilon_2)/2$, $K[m]$ is a complete elliptical integral of the first kind and $r = a/b$. It is assumed for an interdigitated pattern that the far-edge distance lies in the center of the conductor strips. In this case the total capacitance (neglecting the "end effect" arising from the lower potential distribution on the outermost fingers) is given by

$$C_T = (N-1)C_s W \tag{19}$$

Where N is the number of finger pairs and W is the finger overlap. When N is large this can be further simplified by writing $(N - 1) = N$. Similar calculations have been given by Auld [98] based upon the earlier work of Engan [99].This leads to a different form of equation 17, however:

$$C_s = (\epsilon_0 + \epsilon_p^T) \frac{K[k]}{K[(1-k^2)^{\frac{1}{2}}]} \tag{20}$$

$$\text{where } k = \cos\left(\frac{\pi}{2}(1-\alpha)\right) \tag{21}$$

ϵ_0 is the permittivity of free space, ϵ_p^T is the zero-stress permittivity, and a = d/2b (d is the finger width and r = 1 - α). Auld and Kino later gave equation 21 with k expressed as k=sin(πβ).

where β = d/λ = α/(1 + α). If, however, the same assumption is made regarding the far-edge distance then β= d/2b = α, and it can be shown that equation 18 is then identical to equation 20 except that the sine term differs by a factor of 1/2.

It is not easy to determine the origins of these differences, but their effects can be calculated for various values of r. Equations 19 and 21 give values of C_s ,that are the same for r = 1 and r → 0. The maximum difference with a = 7.5 μm occurs for r ≈ 0.73, the value from equation 17 being 18% larger. The use of equation 20 for k in equation 21 results in much lower values of C_s, with C_s increasing with increasing r not like the expressions of Scapple and Engan. If equation 20 is used with β= α, the value of C_s passes through a maximum at r≈0.5. The three different expressions for C_s gives similar results only for r ≥ 0.85, and only then if the far-edge distance assumption is made. Since the capacitance of a parallel plate capacitor is proportional to the area over the separation, Auld and Kino's expression with β = α probably gives the most realistic values.

Recently, Endres and Drost[100] have used equation 17 with a modification of equation 20 to account for a third medium between the fingers of an interdigital capacitor (Figure 2.9(a)) with capacitance

$$C_3 = \epsilon_0\epsilon_3(\frac{h}{a}) \qquad\qquad (22)$$

where e_3 is the relative dielectric constant of the medium and h is the finger height so that

$$C_T = (N\text{-}1)(C_3 + C_S)W \qquad\qquad (23)$$

Combining equation 23 with equations 20, 21, and 22 allows us to calculate the capacitance of a single IDT. In the case of a semi infinite medium contacting the IDT and filling the gaps between the fingers the effect on C_T can be large. The effect is obviously much smaller when the medium only fills the region between the fingers (with gas or a vacuum above this) but can still be significant, especially for highly polar substances.

2.7.2 Capacitance Effects and Sensor Response

David C Stone et. al.[39] studied that circuit capacitance can have a powerful effect on SAW sensor response and stability. Comparison of the total capacitance (C_T) values for a single IDT coated with different materials with the range of added capacitance values strongly suggests that coating the IDTs of a SAW device with a film or liquid layer will change the net circuit capacitance and so control sensor response.

It is important to realize that when the IDTs are coated with a polymeric film or exposed to adsorbing sample vapors, it is not just the acoustic propagation velocity that is perturbed; the whole oscillator circuit is also being modified to some extent as C_T is varied through addition of a dielectric medium over the transducer fingers. It is rather possible that this could seriously affect SAW sensor response and stability, In particular if tuning and impedance matching components are present in the Circuit.

In general terms, smaller capacitances have a greater effect at higher frequencies so it might be expected that capacitance effects will be more important for higher frequency devices. It also seems reasonable that if impedance matching and tuning components are used in practical SAW oscillator circuits, it will be necessary to take into account the effect of any high dielectric films used in chemical sensing applications. C_T values could however be determined experimentally at the desired operating frequencies by forming the IDTs on a nonpiezoelectric substrate having the same dielectric constant as the piezoelectric substrate to be used. Combined with careful consideration of the measurement circuit or experimental characterization through impedance analysis, this would allow such evaluations to be performed [95].

2.8 Advanced SAW-based Gas Sensors

Surface acoustic wave gas sensors are very famous because of their notable sensitivity which is due to changes in the boundary conditions for the propagating wave, given by the interaction of sensitive material with target gas molecules. This noticeable sensitivity results from the simple fact that most of the wave energy is concentrated near the crystal surface within 1 or 2 wavelengths. Consequently, the surface wave is in its first approximation highly sensitive to any changes of the physical or chemical properties of the thin sensing layer deposited on the crystal surface. As long as the thickness of the sensing material, h, is substantially less than the surface wave wavelength, λ, one can claim a perturbation of the Rayleigh wave. Otherwise, one can take into account other types of waves, such as Love waves, which can propagate in layered structures [101].

The fundamental nature of gas sensors can be presented in the form of three basic type's couplings; we can differentiate the first coupling between gas molecules and sensing element parameters, which is the essential from the sensor point of view. The next is between sensing element parameters and the detection hardware. Here, the important fact is the t detection system must "sense" the slight changes of the sensing element parameters. The third coupling depends on signal analysis and conversion to gas concentration. Figure 2.10 shows the three fundamental couplings in SAW based gas sensors.
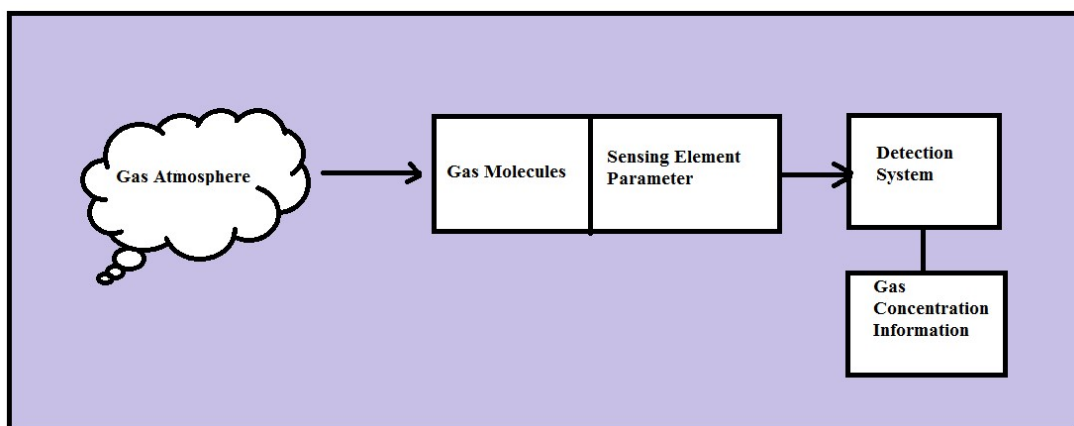
Fig. 2.10 Basic coupling in SAW gas sensors

In case of the SAW based gas sensors the second coupling is indirect. One can observe the changes of the sensing elements parameters as a result of SAW wave velocity and/or wave attenuation change. According to the above mentioned 3 basic couplings, there are 3 main directions of evolution using SAW based gas sensors. The 1st direction is concerned with improvement of the 1st coupling, same as new sensor materials of the sensing elements. For   example cyclodextrin for organic vapors made by self assembled minelayers (SAM) and sol–gel technology [102]. It is reported that metal ion/cryptand-22 complex like Ag(I)/cryptand-22 are very good cover for alkene and alkyne detection [103]. The UV cross linked polysiloxanes with different side group addition for organic vapors detection [104]. The rf sputtered InOx and PECVD SiNx films for H_2 and O_3 detection at different operating temperatures [105]. Other than these, carbon nanotubes (CNTs) have been used for carbon dioxide [106] and organic vapors sensing as well [107]. Later a modified diamond nanoparticles were used as coatings for volatile chemicals detection [108]. The 2nd coupling improvement is connected with modification in sensor parameters and the influence on the velocity and attenuation (insertion loss) of the SAW. Here we can differentiate between multi-strip couplers suppressing bulk acoustic waves [109], single phase unidirectional transducer (SPUDT) is applicable in SAW sensors improving the wave excitation [110], and layered sensor structures enabling acoustoelectric interactions based on the conductivity effect are described further. The 3rd coupling depends on SAW sensor signal analysis and conversion to corresponding gas concentration. Here one can implement most suitable methods such as artificial neural analysis or pattern recognition.

2.8.1 Layered sensor structures

In SAW-based gas sensors, mainly the single sensor structures were used to detect specific gas concentrations [29]. The example is a single ZnO film, can be used for ammonia molecules detection [30]. The layered sensor structures (like

bilayer of semiconductor and metal) on a piezoelectric substrate, creates new possibilities for detecting gas molecules in a SAW sensor system. Such a structure has its resultant electrical conductivity much better fitted to the high sensitivity range the "Semiconductor+metal" region in Fig. 2.11. Consequently, one can use an acoustoelectric coupling between the surface wave and the sensor structure in a high sensitivity region (Fig. 2.11). In a layered sensor structure we can use the much stronger acoustoelectric effect in the SAW sensor system as the main detection mechanism [13]. This effect can be many times greater than the mass effect, which can be dominant in non-conductive polymer films and simple metal and dielectric films in SAW-based gas sensor systems [87].
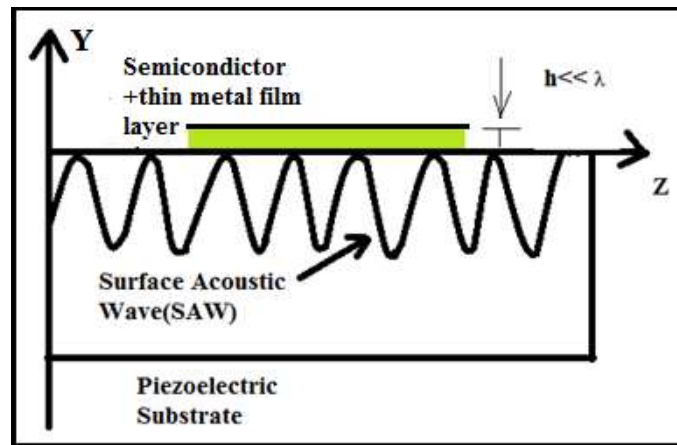
Fig.2.11 SAW device with nanostructure layer (metal + semiconductor)

2.8.2 Sensor Response Measurement

Figure 2.12 shows a block diagram of a measurement scheme that can be used in measuring the characteristics of SAW sensor. The IDTs can be excited using network analyzer and from the scattering parameter of the device one can characterize the SAW senor. The measurement of the experimental part of the thesis is entirely done using network analyzer (E5062A)[79]. A recording device or a computer can be interfaced with the network analyzer to record the output. Other than this oscillator and a frequency counter can also be employed for SAW device response measurement.
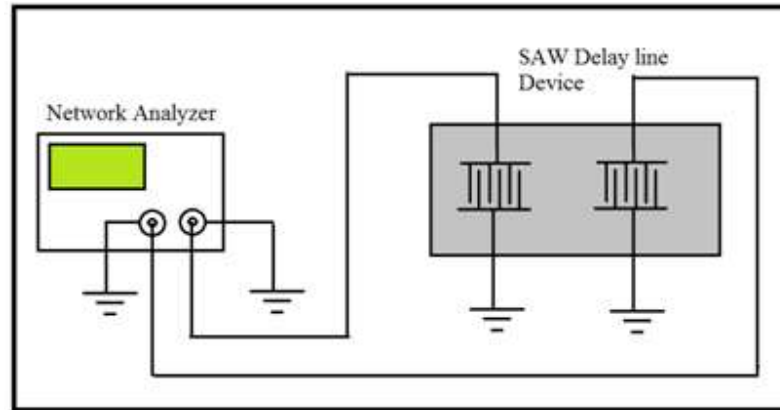
Fig. 2.12 Setup for measuring SAW sensor Characteristics using network analyzer [79]

2.9 SAW Sensor Applications

There are several reports in literature on SAW sensors to detect chemicals, gases, vapors, temperature, voltage, liquids, biomolecules, force, pressure etc. All these sensors works on the principles of change in SAW properties due to perturbation in the SAW path caused by the measurand. There are several reports on SAW gas sensors working on the principle of mass loading effect, for example as reported by Lokesh Rana et. al. the NO_2 gas sensor using ZnO thin film is the one of the good examples of mass loading based SAW sensor[110] in 2017. In this case the sensing film is coated over its acoustic path. It's reported that in the presence of NO_2 the ZnO film material density decreases and Young's modulus increases. Further, the volume of the film increases due to the addition of NO_2 molecules to the film [111]. These changes in sensing film properties introduce mass loading to the SAW device and hence changes the SAW properties and corresponding NO_2 concentration is measured. Table 4 shows list of various SAW sensors reported in last three decades. The table also shows the type of wave, principle of operation, sensing medium used, measurand and reference.

Table 2.3. List of selected reports of SAW sensors used in various sensing applications

Sr. No.	Type of acoustic wave	Principle	Sensing medium	Measurand	Reference and year
1	Rayleigh	Strain	No medium	Pressure	Reeder et. al.[112]1975
2	Rayleigh	Mass loading	Dow corning 970V vacuum grease,squalane,Apiezon L vacuum grease, di-n- decyl phthalate , and Carbowax 20 M.	Vapour pressure	Wohltjen et. al.[113] 1979
3	Rayleigh	Mass loading	Palladium thin film	Hydrogen	Amico et. al.[111] 1982
4	Rayleigh	Voltage/strain	Metal coating	Voltage	Gatti et. al.[114] 1983
5	Rayleigh	Conductivity change	lead Pathalocya-nine film	Nitrogen di oxide	Ricco et.al. [4] 1985
6	Rayleigh	Mass loading	Platinum thin film	Ammonia	Amico et. al.[3] 1987

Sr. No.	Type of acoustic wave	Principle	Sensing medium	Measurand	Reference and year
7	Flexural plate mode (FPM)	Mass loading	Zinc oxide and siliconnitride films	Vapors of tolunes, trichloethane,and carbon tetrachloride	Wemnzel et.al. [5] 1989
8	Rayleigh	Conductivity charge	Tungusten oxide film	Hydrogen sulphide	Falconer et. al.[6] 1990
9	Rayleigh	Mass loading	Polymer	Methanol in fuel	J. Retchert et. al .[7] 1993
10	Rayleigh	Mass loading	Polyisobutane (PIB) film	CCl_4	Pfelfer et. al. [115] 1994
11	SH Wave	Conductuuty change	Urease enzyme	Urea content in blood	Kondoh et. al. [116] 1994
12	Rayleigh	Conductivity change	Copper Pathalocyanine	NO_2	Beck et. al. [38] 1999
13	SH - wave	Mass loading	Antibody	Biochemical's	Josse et. al. [36] 2001

Sr. No.	Type of acoustic wave	Principle	Sensing medium	Measurand	Reference and year
14	Rayleigh	Mass laoding	Antibody	Uranine vapor , Alexa vapor(Electronic nose)	Stubbs et. al. [37] 2002
15	SH-wave	Conductivity change ,Viscosity change	No medium	Milk, orange Juices, and water (Smart Tonuge)	Cole et. al. [117] 2004
16	Rayleigh	Voltage / strain	No medium	Strain/pressure	Jiang et. al. [118] 2005
17	Rayleigh	Mass loading/ conductivity	Chemical warefare agents	Various polymers	Joo et. al. [119] 2007
18	Rayleigh	Mass loading and condutivity change	Graphene sheet	CO and H_2	Arsat et. al. [120] 2009
19	Rayleigh	Mass loading	PNVP film	Ammonia	Yi-Tian Li et. a;. [121] 2011

Sr. No.	Type of acoustic wave	Principle	Sensing medium	Measurand	Reference and year
20	Rayleigh	Elastic loading ,mass loading	ZnO thin film	Liquor ammonia	V. Bhaskar Raj et. al. [122]2012
21	Rayleigh	Elastic loading	ZnO thin film	DMMP(Dimethyl methylphos phonate)	Raj et. al.[123]2015
22	Rayleigh	Mass laoding	ZnO thin film	NO_2	Lokesh Rana et. al.[110] 2017

2.10 Conclusion

The literature study in the beginning covers various aspects of SAW devices that include the well known phenomenon "piezoelectric effect" which is the backbone of all SAW devices. The different types of SAW devices such as Rayleigh SAW, Shear horizontal-SAW (SH-SAW), Love wave SAW, Lamb Wave SAW, etc. are briefly reviewed in the form of table content highlighting their suitability for gas and liquid sensing. The details of SAW device design along with their different configurations are emphasized. Various way of SAW generation such as wedge transducer, IDTs and edge transducer are available, among these the IDTs are very famous due to their ease of fabrication. Different factors perturbs the SAW wave during gas and vapor sensing these are temperature, pressure, stiffness of film, mass loading and conductivity.

Many SAW chemical and biosensors have been developed by various researchers including mass loading and acoustoelectric effects due to deposition of sensing

layers suitable for different gases and vapor detection. Mass loading is applicable for non-conducting sensing layers, while acoustoelectric effect is applicable for conducting sensing layer. Acoustoelectric response effect gives larger sensing response in some cases as compared to mass loading effect. Few SAW based chemical sensors have been developed based on the viscoelastic properties of sensing layers with relatively large changes in viscosity from analyte interactions.

In gas sensing, the very important characteristics are sensitivity, selectivity, stability, repeatability and response time. The SAW device sensitivity depends on the type of piezoelectric substrate; the substrate with high electromechanical coupling capacitor increases the sensing response. The SAW device designed for high operating frequency also improves the sensitivity of the SAW sensor. The sensing layer which is thin and porous also contributes for increase in sensitivity. Taking these all factors in account we have proposed to develop a SAW sensor for gas sensing applications, with high sensitivity and better selectivity using highacoustic velocity, high coupling coefficient factor piezoelectric device and the suitable sensing materials for the target gases.

After considering all the above factors, development of SAW delay line sensor for gas sensing applications has been done. For designing high sensitivity and better selectivity SAW sensor, the high acoustic velocity, high electromechanical coupling coefficient factor piezoelectric substrate and the suitable sensing materials is used. The design, model simulation and development of SAW delay line sensor along with development of chemiresistor is discussed in next chapter

References

1] J.W. Garder, V. K. Varaden, and O.O.Awadelkarim, *Microsensors MEMS and Smart Devices,Chichester*, U.K. : John Wiley & Sons,2002.

[2] Grate J. W., Martin S. J. and White R. M., "Acoustic Wave Micro sensors-Part 1",Analytical Chemistry, Vol. 65, No. 21, pages 940A-948A, 1993.

[3]Ballantine Jr. D. S. and Wohltjen H., "Surface Acoustic Wave Devices for ChemicalAnalysis", Analytical Chemistry, Vol. 61, No. 11, pages 704A-712A, 1989.

[4] Calabrese G., Wohltjen H. and Roy M. K., "Surface Acoustic Wave Devices as chemical Sensors in Liquids. Evidence Disputing the Importance of Rayleigh Wave Attenuation", Analytical Chemistry, Vol. 59, pages 833-837,1987.

[5] D 'Amico A. and Verona E., "SAW Sensors", Sensors and Actuators, Vol. 17, pages55-66,1989.

[6]Atashbar M. Z. and Wlodarski W., "Design, Simulation and Fabrication of Doped TiCVCoated Surface Acoustic Wave Oxygen Sensor", Journal of Intelligent MaterialSystems and Structures, Vol. 8, pages 953-959, 1997.

[7] Varadan V. V., Roh Y. R. and Varadan V. K., "Local/Global SAW Sensors for Turbulence", Proceedings of the IEEE Ultrasonics Symposium, pages 591-594, 1989.

[8]Mc Cormack, Brian, Dermot Geraght, and Margaret O'Mahony."Design and Manufacture of Surface Acoustic Wave Sensors for Real-Time Weigh-in-Motion." *Instrumentation and Measurement Technology Conference* (2005). *IEEEXplore*. IEEE. Web. 6 Dec. 2010.

[9] Rodolfo Almar, Brian Lewis, And Edward G. **S.** Paig, "SAW interdigital Transducers with Harmonic Responses Insensitive to Variations in Finger Widths"IEEETransactions On Sonics And Ultrasonics, Vol. 30, No. 1, January 1983.

[10] Evan R. Hirst , Yong J. Yuan , W.L. Xu , J.E. Bronlund ," "Bond- Rupture Immunosensors—A Review." Biosensors and Bioelectronics 23 (2008): 1759-1768.

[11] Yoshida, H., H. Fujimori, T. Kaneko, S. Abe, and H. Morita. "Attenuation of Surface Acoustic Wave Through Sputtered Multi-Layered Nickel Films." *Journal De Physique* 49 (1988). *HAL*. Centre Pour La Communication Scientifique Directe. Web. 6 Dec. 2010.

[12] Chin, Matthew L. "A Fabrication Study of a Surface Acoustic Wave Device for Magnetic Field Detection." Thesis.Oregon State University, 2006. *Scholars Archive at OSU*.Oregon State University, 5 June 2006. Web. 5 Dec. 2010.

[13] Joachim W. Mrosk, Lothar Berger, Christoph Ettl, Hans-Jörg Fecht, G. Fischerauer, and A. Dommann," Materials Issues of SAW Sensors for High-Temperature Applications", Ieee Transactions On Industrial Electronics, Vol. 48, No. 2, April 2001.

[14]https://www.google.co.in/search?biw=1366&bih=664&tbm=isch&sa=1&ei=UR5WuoNorNvgSS9JwDA&q=SAW+wedge+transducer&oq=SAW+wedge+transducer&gs_l=psyab.3...4848.7392.0.8618.5.4.1.0.0.0.422.818.0j3j41.4.0....0...1c.1.64.psy-ab..0.0.0....0.Hft_cRZxys4#imgrc=RqE_IWTmWO1EiM.

[15]Didit Yudistira,1,a Sarah Benchabane,1 Davide Janner,1 and Valerio Pruneri," Surface acoustic wave generation in ZX cut-LiNbO$_3$ superlattices using coplanar electrodes", Applied Physics Letters 95, 052901 2009.

[16] Morgan D. P., "History o f SAW Devices", Proceedings of the IEEE International Frequency Control Symposium, pages 439-460, 1998.

[17] Reindl L., Scholl G., Ostertag T., Scherr H., W olff U. and Schmidt F., "Theory andApplication of Passive SAW Radio Transponders as Sensors", IEEE Transactions on Ultrasonics, Ferroelectrics and Frequency Control, Vol. 45, No. 5, pages 1281-1292,1998.

[18] D. Morgan , Surface Acoustic Wave with Applications to electronic Communication and Signal Processing, London, U.K.,: Elsevier,2007.

[19] Key-ya Hashimoto." Surface acoustic wave devices in telecommunications: modeling and simulation", Springer,,ISBN3-540-67232-X

[20] Campbell C. K., "Surface Acoustic Wave Devices for Mobile and Wireless Communications", Academic Press Inc., 1998.

[21]Jakubik, W.P.,"Surface acoustic wave-based gas sensors.", Thin Solid Films2011, *520*, 986–993.

[22]Ricco A. J., Martin S. J. and Zipperian T. E., "Surface Acoustic Wave Gas SensorsBased on Film Conductivity Changes", Sensors and Actuators, Vol. 8, pages319-333,1985.

[23]Hivert B., Hoummady M., Henrioud J. M. and Hauden D., "Feasibility of SAW Sensor Array Processing with Formal Neural-Networks", Sensors and Actuators B,18-19, pages 645-648, 1994.

[24] Grate J. W., Rose-Pehrsson S. L., Venezky D. L., Klusty M. and Wohltjen H., "smartSensor System for Trace Organophosphorus and Organosulfur Vapor Detection employing a Temperature-Controlled Array of Surface Acoustic Wave Sensors,Automated Sample Preconcentration and Pattern Recognition", Analytical Chemistry, Vol. 65, pages 1868-1881,1993.

[25]Hoummady M., Campitelli A. and Wlodarski W., "Acoustic Wave sensors: design,sensing mechanisms and applications", Smart Materials and Structures, Vol.6,pages647-657, 1997.

[26]Davide F. A. M. and D 'Amico A., "Pattern Recognition from Sensor Arrays:Theoretical Considerations", Sensors and Actuators A, Vol. 32, pages 507-518, 1992.

[27]Di Natale C., Davide F. A. M. and D 'Amico A.. "A Self-Organizing System for Pattern Classification: Time Varying Statistics and Sensor Drift Effects", Sensors and Actuators B, 26-27, pages 237-241, 1995.

[28]Hauden D., Jaillet G. and Coquerel R., "Temperature sensor using SAW delay line",Proceedings of the IEEE Ultrasonics Symposium, pages 148-151, 1981.

[29] Bao X. Q., Burkhard W., Varadan V. V. and Varadan V. K., "SAW temperature sensor and remote reading system", Proceedings of the IEEE Ultrasonics Symposium,pages 583-585, 1987.

[30] Talbi A., Sarry F., Le Brizoual L., Elmazria O. and Alnot P., "Development of SAWpressure sensor using ZnO/Si structure", Proceedings of the 2004 IEEE InternationalFrequency Control Symposium and Exposition, pages 566-570, 2004.

[31] Schimetta G., Dollinger F., Scholl G. and Weigel R., "Wireless Pressure and Temperature measurement using a SAW Hybrid sensor", Proceedings of the IEEE Ultrasonics Symposium, 2000.

[32] Vlassov Yu. N., Kozlov A. S., Pashchin N. S. and Yakovkin I. B., "Precision SAWPressure Sensors", Proceedings of the IEEE International Frequency Control Symposium,pages 665-669,1993.

[33]Buff W., Rusko M., Vandahl T., Goroll M. and Moller F., "A Differential Measurement SAW Device for Passive Remote Sensoring", Proceedings of the IEEEUltrasonics Symposium, pages 343-346, 1996.

[34]Haueis R., Vellekoop M. J., Kovacs G., Lubking G. W. and Venema A., "A Love Wave Based Oscillator for Sensing in Liquids", Proceedings of the Fifth International Meeting of Chemical Sensors, Vol. 1, pages 126-129, 1994

[35] Gizeli E., Goddard N. J., Lowe C. R. and Stevenson A. C., "A Love Plate BiosensorUtilising a Polymer Layer", Sensors and Actuators A, Vol. 6, pages 131-137, 1992.

[36] [20] Ricco A. J. and Martin S. J., "Acoustic Wave Viscosity Sensor", Applied PhysicsLetters, Vol. 50, No. 21, pages 1474-1476,1987.

[37] Hoummady M. and Bastien F., "Acoustic Wave Viscometer", Review of ScientificInstruments, Vol. 62, No. 8, pages 1999-2003,1991

[38] Campitelli A. P., Wlodarski W. and Hoummady M., "Identification of Natural Spring Water Using Shear Horizontal SAW based Sensors", Sensors and Actuators B., Vol. 49, No. 3, pages 195-201,1998.

[39] David C. Stone and Michael Thompson,, "Interdigital Capacitance and Surface Acoustic Wave Sensors",Anal. Chem. 1993, 65, 352-362

[40] David C. Stone and Michael Thompson,, "Interdigital Capacitance and Surface Acoustic Wave Sensors",Anal. Chem. 1993, 65, 352-362.

[41]Wohltjen, H. Sensors. Actuators 1984, 5, 307-325.

[42] Wohltjen, H.; Snow, A. W.; Barger, W. R.; Ballantine, D. S. IEEE Trans. Ultrasonic. Ferroelectric . Freq. Control 1987, UFFC-34, 172-178. [Cross reference].

[43]Grate, J. W.; Klusty, M.; McGill, R. A.; Abraham, M. H.; Whiting [cross reference]

[44] Frye, G. C.; Martin, S. J.; Ricco, A. J. Sens. Mater. 1989,1, 335-357.[cross reference]

[45] Frye, G. C.; Martin, S. J.; Ricco, A. J. Sens. Mater. 1989,1, 335-357. .[cross reference]

[46] Grate, J. W.; Klusty, M.; McGill, R. A.; Abraham, M. H.; Whiting, G.; Andonian-Haftvan, J. Anal. Chem. 1992, 64, 610-624.

[47]) Baer, R. L. and Flory, C. A. Some Limitations on the use of Leaky SAW Mode Sensors in Liquids. Presented at the IEEE Ultrasonics Symposium, Lake Buena Vista, FL, December 1991. .[cross reference]

[48] Alder, R. IEEE Trans. Sonics Ultrasonics. 1971, SU-18, 115-118. .[cross reference]

[49] Martin, S. J.; Frye, G. C.; Ricco, A. J.; Zipperian, T. E. IEEE Ultrason. Symp. Proc. 1987, IEEE Cat. No. 87CH2429-7, 1, 563-567. .[cross reference]

[50] Frye, G. C.; Ricco, A. J.; Martin, S. J.; Brinker, C. J. In Better Ceramics Through Chemistry III. Brinker, C. J., Clark, D. E., Ulrich, D.R., Eds.; Mat. Res. Soc. Symp. Proc. 1988, 121, 349-354. .[cross reference]

[51] Roederer, J. E.; Bastiaans, G. J. Anal. Chem. 1983,55,2333-2336.[cross reference].

[52] Calabrese, G. S.; Wohltjen, H.; Roy, M. K. Anal. Chem. 1987,59,833-837.[cross reference].

[53] Cheeke, J. D. N.; Morisseau, P. J. Low Temp. Phys. 1982, 46,319-330..

[54] Bryant, A.; Poirier, M.; Riley, G.; Lee, D.L.; Vetelino, J.F.," Gas detection using surface acoustic wave delay lines", Sensors. Actuator 1983, 4, 105–111.

[55]. Mujahid, A.; Dickert, F.L," SAW and Functional Polymers. In Gas Sensing Fundamentals", Kohl, C.-D.,Wagner, T., Eds.; Springer: Berlin/Heidelberg, Germany, 2014; pp. 213–245.

[56]Dorozhkin, L.M.; Rozanov, I.A.," Acoustic wave chemical sensors for gases",. J. Anal. Chem. 2001, 56, 399–416.

[57] Wohltjen, H.," Mechanism of Operation and Design Considerations for Surface Acoustic-Wave Device Vapor Sensors", Sensors. Actuator 1984, 5, 307–325.

[58] Ali, Z.; Pavey, K.; Robens, E.," Survey on mass determination with oscillating systems—Part III. Acoustic wave mass sensors for chemical and biological sensing",. J. Therm. Anal. Calorim. 2003, 71, 31–35.

[59] Dickert, F.L.; Forth, P.; Bulst, W.-E.; Fischerauer, G.; Knauer, U.."SAW devices-sensitivity enhancement in going from 80 MHz to 1 GHz",. Sens. Actuators B Chem. 1998, 46, 120–125. [

[60] Venema, A.; Nieuwkoop, E.; Vellekoop, M.J.; Nieuwenhuizen, M.S.; Barendsz, A.W., "Design aspects of saw gas sensors". Sensors. Actuators 1986, 10, 47–64.

[61] Afzal, A.; Iqbal, N.; Mujahid, A.; Schirhagl, R. ,"Advanced vapor recognition materials for selective and fast responsive surface acoustic wave sensors: A review". Anal. Chim. Acta 2013, 787, 36–49.

[62]Penza, M.; Antolini, F.; Antisari, M.V.,"Carbon nanotubes as SAW chemical sensors materials.", Sensors. Actuators B Chem. 2004,100, 47–59.

[63] Afzal, A.; Dickert, F.L.," Surface acoustic wave sensors for chemical applications.." Chem. Sensors. Compr. Sensors. Technol. 2011, 3, 447–484.

[64]Mujahid, A.; Dickert, F.L. SAW and Functional Polymers. In *Gas Sensing Fundamentals*; Kohl, C.-D.,Wagner, T., Eds.; Springer: Berlin/Heidelberg, Germany, 2014; pp. 213–245.

[65]Fisher, B.H.; Malocha, D.C.," Study of the acoustoelectric effect for SAW sensors.", IEEE Trans. Ultrason.Ferroelectr. Freq. Control 2010, 57, 698–706.

[66]Luo, W.; Fu, Q.; Zhou, D.; Deng, J.; Liu, H.; Yan, G.," A surface acoustic wave H2S gas sensor employing nanocrystalline SnO2 thin film.", Sensors. Actuators B Chem. 2013, 176, 746–752

[67]Liu, B.; Chen, X.; Cai, H.; Mohammad Ali, M.; Tian, X.; Tao, L.; Yang, Y.; Ren, T,". Surface acoustic wave devices for sensor applications.", Journal of Semiconductors. 2016, *37*, 021001.

[68] Tasaltin, C.; Ebeoglu, M.A.; Ozturk, Z.Z," Acoustoelectric Effect on the Responses of SAW Sensors Coated with Electrospun ZnO Nanostructured Thin Film.", Sensors2012, *12*, 12006–12015

[69]Wohltjen, H.; Dessy, R.," Surface Acoustic-Wave Probes for Chemical-Analysis.2. Gas-Chromatography Detector.:, Anal. Chem. 1979, *51*, 1465–1470

[70] Calabrese, G.S.; Wohltjen, H.; Roy, M.K. A Study of SAW Delay Line Behavior in Liquids. In Proceedings of the IEEE 1986 Ultrasonics Symposium, Williamsburg, VA, USA, 17–19 November 1986.

[71] Grate J. W., Wenzel S. W. and White R. M., "Flexural Plate Wave Devices for Chemical Analysis", Analytical Chemistry, Vol. 63, pages 1552-1561, 1991

[72] Nimal, A.T.; Mittal, U.; Singh, M.; Khaneja, M.; Kannan, G.K.; Kapoor, J.C.; Dubey, V.; Gutch, P.K.; Lal, G.;Vyas, K.D.; et al.,"Development of handheld SAW vapor sensors for explosives and CW agents",. Sensors. Actuators B Chem. 2009,135, 399–41.

[73] Hamidon, M.N.; Yunusa, Z,"Sensing Materials for Surface Acoustic Wave Chemical Sensors.", In Progresses in Chemical Sensor; Wang, W., Ed.; InTech: Rijeka, Croatia, 2016.

[74] Afzal, A.; Iqbal, N.; Mujahid, A.; Schirhagl, R.," Advanced vapor recognition materials for selective and fast responsive surface acoustic wave sensors: A review.", Anal. Chim. Acta 2013, 787, 36–49.

[75]Sayago, I.; Fernández, M.J.; Fontecha, J.L.; Horrillo, M.C.; Terrado, E.; Seral-Ascaso, A.; Muñoz, E. Carbon Nanotube-Based SAW Sensors. In Proceedings of the 2013 Spanish Conference on Electron Devices,Valladolid, Spain, 12–14 February2013;pp.127–130.

[76]. Asad, M.; Sheikhi, M.H. Surface acoustic wave based H2S gas sensors incorporating sensitive layers of single wall carbon nanotubes decorated with Cu nanoparticles. *Sens. Actuators B Chem.* 2014, *198*, 134–141.

[77]. Sayago, I.; Fernández, M.J.; Fontecha, J.L.; Horrillo, M.C.; Vera, C.; Obieta, I.; Bustero, I. New sensitive layers for surface acoustic wave gas sensors based on polymer and carbon nanotube composites. *Procedia Eng.*2011, *25*, 256–259

[78] Robinson, A.L.; Stavila, V.; Zeitler, T.R.; White, M.I.; Thornberg, S.M.; Greathouse, J.A.; Allendorf, M.D.Ultrasensitive Humidity Detection Using Metal–Organic Framework-Coated Microsensors. Anal. Chem. 2012, 84, 7043–7051.

[79] Joo, B.-S.; Huh, J.-S.; Lee, D.-D. Fabrication of polymer SAW sensor array to classify chemical warfare agents.Sens. Actuators B Chem. 2007, 121, 47–53.

[80] Raj, V.B.; Singh, H.; Nimal, A.T.; Tomar, M.; Sharma, M.U.; Gupta, V. Effect of metal oxide sensing layers on the distinct detection of ammonia using surface acoustic wave (SAW) sensors. Sens. Actuators B Chem. 2013,187, 563–573.

[81] Thomas, S.; Cole, M.; De Luca, A.; Torrisi, F.; Ferrari, A.C.; Udrea, F.; Gardner, J.W. Graphene-coated Rayleigh SAW Resonators for NO2 Detection. Procedia Eng. 2014, 87, 999–1002..

[82] Liu, X.; Cheng, S.; Liu, H.; Hu, S.; Zhang, D.; Ning, H. A Survey on Gas Sensing Technology. Sensors 2012, 12,9635.

[83] Ippolito, S.J.; Kandasamy, S.; Kalantar-Zadeh, K.; Wlodarski, W. Layered SAW hydrogen sensor with modified tungsten trioxide selective layer. Sens. Actuators B Chem. 2005, 108, 553–557.

[84] Giffney, T.J.; Ng, Y.H.; Aw, K.C. A Surface Acoustic Wave Ethanol Sensor with Zinc Oxide Nanorods.Smart Mater. Res. 2012, 2012, 1–4

[85] Sadek, A.Z.; Wlodarski,W.; Shin, K.; Kaner, R.B.; Kalantar-zadeh, K. A layered surface acoustic wave gas sensor based on a polyaniline/In2O3 nanofibre composite. Nanotechnology 2006, 17, 4488

[86] Venema, A.; Nieuwkoop, E.; Vellekoop, M.J.; Nieuwenhuizen, M.S.; Barendsz, A.W. Design aspects of saw gas sensors. Sens. Actuators 1986, 10, 47–64.

[87] Jakubik,W.P. Investigations of thin film structures of WO_3 and WO_3 with Pd for hydrogen detection in a surface acoustic wave sensor system. Thin Solid Films 2007, 515, 8345–8350.

[88] Jakubik,W.P.; Urba´ nczyk, M.W.; Kochowski, S.; Bodzenta, J. Bilayer structure for hydrogen detection in a surface acoustic wave sensor system. Sens. Actuators B Chem. 2002, 82, 265–271.

[89] McGill, R.A.; Chung, R.; Chrisey, D.B.; Dorsey, P.C.; Matthews, P.; Pique, A.; Mlsna, T.E.; Stepnowski, J.L.Performance optimization of surface acoustic wave chemical sensors. IEEE Trans. Ultrason. Ferroelectr. Freq. Control 1998, 45, 1370–1380.

[90] Pestov, D.; Guney-Altay, O.; Levit, N.; Tepper, G. Improving the stability of surface acoustic wave (SAW) chemical sensor coatings using photopolymerization. Sens. Actuators B Chem. 2007, 126, 557–561.

[91] Buff,W. SAW sensors. Sens. Actuators A Phys. 1992, 30, 117–121. [Cross Reference]

[92] Wang,W.; Lee, K.;Woo, I.; Park, I.; Yang, S.," Optimal design on SAWsensor for wireless pressure measurement based on reflective delay line", Sensors. Actuators A Phys. 2007, 139, 2–6.

[93] Caliendo, C.; Verardi, P.; Verona, E.; Amico, A.D.; Natale, C.D.; Saggio, G.; Serafini, M.; Paolesse, R.; Huq, S.E.Advances in SAW-based gas sensors. Smart Mater. Struct. 1997, 6, 689. [Cross Refernce].

[94] Xu, F.-Q.; Wang, W.; Xue, X.-F.; Hu, H.-L.; Liu, X.-L.; Pan, Y. Development of a Wireless and Passive SAW-Based Chemical Sensor for Organophosphorous Compound Detection. Sensors 2015, 15, 30187–30198.

[95] Jagannath Devkota , Paul R. Ohodnicki and David W. Greve,"SAW Sensors for Chemical Vapors and Gases",Sensors 2017, 17, 801; doi:10.3390/s17040801.

[96] Rebière, D.; Duchamp, G.; Pistré, J.; Hoummady, M.; Hauden, D.; Planade, R. Surface acoustic wave NO2 sensor: Influence of humidity. Sens. Actuators B Chem. **1993**, 14, 642–645. [Cross Ref].

 [97] Jasek, K.; Pasternak, M. Influence of Humidity on SAWSensor Response. Acta Phys. Polonica A **2013**, 124,448–450.

[98] Müller, C.; Nirmaier, T.; Rügemer, A.; Schickfus, M.V. Sensitive NO2 detection with surface acoustic wave devices using a cyclic measuring technique. Sens. Actuators B Chem. 2000, 68, 69–73. [CrossRef]

[99] Wen, C.; Zhu, C.; Ju, Y.; Xu, H.; Qiu, Y. A novel NO2 gas sensor using dual track SAW device. Sens. Actuators A Phys. 2010, 159, 168–173.

[100] Endres, H.-E.; Drost, S. Sens. Actuators B 1991, 4, 95-98.

[101] C.S. Kim, K. Yamanouchi, et al., Japan. J. Appl. Phys. 13 (1974) 24.

[102] DeQuan Li, Min Ma, Sens. Actuators B 69 (2000) 75[CrossRef].

[103] Hsu Hui Ping, J.S. Shih, Sens. Actuators B 114 (2006) 720[CrossRef].

[104] N. Barie, et al., Sens. Actuators B 46 (1998) 97[CrossRef].

[105] A. Fechete, et al., Sens. Actuators B 118 (2006) 362[CrossRef].

[106] S. Sivaramakrishnan, et al., Sens. Actuators B 132 (2008) 296[CrossRef].

[107] M. Penza, et al., Thin Solid Films 472 (2005) 246[CrossRef].

[108] E. Chevalier, et al. Sens. Actuators (2010) in print[CrossRef].

[109] Ch. Wen, et al., Sens. Actuators A 159 (2010)[CrossRef].

[110] Vellekoop M. J., Lubking G. W., Sarro P. M. and Venema A., "A Multi-Purpose SmartAcoustic Lamb Wave Sensor System", Proceedings of the Seventh InternationalConference on Solid-State Sensors and Actuators, Transducers'93, pages1052-1055,1993.

[111] Lucklum R., Behling C., Hauptmann P., Cemosek R.W. and Martin S.J., "ErrorAnalysis of Quartz Crystal Resonator Applications", Proceedings of the Ninth International Conference on Solid-State Sensors and Actuators, Transducers'97, pages1347-1350, 1997.

[112]ickert J., Weiss T. and Gopel W., "Self-Assembled Monolayers for Chemical Sensors: Molecular Recognition by Immobilised Supramolecular Structures", Sensorsand Actuators B, 31, pages 45-50, 1996.

[113] Rickert J., Weiss T., Kraas W., Jung G. and Gopel W., "A New Affinity Biosensor:

Self-Assembled Thiols as Selective Monolayer Coatings of Quartz Microbalances", Transducers'95-Eurosensors IX, pages 528-531, 1995.

 [114] Muramatsu H., Kajiwara K., Tamiya E. and Karube I., "Piezoelectric Immuno Sensor for the Detection of Candida albicans Microbes", Analytica Chemica Acta, 188, pages 257-261, 1986

[115]Kondoh J. and Shiokawa S., "Liquid Identification Using SH-SAW Sensors", Transducers'95-Eurosensors IX, pages 716-719, 1995.

[116] Kondoh J. and Shiokawa S., "A Liquid Sensor Based on a Shear Horizontal SAWDevice", Electronics and Communications in Japan, Part 2, Vol. 76, No. 2, pages 69-82,1993.

[117] Gardner J. W., Varadan V. K. and Awadelkarim 0 . 0 ., "Micro Sensors, MEMS andSmart Devices", John Wiley & Sons, England, 2001.

[118]Ricco A. J., Martin S. J., Frye G. C. and Niemczyk T. M., "Acoustic Plate ModeDevices as Liquid Phase Sensors", Proceedings of the IEEE Ultrasonics Symposium,pages 23-26, 1988

[119] Josse F. and Shana Z., "Acoustoionic Interaction of SH Surface Waves with DiluteIonic Solutions", IEEE Transactions on Ultrasonics, Ferroelectrics and FrequencyControl, Vol. 38, No. 3, pages 297-304,1991.

[120] Andie J. C., Weaver J. T., Vetelino J. F. and McAllister D. J., "Application of Unidirectional Transducers in Acoustic Plate Mode Biosensors", Proceedings of theIEEE Ultrasonics Symposium, pages 331-335, 1993.

[121] Dejous C., Savart M., Rebiere D. and Pistre J., "A Shear-Horizontal Acoustic Plate Mode (SH-APM) Sensor for Biological Media", Sensors and Actuators B, 26-27, pages 452-456,1995

[122]Schweyer M. G., Andie J. C., McAllister D. J. and Vetelino J. F., "An Acoustic Plate Mode Sensor for Acquous Mercury", Sensors and Actuators B, 35-36, pages 170-175,1996

[123] Lucklum R., Rosier S., Hartmann J. and Hauptmann P., "On-line Detection of Organic Pollutants in Water by Thickness Shear Mode Resonators", Sensors and Actuators B, 35- 36, pages 103-111, 1996.

CHAPTER 3

DESIGN, SIMULATION AND DEVELOPMENT OF SURFACE ACOUSTIC WAVE SENSORS

3.1 Introduction

In previous chapter we have discussed the theory of SAW including working principle, types of SAW device, configuration of SAW devices, factors affecting the performance of SAW devices and its use as gas sensor using polymer nanocomposite materials. On the basis of the theoretical study the design of the proposed SAW delay line device is explained here. After design the device is modeled and simulated using the MATLAB and COMSOL multiphysics software's. The SAW device fabrication is carried out using the conventional photolithography and simultaneously interdigital transducers (IDTs) using glass epoxy, fabricated for testing the performance of developed sensing materials. All these steps are explained in this chapter.

3.2 Design of SAW Devices

In SAW devices interdigital transducers (IDTs) are the backbone for their operation. The SAW generation and detection is the main job of IDTs, so their performance plays the vital role when SAW devices are operated for specific applications [1]. An optimum design of interdigital transducers (IDT) may take multiple iterations because the frequency, bandwidth and time response of the IDT are variables that are controlled by a number of factors: number of finger pairs, distance between input and output IDTs, aperture width, finger width, and spacing between adjacent fingers[2,3].

The most of the SAW devices are used for chemical and biosensing applications [4], where the two port configuration of SAW device is widely utilized. In this configuration one IDT act as transmitter and another as a receiver [5]. For two port device, two options are available one is the delay line device and the other is two port resonator [1, 6, 7]. We employed delay line devices for the present work. The schematic of this configuration is shown in figure 3.1
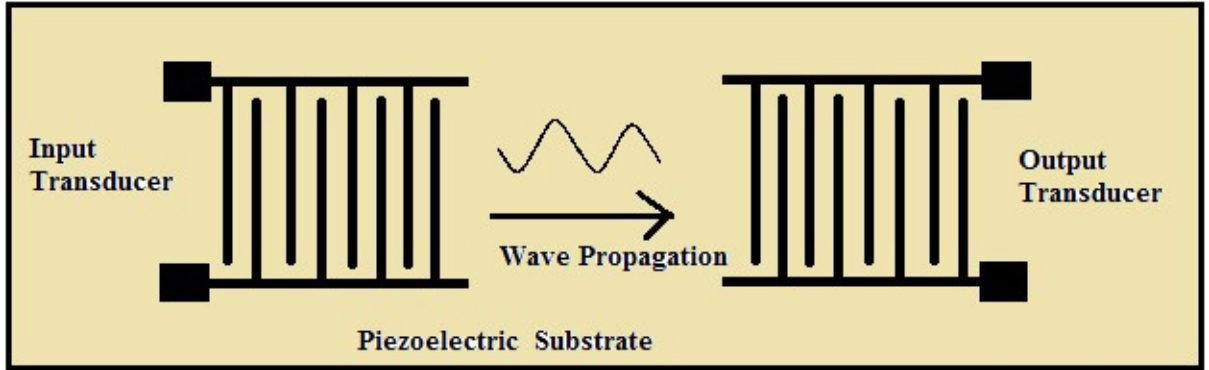
Fig.3.1 SAW delay line device

The SAW devices design starts with the important equation:

$$f_0 = \frac{v}{\lambda}$$
(1)

Where f₀ is the device resonant frequency, v is the acoustic velocity of the piezoelectric substrate used for SAW device, λ is the SAW wavelength which is equal to the IDT pitch (p).

The important parameter of a SAW delay line is the distance between IDT centers .To avoid direct electromagnetic coupling between the input and output IDTs should be separated by 100-300 acoustic wavelengths [2,6 7].

The simplest IDT configuration is a single split finger design with equal finger width and spacing.In this case the acoustic wavelength λ is given by:

$$\lambda = 4d$$
(2)

where d is the finger width. Since the SAW frequency is inversely proportional to the acoustic wavelength, operation at very high frequencies requires small finger width/spacing.However, fabrication becomes difficult when dimensions become too small due to the physical limitations of photolithography. To increase device sensitivity for measurand and surface perturbations and to decrease overall size, it is desirable to design and operate the device at a higher frequency [8, 9].To overcome this problem, more sophisticated transducer designs that are

unidirectional have been realized. Utilizing these unidirectional IDTs permits insertion loss (IL) to be decreased beyond the -6 dB limit.

Other important design parameters to consider are the number of finger pairs and IDT aperture length (finger overlapping), which determine the bandwidth of the frequency response and the impedance respectively [10]. Table 3.0 below lists the parameters for one design of SAW delay line device which is used for the present research work.

Table 3.1 SAW delay line parameters

Parameters	Value/s
Substrate	128^0 YX cut LiNbO$_3$
Acoustic Velocity	3992 m/s
Wavelength	360 µm
Resonant frequency	11.08 MHz
Number of finger pairs in both IDTs	10
Aperture length(30λ)	10.80 mm
IDT gap(12λ)	4 .32mm

For both the theoretical and experimental studies in this work, we utilized the simple split finger design. Though it is simple in structure there is one inherent problem; IDTs with this configuration are bi-directional and therefore generate SAWs in opposing directions. As a result,3 dB of loss will occur for each transducer because 50% of the power is directed away from the proposed direction. In other words, if no other loss mechanisms exist the insertion loss (IL) would be -6dB for a delay line SAW device.

There are various substrates that one can select from but the most common are quartz, lithium tantalate and lithium niobate. When choosing an appropriate substrate, factors such as the material's acoustic velocity, coupling coefficient (K^2), and temperature coefficient of frequency (TCF) are important [8]. However, if

sensing is taking place in a liquid medium the most important consideration is particle polarization. To avoid excessive dissipation of acoustic energy the particles must be polarized in the shear-horizontal (SH) direction. This requires a certain class of piezoelectric materials. 128^0 YX cut Lithium niobate was selected as a substrate due to its high electromechanical coupling coefficient, high acoustic wave velocity and to avail the benefits of strong acoustoelectric effect in sensor response [11]. Since the application is gas sensing, the Rayleigh SAW generated on this substrate are useful. Themost commonly used substrate materials used for SAW sensor application and their properties such as acoustic velocity, electromechancial coupling coefficient (K^2),substrate orientation are listed out in the appendix-A.

Some of the important criteria to be considered in fabricating the SAW devices for our research are as follows:

1. The IDT structures have been designed for the specified resonance frequency and 50 Ohm impedance. The SAW delay line devices with resonance frequency 11.08MHz are designed to use them for gas/vapor sensing application.

2. The size of the device is suitable for the gas sensing application.

3. Bond pad size is to be designed such that the wires can be bonded over them using silver paste.

4. The dimensions of delay line are decided such that it offers minimum attenuation to SAW and sufficient space should be left to apply to deposit the sensing film on the delay line part.

3.3 Modelling and Simulation

Computer models for SAW devices are continuously improved to meet the demanding design requirements for key components in sensor applications. This often leads to the increase in simplicity of the simulation codes and reduction in run time of the program. Several analytical and numerical modelling techniques are helpful to model the device characteristics before designing a device. The relationship between system parameters and device characteristics like impulse

and frequency response are more complicated. For determining the design parameters for a specific SAW sensor, several device characteristics are taken into consideration like size of the device (including IDT dimensions), device operating frequency, Impulse response, frequency response and Bandwidth of the devices etc[12]. Different models are available for modelling and simulation of SAW devices. The commonly used models are P matrix, coupling of model (COM) model, finite element method (FEM) model, cross field equivalent circuit model etc. P matrix model is basically combination of S (scattering) and Y (admittance) matrix [13].

3.3.1 Modelling of SAW delay line using Matlab

A first order model of a SAW Delay line has been created using MATLAB .The model implements the Impulse Response method to calculate the frequency response, impedance, and insertion loss. This is a first order model that does not take into account any second order effects such as reflections, however, it does model the piezoelectric, mechanical and electrical behaviors of the SAW device. This model is only valid for transducers where the IDTs are un-weighted (unapodized). The model assumes that the finger overlap or aperture is constant and that the metallization ratio between the fingers and spaces is 0.5. This model calculates the frequency response, conductance, susceptance, impedance, and other electrical parameters. The Impulse response method uses the Mason equivalent circuit shown in Figure 3.2. In the circuit Ga(f) is the radiation conductance, Ba(f) is the acoustic susceptance, and C_T is the total capacitance.
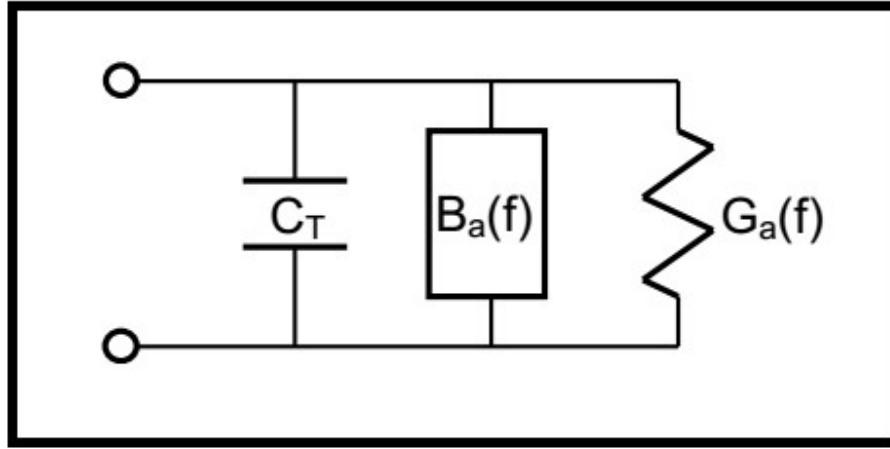
Fig.3.2 Mason Equivalent circuit model [21]

3.3.2 MATLAB Simulation results for equivalent circuit model

Figure 3.3 shows the acoustic susceptance, radiation conductance, and frequency response and insertion loss as a function of frequency for the SAW device with operating frequency at 11.08 MHz. Here the insertion loss and transfer function values are expressed in numeric form instead of dB values. The observed bandwidth from the simulation is 2MHz. Thus the simulated results were in good agreement with theoretical predications [21].
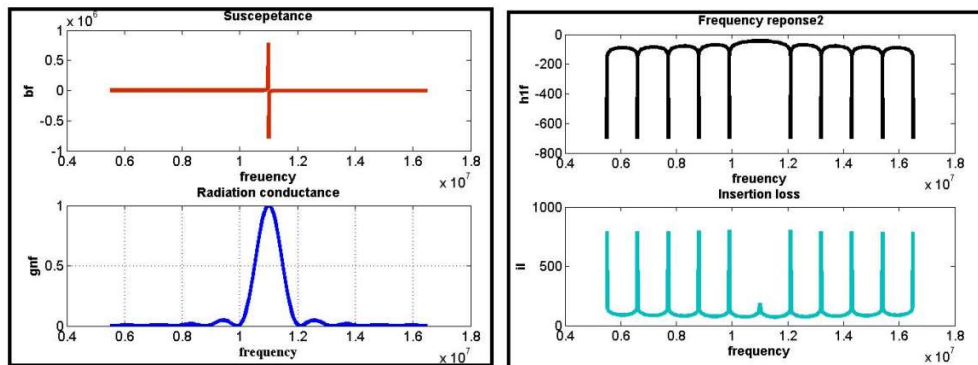
Fig.3.3 (a) Upper part shows the acoustic susceptance, lower part shows the radiation conductance, (b) Upper part shows frequency response, lower part shows the insertion loss

3.3.3 Transmission matrix modelling for the SAW delay line device

Figure 3.4 shows the schematic of the SAW delay line described in terms of the constituent matrices. The acoustic wave amplitudes at the left side of the input transducer can be written as

$$[U_0] = [M][I_3] + \begin{bmatrix} t_{13} \\ t_{23} \end{bmatrix} V_{in} + [K]V_{out} \tag{3}$$

Where $[M] = [t_1][D_2][t_3]$ and subscripts 1,2,3 refer to input IDT ,delay, and output IDT respectively, $[t] = \begin{bmatrix} t_{11} & t_{12} \\ t_{21} & t_{22} \end{bmatrix}$ and the matrix [D] is defined as

$$D = \begin{bmatrix} e^{j\beta d} & 0 \\ 0 & e^{-j\beta d} \end{bmatrix} \tag{4}$$

The matrix $[K] = [t_1][D_2] \begin{bmatrix} t_{13} \\ t_{23} \end{bmatrix}$ \tag{5}

The currents in input and output transducers can be written as

$$I_{in} = [P][U_3] + [L]V_{out} + (t_{33})V_{in} \tag{6}$$

$$I_{out} = [t_{31}, t_{32}]_3[U_3] + (t_{33})_3 V_{out} \tag{7}$$

Where[P] = [t₃₁ t₃₂]₁[D₂][T₃] and [L]= [t₃₁ t₃₂]₁[D₂]$\begin{bmatrix} t_{13} \\ t_{23} \end{bmatrix}_3$

Since no acoustic power incidenton the two acoustic ports U_0^+ =0 andU_0^-
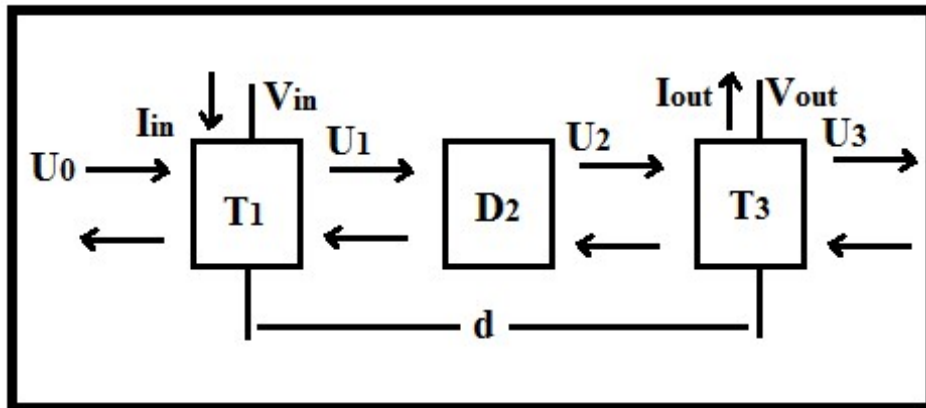
Fig. 3.4 SAW delay line building blocks

Using the above equations, the expressions for admittance or Y-parameters were first obtained and were used to determine the scattering or s-parameters. The Y parameters for a two-port network are defined as [14]:

$$\begin{bmatrix} I_{in} \\ I_{out} \end{bmatrix} = \begin{bmatrix} Y_{11} & Y_{12} \\ Y_{21} & Y_{22} \end{bmatrix} \begin{bmatrix} V_{in} \\ V_{out} \end{bmatrix} \tag{8}$$

$$Y_{11} = \frac{I_{in}}{V_{in}} \mid \text{Vout} = 0 \tag{9}$$

Substituting V_{out}=0 in equation (3) we, get

$$\begin{bmatrix} 0 \\ U_0^- \end{bmatrix} = [M] \begin{bmatrix} U_3^+ \\ 0 \end{bmatrix} + \begin{bmatrix} t_{13} \\ t_{23} \end{bmatrix}_1 V_{in} \tag{10}$$

From this we can get $U_3^+ = -\frac{t_{131}}{M_{11}} V_{in}$

Substituting $V_{out} = 0$ in equation (6), we get

$$I_{in} = [P] \begin{bmatrix} U_0^+ \\ 0 \end{bmatrix} + (t_{33})_1 V_{in} \tag{11}$$

Substituting the expression for $U_3^+ = 0$ in equation (7), we obtain

$$I_{in} = -\frac{P_{11} t_{131}}{M_{11}} V_{in} + t_{331} . V_{in} \tag{12}$$

Combining equation (9) and (12), we get

$$Y_{11} = -\frac{P_{11} t_{131}}{M_{11}} + t_{331} \tag{13}$$

Using similar procedure, the other Y parameters were obtained by substituting boundary
Conditions in Equation (3), Equation (4) and Equation (5).

The Y-parameters for the SAW delay line were then determined as illustrated below:

$$Y_{21} = \frac{I_{out}}{V_{in}} \mid V_{out} = 0 = -\frac{t_{313} t_{131}}{M_{11}} \tag{14}$$

$$Y_{12} = \frac{I_{in}}{V_{out}} \bigg| V_{in} = 0 = -\frac{P_{11}K_{11}}{M_{11}} + L_{11} \qquad (15)$$

$$Y_{22} = \frac{I_{out}}{V_{out}} \bigg| V_{in} = 0 = -\frac{t_{313}K_{11}}{M_{11}} + t_{333} \qquad (16)$$

By knowing the expressions for Y- parameters, the expressions for S- parameters can be easily obtained

3.3.4 MATLAB simulation results for transmission matrix method
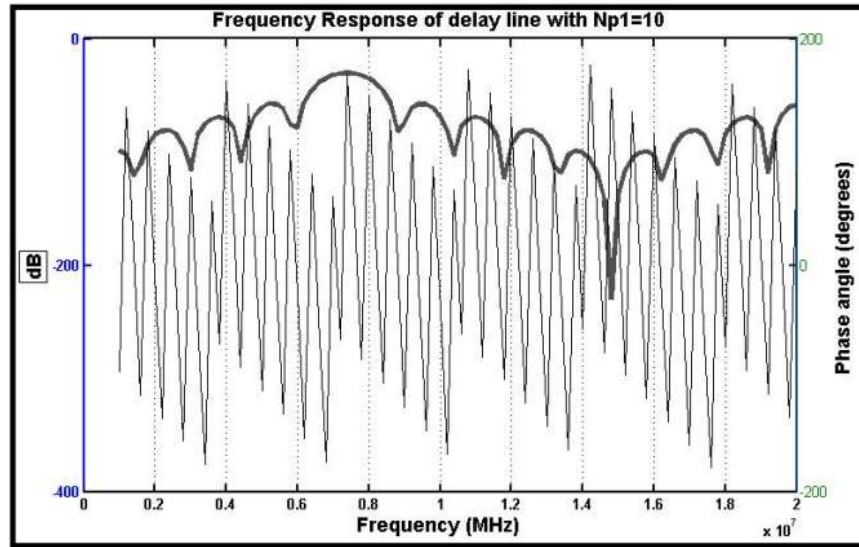
Fig. 3.5 (a) Frequency and phase response of SAW device
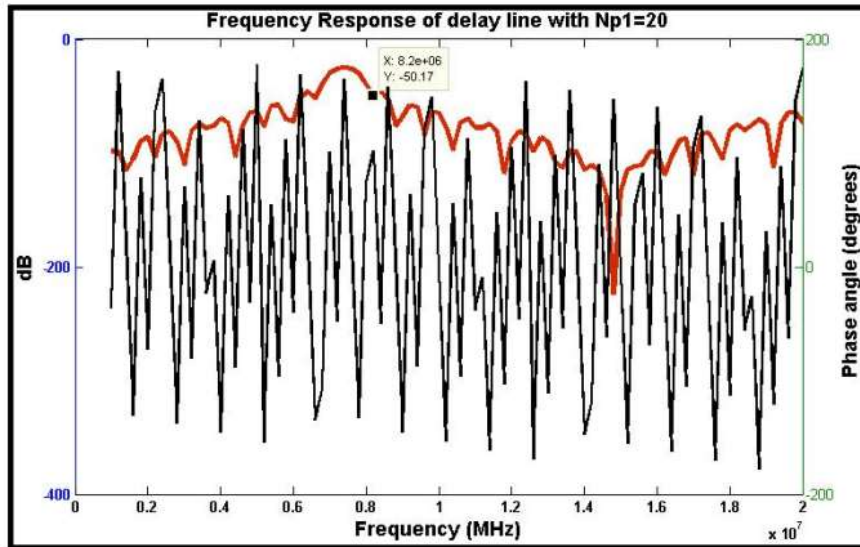
Fig.3.5 (b) Frequency and phase response of SAW device operating at 6.66 MHz with Np1 =10Operating at 6.66 MHz with Np1 =20.
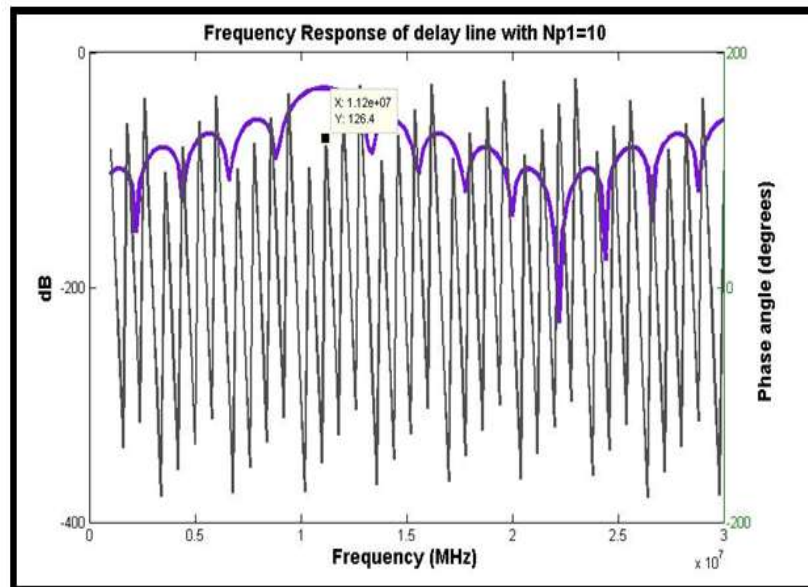
Fig.3.6 (a) Frequency and phase response of SAW device
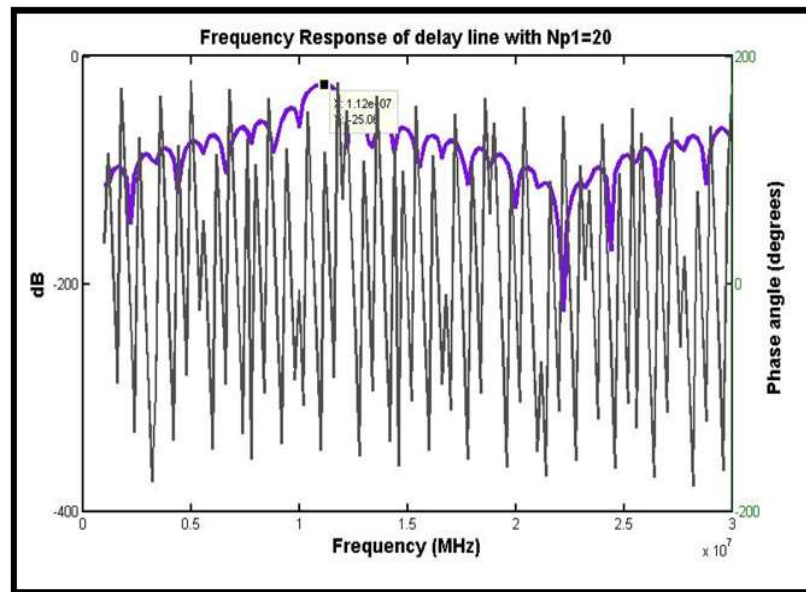
Fig.3.6 (b) Frequency and phase response of SAW device operating at 11.08 MHz with Np1 =10. Operating at 11.08 MHz with Np1 =20.

(a)   (b)

(c)

(d)
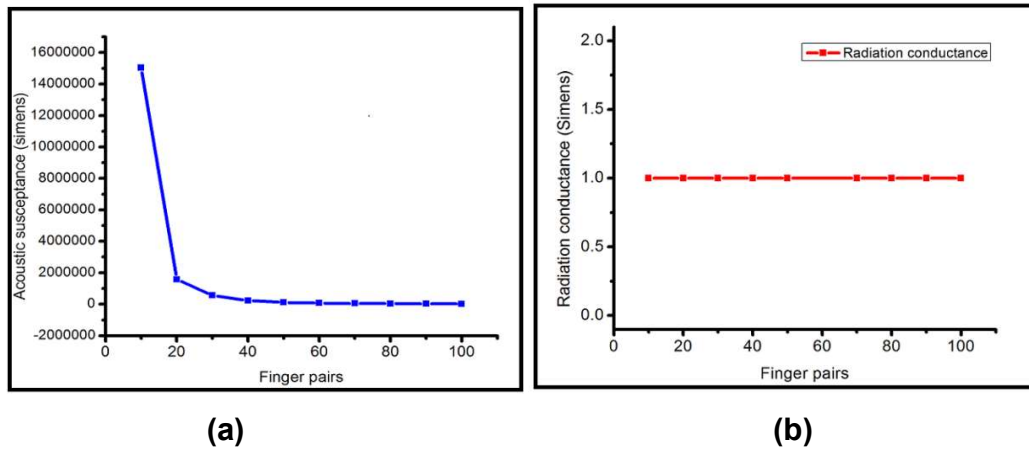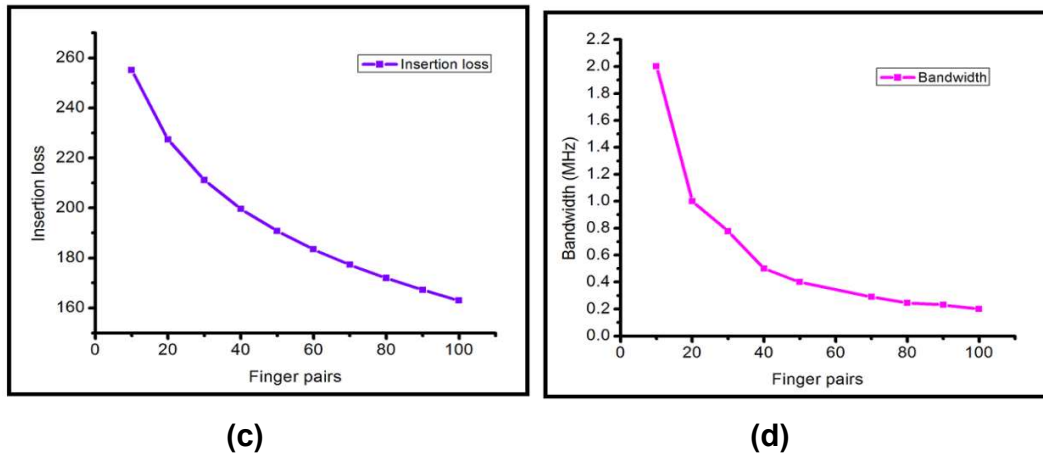
Fig. 3.7 Effect of finger pair change on (a) acoustic susceptance (b) Radiation conductance (c) Insertion loss (d) Bandwidth of SAW device.

(a)

(b)

(c)

(d)
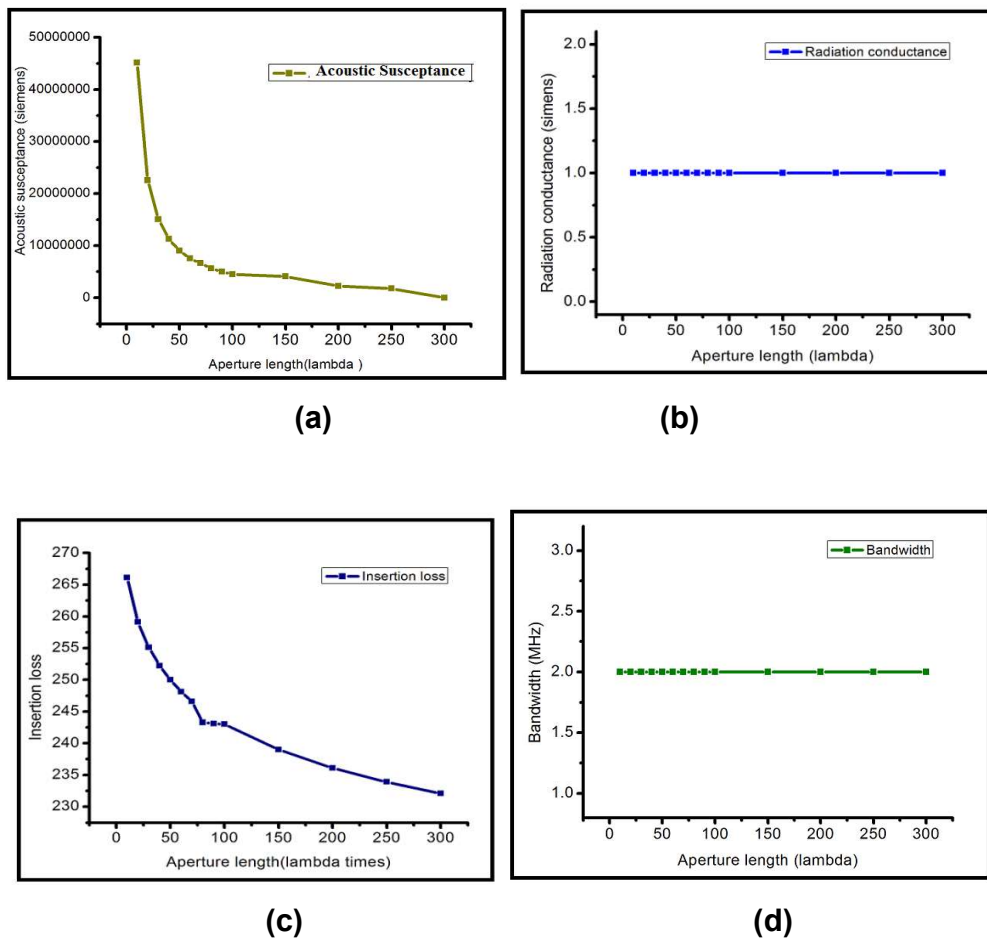
Fig.3.8 Effect of aperture length change on (a) acoustic susceptance (b) Radiation conductance (c) Insertion loss (d) Bandwidth of SAW device.

(a)

(b)

(c)

(d)
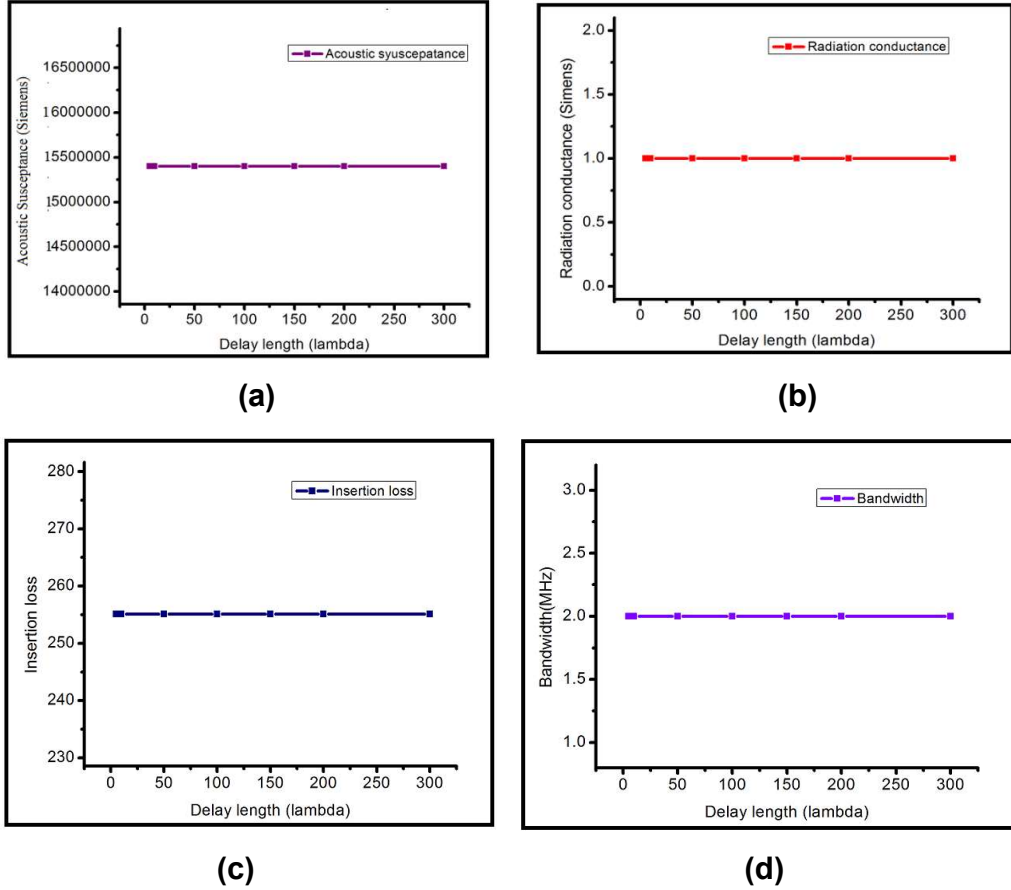
Fig. 3.9 Effect of Delay length change on (a) acoustic susceptance (b) Radiation conductance (c) Insertion loss (d) Bandwidth of SAW device.

Different SAW device designs were simulated using the transmission matrix method in MATLAB 11. Figure 3.5, 3.6   shows the magnitude and phase of S12 of a SAW delay line with resonance frequencies 6.66 MHz and 11.08 MHz respectively the other specifications are as follows:

128^0 YX cut $LiNbO_3$ as a piezoelectric substrate with acoustic velocity=3992 m/s, electromechancial coupling capacitance =5.6 %, the number of finger pairs in input and output IDTs =10, the aperture length= 30λ, the IDT separation = 12λ. Capacitance per finger pair =5 pF/cm. The ripples in the frequency response may

be due to reflection between fingers and mismatch of source and load impedance used in simulation [14,15]. The ripples in passband could be due to the triple transit interference (TTI) and electromagnetic interference (EMI). The presences of sidelobes levels are due to the fact the apodization is not implemented in IDTs to suppress the sidelobes. The bandwidth (BW) between the first nulls on either side of the center frequency depends on the number of finger pairs in the input IDT, which is expressed as [8],

Bandwidth (BW) $=\frac{2f_o}{N}$ (17)

Where f_o is the resonance frequency of the SAW device and N is the number of finger pairs in both the IDTs. Thus as the number of finger pairs decreases the bandwidth increases. From figures 3.5(a)-(b) and 3.6(a)-(b) shows the frequency responses of two different delay line devices having all parameters same except the number of finger pairs in the input transducers. Here the bandwidths are different for both the designs due to variation in finger pairs in the devices. In these figures the phase response of the SAW devices is also shown. The phase variation also occurs with change in number of finger pairs. In this simulation we also studied the effect of change in finger pairs, aperture length (finger overlap) and delay line (or delay) length on acoustic susceptance, radiation conductance, insertion loss and bandwidth of the device. Figure 3.7, 3.8and 3.9 shows the results of the same. From the results it is found that:

1. The acoustic susceptance decreases with increase in finger pairs and aperture length but there is no effect of change in delay line length on it.

2. There is no effect of change in finger pairs, aperture length and delay line length on radiation conductance.

3. Insertion loss decreases with increase in aperture length and number of finger pair.

4. Bandwidth decreases as the number of pairs increases.

5. It is also found that the insertion loss decreases after delay line length of 300λ.

3.3.4 Finite Element Method (FEM)

The FEM is used almost in every discipline of science and engineering, for example in the areas of stress/strain analysis of solid substrate, fluid dynamics, multibody dynamics module, MEMS module etc [14]. FEM is used to get a 3D view for SAW delay line and explain some results that cannot be explained by impulse response model, matrix model [15, 16]. Only few basic procedures and techniques use in FEM are presented here.

3.3.4.1 Input and output information in FEM

In the FEM, following input information about the structure and material are to be provided,

1. Profile of the structure geometry
2. Suitable coordinate systems according to the geometry in two dimensional and three dimensional systems.
3. Properties of the materials used in the model.
4. Boundary conditions to the boundaries of the structure are to be provided.

The problem domain is to be discretized into smaller regions called elements which are connected at specific points called node. The elements created may be two or three dimensional and can be of any shape such as triangular, quadrilateral, tetrahedral or brick shape depending on the dimensionality. The output information in this case of stress /strain analysis in piezoelectric material involves nodal and elemental information. The solution to the primary unknown quantities, the displacements in all directions and the determined at modes and these are known as degree of freedom.

3.3.4.2 Finite element formulation

This process starts with dividing a scale into an assembly of elements interconnected at nodes. Figure 3.10 shows this idea.
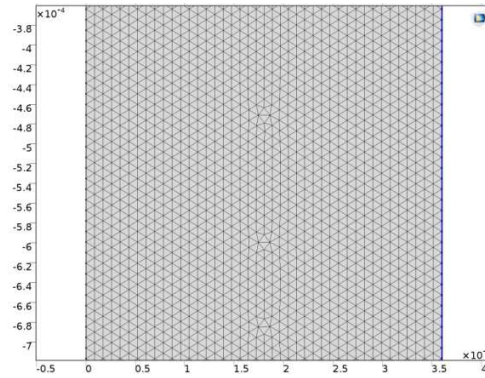
Fig. 3.10 Illustration of solid body discretized into finite number of elements.

It can be seen that after discretization, the original curved boundaries are approximated by straight edges of the elements of the boundary. The primary unknown quantities for the case of stress/strain analysis of piezoelectric material are the displacement u(r, t) and voltage v(r, t) where r denotes position vector and t denotes time. This position vector represents the spatial coordinates (x_1, x_2, x_3) or cylindrical polar coordinates (r, z) for an axis symmetric solid. The continuity of the solution is taken care, by the introduction of shape functions or interpolation functions. The selection of these functions determines how the field varies across a single element domain. Generally, a polynomial function is chosen as a shape function and the number of nodes assigned to a particular element defines the order of the polynomial. The mathematical expression for discretization can be expressed as:

u(r, t) = [N(r)]{u}   (18)

where [N(r)] is the interpolation function and the vector {u} is the corresponding nodal displacement components. The values of primary unknown quantities at the nodes of an element can be related to the applied nodal loads as $\{K_e\}\{u\} = \{Q_e\}$ where, $\{K_e\}$ is the element coefficient matrix,$\{ Q_e\}$ is the applied load, in case of stress/strain analysis of piezoelectric material the applied loads are force and applied electric potential. A system of equations in terms of unknown nodal values is formulated for that element and subsequentially for the complete domain. This system of equations can be solved by suitable numerical techniques. In the present

thesis work numerical techniques used in commercial FEM software COMSOL Multiphysics were used to for solving the system of equations.

3.3.5 SAW device Simulation using FEM

FEM simulations of SAW devices have been reported by other researchers are discussed here. Yi-Gui Zhao et.al.[5] have followed A finite element method (FEM) simulation approach of surface acoustic wave (SAW) organic vapor sensors. The effects of the polymer coating on the propagation characteristics of the SAW were studied by FEM modeling in the absence and presence of vapor. They computed the sensitivities for each vapor-coating combination. Comparisons of the simulation sensitivities of SAW vapor sensors with the experimental values reported by Edward T. Zellers and co-workers confirm the general validity of the approach. The approach is expected to select polymer, which offers the best sensitivity for particular vapor.In2010 C.G. Bostan et al.[2] used FEM model to simulate SAW gas sensors with polymer layers.By solving the damped eigenvalue problem they have calculated the sensor response in terms of frequency and attenuation shifts with vapor concentration. The correlated the simulated results with the experimental values.N. Ramakrishnana et al.[8] studied a 2D-finite FEM simulation of SAW delay line model using COMSOL Multiphysics. They have modeled a Rayleigh wave type SAW device choosing YZ - Lithium Niobate as the substrate. The major contribution of this work is the application of periodic boundaries to the transmitter interdigital transducer (IDT) to reduce the number of degrees of freedom of a SAW delay line model solution. Accordingly the computation complexity and memory usage of the machine is considerably reduced.The proposed SAW delay line model for FEM simulation can be extended to simulate a SAW sensor by placing sensing material in the delay line path. Shahrzad Arabshahi et al.[9] reported the study about modeling and simulation using the finite element method of COMSOL Multiphysics, in piezo plane strain, convection and diffusion and incompressible Navier stroke modes of a 2 - dimensional SAW sensor with Zinc oxide thin film for detecting NO_2 gas. XY $LiNbO_3$ piezoelectric substrate is used and simulations are performed to study the

behavior of the sensor in the absence and presence of NO$_2$. As a result of the simulations, total displacement of the wave is obtained. Xiao-Dong Lan et al.[10], simulated the characterizations of Rayleigh wave and Love wave humidity sensors based on the `1120˘ZnO/R-sapphire structures by the FEM model with COMSOL software. The results can provide more detailed understanding on the mechanisms of the humidity sensing of the SAW sensors and also provide valuable information to optimize the structures of the sensors.

In most of the earlier work the number of degree of freedom (DOF) to solve DOF for the complete SAW device structure needs high computing facility and consumes time in computation. Thus valid approximation and simplified model is necessary to perform FEM simulation of SAW sensors.

3.3.6 FEM simulation of a SAW delay line using COMSOL Multiphysics

3.3.6.1 The mathematical model for a SAW delay line

The interdigital transducer (IDT) used in SAW device converts electrical energy to mechanical energy and vice versa. The mathematical model of a SAW delay line given by Feng et al. and also discussed by other researchers [17, 18] is adopted here for simulation of proposed device. In this case the SAW launching IDT is considered as a force generator, which converts electrical voltage to mechanical forces. These forces travel a SAW on the piezoelectric substrate. Consider a launching IDT as shown in figure 3.11and with the number of force generators (IDT fingers) of N equal to 4. If the force generated at each finger of launching IDT is proportional to the applied voltage, the force at n^{th} finger pair can be expressed as

$$f_n(t) = K_1 V_{in}(t) \qquad\qquad (19)$$

where K_1 is the proportionality constant of the transducer ,$V_{in}(t)$ is the input voltage. The displacement of the wave u at the edge of IDT of N finger pair can be written as

$$u(t) = \frac{1}{2v} \sum_{n=1}^{N} fn\left(t - \frac{n\lambda}{v}\right) \qquad\qquad (20)$$

The displacement of the wave at receiver IDT of the SAW delay line device with delay line length L can be written as

$$U(t) = \frac{1}{2v}\sum_{n=1}^{N} fn(t - \frac{n\lambda + N\lambda + L}{v}) \qquad (21)$$

where N is the number of finger pair at the receiving IDT . Let qo denotes the electric charge produced when the electrodes are subjected to local strain. By considering that the charge produced is the sum of the charges from each finger and is proportional to displacement,

$$q_o(t) = K_2\sum_{l=1}^{N} u_l(t) \qquad (22)$$

Thus assuming the output voltage is proportional to charge,

$$V_o(t) = K_3 q_o(t) \qquad (23)$$

K_2 and K_3 are proportionality constants, thus combining the above equations the output voltage can be expressed as

$$V_o(t) = \frac{K_1 K_2 K_3}{2v}\sum_{l=1}^{Ng}\sum_{n=1}^{N_\tau} V_{in}(t - \frac{n\lambda + N\lambda}{v}) \qquad (24)$$

If an IDT of 50 pair and displacement at edge of point 4th pair from equation (21) can be rewritten as

$$u(t) = \frac{1}{2v}\sum_{n=1}^{N=50} f_n(t - \frac{n\lambda}{v}) - \frac{1}{2v}\sum_{n=5}^{N=50} f_n(t - \frac{n\lambda}{v}) \qquad (25)$$

$$u(t) = u_a(t) - u_b(t) \qquad (26)$$

The above equation can be further realized in terms of time t as below

$$u_a(t) = \frac{1}{2v}\sum_{n=1}^{N=50} f_n(t - \frac{n\lambda}{v}) \text{ for all t} \qquad (27)$$

$$u_b(t) = \frac{1}{2v}\sum_{n=1}^{N=45} f_n(t - \frac{n\lambda}{v}) \text{ for t >= n}\lambda\text{/v} \qquad (28)$$

In general, equation (27) can be realized as a one port SAW resonator consisting of single IDT with 50 finger pairs. Thus , it is convenient to model equation (27) and (28) by applying infinite boundary conditions to a section of SAW resonator of length nλ consisting of single or pair of IDT. The simulation procedure used for

the SAW delay line model is explained in the following section.
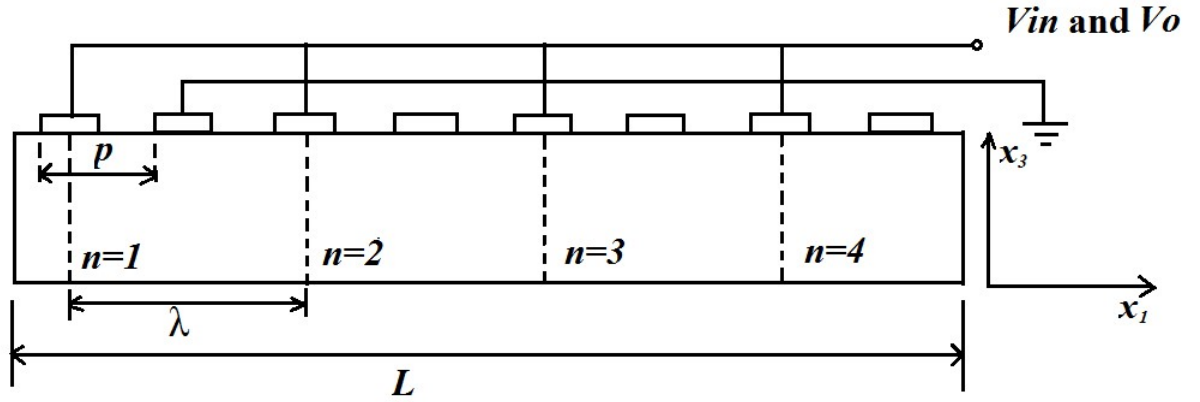
Fig. 3.11 A Typical interdigital transducer structure with four pairs of electrodes.

3.3.6.2 Simulation Methodology

128 YX lithium niobate piezoelectric crystals are assumed as the piezoelectric substrate in the simulation.
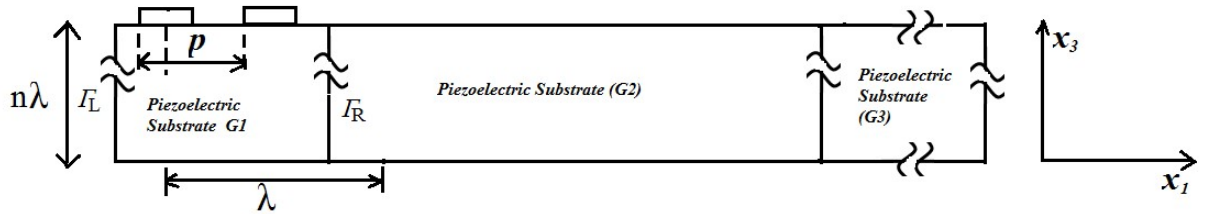
Fig. 3.12 SAW delay line structure used for simulation in COMSOL multiphysics

The alternate fingers are shorted and given input voltage. The SAW delay line structure used in simulation consist of two blocks, the transmitter IDT*(G1)* to generate the Rayleigh waves, delay line*(G2)* as shown in above figure. The SAW delay line structure consist of transmitter and receiver IDT with two electrodes of each 90 µm in width (with λ=360 µm) and a delay line of ~12λ in length. Standing waves at the transmitter IDT propagates SAW in both directions of the IDT [19]. Periodic boundary conditions were applied for transmitter and receiver IDTs as

discussed in previous section. Critical damping was assumed at the edge of the receiver *(G3)* and bottom of the whole device to avoid reflections to the delay line. The equations relating to critical damping are provided in appendix C. To analyze propagation of SAWs waves over the delay line, the frequency domain analysis is used with the input frequency range 1MHz-20MHz with the increment of 0.1 MHz and input voltage of 1V. The linear stationary solver is used for simulation. The statistics of Mesh is given in following table 3.1. The number of degree of freedom solved for 780224 shown in figure 3.14. Complete mesh consists of 16414 boundary elements. The finalized geometry consists of 9 domains and 54 boundaries, 108 edges and 72 vertices. The total time taken for simulation was18 hrs 28 min and 42 sec.

3.3.6.3 Results and discussions on FEM simulation of SAW delay line

Table 3.2 Mesh Statistics for Simulation

Property	Value
Minimum element quality	8.905E-4
Average element quality	0.6311
Tetrahedral elements	144810
Pyramid elements	0
Prism elements	0
Hexahedral elements	0
Triangular elements	16414
Quadrilateral elements	0
Edge elements	3314
Vertex elements	72

Table 3.2 Shows the statistics of mesh used for device simulation. It shows the minimum element quality as 8.906E-4 with average element quality of 0.6311 ant the total tertahedral elements as 144810.
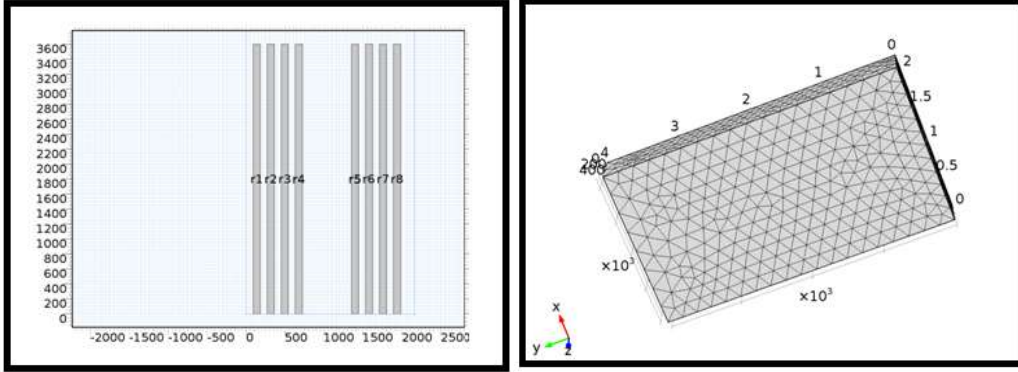
Fig. 3.13 Geometry for Simulation Fig.3.14 Device meshing used in simulation.
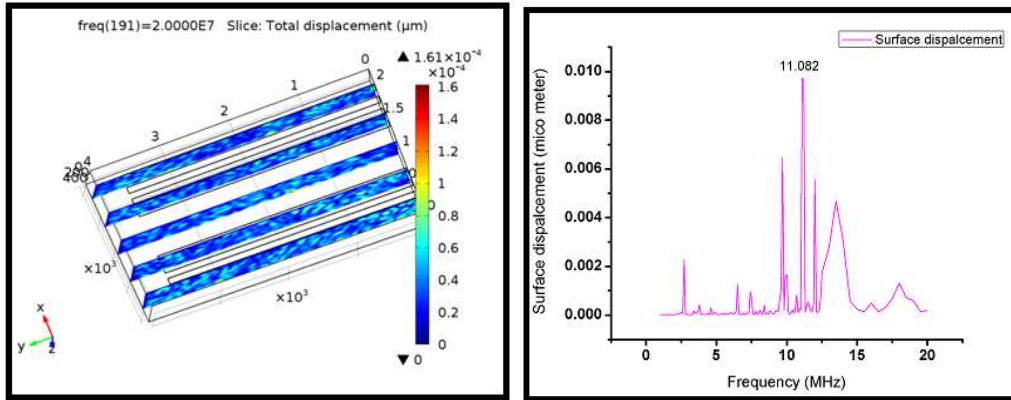
Fig.3.15. Total displacement at input Frequency of 20MHz **Fig. 3.16 frequency Vs surface displacement.**

Figure 3.13 shows the geometry used for the SAW delay line simulation. It consists of two finger pairs in input as well as output IDTs. The height for simulation was selected to be 10λ with λ =360μm and finger width of 90 μm. Figure 3.14 shows the meshing structure used in simulation with its details as listed in table 3.1.

Figure 3.15 shows the total surface displacement of the device in μm with the input frequency of 20MHz. The displacement was measured for the input frequency range of 1-20 MHz and the resultant graph of total surface displacement vs. frequency is as shown in figure 3.16. From the figure it is observed that the maximum displacement occurs at resonance frequency (11.08 MHz). This shows the response of the SAW device is good at the designed frequency and can be used for gas sensing application.

3.4 Fabrication of SAW devices

Low frequency devices up to 200 MHz were fabricated by using traditional optical lithography while the high frequency devices (> 900 MHz) were fabricated by using electron beam lithography because of submicron line widths. For high frequency devices (f >900 MHz) the electron beam lithography is more suitable while for low frequency devices upto 200 MHz can be fabricated using a well known photolithography patterning techniques used for the semiconductor devices. There are two processes that are commonly used to pattern interdigital transducers (IDTs): etching and lift off. Though both are used for fabricating SAW devices, lift-off is more suitable to develop IDT device structure of feature size less than 5µm. However the etching process is quite simple and easy to form IDT patterns of low resolution [20].

In present work etching processes was adopted and the minimum feature size was of the order of 70 µm. The basic steps involved in fabricating SAW devices in this case were: substrate selection, layout design, and mask preparation, dicing of the wafer, cleaning of the samples, and metal deposition over the cleaned piezoelectric samples, photolithography, etching and stripping of photoresist. The SAW delay line devices were fabricated on 128^0 YX cut lithium niobate wafers of thickness 0.5mm and diameter of 3 inch. One face of the wafer was mirror polished while the other surface was lapped.

The following fabrication steps were carried out for our devices.

a. Layout design and mask preparation

The design of a mask will vary according to one's specific application. The first step is to design the device and identify the layers, which will comprise the final device followed by the layout in any CAD software. The next step is to make a photomask which can be used to transfer pattern on many wafers. Photomasks can be fabricated on various types of fused silica [20]. The most important properties of the mask include a high degree of optical transparency, a small

thermal expansion coefficient and a flat highly polished surface that reduces light scattering. On one surface of this glass is a patterned layer, mostly of chromium. In present research work, the layouts of the designed dimensions are prepared using AutoCAD and CorelDraw software's. The masks were prepared on simple transparency paper. It is one of the low cost methods of mask preparation. It also produces fine line definition and works well upto 30-40 µm line definition. Figure 3.17 shows the mask layout structure for the proposed SAW devices.
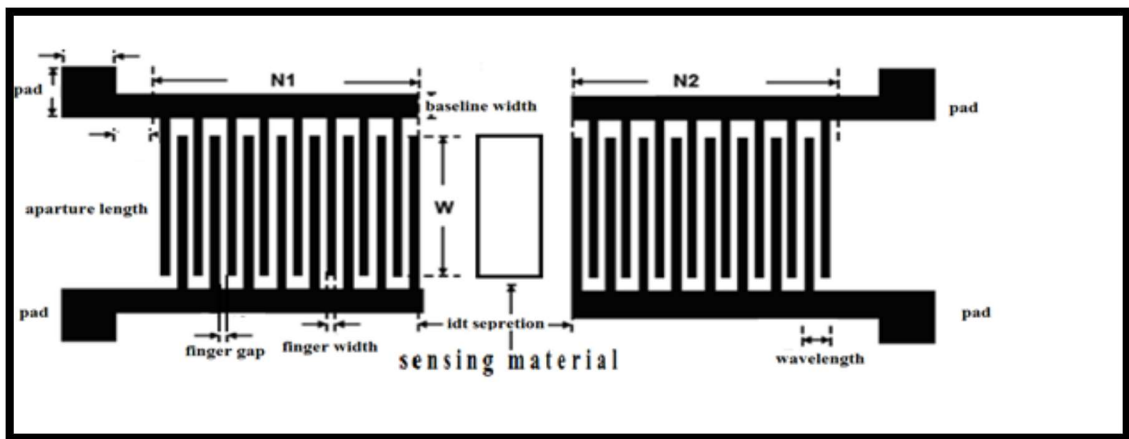
Fig. 3.17 Layout of SAW delay line device [22]

b. Dicing of the Wafer

Due to lithography limitations, at our laboratory the whole 3 inch wafer were not processed directly. The wafer was diced into small rectangular pieces. The dicing of wafer was done using dicing machine at C-MET Pune. The size of the individual samples was 2.4mm x 2.4mm. This was calculated from the physical dimensions of the designed device.

c. Cleaning of LiNbO$_3$ samples

The samples were placed inside a beaker containing acetone bath and were cleaned by placing the beaker in ultrasonic bath for 5 minutes. Further, the samples were placed in methanol for 5 minutes to remove the residual acetone. Finally, the samples were placed in de-ionized (DI) water and dried in clean atmosphere using IR lamp.

d. Metallzation

After cleaning the samples, using thermal evaporation deposition system (Hind High Vacuum) an aluminum metal of 200nm -300 nm is coated over the samples. The 99.99 % pure aluminum wire were cleaned using acetone and small pieces of this wire were kept on tungsten filament and evaporated by passing sufficient amount of current through the filament. After the deposition the thickness of aluminum film was measured using tally – step method.

e. Photoresist Coating

The aluminum deposited sample was placed inside the spin coater. It is ensured that the sample is exactly aligned with spinner. LPR 2010 photoresist was dispensed from the bottle and spread all over the sample. The wafer is spun for a speed of 3000 rpm for 1 minute. By this method a photoresist coating of ~1µm.thickness was achieved over the sample.

f. Soft baking

The wafer with the photoresist coating was soft baked by placing it on a hot plate at a temperature of 75^0C for 3 minutes. To avoid sample (wafer) getting stuck to the hotplate, it was placed on glass slide.

g. Exposure and development

The sample (wafer) was placed in labmade holder with proper alignment of mask for UV light exposure. The assembly was kept in the UV exposure unit for 5 minutes. The intensity of UV light was 19 Lux. The patterns were transferred to the sample by UV exposure. The sample was then rinsed in LPR developer for 1min-1.5min, the wafer was taken out from the developer solution once the patterns are identified in the sample. If the sample is placed for excess time it will lead to over development and finally ends with poor features on the wafer. The exposure and development were optimized after 5-6 trials.

h. post baking

The developed patterns were cross checked with optical microscope. The wafers were hard baked by placing them on hot plate for the temperature of 90^0 C for 3-4 minutes.

i. Aluminum etching

Aluminum etchant was prepared by mixing KOH pellets in DI water the concentration value was 2 palates (~0.270 gm)/80 ml. Another solution that is used for etching was phosphoricAcid (73%)+ Nitric Acid (3%) +Acetic Acid (3.3%) + DI Water (20.6%) is good for aluminum etching. The etchant was prepared in bulk and stored in glass bottle. The post baked wafer was placed in etchant solution for 1 to 2 minutes. Once the aluminum is etched out the sample were immediately taken out from the etchant solution and placed in DI water. Excessive time in etching will lead to undercut in the IDT electrode. Therefore the samples (IDT devices) were continuously monitoredunder microscope for every 30 seconds during the etching process. The samples were dried under IR light in clean environment.

j . Removal of photoresist

The samples were placed in acetone for 1-2 minutes, followed by methanol and DI water and subsequently dried under IR light. The fabricated SAW delay line device is shown in figure 3.19

The final process was decided after 5 trials runs of spinning and development for the samples.

k. connecting wire for testing

After the SAW delay line device was fabricated successfully. To test the device for its scattering parameters the gold plated SMA connectors were joined to the device using 2 cm long, 200 µm diameter copper wires, silver paste and soldering. The

assembly is shown in figure 3.19. Figure 3.18 shows the lithography steps used to fabricate the SAW devices[22]
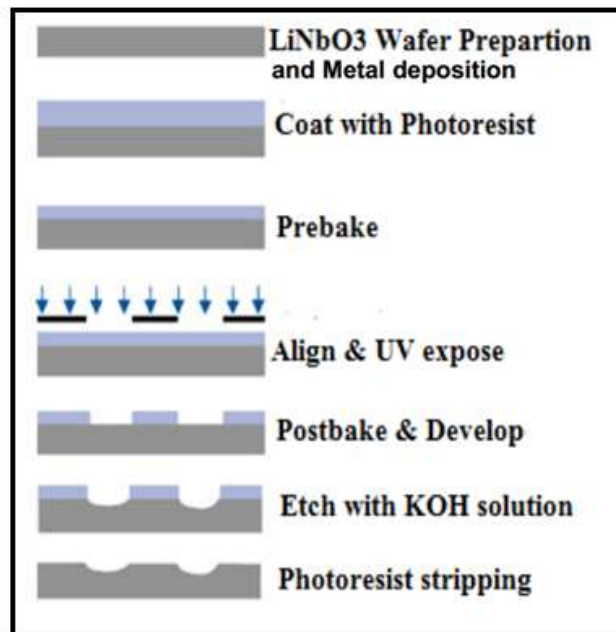
Fig.3.18 Saw Device Fabrication Steps
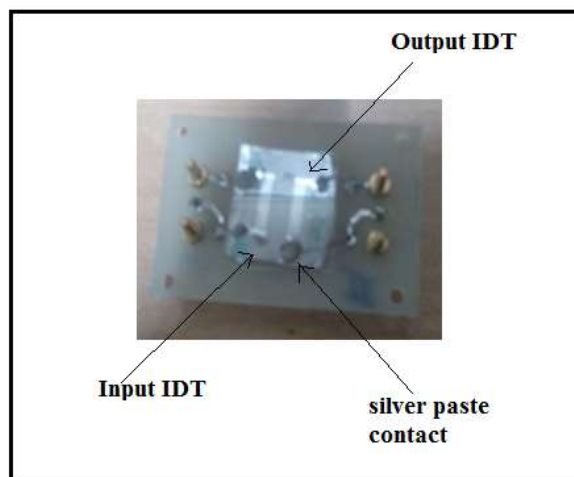
Fig. 3.19 Labmade SAW delay line device snapshots

Table 3.3. Lithography Parameters

Parameter	Value	Parameter	Value
Amount of resist	0.5ml	Exposure time	15 minutes
Spin speed	3000rpm +/- 100 rpm	Developer time	10-15 sec.
Spin time	1minute +/- 5sec.	Exposure intensity	19 Lux.
Baking time	5 minutes	Etching concentration	2 palates (~0.270 gm)/80 ml
Baking temperature	90^0 C +/-5^0 C	Etch time	2-3 minutes

3.4.1 Problems faced during SAW device fabrication

Following are some of the problems faced during the SAW device fabrication

1. Samples (wafer) cracks and breaks during baking process.
2. Baking parameters for glass samples were not same for $LiNbO_3$.
3. Baking parameters needs to be optimized for aluminum film adhesion on $LiNbO_3$.
4. Mask need to be replaced after every cycle of exposure due to photoresist traces on the mask.

3.4.2 Dimensions of Fabricated SAW delay line devices

The finger width, finger gap and finger length are observed under digital microscope (Leica).The images /snapshots of the same are as shown in figure 3.20
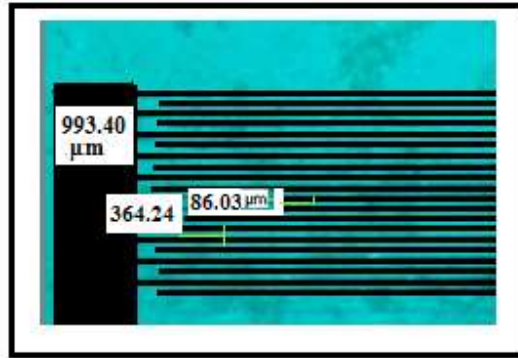
Fig. 3.20 Dimensions of fabricated SAW devices showing finger width, pitch and baseline width (f_0 =11.08MHZ).

3.4.3 SAW Device Characterization

The response a SAW device to an external perturbation for chemical sensing can be better understood if the device frequency response is known in advance. Measurement of the frequency response is also important if the most stable and accurate measurement system is to be designed for a particular device. It is very useful to monitor velocity and attenuation both simultaneously. Most of the acoustic sensor research solely depends on the measurement of velocity perturbations [2,20]. Such an approach is adequate if it is known in advance that all perturbations will affect wave velocity alone; such perturbations include mass effects and changes in the elastic and mechanical properties. The complete characterization of an acoustic wave device is always obtained from a complete frequency response spectrum including all the scattering(s) parameters.

The S parameters are set of parameters explaining the scattering and reflection of travelling waves, when a network is inserted into a transmission line. S parameters are normally used to characterize high frequency networks, where simple models valid at lower frequencies cannot be applied. S parameters are normally measured as a function of frequency of applied signal.

All the SAW devices were characterized by Agilent E 5062A Network Analyzer. Network analyzer with all the test leads and terminations were calibrated by using calibration kit 85032E. The maximum center frequency of every device fluctuates between +/- 1 KHz depending on the external noise, vibrations and test fixture stability.

Before measurements, devices were checked by using multimeter for any shorts. A simple continuity test was carried out between each pair of bonding pads. The S_{21} and S_{11} curves measured by network analysis were compared with the characteristic curves of a SAW device. Some S-parameter curves for SAW devices with center frequency 6.66 MHz and 19.8 MHz, respectively, are shown in Figures 3.17 and 3.18.

The results of five different devices are as shown in following table.

Table 3.4. SAW delay line devices with their frequency and Insertion loss

Device /Sample No	Resonant Frequency From actual dimensions(MHz)	Observed Resonant frequency (MHz)	Attenuation (dB)
1	6.66MHz	6 MHz	-26.37
2	9.98MHZ	11.08 MHz	-30.75
3	6.66MHz	7MHz	-25.03
4	13.31 MHz	14 MHz	-33.47
5	13.31 MHZ	19.8MHz	-25.51
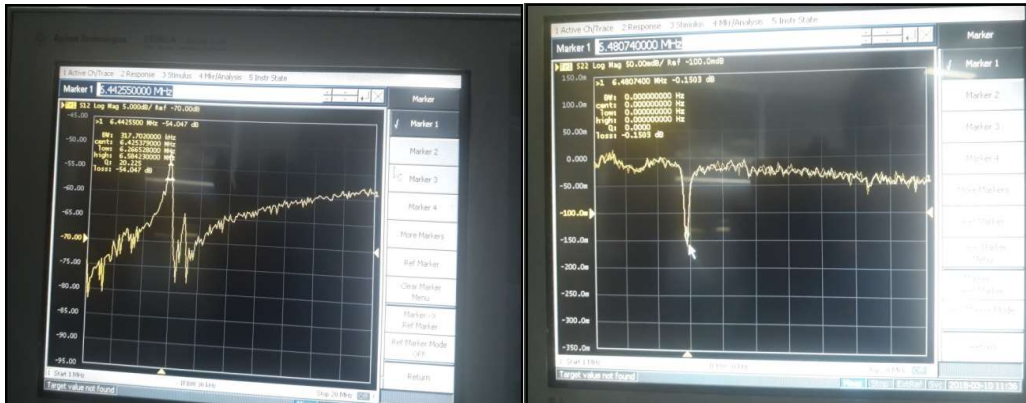
Fig.3.21 (a) S$_{12}$ of SAW   (b) S$_{22}$ of SAW

Fig. 3.21(a), (b) Shows the S$_{21}$ transmission curve with the peak frequency near designed frequency of 6.66 MHz and S$_{22}$ reflection curve showing a dip near resonance frequency with moderate insertion loss.
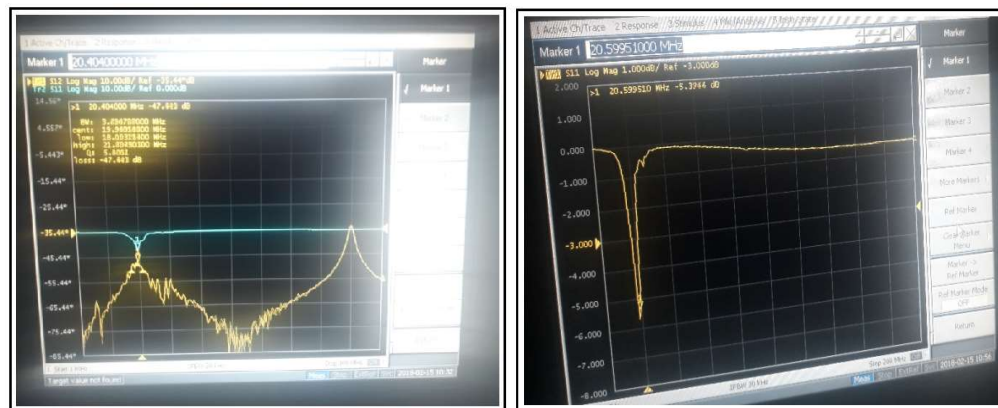
Fig.3.22 (a) S12 of SAW   (b) S11 of SAW

Fig.3.22(a),(b) Shows the S$_{21}$ transmission curve with the peak frequency near designed frequency of 19.8 MHz   and S$_{22}$ reflection curve showing a dip near resonance frequency with moderate insertion loss.

We also characterized the SAW IC (SIPAT) LB 211 DS 01 using the network analyzer E5062A and its parameters are listed in table 4. Figure 3.23 Shows the SAW IC assembly with its matching network.

Table 3.5 SAW IC LB 211 DS 01 S- parameters

Parameter	Value
S11	-6.421 dB
S21	-9.66 dB
S12	-13.769 dB
S22	-2.096 dB
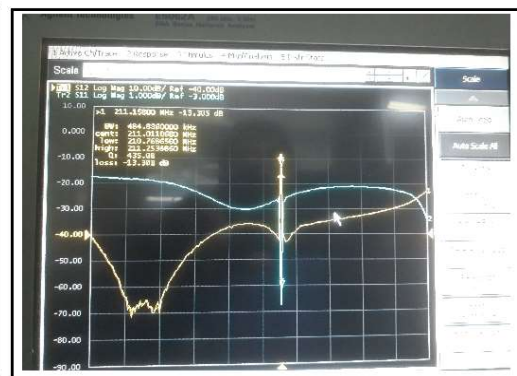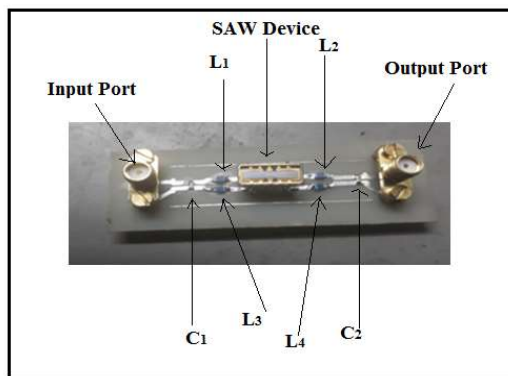
Fig. 3.23 SAW IC LB 211 DS 01 with its Fig. 3.24 S_{12} of SAW IC LB 211 DS01Matching network
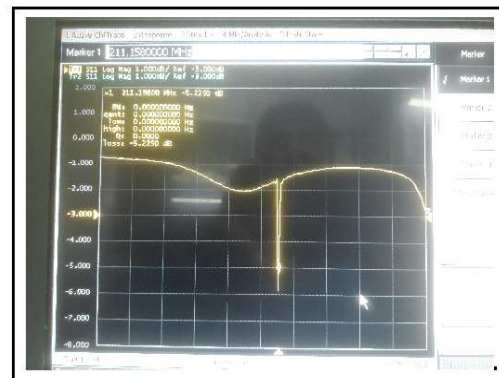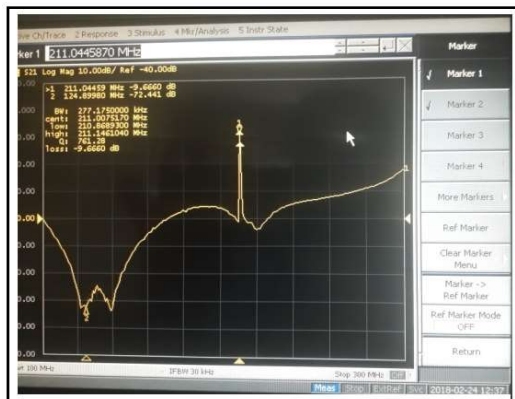
Fig.3.25 (a) S_{21} of SAW IC LB 2011 (b) Fig. S_{11} of SAW IC LB 2011 DS 01

Fig.3.25 ,3.21(a) and 3.21(b) Shows the S_{12}, S_{21}, and S_{11} for SAW device with the resonsnat frequency 211MHz. the measured parameters are in good agreement with the parameters listed in data sheet.
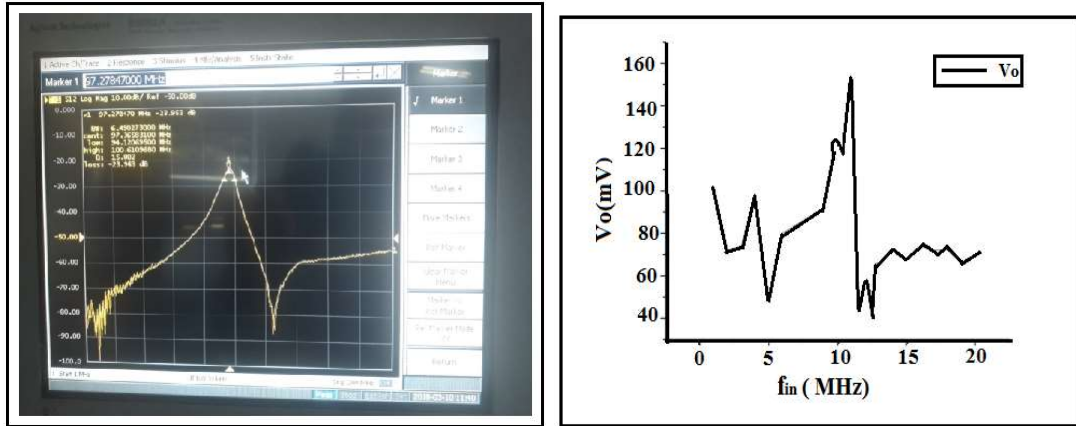
Fig. 3.26 (a) S$_{12}$ of SAW device operating at harmonic frequency 97.27 MHz , (b) Frequency response of SAW device measured on DSO and Arbitrary function generator as a RF source at (Vin =5V).

Figure 3.26 (a) shows the S$_{12}$ of SAW device operated at harmonic frequency 97.27 MHz. Figure 3.26(b) shows the frequency response of SAW device with resonance frequency 11.08MHz measured on DSO with arbitrary function generator as a RF source at (Vin =5V). In this case the attenution is quite large due to impedance mismatch of the device and measuring instruments.

3.5 Development of Chemiresistors for Gas Sensing Application

We have designed and fabricated the interdigital transducer structures on glass epoxy as well as on glass substrates. The three different layout designs are shown in following figure 3.23. Their physical dimensions are listed in table 5. The electrical parameters of these devices were measured on LCR meter at 1 KHz frequency and some of them are reported in table 6.
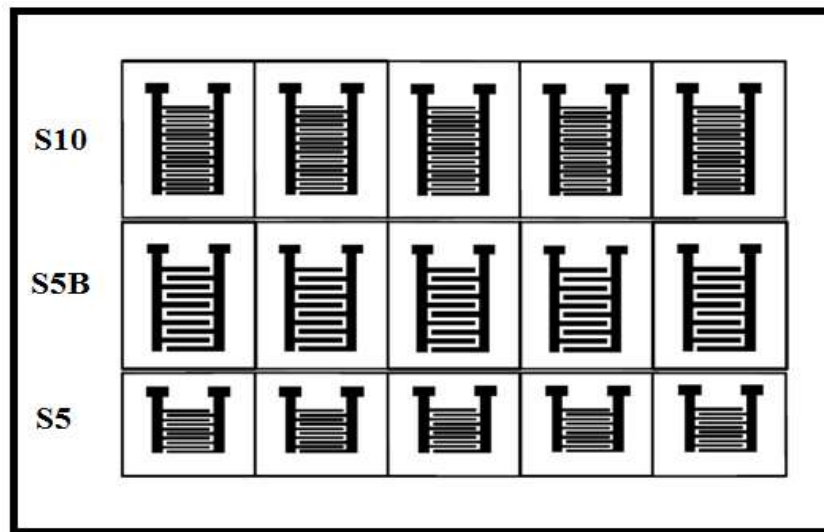
Fig. 3.27 IDT structures used as chemiresistors

Table 3.6 Chemiresitor Physical Dimensions

Parameter	IDT1	IDT2	IDT3
Base line width	2mm	2mm	2mm
Finger Width	0.5mm	1 mm	0.5mm
Finger Gap	0.5mm	1 mm	0.5mm
Finger length	10 mm	10 mm	10 mm
No. of finger pairs	10	5	5

Table 3.7. Parameters of IDTs

Sample	Cp (pF)	R (Mega Ohm)	X (Mega Ohm)	Z (Mega Ohm)	Change	% Change
S10-1	5.96	0.945	26.73	26.75	R =0.18	16.36
S10-3	5.338	1.10	29.82	29.82	Cp=0.817	13.27
S10-5	6.155	0.920	25.87	25.90	Z=3.92	13.14
S5-1	2.524	2.54	63.86	63.86	R =0.46	18.11
S5-3	3.404	2.08	46.70	46.75	Cp= 0.88	25.82
S5-5	2.977	2.21	53.41	53.44	Z=17.11	26.79
S5B-1	2.980	2.17	55.31	54.47	R =0.37	17.05
S5B-3	3.11	2.04	51.42	51.50	Cp= 0.93	23.78
S5B-5	3.91	1.80	40.60	40.61	Z=13.86	25.46

Chemiresitor characterization

The Electrical parameters of IDTs are measured using LCR meter and reported in table 5. It is observed that:

Reactance (X) and impedance (Z) values for each sample are same; Resistance (R) value is different for the samples, and as number of finger pairs increases Cs and Cp increases & Lp, Rs, R decreases. It is also observed that the electrode width variation does not cause any significant increase in capacitance (Cp) Value.

3.6 Conclusion

In this chapter we have discussed the design, model simulation and fabrication of SAW delay line devices. Different models are available for simulation of SAW devices. In present study we used equivalent circuit model, transmission matrix method and finite element method for the proposed device. The first two methods are implemented using MATLAB. The effect of aperture length, number of fingers, and delay line length on acoustic susceptance, radiation conductance, insertion

loss and bandwidth has been studied. The finite element method is implemented using commercial software COMSOL multiphysics. The SAW delay line was modeled and simulated using COMSOL multiphysics. The results of simulation were in good agreement with theoretical calculations.

The device was designed for five different frequencies out of which we emphasized on two of them. 128^0 YX cut Lithium niobate was considered as piezoelectric substrate with taking account all its important characteristics. Five SAW delay line devices were fabricated using standard photolithography technique, to study the gas sensing of application of SAW devices. We optimized the process parameters to fabricate the SAW devices with available resources, also discussed the problems faced during fabrication process. The characterizations of developed devices have been undertaken and obtained results are close to the expected values.

The developed of SAW delay line can be used for gas sensing applications. For gas sensing (ammonia and VOCs) polyaniline and polyaniline -SnO_2 nanocomposite materials were used as sensing layers. Next chapter deals with the synthesis and characterization of polyaniline (PANI) and polyaniline -SnO_2 nanocomposites.

References

[1] A. D' Amico, A. Palma and E. Verona,"Surface Acoustic wave hydrogen sensor", Sensors and Actuators, Vol-3, pp-31-39, 1982.

[2] D. S. Ballantine, Jr., Robert M. White, S. J. Martin, Antonio J. Ricco, E. T. Zellers, G. C. Frye, H. Wohltjen, Moises Levy, Richard Stern, "Acoustic Wave Sensors, Theory, Design, and Physico-Chemical Applications", New York: Academic Press limited.,1996.

[3] Ricco A. J. and Martin S. J., "Acoustic Wave Viscosity Sensor", Applied Physics Letters, Vol. 50, No. 21, pages 1474-1476,1987.

[4]Andie J. C., Weaver J. T., Vetelino J. F. and McAllister D. J., "Application of Unidirectional Transducers in Acoustic Plate Mode Biosensors", Proceedings of the IEEE Ultrasonics Symposium, pages 331-335, 1993.

[5]Andie J. C. and Vetelino J. F., "Acoustic Wave Biosensors", Sensors and Actuators A,Vol. 44, pages 167-176, 1995.

[6] Key-ya Hashimoto." Surface acoustic wave devices in telecommunications: modeling and simulation", Springer,,ISBN3-540-67232-X.

[7] Campbell C. K., "Surface Acoustic Wave Devices for Mobile and Wireless Communications", Academic Press Inc., 1998.

[8] Chin, Matthew L. "A Fabrication Study of a Surface Acoustic Wave Device for Magnetic Field Detection." Thesis.Oregon State University, 2006. *Scholars Archive at OSU*.Oregon State University, 5 June 2006. Web. 5 Dec. 2010.

[9] Morgan D. P., "History o f SAW Devices", Proceedings of the IEEE InternationalFrequency Control Symposium, pages 439-460, 1998.

[10] Evan R. Hirst, Yong J. Yuan, W. L .Xu, J. E. Bronlund," Bond-rupture immunosensors- A Review", biosensors and Bioelectronics 23 (2008); 1759-768.

[11] Calabrese G., Wohltjen H. and Roy M. K., "Surface Acoustic Wave Devices as chemical Sensors in Liquids. Evidence Disputing the Importance of Rayleigh Wave Attenuation", Analytical Chemistry, Vol. 59, pages 833-837,1987.

[12] R. Banu Priya, T. Venkatesan, Haresh M. Pandya," Modelling, Simulation and Validation of Surface Acoustic Wave (SAW) Delay Line by P Matrix Mode",J. Sci. Res. Adv. 4 (2017) 419-424.

[13] Yi-Gui Zhao, Ming Liu *, Dong-Mei Li, Jing-Jing Li, Jie-Bin Niu,"FEM modeling of SAW organic vapor sensors",Sensors and Actuators A 154 (2009) 30–34.

[14] Sridevi Krishanamuti,"Wireless Passive Surface Acoustic Wave (SAW) Sensing System", Thesis Western Michigun Univeristy. August 2007.

[15] M.M. Elsherbini, M. F. Elkordy, A. M. Gomaa," Using COMSOL to model high frequency surface acoustic wave(SAW) device", Journal of Electrical and Electronics Engineering Research, Vol(8), pp. 1-8 July 2016.

[16] Moataz Mostafa Elsherbine, Mohamad Fahim Elkordy, Aly Mohamed Gomaa, "Transient Analysis for 70 MHz LiNaBo$_3$ delay line", Journal of Scientific Research and Advances, 2015 2(2),80-83.

[17] Moulic J. R. " A broadband surface -wave filter with 50 dB stopbands and 1-dB passband ripples", Proceedings of the Ultrasoncis Symposium, pages 673-674,1977(cross reference).

[18] Z. C. Feng.and C. Chicone ," A delay differential equation for surface acoustic wave sensors", Sensors and Actuators A, vol. 104,pp,171-178,2003.

[19] COMSOL Multiphysics Version 3.4 documentation COMSOLAB, Stockholm, Sweden 2007[cross referemce].

[20] Jared Kirschner ," Surface Acoustic Wave Sensor(SAWS): Design and applications, December 6, 2010.

[21]P. S. Varade, S. A. Gangal, A.D. Shaligram," simulation of SAW Dealy line Sensor using MATLAB", Bionano Frontier, Vol. 10 Issue-2.July 2017.

[22]P.S. Varade, A.D. Shaligram, *"Evaporation studies of volatile organic compounds using SAW devices",* American Institute Physics, **(Accepted)** ETMN 2017 AIP online conference series.

CHAPTER 4

SYNTHESIS AND CHARACTERIZATION OF POLYANILINE AND POLYANILINE – NANOCOMPOSITES

4.1 Introduction

Polyaniline (PANI), Polythiophene (PTH), Polypyrrole (PPy), poly(3,4-ethylenedioxythiophene) (PEDOT), trans-polyacetylene, and poly(p-phenylene vinylene) (PPV)and their derivatives are known as conducting polymers, which have been widely used as an active layer for development of room temperature gas sensors[1,2]. Sensors developed using these conducting polymers has improved characteristics such as high sensitivities and faster response time at low temperatures around room temperature. Conducting polymers are easy to be synthesized through chemical or electrochemical processes, and their molecular chain structure can be modified conveniently by copolymerization or structural derivations. Furthermore, conducting polymers have good mechanical properties, which allow a simple fabrication of sensors. But they possess a main drawback of having poor selectivity as they sense most of the gases. The sensitivity of these sensors arises from change in redox levels due to the transfer of electrons from or to the gas. Therefore lot of care has been taken while fabricating sensors from conducting polymers [3].

The inclusion of carbon nanotubes (CNT), nanoparticles of different metal oxides such as SnO_2, TiO_2, WO_3, MnO_2 materials into a polymer matrix in order to prepare conductive nanocomposites appear also as a very capable direction to prepare active elements for gas sensors [4,5,6]. For conductivity type gas sensors, the active material of the sensor should have adequate electrical conductivity at low nanoparticles content. The major requirement for the latter is the good dispersion of nanoparticles in the polymer matrix which is strongly dependent on the polymer-nanoparticles interactions [4]. Further, conducting polymers that have been investigated for chemical sensors are polypyrrole, polyacetylene, polyaniline, polythiophene, porphyrin and N-vinylcarbazole. Among these polymers, polypyrrole and polyaniline are widely investigated for ammonia (NH_3) sensing. Polypyrrole was the first polymer used for NH_3detection;however its sensitivity was quite low and response was also irreversible. Polypyrrole films are not easily

processable whereas polyaniline is soluble in common organic solvents from which free standing films can be cast. Polyaniline is also considered to be one of the most promising conducting polymers because of its easy preparation, low cost, and relatively stable electrical conductivity in air. By taking in to account of all the advantages of polyaniline we proposed the synthesis of polyaniline for gas sensing applications. This chapter presents the work carried out on synthesis and characterization of polyaniline and polyaniline-SnO_2 nanocomposites.

4.2 Polyaniline and Its Synthesis

Polyaniline is the oxidative polymeric product of aniline under acidic conditions and has been known since 1862 as aniline black. Among all the conducting polymers, polyaniline (PANI) is the most promising polymer due to its easy synthesis, controllable electrical conductivity in doped state, good environmental stability and simple non-redox doping by protonic acids. Polyaniline is a typical phenylene based polymer having a chemically flexible –NH– group in the polymer chain flanked either side by phenylene ring. The protonation, deprotonation and various other pysico-chemical properties of polyaniline are due to the presence of this –NH– group.

It is well known that PANI exists in three different oxidation states such as leucoemeraldine, emeraldine and pernigraniline. Among these only polyemeraldine is electrically conductive. The electronic transport properties of PANI can be changed by doping either by electrochemically or chemically with some anions. In the recent years, PANI has been one of the most extensively investigated conducting polymers due to its electronic, electrochemical, and optical properties. In addition, PANI has thermal stability, particularly in the conducting emeraldine salt form and is a candidate for potential commercial application, such as in light emitting diodes, lightweight battery electrodes, sensors, electro-optics, electromagnetic shielding materials, biochemical capacitors, and anticorrosion coating[7].

Polyaniline in the emeraldine oxidation state can be reversibly switched between electrically insulating emeraldine base and conducting emeraldine salt forms [8].

The conductivity of polyaniline can be varied by 10 orders of magnitude by controlling the degree of imine nitrogen protonation (doping). The doping level can be changed by using variable amounts of a wide variety of protonic acids. The dopants can be removed by a reversible reaction with any strong base such as ammonium hydroxide [9]
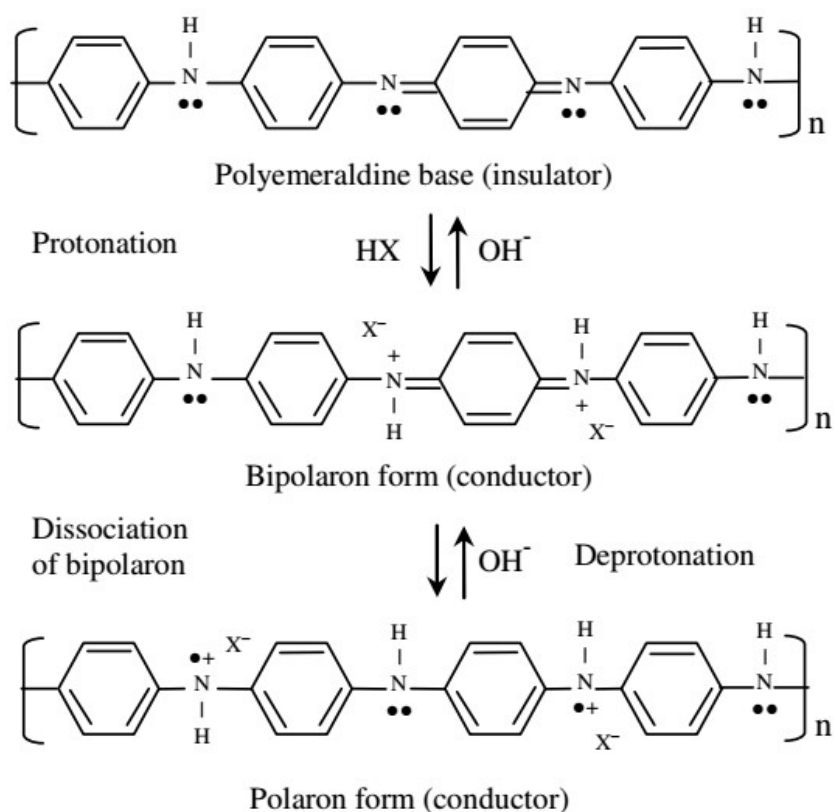
Fig 4.1: Polyaniline in the emeraldine oxidation state can exist in either its undoped (top), intermediate bipolaron (middle) or fully doped acid form (bottom).

The polyemeraldine form consists of amine (-NH-) and imine (=N-) sites in equal proportions. The imine sites are prorogated preferentially to achieve an intermediate bipolaron form (Fig. 4.1: middle), which further undergoes dissociation to form a delocalized polaron lattice (Fig. 4.1: bottom)[10]. A polarons can be considered a type of electronic defect that occurs within the π orbital's of the polymer backbone and is the charge carrier responsible for the relatively high conductivity of doped polyaniline. By controlling the pH of the dopant acid solution any desired quantity of dopants can be added until all imine nitrogen's are prorogated. The conductivity of polyaniline depends on both the degree of protonic acid doping of the imine sites and the oxidation state of the main polymer chain [11]. Any interaction with polyaniline that alters either of these processes will affect its conductivity. Reduction (n doping) or oxidation (p-doping) of the conducting polyaniline emeraldine salt by chemical or electrochemical processes change the number of electrons associated with the polyaniline backbone making the polymer to the insulating leucoemeraldine or pernigraniline oxidation states, respectively.

As a result, redox active chemicals and gases can affect the conductivity of polyaniline by changing its intrinsic oxidation state. Neutral, volatile organic compounds are able to change the conductivity of doped polyaniline films through physical effects as a result of polymer swelling, alignment, crystallization, solvation, or by affecting the doping level [12].It was reported that partial electron transfer occurs between the polyaniline and the volatile organic compound analytes which may increase or reduce the concentration of the charge carriers along the polymer backbone, and hence polymer conductivity [13].Functional additives incorporated into the polyaniline structural matrix, such as metals, metal oxides, enzymes, etc. can change the electrical characteristics of polyaniline. This versatility has made polyaniline attractive for a broader scope of design and development of highly efficient sensors [14].

4.2.1 Polyaniline preparation Methods

The polyaniline can be chemically and electrochemically synthesized by the oxidative polymerization of aniline monomer in the presence of aqueous acid e.g. 1M HCl solution. The resultant polymer is called as an emeraldine salt.For chemical synthesis there are many different oxidizing agents, including hydrogen peroxide, ammonium per sulphate, ferric chloride, ceric nitrate and sulphate.

Typically the ratio of oxidizing species to aniline has been reported to be oxidant /aniline 1:25[15, 16].In this thesis we have reported polyaniline synthesis by using chemical method by using two different oxidizing agents: potassium dichromate and ammonium persulphate with HCl and PTSA as the doping agents respectively. The process of synthesis and corresponding characterization of the resultant polyaniline is explained in the following section.

4.2.2 Distillation of Aniline

To remove impurities if any, in the aniline, its purification is done using condenser method. Figure 4.2 shows the setup for aniline purification. The amount of aniline taken for distillation was 20ml. The time taken to start the distillation was 40 minutes and the temperature was in between 90-100 ^{o}C. The collected pure aniline was kept in refrigerator for further use. The chemical structure of aniline was analyzed using Fourier transform infrared spectroscopy (FT-IR) in the range 400-4000 cm^{-1}.The observed results were similar to the standard results reported in literature [17].
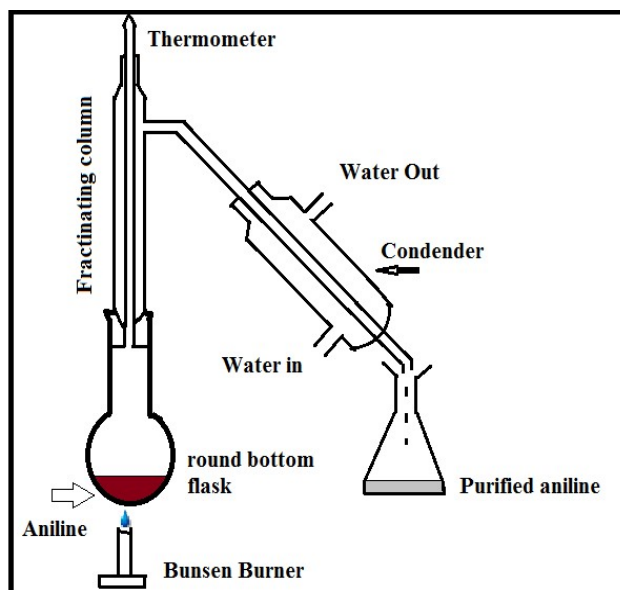
Fig.4.2 Aniline purification using condensar method

4.2.3 Polymerization of Aniline using Potassium Dichromate

The synthesis of polymer was carried out in a three different flasks that was kept at room temperature (27-32 °C). Small volume of distilled water, 20 ml concentrated HCL and aniline of different required volumes were taken in the flask. 25 ml Potassium dichromate solution (0.44 M) was added slowly with vigorous stirring by a magnetic stirrer. The total volume of the reaction mixture was made to 100 ml by distilled water. The precipitated polyaniline salt was filtered and then washed with distilled water until the washing liquid was completely colorless. The material was dried at room temperature for 48 hours in normal atmosphere in the laboratory. The synthesized polyaniline was finally grinded and the product is obtained in the form of fine green powder and the observed weight of the powder was 6.81 gm. The polymer yield (PY) was calculated using the formula [18]:

$$PY = \frac{Amount\ of\ PANI\ produced\ in\ gram}{Amount\ of\ aniline\ charged\ in\ gram}\ x\ 100$$

This is verified for different mole ratio of aniline/dichromate. The typical range of 2.0 to 2.4 produces better yield.

4.2.4 Structural and morphological characterization of polyaniline

Fourier transform infrared (FT-IR) spectrum was recorded on a Perkin-Elmer Spectrum RXFTIR system in the range of 4000-400 cm^{-1} using KBr pellets. Thermal degradation studies TGA were performed under pure air using Detector: DTG-60H for the temperature range 45.04^{0}C to 499.27^{0}C. The weight loss observed is 4.325mg (-67.002%).X-ray diffraction patterns of the polyaniline powder were obtained by employing JEOL JDX Services diffractometer using CuKα (Kα =1.54056 Å) radiation. The diffractometer was operated at 40Kv and 40mA. A scanning step of 0.1^0 in 2θ with a dwell time of 10s per step was used. The samples used for x-ray were in powder form. The electrical characterization studies were performed by forming thin films on glass plates and by preparing bulk pellets using KBr pressing machine. The resistance of both structures are measured using electrometer, LCR meter and by potential divider method.

4.3 Results And Discussions

4.3.1 XRD of Polyaniline

 Crystalline orientation of conducting polymer are of much interest, because more highly ordered systems could display a metallic property such as like conductive state. The XRD pattern for PANI doped with HCl in chemical oxidative synthesis has been assessed as shown in Fig 4.3. The profile of the characteristic peak of PANI at 2θ≈25^0 The XRD spectrum for free PANI does not show any sharp peaks suggesting a non-crystalline nature of PANI. However, the polymer displays a diffuse broad peak ranging from 20^0 to 30°, which is consistent with the results obtained by other research groups [19, 40]. We also observe a small peak at 28^0 which results due to the periodicity parallel and perpendicular(preferred orientation) of the X- ray to the polymer chain reported by Hui Xu et al. and Sreela Pal Bask and et al. [24, 25].   This confirms lower crystallinity and conductive emeraldine salt structure of PANI. Figure 4.3(c) shows the XRD for amorphous

PANI reported by S. D. Charpe et al [43]. This shows that the nature of developed PANI is not amorphous.
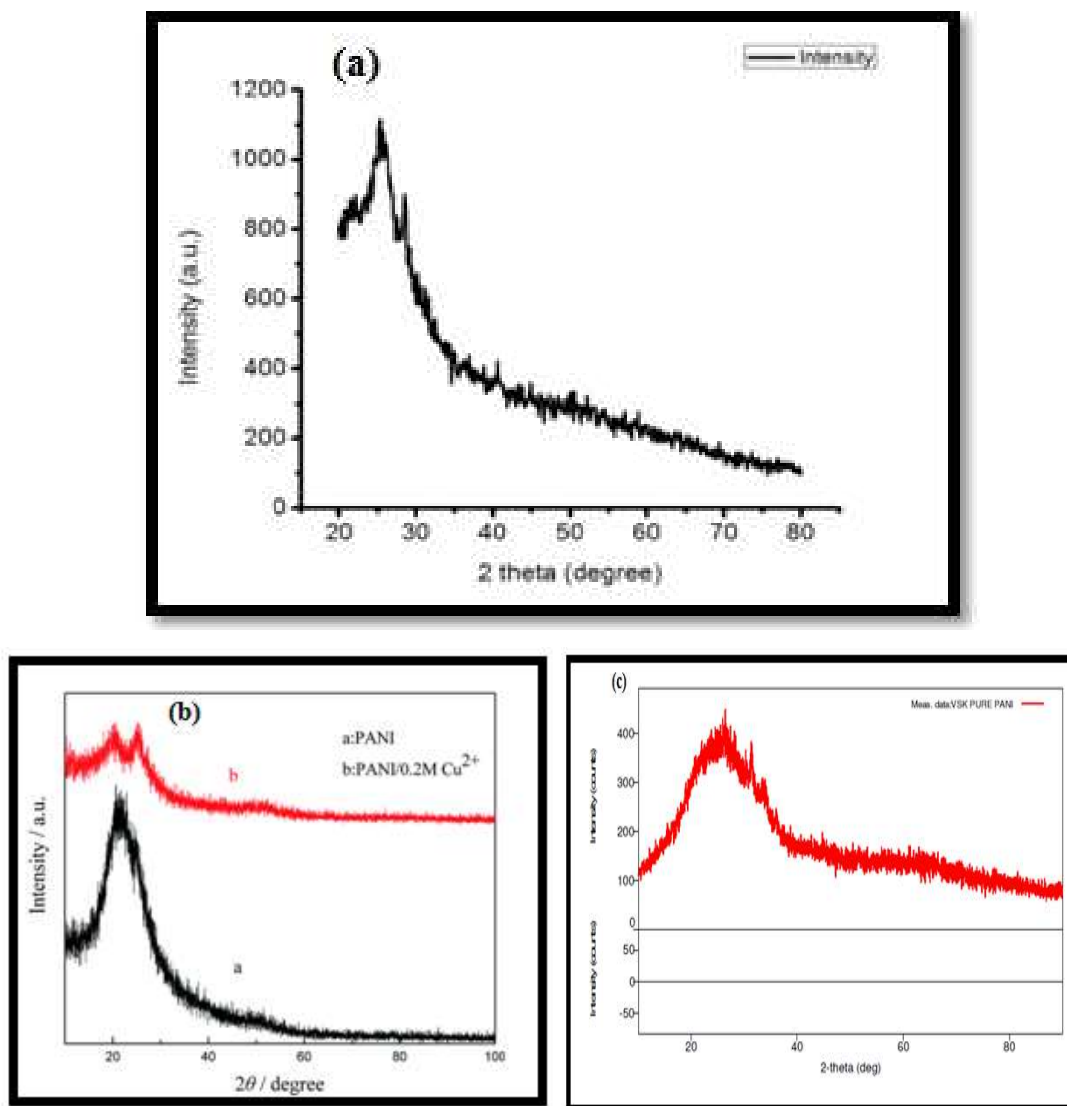
Fig. 4.3 XRD of Polyaniline(a) our result (b) Source- Ref[25] (c) Source-Ref[43]

4.3.2 Fourier Transform -Infrared Spectroscopy (FT-IR) of Polyaniline

The main objective of FT-IR spectroscopic analysis is to determine the chemical functional groups in the sample of study. Different functional groups absorb the characteristics frequencies of IR radiation. Thus it is well known tool for structural clarification and compound identification.
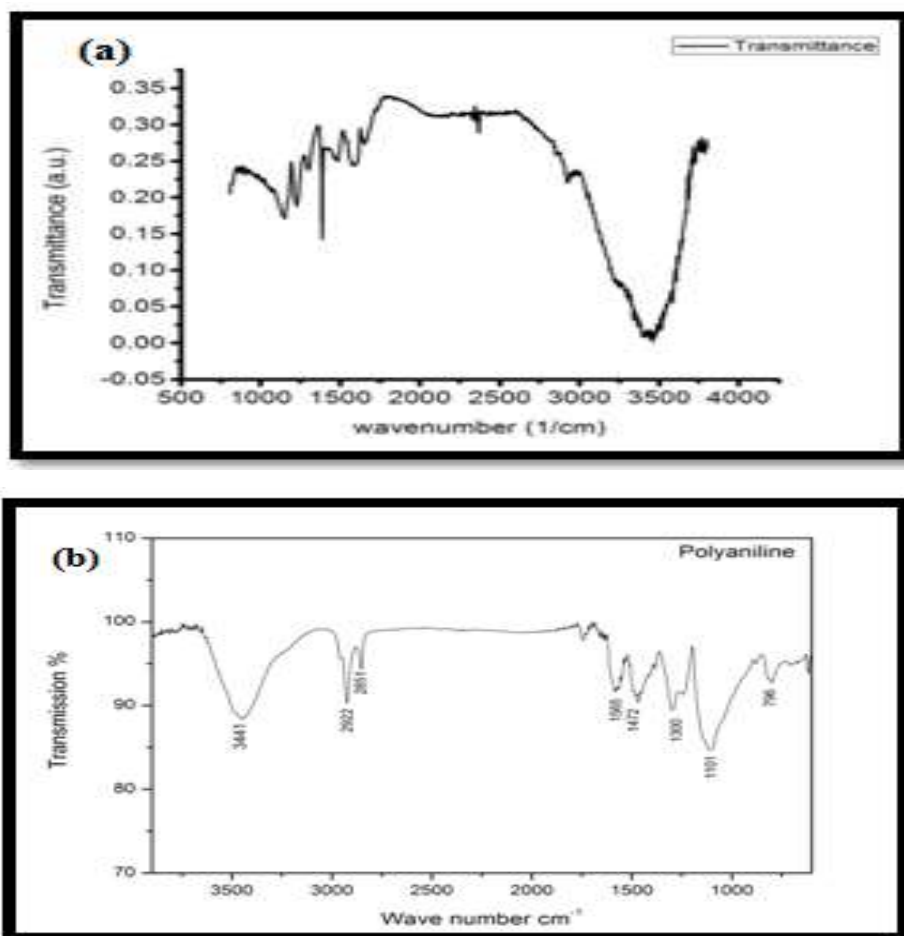
Fig. 4.4 FTIR of Polyaniline (a) Our result (b) Source- Ref[44]

FT-IR spectra of PANI samples with HCl acid is shown in figure 4.4. In a spectrum the band observed at 3449.529 cm^{-1} is due to N-H stretching. The polymer shows the absorption at 2927.686cm^{-1} is due to C-H stretching vibrations. The absorption peaks observed at 1597.805 cm^{-1} is attributed to C-H stretching in aromatic compounds. Absorption bands at 1480.250 & 1384.326 cm^{-1} evidenced to C=N

stretching in aromatic compounds. The polymer shows absorption peak at 1224.46 cm^{-1} confirms C-N stretching of primary aromatic amines. The absorption peak appeared at 1150.186 revels the C-H bending vibrations. Anil sonkusare et al [44] also reported the FTIR of polyaniline nano particles. The most of the characteristic peaks are similar with minor shift. The shift could attribute to nanosize of the polyaniline material particles. The same findings have been reported in reference [21]. This shows that the synthesized polyaniline material has some crystallinity.

4.3.3 TGA-DTA of Polyaniline

The analysis of the change in mass of a sample on heating is known as "Thermo-gravimetric analysis(TGA)". TGA measures the mass changes in a material as a function of temperature or time under a controlled atmosphere. It is basically used to find material's thermal stability and composition. TGA is commonly useful for decomposition, desorption, dehydration and oxidation process. The most commonly used thermal method of analysis is "Differential thermal analysis (DTA)".

(a)

(b)   (c)
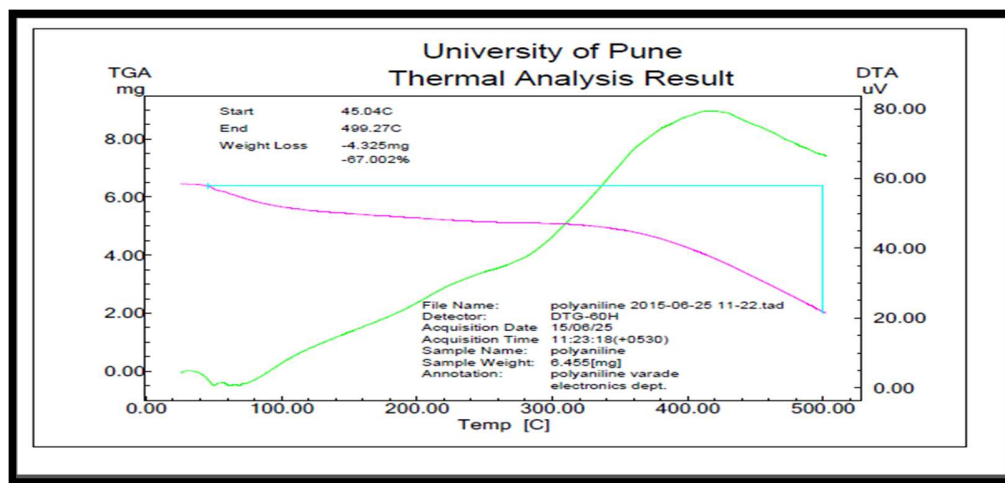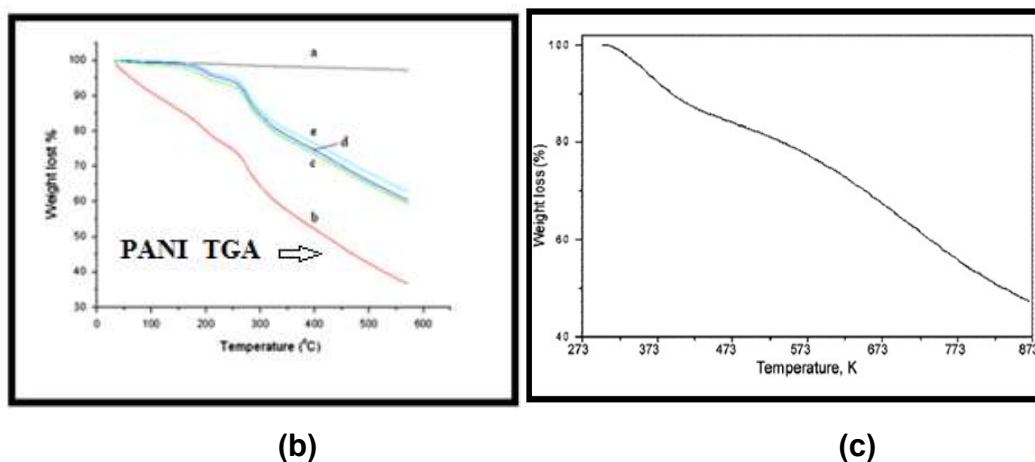
Fig. 4.5 TGA -DTA of Polyaniline (a) Our results (b) Source - Ref[45] (C)Source- Ref [46]

In this method the temperature of a sample is compared with that of an inert reference material during a programmed change of temperature. The temperature should be the same until thermal event occurs (melting, decomposition or the change in crystal structure). Figure 4.5 shows the TGA- DTA report of the polyaniline powder. TGA of polyaniline sample was performed under pure air atmosphere. The weight loss is in two steps. First for the temperatures range 45^0C to 340 ^{0}C and second, mass decrease between the temperature 340 to 500 ^{0}C. The total weight loss is 4.325 mg (67.002%). The first step of weight loss is due to the loss of moisture and the removal of dopants while second step of loss is for decomposition of polyaniline material. The TGA analysis of polyaniline reported by Amir Mostafaei et al. [45] and Amar Melad et al. [46] are also confirms our results. The polyaniline developed by us has more stability as seen from the graph.

4.3.4 Preparation of Polyaniline pellets and resistance measurement

It is difficult to find the resistance of the developed material. Therefore, pellets of PANI powder were prepared using the KBr pressing machine at C-MET, Pashan. The pressure applied for pellet preparation was 3 tones. The diameters and thickness of two pellets were 10mm & 2mm respectively. Contact leads were connected to the pellets using silver paste. The resistance measured using LCR

meter at frequency of 1KHz. (Agilent 4284A) and the observed values were 1.613 MΩ & 1.523 MΩ. The resistances of the pellets were also measured using potential divider method. Figure 4.6 shows the potential divider arrangement used for measurement of pellet resistance. The fixed resistor used in this case was 0.47MΩ. The observed values were ~ 6.520 MΩ and 5.275 MΩ for pellet 1 and 2 respectively under neutral conditions. The variation in resistance could be attributed to the change in contact resistance and minor variation in the pellet dimensions.

4.3.5 Electrical Properties

Thin films of PANI were formed on soda lime glass substrates of 1cm x 1cm dimensions by spin coat. Silver paste (99.9 % pure) was used to make contact using the copper wire with 200 μm diameter. The DC voltages were applied (0-35 volts) applied to the polyaniline films and current values were measured using Keithley's digital multimeter (2000 series).Figure 4.7 shows the resistance variation of PANI sample at room temperature. The I-V curve is quite linear and indicates that the resistance value is constant. It is in the order of 250 MΩ. The higher resistance could be attributed to film thickness.
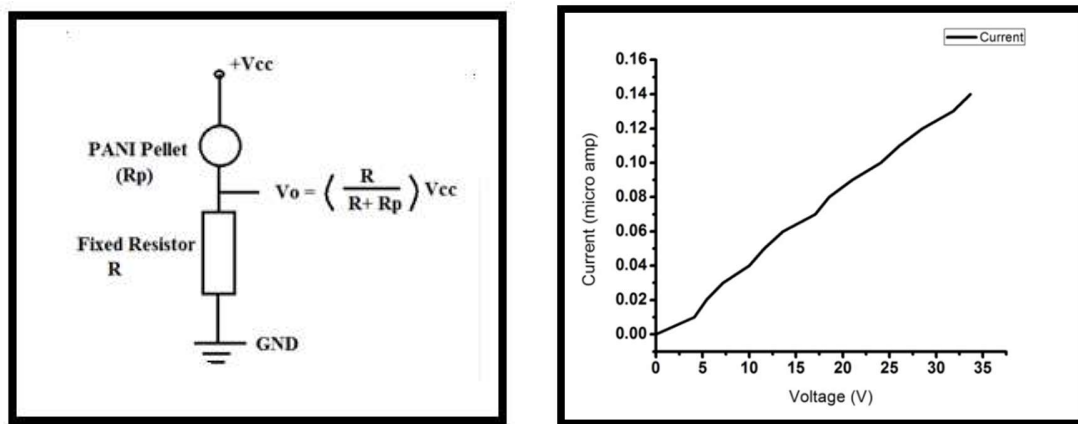
Fig.4.6 Potential divider arrangement Fig. 4.7 I-V characteristics of

Polyanilineto find pellet resistance

4.4 PANI Preparation and Characterisation (Sample 2)

To check the effect of method of preparation on polyaniline nature, we prepared another polyaniline material using p-toluene sulphonic acid (PTSA).First the 0.55 M solution of ammonium persulphate and 1.5M solution of PTSA were prepared. 0.5 ml aniline was mixed with PTSA solution. Ammonium persulphate were added to the mixture drop by drop and stirred the solution for 24 hours. The solution was filtered using Whatmen filter paper and Buckner flask (Time required = 5Min).The precipitate were collected and dried under IR for 25 minutes. The small chips of polyaniline were collected and powder is prepared from the same. The colour of the PANI powder was dark green indicating that PANI Emeraldine salt was formed. Weight of powder was 2 gram.

4.4.1 Structural and Morphological Characterisation of Polyaniline (Sample 2)

FT-IR spectrum was recorded on a Perkin-Elmer Spectrum RXFTIR system in the range of 4000-400 cm^{-1} using KBr pellets. X-ray diffraction patterns of the powder were obtained by employing JEOL JDX Services diffractometer using CuKα (Kα =1.54056 Å) radiation. The diffractometer was operated at 40Kv and 40mA. A scanning step of 0.1^0 in 2θ with a dwell time of 10s per step was used. The samples used for XRD were in powder form. The surface morphology was studied using scanning electron microscope (SEM) JEOL format (JSM-6360, Oxford instruments).

4.4.2 Results and Discussion

4.4.2.1 FT-IR Analysis

FT-IR spectra of PANI samples with PTSA are shown in figure 4.8. Out-of-plane bending deformation of C–H is observed at 569.54 cm^{-1} for PANI-(PTSA)[29]. The peaks at 677.76 cm^{-1} and 717.56 cm^{-1} with very weak intensities are attributed to out of plane wagging vibrations, which could be attributed to conformational deformation of rings in polymeric chain as reported by Manju Arora et al[47]. This indicates the polyaniline ES is formed with some deformations [15,20].
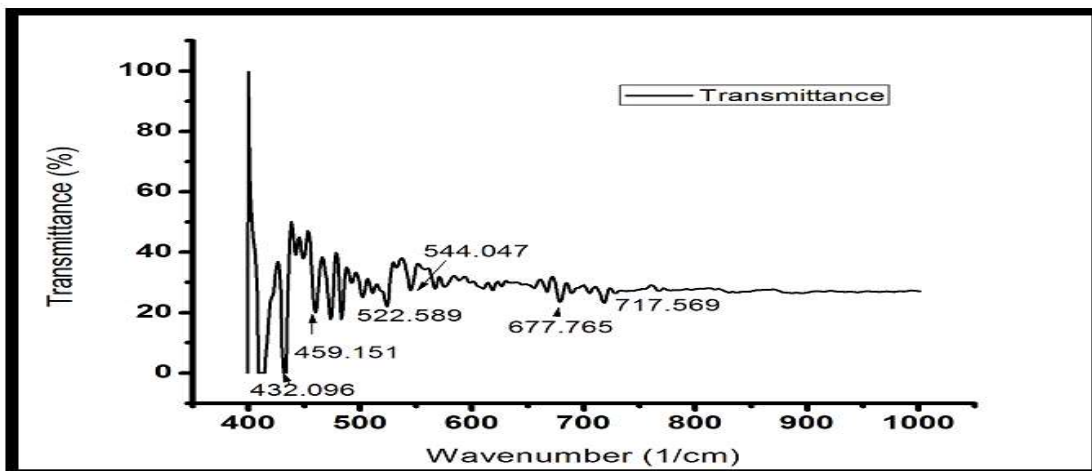
(a)
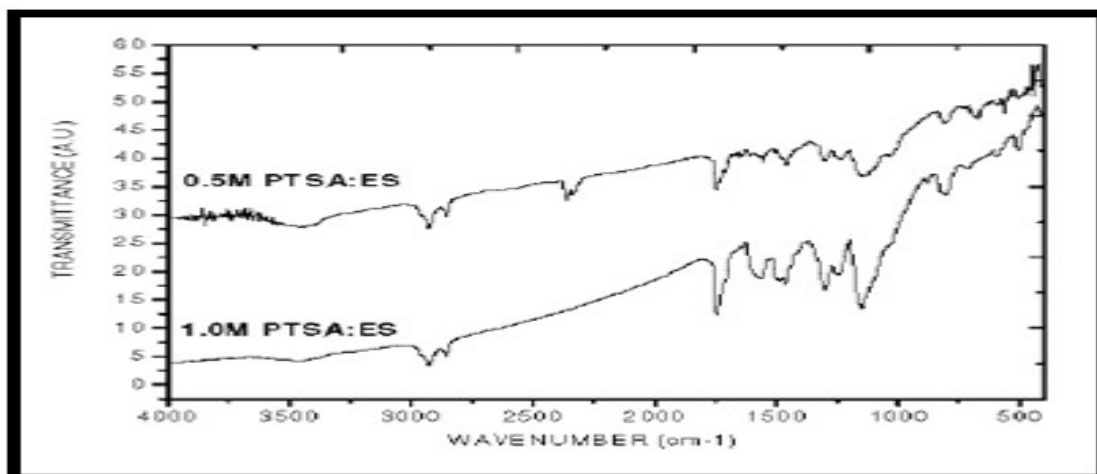
(b)
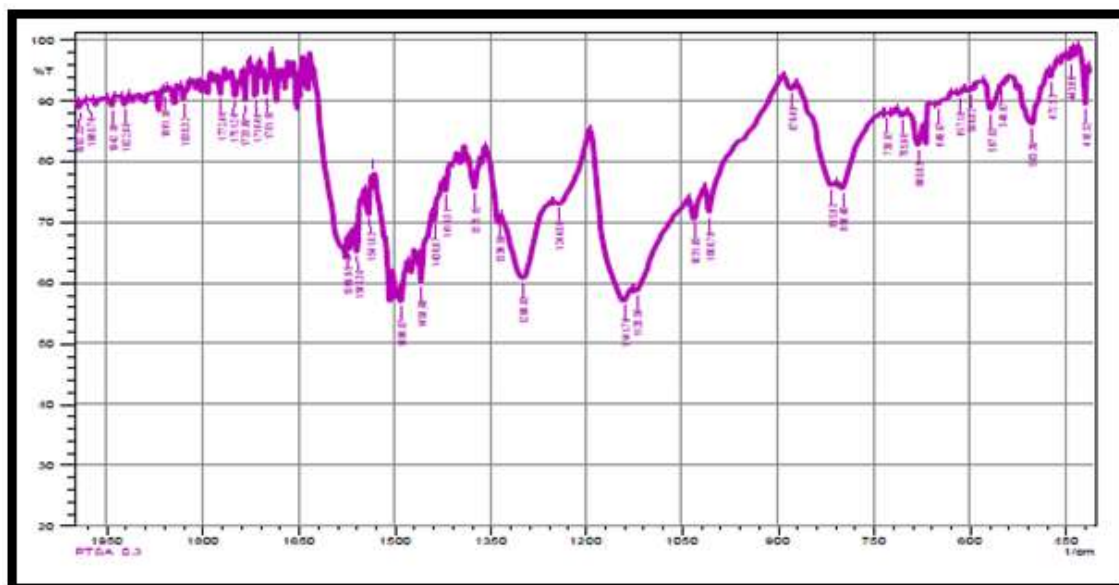
(c)

Fig. 4.8 FT-IR of Polyaniline (Sample 2) (a) Our results (b) Source-Ref[47](c) Source- Ref[29]

4.4.2.2 XRD Studies
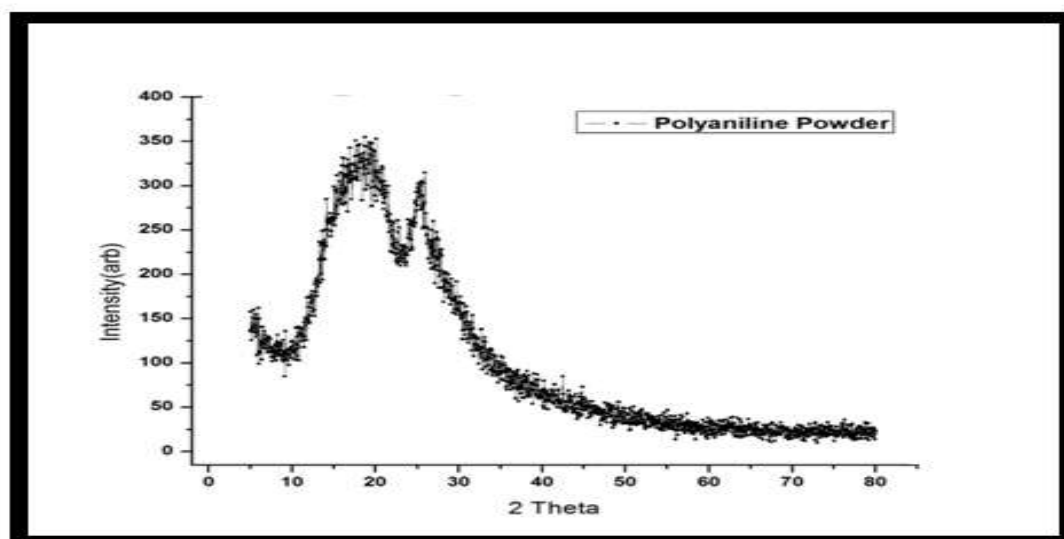
(a)
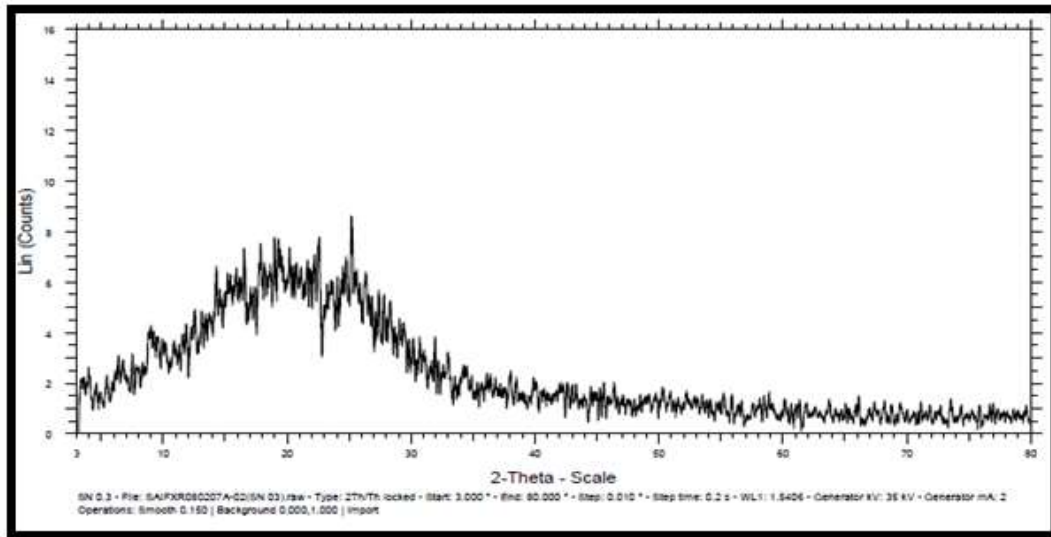
(b)

Fig. 4.9 XRD of Polyaniline (Sample 2) (a) Our results (b) Source- Ref [29]

Figure 4.9(a) shows the X-ray diffraction pattern for synthesized polyaniline. It shows the two peaks at $2\theta=18.88^0$ and 28^0 in the background of amorphous shoulder [24, 25], indicating that some part of the polyaniline sub chains become rigid and well ordered. Doped polyaniline is considered as the polymer cation-anion complex. Polyaniline could be treated as a poly-cation while TSA acts as an anion that allows an increase in interchain packing and thus higher structural order. This is similar to the accepted results of HCl doped polyaniline indicating the doped state is of the polyaniline emeraldine. The two peaks indicate significant crystallization of PANI on protonation indicating the conducting emeraldine phase of the polymer [29].Figure 4.9(b) shows the XRD of polyaniline studied by H Tui et al[29] ,which also shows that peaks indicate the same amount of crystallinity present in the developed material.

4.4.2.3 SEM Studies

In order to get the information regarding the structural arrangement of the material and surface morphology, SEM images were studied. Figure 4.10 shows the SEM

micrograph of polyaniline sample 2. This shows the more homogeneous and compacted agglomerated structure of polyaniline powder [26].
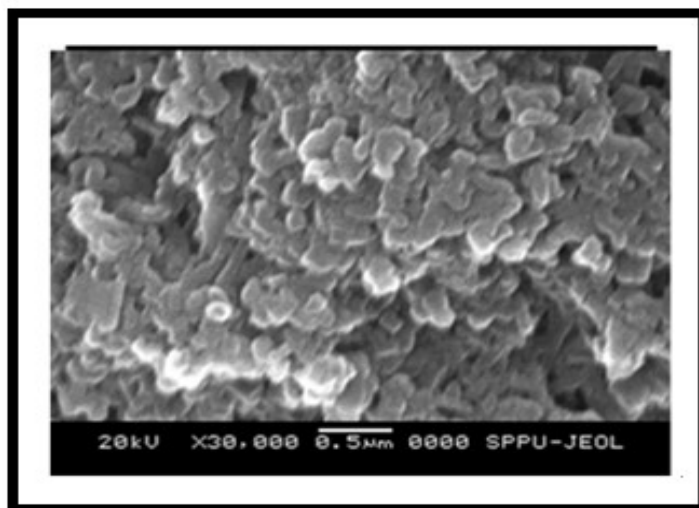
Fig.4.10 SEM of Polyaniline (Sample 2)

4.4.2.4 Electrical properties
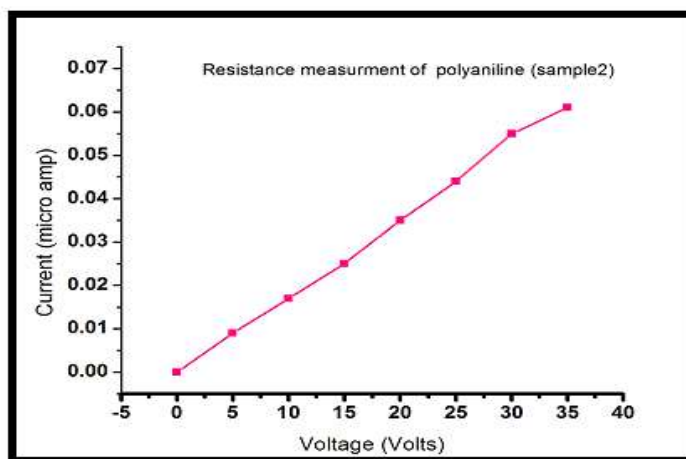
Fig. 4.11. Resistance measurement of Polyaniline thin film

Thin films of PANI were formed on soda lime glass substrates of 1cm x 1cm dimensions by spin coat. Silver paste (99.9 % pure) was used to make contact

using the copper wire with 200 µm diameter. The DC voltages were applied (0-35 volts) applied to the polyaniline films and current values were measured using Keithley's digital multimeter (2000 series). Figure 4.11 shows the resistance variation of PANI sample at room temperature. The I-V curve is quite linear and indicates that the resistance value is constant. It is in the order of 500 MΩ. The higher resistance could be attributed to film thickness and type of doping material used for polyaniline synthesis.

4.4.3 Conclusion

Polyaniline preparation is done using aniline and two different oxidant materials: potassium dichromate and ammonium persulphate. For the first case HCl aqueous solution was used as doping and for second case p-toluene sulphonic acid (PTSA) was used as doping. The structural and morphological characterization of both the materials was done using TGA-DTA, XRD, FTIR, and SEM. The conductivity depends on the doping concentration. In case of PTSA based synthesis the maximum yield were achieved for aniline/dichromate ratio of 2.0 to 2.4.

The XRD study of both the samples shows, small amount of crystallinity indicating the conducting nature of prepared polyaniline. The X-ray diffraction pattern obtained shows that the intensity in HCl doped polyaniline is higher than the PTSA doped polyaniline. This may results in higher crystallinity of HCl doped PANI than PTSA doped. This also shows that HCl doped polyaniline has better conductivity than the PTSA doped polyaniline.

FTIR measurement of the both samples shows the major characteristics peaks which are quite similar to reported by other researcher which confirm the chemical structure of the polyaniline is formed. The TGA study of the sample 1 shows the better thermal stability of the polyaniline material. SEM micrograph of the sample 2 shows the homogeneous and compacted agglomerated structure of the polyaniline obtained.

The electrical characterization of both the samples of polyaniline is done. For the first sample characterization the pellet is prepared and its resistance is calculated

using potential divider method. It showed the resistance of the order of 6 MΩ. Thin film of the same sample is prepared on glass substrate and I-V characteristics are studied by applying Ohm's law and the measured resistance was in the order of 250 MΩ. Same process is also applied to sample 2 and its measured value of resistance found to be in the order of 500MΩ. This shows that the polyaniline doped with HCl has higher conductivity than the PTSA doped polyaniline sample.

4.5 Synthesis of Polymer Nanocomposites

As discussed above the polyaniline is one of the most attractive materials among the variety of conducting polymers due to its unique electrical properties, environmental stability, easy fabrication process, and intrinsic redox reaction. However, the problems with these conducting polymers are their low processing ability, poor chemical stability, and mechanical strength [27]. There is a tremendous approach for the enhancement of the mechanical strength and characteristics of sensors by combining the organic materials with inorganic counterparts to form composites [27, 28].Accordingly, organic inorganic nanocomposite sensors have been developed by several research groups. Among the available inorganic materials, nanocrystalline SnO_2 is one of the most attractive and extensively used materials for detection of ammonia (NH_3), $H_2$and VOCs.

A number of researchers have already developed polyaniline/inorganic nanocomposite sensors. Conn et. al. [29] developed a polyaniline/PtO_2 based selective H_2 sensor and reported that the conductivity of polyaniline increases with H_2 exposure, due to the formation of water. It is known that water present in the polymer takes part in charge transfer promote to an increase in the conductivity of polyaniline which is reversible [30]. Wang et al. [31]developed polyaniline intercalated MoO_3 thin film sensors and reported that the conductivity change is due to the reversible absorption of analyte. Parvatikar et al. [32] developed polyaniline/WO_3 composite based sensors and reported that conductivity of the film increases with increasing humidity. Ram et. al. [33] developed conducting polymer/SnO_2 andTiO_2 nanocomposite thin film based sensors and found that conductivity of the film increases with NO_2 exposure. Geng et. al. [34] synthesized

polyaniline/SnO_2 hybrid materials by a hydrothermal process for gas sensing applications. They found that hybrid materials are sensitive to ethanol and acetone vapor at 60 to 90°C.

Tai et.al [28] fabricated TiO_2 nanocomposite for NH_3 and CO and reported that the films exhibits better response to ammonia NH_3 as compared to CO. They have used in-situ polymerization of polyaniline in presence of TiO_2 nanoparticles on the sensor substrate at different temperatures. The main drawback of this process is one cannot control the amount of TiO_2 nanoparticles going in the film. In case of nanocomposite, the ratio of the organic in-organic plays an important role in the morphology and gas sensing properties. Since SnO_2 is an n-type material and the polyaniline is a p-type semiconductor in nature their composite is expected to show a p-n junction diode characteristics as reported byN. G. Deshpande et.al. [20]. Thus, the electrical characteristics will be modulated by the ratio of polyaniline and SnO_2. Kondawar et. al. [19] also reported that polyaniline - SnO_2 nanocomposite formed by in-situ method of synthesis shows higher sensitivity to ammonia at room temperature. To take the advantage of this increased sensitivity of polyaniline - SnO_2 nanocomposite with additional sensitivity of SAW device. We proposed the SAW based polyaniline - SnO_2 nanocomposite gas sensor for the effective detection of ammonia and volatile organic compounds (VOCs).

In the Thesis, we have reported polyaniline- SnO_2 nanocompositethin film gas sensors working at room temperature. The nanocomposites were prepared by following solution route and in-situ method and compared the samples for characterization using XRD, FTIR and FE-SEM. The results of both the materials are compared on the basis of gas sensing responses.

4.6 Synthesis of Polyaniline- SnO_2 Nanocomposites

Nanocomposite preparation are usually based on two routes : (a) In-situ polymerization where pre-synthesized nanoparticles are mixed into the monomer solution followed by chemical or electrochemical polymerization.(b) one step redox reactions where simultaneous polymerization of aniline and formation of

nanoparticles takes place [1]. In the present research work we followed both the strategies to synthesize polyaniline- SnO_2 nanocomposite material and are explained in this section.

4.6.1 Synthesis of SnO_2 Nanoparticles

Sol-gel method was used for the synthesis of SnO_2 nanoparticles. In a typical method, 0.1M $SnCl_4$:H_2O was added in 1M starch solution and the mixture was stirred for half an hour. Then 0.2M ammonia was added drop wise in the solution under constant stirring. The stirring was continued for further 3 hours and then the solution was allowed to settle overnight. Supernatant liquid was then discarded carefully andthe remaining solution was centrifuged for 15 minutes and then filtered. The precipitate of SnO_2 was washed completely using distilled water to remove byproduct and the excessive starch those were bound with the nanoparticles. The product was dried in hot air oven at 90°C for overnight. Then powder was sintered at 700°C using oven for 6 hours and nanocrystalline SnO_2 was obtained [18,19, 22,48].

4.6.2 Synthesis of Polyaniline-SnO2 Nanocomposite

Sample 1.

Polyaniline - SnO_2 nanocomposite was synthesized by an in-situ polymerization of aniline in presence of synthesized SnO_2 nanoparticles using ammonium persulphate (APS) as an oxidant in acidic medium.Aniline (0.1M) and APS (0.1M) were dissolved separately in 1M HCl solution and stirred for 80 minutes. As-synthesized SnO_2 nanoparticles were suspended separately in 1 M HCl (100 ml) solution and sonicated for 90 minutes to reduce aggregation of SnO_2nanoparticles. 100 ml aniline solution and 10 ml SnO_2 nanoparticles suspension were mixed and further sonicated for 90 minutes. 100 ml APS solution was then slowly added drop wise to well disperse suspension mixture with continuous stirring. After 2 hours, a good degree of polymerization was achieved. The green color precipitate was obtained. The precipitate produced in the reaction was removed by filtration, washed repeatedly with 1 M HCl and dried at room temperature in dust free

environment. The composite powder was in conductive emeraldine salt (ES) form of polyaniline -SnO_2 nanocomposite [18, 19, 22,48].

Sample 2

The solution route technique was used to synthesize polyaniline- SnO_2 nanocomposite. In this technique, formation of nanocomposite process through an inorganic/organic interface reaction. 4g of $SnCl_4.5H_2O$ in 100 ml of double distilled water was stirred for half an hour and its pH was maintained ≤ 4 using 0.1M HCl. 20 ml hydrogen peroxide (H_2O_2) was added in the above solution, which oxidized tin ions to tin oxide. The solution turned into a white colour suspension of SnO_2 and this reaction mixture was mixed with 0.1M aniline and kept below 4°C.0.1M ammonium persulphate solution was added in the above mixture at room temperature, the colour of the solutions was turned to blue and then to green after few minutes. The precipitate produced in the reaction was removed by filtration, washed repeatedly with 1 M HCl and dried under vacuum for 30 hours. The composite powder was conductive emeraldine salt (ES) form of polyaniline-SnO_2 nanocomposite[18, 22,48]. Figure 4.12 illustrates the process of PANI- SnO_2 nanocomposite formation.
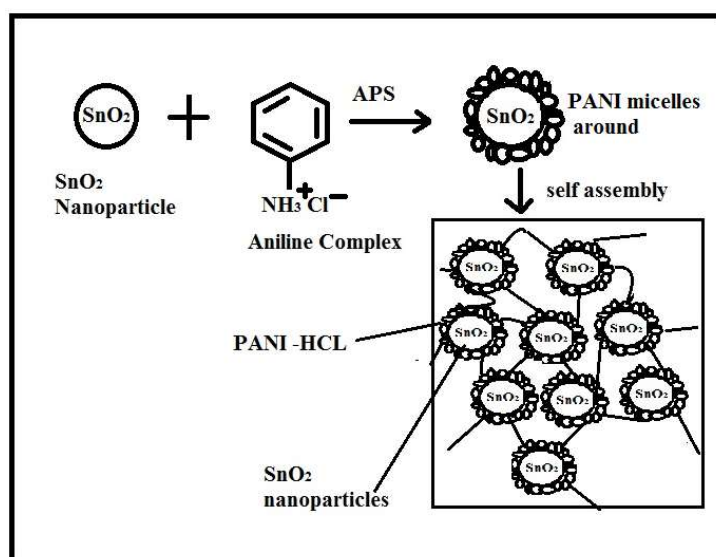
Fig.4.12 PANI -SnO_2 nanocomposite formation (for Sample 1)

4.6.3 Structural and Morphological Characterisation of PANI -SnO₂ Nanocomposite

The FTIR spectra of synthesized product were recorded by using Bruker spectrophotometer in the wavenumber range of 400-4000 cm^{-1}. Phase identification of the composite was done by X-ray diffraction using Bruker AXSD8 diffractometer with Cu-Kα radiation source. The morphological study of the composite was carried out by field emission scanning electron microscope (FESEM- Nova NanoSEM NPEP303), and SEM JEOL, OXFORD instruments.

4.7 Results and Discussions

The results on the morphological and structural analysis of polyaniline,SnO_2 nanoparticles and polyaniline -SnO_2 nanocomposite are described and discussed in this section

4.7.1 SEM Study of Tin-dioxide Nanoparticles

Figure 4.13 shows the SEM micrograph image of synthesized SnO_2 nanoparticles. The micrograph shows that the particle size is not uniform. The minimum particle size observed was close to 100nm. Shape of the particles was spherical as well as rod shape.
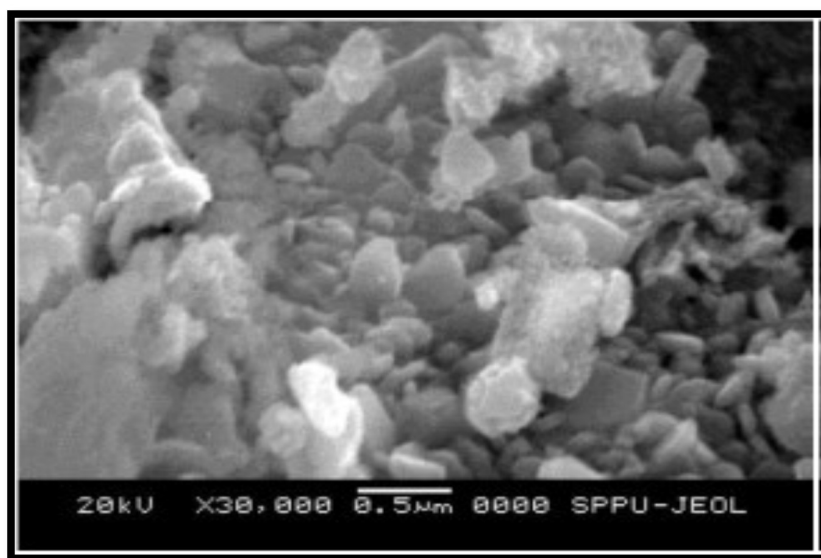
Fig .4.13 SEM of SnO₂ nano particles[48]

4.7.2 EDAX of SnO₂ Nanoparticles
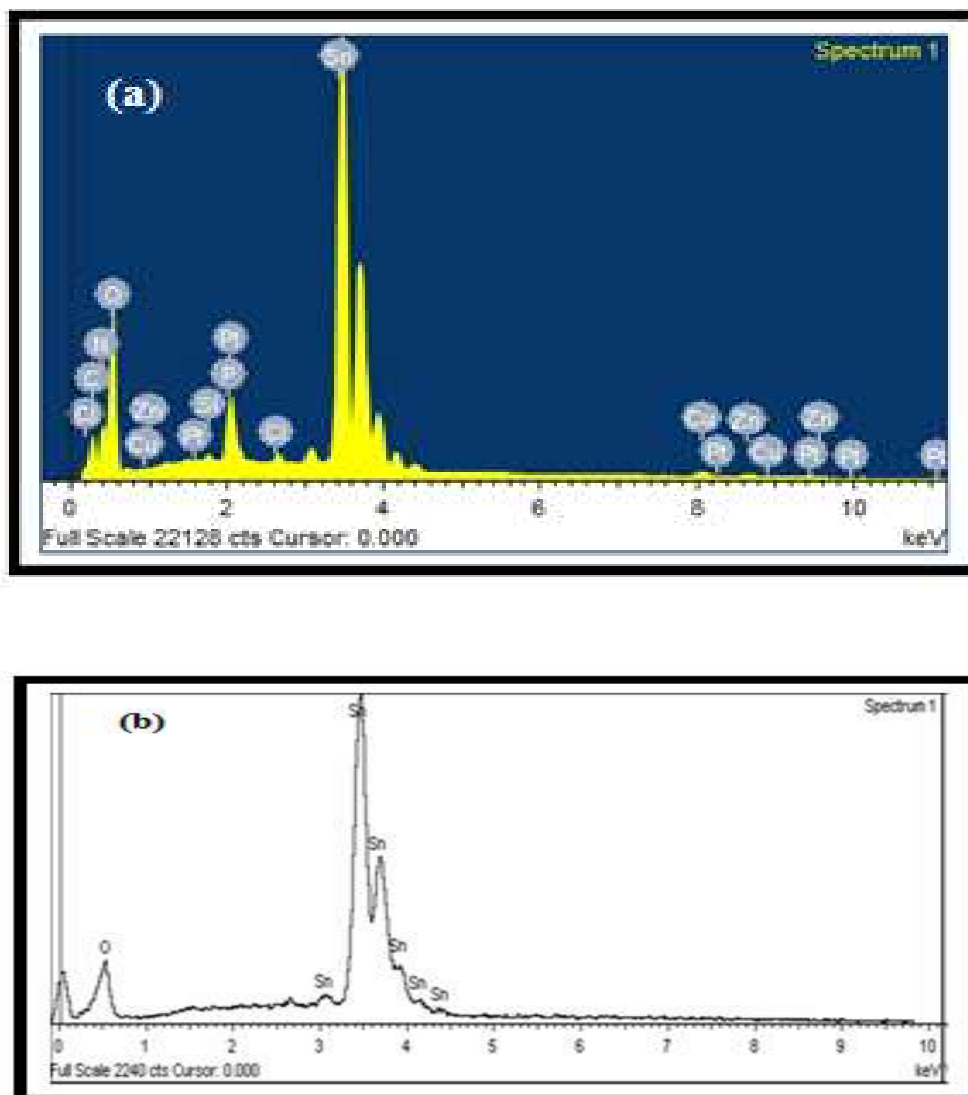
Fig.4.14 EDAX of SnO₂ nanoparticles (a) Our Results (b) Source- Ref[36].

Table 4.1 EDX Spectra showing the Atomic percentage of Sn and O species

Elements	C	O	N	Sn	Cl
Atomic Weight %	19.07	67.15	4.78	7.22	0.15

The chemical composition analysis of SnO_2 nanoparticles was performed by energy dispersive analysis by X-ray (EDAX). Figure 4.14 shows the EDAX spectra of SnO_2 nanoparticles. The EDAX analysis exhibits prominent peaks of **Sn** and **O** elements, which indicates the existence of Sn: O elements. Table 4.1 illustrating their atomic percentages. The peak of 0.3 keV represents the carbon film holder used for the analysis [42]. In graph the Pt peak was observed at 2 keV which shows the contact material used for analysis was platinum. Other impurities could be added during sample preparation for SEM analysis. The results confirm that final nano powder is comprised of pure tin oxide, with Sn:O atomic percentage only determined in the sample. This confirms the formation of SnO_2 nanoparticles. Figure 4.14(b) reported by S. Blessi and et al. shows the similar nature of Sn and O peaks.

4.7.3 FTIR of SnO_2 Nanoparticles
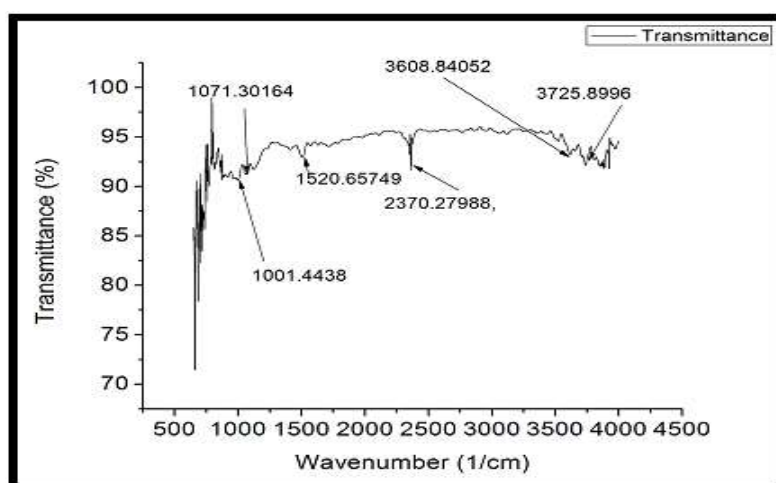
(a)
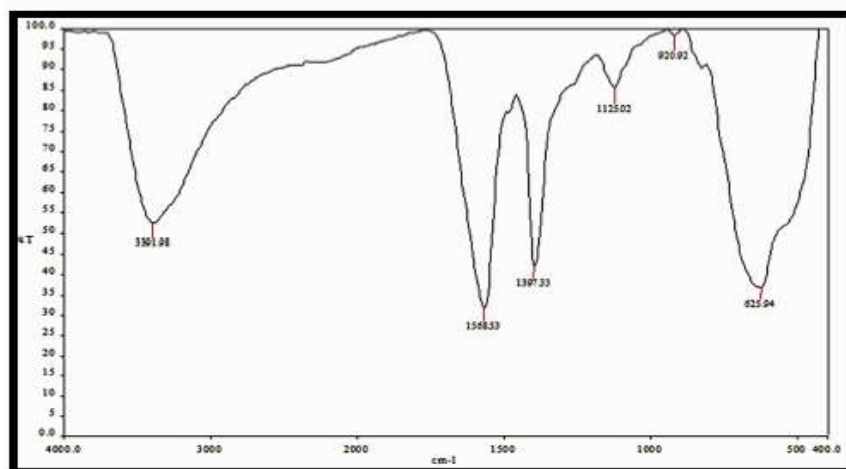
(b)

Fig.4.15 FT-IR of SnO$_2$ nanoparticles (a) our results (b) Source- Ref[36]

The chemical structure of the nanoparticles was characterized by Fourier Transform Infrared (FTIR) spectroscopy. Figure 4.15 shows the FTIR of SnO$_2$ nanoparticles. In the FTIR spectrum the characteristic peaks at 3608 cm^{-1}is attributed to OH groups of adsorbed water bound at SnO$_2$ surface while peak at 1001cm^{-1}and 1071cm^{-1} is due to C-H stretching mode. Peak at 1520cm^{-1} may also be related to bending vibrations of water molecules in SnO$_2$ sample [17, 18, 19]. The similar spectra were observed by S. Blessi[36] as shown in the figure 4.15(b). In this figure the scale is taken with lower values to observe the spectra properly. Thus it shows the characteristics of tin-dioxide and we can say the resultant material is SnO$_2$ nanoparticles.

4.7.4 FTIR of Polyaniline-SnO$_2$ Nanocomposites

Figure 4.16 shows the FTIR spectra of polyaniline-SnO$_2$ nanocomposites (sample 1 and sample 2). All the major characteristics peaks are present in both the spectrum. In the FTIR spectrum the characteristic peaks at 3062.45cm^{-1}, 3204.24 cm^{-1}& 1681.24cm^{-1} correspond to C-H stretching vibrations, and C=C stretching vibrations respectively. Peaks at 1607.
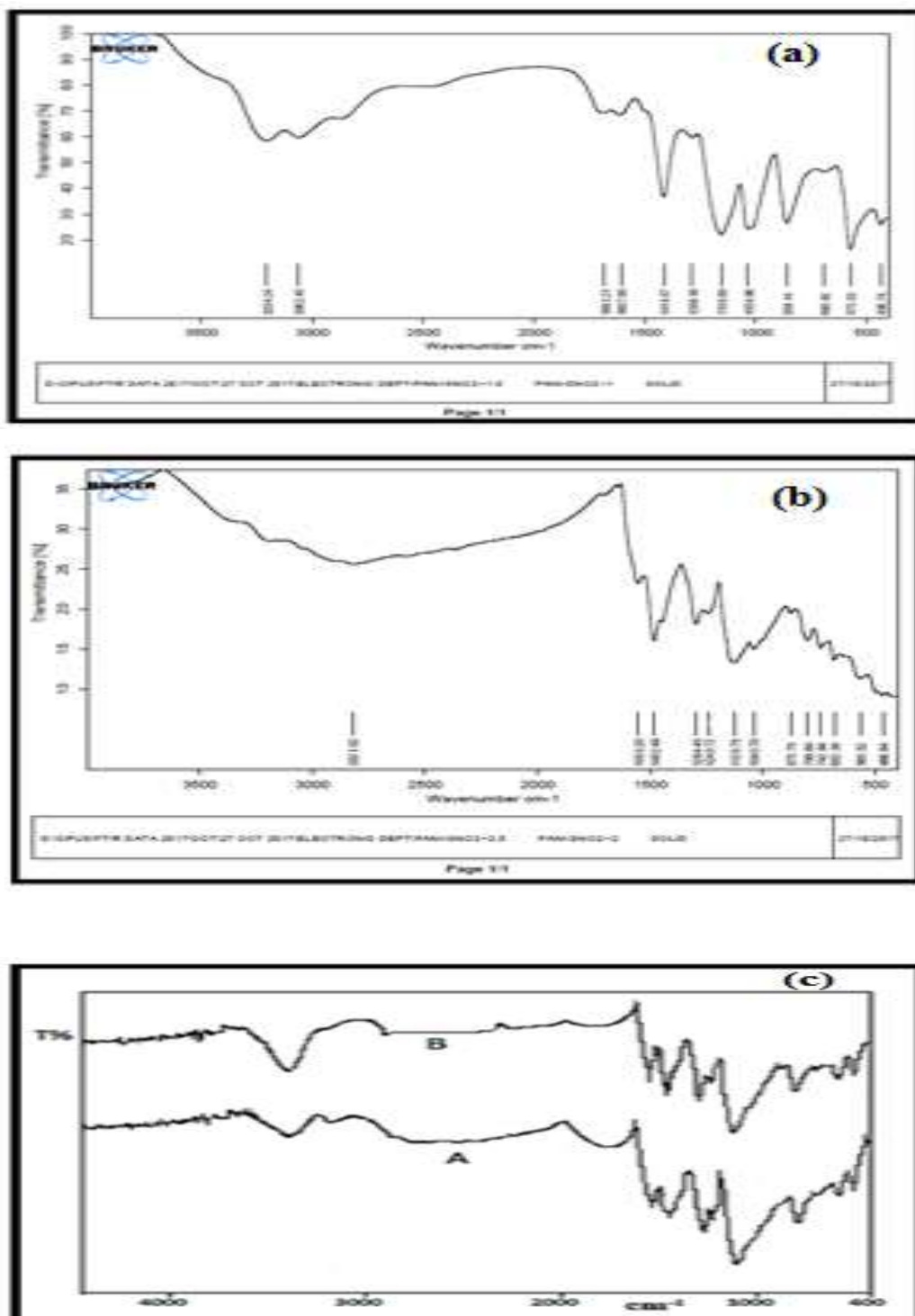
Fig. 4.16 FT-IR spectra of polyaniline-SnO2 nanocomposite (a) Sample1 (b) Sample 2 (C) FTIR of PANI-SnO$_2$[source- Ref.[19].

80cm^{-1} and 1414.57cm^{-1} correspond to quinoid and benzene rings of polyaniline, while the peak at 690.92 cm^{-1} corresponds to the anti-symmetric Sn-O-Sn mode [21, 13]. Kondawar et al observed similar results for tin oxide-polyaniline nanocomposite, thus, it shows the characteristics of polyaniline as well as the tin oxide. The peaks are slightly shifted; this could be due to the method of material preparation carried out.

4.7.5 XRD of Polyaniline –SnO$_2$ Nanocomposite

(a) [48]   (b)

(c)   (d)
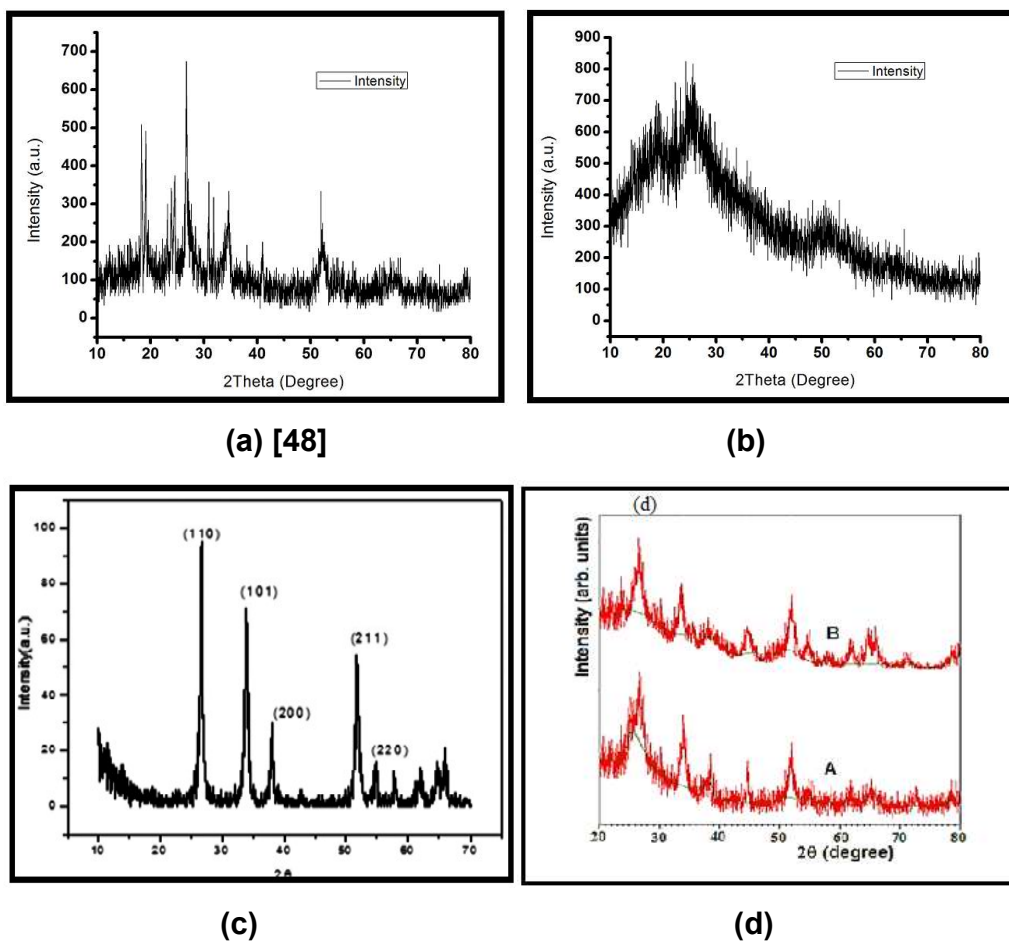
Fig 4.17 XRD of polyaniline -SnO$_2$ Composite (a) Sample 1(b) Sample 2 (c) XRD of PANI, SnO$_2$ and PANI- SnO$_2$ nanocomposites[Source-Ref.[36] (d) XRD of PANI- SnO$_2$ nanocomposites [Source-Ref[19].

Figure 4.17 shows the XRD pattern of the obtained polyaniline-SnO_2nanocomposites. It can be seen that the nanocrystalline SnO_2 peaks are observed (figure 4.17(a)) at 2θ values of 26.58^0 4.90^0, 38.14^0, 52.13^0, 66.12^0 and matched with those peaks along planes (1 1 0), (1 0 1), (2 0 0), (2 1 1), and (3 0 1) having primitive tetragonal structure (*JCPDS DATA CARD 41-1445*). The XRD spectrum peaks are close to the standard XRD of SnO_2. However, these peaks show a small shift (0.20^0 to 0.50^0) from their respective standard positions which may be due to polyaniline matrix. In addition, we observed relatively larger peak broadening, compared with XRD of pure SnO_2 [19, 48].This suggests that tin oxide is present in the polyaniline matrix, and presence of polyaniline has influenced the preferred orientation of tin oxide grains in the composite to some extent. The lattice constant was found to be *a* = *b* = 4.741 Å, *c* = 3.31. Peaks in Figure 4.17 are similar to those observed by other researchers as shown in figure 4.17(c) and figure 4.18(d) reported by S. Blessi and S. Kondawar respectively[19,20,36]. This confirms the formation of polyaniline- SnO_2 nanocomposites (sample 1). But some of the peaks are missing and few broad peaks were observed at 2θ = 20^0, 27 ^{0}&52.13^0 in figure 4.17(b) for sample 2. This clearly indicates that the sample 2 has less crystallinity as compared to sample 1 and the composite is PANI dominant.

4.7.6 FE-SEM of Polyaniline-SnO_2 Nanocomposites

The surface morphology of synthesized PANI - SnO_2 nanocomposite was analyzed by Field emission - scanning electron microscopy (FE- SEM). Figure 4.18 shows the field emission scanning electron microscopic (FE-SEM) image of polyaniline-SnO_2 nanocomposite (sample1 and sample 2). The images were taken at different points on the material. At few places particle structure were observed like the fibrous nano rods as shown in figure 4.18(a)-(b). As shown in figure 4.18 (c)-(d) the shape of nanoparticles were nanorods as well as nano pellets with their length varying from ~450-700nm. The average diameter of the particles was around 100 nm. Many researchers showed that SnO_2nanoparticles exhibits granular structure [38-40]. From figure 4.18 (b), it is also observed that there are

large globules present, which proves that PANI cells get deposited on SnO_2 particles. Thus, the results of XRD, FTIR and FESEM have provided clear evidence that polymerization of aniline has been successfully achieved on the surface of SnO_2 nanoparticles.
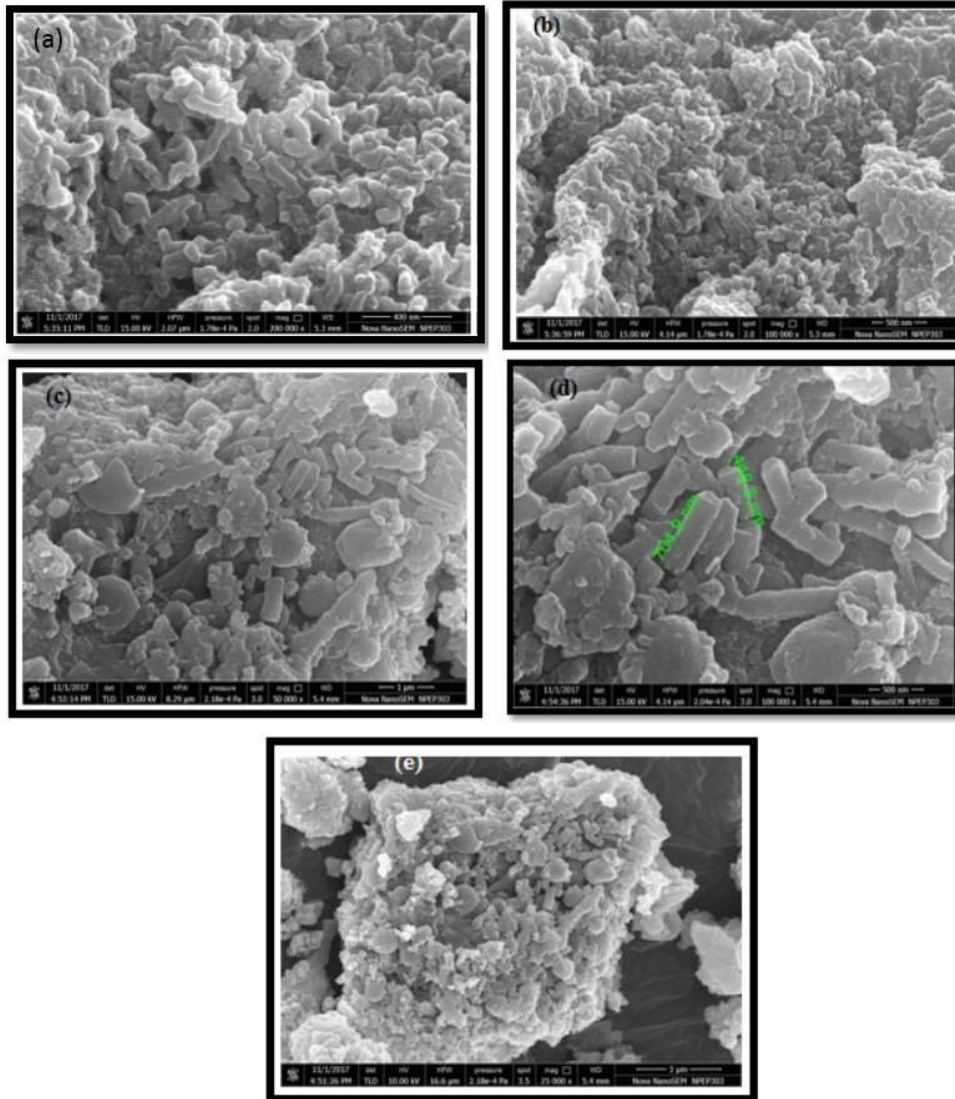
Fig. 4.18 FE-SEM of polyaniline-SnO_2 Nanocomposite (a) - (b) Sample1, (b) - (e) Sample 2

4.7.7 EDAX of Polyaniline-SnO₂ Nanocomposites
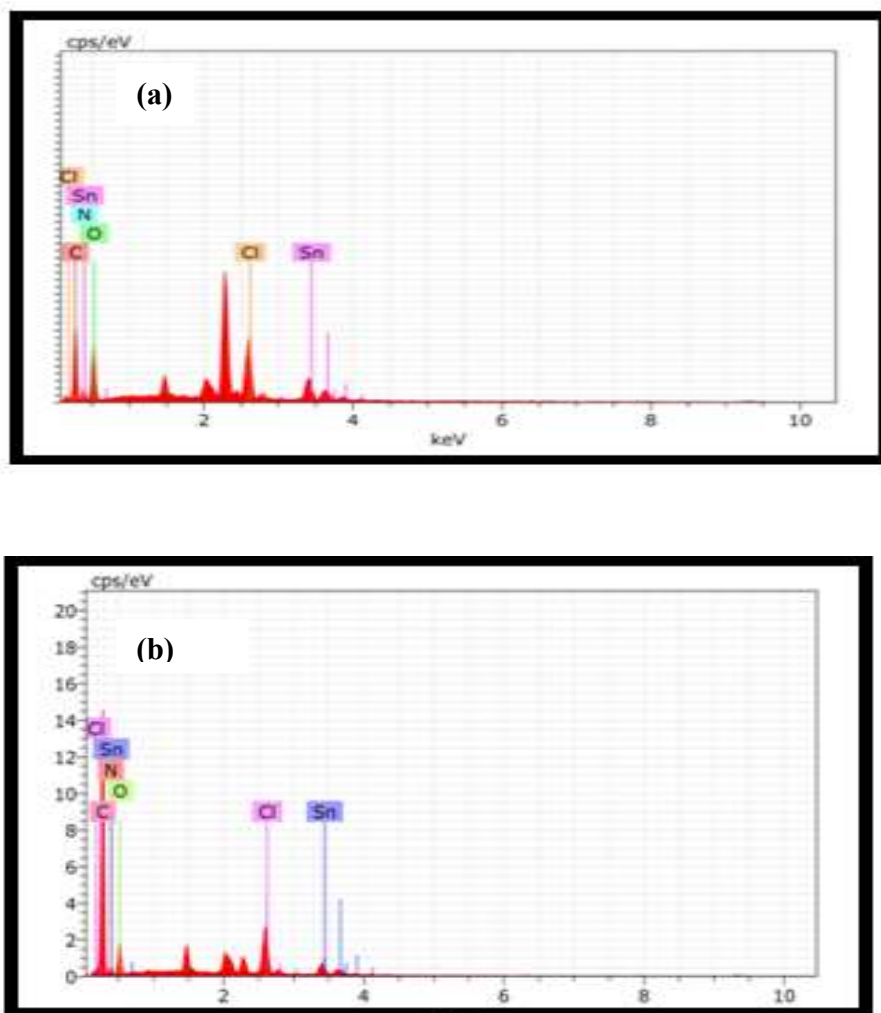
Fig 4.19 EDAX of PANI-SnO₂ nano composite (a) Sample 1 (b) Sample 2.

Study of the chemical composition of samples by the technique of EDAX microanalysis is shown in Figure 4.19. The figure shows the prominent peaks for Sn, O, C, and N.I t also shows the peaks chlorine(Cl) with very small percentage. This could be due to the impurities present during composite formation or during measurement. Measurements were performed in different regions of the sample surfaces [4].

Table 4.2 EDX Spectra showing the Atomic percentage of Sn, O, C species (sample 1)

Elements	C	O	N	Sn	Cl
Atomic Weight %	48.86	30.33	16.39	1.42	3.00

Table 4.3 EDX Spectra showing the Atomic percentage of Sn, O, C species (sample 2)

Elements	C	O	N	Sn	Cl
Atomic Weight %	73.35	12.78	11.03	0.74	2.00

Table 4.2 and 4.3 lists atomic weight values of Sn, O and C. The higher percentage of C indicates the PANI is also present into the composite. The presence of Sn, O, and C confirms the formation of SnO_2 nanoparticles in polymer matrix [48]. Both the table shows the variation in the atomic weight percentage of C, O, Sn, This could be attributed to the synthesis method of PANI -SnO_2 nanocmoposite. Table 4.3 show the higher percentage of C than as reported in table 4.2, which could be attributed to the higher percentage of PANI than tin oxide in sample 2.

4.8 Conclusions

Polyaniline-SnO_2nanocomposite were prepared by using two different methods :(a) By an in-situ polymerization of aniline in presence of synthesized SnO_2 nanoparticles using ammonium persulphate (APS) as an oxidant in acidic medium, where the nanoparticles were prepared using sol-gel method (b) The solution route technique was used to synthesize polyaniline-SnO_2 nanocomposite. SEM and EDX study of nanoparticles were carried out and it showed the appropriate content of Sn, O elements with negligible content of other impurities which could be added during synthesis process. The structural and morphological study of PANI-SnO_2 nanocomposite was carried out using XRD, FTIR and FE-SEM. XRD study showed the crystalline peaks indicating that tin nanoparticles are formed in the polymer

matrix. These peaks show a small shift (0.20^0 to 0.50^0) from their respective standard positions which may be due to polyaniline matrix. From XRD study, it can be observed that the sample 2 has less characteristics peaks as compared sample 1 which could be attributed to less crystallinity. The FT-IR study showed all the absorption peaks for N-H, C-H stretching, bending, quinoid, benzene aromatic rings, and also anti-symmetric Sn-O-Sn mode. This proves the PANI- SnO_2 composite is formed. FE-SEM study showed the composite with nanorods present having length around 450-700 nm and average diameter close to 100 nm. The EDAX spectrum also proves the presence of required (Sn, O, C) elemental composition for polyaniline- SnO_2 nanocomposites formation. Thus, using above discussed methods the polyaniline-SnO_2 nanocomposite material can be synthesized for gas sensing applications.

Since both the materials PANI and PANI- SnO_2 nanocomposite has been synthesized well and from their characterization it is found that PANI (sample1) and PANI- SnO_2 nanocomposite (Sample 1) are ready to use as sensing material for ammonia and VOCs. In the next chapter the results o PANI and PANI- SnO_2 nanocomposite based ammonia and VOCs sensing using chemiresistor and SAW device are discussed.

References

[1] Tanushree Sen, Satyendra Mishra and Navinchandra G. Shimpi, "Synthesis and sensing applications of polyaniline nanocomposites: a review"RSC Adv., 2016, 6, 42196–42222.

[2] Alcaser L., Conducting Polymers: Special Applications, Dorhrecht, Holland,(1987).

[3]Tapan K. Das & Smita Prusty,"Review on Conducting Polymers and TheirApplications",Polymer-Plastics Technology and Engineering, 51: 1487–1500, 2012.

[4]Ratheesh and K. Viswanathan, IOSR Journal of Applied Physics (IOSR-JAP)2278-4861. Volume 6, Issue 1 Ver. II PP 01-09, (Feb. 2014).

[5]Advanced Functional Molecules and Polymers, Volume 3, Hari Singh Nalwa,(2001).

[6] Sahoo N. G., Rana S, Cho JW, Li L, and Chan SH. Polymer nanocomposites based on functionalized carbon nanotubes. Prog. Polym Sci 2010; 35: 837-867.

[7]R. Ratheesh and K. Viswanathan,"Chemical Polymerization of Aniline Using Para-toluene Sulphonic Acid"IOSR Journal of Applied Physics (IOSR-JAP).

[8]Y. Liu and M. L. Liu, "Growth of aligned square-shaped SnO2 tube arrays," Adv. Funct.Mater., vol. 15, pp. 57–62, 2005[cross reference]

[9] G. Wallace, G. Spinks, and P. Teasdale, Conductive electro-active polymers. USA: Technomic Pub. Co. Inc., 1997.

[10]]A. Z. Sadek, A. Trinchi, W. Wlodarski, K. Kalantar-zadeh, K. Galatsis, C. Baker and R. B.Kaner, "A room temperature polyaniline nanofiber hydrogen gas sensor," in Proc. of IEEE Sensors Conf., 2005, pp. 207-210[cross reference].

[11] J.C. Chiang and A. G. MacDiarmid, "Polyaniline: Protonic acid doping of the emeraldine form to the metallic regime," Synth. Met., vol. 13, pp. 193-205, 1986[cross reference].

[12] J. G. Roh, H. R. Hwang, J. B. Yu, J. O. Lim, and J. S. Huh, "Oxidant effects on

polypyrrole and polyaniline sensor for several volatile organic gases," J. Macromol.

Sci,

Pure Appl. Chem., vol. A39, pp. 1095-1105, 2002.

[13]K. C. Persaud, "Polymers for chemical sensing," Materialstoday, pp. 38-44, April 2005.

[14] J. N. Barisci, C. Conn, and G. G. Wallace, "Conducting polymer sensors," Trends Polym. Sci., vol. 4, pp. 307-311, 1996.

[15] Alexander V. Streltsov Olga V. Morozova, Nataliya A. Arkharova, Vera V. Klechkovskaya,Irina N. Staroverova, Galina P. Shumakovich, Alexander I. Yaropolov,"Synthesis and Characterization of Conducting PolyanilinePrepared by Laccase-Catalyzed Method in SodiumDodecylbenzenesulfonate Micellar Solutions",Journal of Applied Polymer Science, Vol. 114, 928–934 (2009) @ 2009 Wiley Periodicals, Inc.

[16]Vivek Talwar,"Gas Sensing properties of Polyanilinetin oxide nanocomposites", imperial journal of interdisciplinary Research (IJIR), Vol-2, Issue -9, 2016.

[17] Ch. Gee, S. Douin, C. Crepin, Ph. Brechignac,"Infrred spectroscopy ofaniline($C_6H_5NH_2$) and its cation in a cryogenic argon matrix", Chemical Physics Letters,338,(2001),130-136.

[18] P. Chowdhury ,B. Saha,"Potassium dichromate initiated polymerization of aniline",Indian Journal of Chemical Technology, Vol. 12,November 2005, pp 671-675.

[19] Kondawar SB,S. P. Agrawal, S. H. Nimkar, H. J. Sharma, P. T. Patil"Conductive polyaniline-tin oxide nanocomposites forammonia sensor", Adv. Mat. Lett. 2012,3(5):393-398.

[20] N.G. Deshpande , Y.G. Gudage , Ramphal Sharma , J.C. Vyas , J.B. Kim, Y.P. Lee ,"Studies on tin oxide-intercalated polyaniline nanocomposite for ammonia gas "Sensors and Actuators B 138 (2009) 76–84.

[21] Matnishyan AA et. al, Journal of ContemporaryPhysics, 2010, 45(5):246–250.

[23]L.I.Nadaf, K.S.Venkatesh, M.A.Gadyal, Mohammed Afzal,"Polyaniline-Tin Oxide Nanocomposites: Synthesis and Characterizatio",OSR Journal of Applied Chemistry (IOSR-JAC),e-ISSN: 2278-5736.Volume 9, Issue 2 Ver. II (Feb. 2016), PP 55-61.

[24] Geng Li-na," Gas sensitivty of polyaniline/SnO_2 hybrids to volatile organic compounds",Trans. Nonferrous Maet. Soc. China 19(2009) s678-s683.

[25] Hui Xu,Junlong Zhang, Yong Chen, Hailin Lu ,Junxia Zhuang ," Electrochemical polymerization of polyaniline doped with Cu^{+2} as the electrode material for elecrochemical supercapacitors", RSC Advances 2014,5547-5552.

[26] Sreela Pal Basak, Baishali Kanjilal, Priyabrata Sarkar,Anthony P. F. Turner," Application of electrical spectroscopy and amperometry in polyaniline modified ammonia gas sensor", Synthetic Metals 175(2013) 127-133.

[27] Rosanny C. Silva, Marina V. Sarmento, Roselena Faez, Roger J. Mortimer andAdriana S. Ribeiro,

"Electrochromic Properties of Polyaniline-Based Hybrid Organic/Inorganic Materials",*J. Braz. Chem. Soc.*, Vol. 27, No. 10, 1847-1857, 2016.

[28] S. G. Pawar , S. L Patil , M. A. Chougule ,A. T. Mane, B. T. Raut, P.R. Godse, Shashwati Sen,V. B. Patil, "Room Temperature Ammonia Gas Senor Based on Polyaniline- TiO_2 Nanocomposite", IEEE Sensors Journal Vol. 11 No. 12, December 2011.

[29] H. Tai. Y.Juang, G. Xie, J.Yu, and X. Chen," Fabrication and gas sensitivity of polyaniline -titanium dioxide nanocomposite thin film", Sensors and Actuators B, Vol. 125, pp 664-650,2007.

[30]C.Conn,S.Sestak, A. T. Baker, and J. Unsworth, "A polyaniline-based selective hydrogen sensor," Electroanal., vol. 10, pp. 1137-1141, 1998[cross referewnce].

[31]T.Taka,"Humidity dependency of electrical conductivity of doped polyaniline," Synth. Met., vol. 57, pp.5014-501, 1993[cross referewnce].

[32] J. Wang, I. Matsubara, N. Murayama, S. Woosuck and N. Izu, "The preparation of polyaniline intercalated MoO3 thin film and its sensitivity to volatile organic compounds," Thin Solid Films, vol. 514, pp. 329-333, 2006.

[33] N. Parvatikar, S. Jain, S. Khasim, M. Revansiddappa, S. V. Bhoraskar, and M. A. Prasad, "Electrical and humidity sensing properties of polyaniline/WO3 composites,"Sens. Act. B: Chem., vol. 114, pp. 599-603, 2006. [cross referewnce].

[34]M. K. Ram, O. Yavuz and M. Aldissi, "NO2 gas sensing based on ordered ultra-thin films of conducting polymer and its nanocomposite," Synth. Met., vol. 151, pp. 77-84, 2005.

[35]L. Geng, Y. Zhao, X. Huang, S. Wang, S. Zhang, and S. Wu, "Characterization and gas sensitivity study of polyaniline/SnO2 hybrid material prepared by hydrothermal route," Sens. Act. B: Chem., vol. 120, pp. 568-572, 2007.

[36] S. blessi, M. Maria,Lumina Sonia, S. Vijalaxmi ,S. Pualine," Preparation and characterization of SnO_2 nanoparticles by hydrothermal method", International journal of ChemTech Research,vol.6,No. 3, pp 2153-2155.

[37] R. C. Abruzzi,B. A. Dedavid, J .R. Pires," Characterization of tin dioxide nanoparticles synthesized by oxidation", Ceramica 61(2015) 328-333.

[38] L. Nejati-Moghadam, A.Esmaeill Bafghi-karimabad,M. Salavati - Niasari, H. Safardoust," synthesis and Characterization of SnO_2 nanoparticles prepared by a facile precipitation method", Journal of nanostructures 5 (2015) 47- 53.

[39]Shang Zhan , Dongmei Li, ShengfaLiang, Xin Chen ,Xia Li,"Novel Room temperature Ethanol Gas Sensor based on SnO2 doped poly-iallylimethylammonium,Chloride",Sensors,doi:10.3390130404378;13 (2013)pp 4378-4389.

[40] D. S. Sutrave,G. S. Shahane , V. B. patil, L.P. Deshmukh," Micro-crystallographic and optical studieson Cd,Zn,Se,Thin films", Mat. Chem Phy.;65(2000) pp298-305.

[41]D. R. Patil thesis(2007), North Maharashtra University ,Jalgaon.

[42] Naif Mohammed Al-Hada , ID , Halimah Mohamed Kamari , Anwar Ali Baqer Abdul H. Shaari and Elias Saion,"Thermal Calcination-Based Production of SnO_2 Nanopowder: An Analysis of SnO2 Nanoparticle Characteristics and Antibacterial Activities", Nanomaterials 2018, 8, 250.

[43]S.D. Charpe, F.C.," Raghuwanshi, P.P. Raut , G. T. Lamdhade":Synthesis and Structural Properties of Nanocomposite of PANI/ ZnO by in-situ polymerization" Research journal of Chemical Science, Vol. 6(5), 27-33, May (2016)

[44] Anil G. Sonkusare, 1Sachin Tyagi, 2Ranjan Kumar, 1Sunita Mishra,"Room Temperature Ammonia Gas Sensing Using Polyaniline Nanoparticles Based Sensor", International Journal of Materials Science, Vol. 12, Number 2 (2017), pp. 283-291.

[45] Amir Mostafaei AshkanZolriasatein," Synthesis and characterization of conducting polyaniline nanocomposites containing ZnO nanorods"Progress in Natural Science: Materials International 2012;22(4):273–280.

[46]*Omar Melad and Mariam Jarur,"* Studies On The Effect Of Doping Agent On The Structure Of Polyaniline" Journal of Chemistry and Chemical technology Vol. 10, No. 1, 2016.

[47] Manju Arora and S.K. Gupta,"Vibrational Spectroscopy of PTSA - Doped Polyaniline" American Institute of Physics 978-0-7354-0606-3/08

[48] Varade PS, Gangal SA, Shaligram AD, *"Synthesis, characterization of polyaniline –SnO$_2$ for volatile organic compounds"* December 2017, IJRSE..

CHAPTER 5

EXPERIMENTAL STUDIES ON POLYANILINE AND POLYANILINE - NANOCOMPOSITES BASED GAS SENSORS

5.1 Introduction

In the chapter 4, the synthesis and characterization of PANI and PANI-SnO$_2$ nanocomposite is carried out. From their characterization it is confirmed that the material are ready for gas sensing application. This chapter deals with the study of sensing responses of developed polyaniline(PANI) and polyaniline-tin oxide(PANI- SnO$_2$) nanocomposite materials for ammonia and selected VOCs(Ethanol, methanol, acetone and toluene) for their different concentrations at room temperature. In addition to this the mass loading effect and evaporation studies of VOCs is also reported. The information regarding test gas is also briefed in this chapter. The responses of the developed materials are tested using chemiresistor (IDT) and surface acoustic wave (SAW) devices. The materials are tested for 25-100 ppm of ammonia concentration and 200-1000 ppm of ethanol, methanol and acetone. For toluene the materials were tested within 100-300 ppm range. The response -recovery time and percentage response were measured for the sensors and are discussed. The response of laboratory developed SAW delay line performance is compared with the responses of SAW IC SIPAT (LB 211 DS 01) for the ammonia and VOCs.

5.1.1 Test Gas Information

Need for acetone gas sensing

Acetone (C$_3$H$_6$O) is a colourless liquid, with characteristics odor. The vapor is heavier than air and may travel along the ground. The distant ignition is possible. Acetone is commonly used as a chemical reagent in industries and it easily evaporates at room temperature. Continuous exposure to acetone may cause headache and fatigue to the workers [1]. It irritates the eyes and the respiratory part. Acetone also reacts with chloroform and bromoform under basic conditions, causing fire and explosion hazard. It may have effects on the blood and bone marrow, therefore detection and measurement of acetone concentration in the

workplace is necessary for our safety and health. Hence there is need to develop gas sensors to detect acetone.

Need for ethanol gas sensing

Ethanol (CH_3CH_2OH) is one of the volatile and flammable liquids. It is colourless liquid and burns with a smokeless blue flame which is not visible sometimes in normal light. Ethanol is a powerful psychoactive drug and is not a carcinogen. But the first metabolic product of ethanol in the liver is acetaldehyde, which is more toxic, mutagenic, and carcinogenic. Pure ethanol will irritate the skin and eyes. It is widely used as anti-tissues agent in laboratories. Its exposure may lead to nausea, omitting and intoxication which are the symptoms of ingestion. Long term exposure can result in serious liver damage. Hence it is necessary to develop gas sensors which may effectively detect the ethanol.

Need for methanol sensing

Though methanol(CH_3OH) is an alcohol similar to ethanol, it is very dangerous in large quantities. While methanol does form in small amounts during fermentation and is fine to consume in things like commercially produced wine or beer, the concentration you find in things like home brewed gin, rum and other spirits can poison you. Unlike ethanol, when consumed, methanol in the human body is converted into formic acid. The same substance found in ant poison. A build-up of formic acid resulting from this can cause transmission problems, liver damage and a number of other symptoms up to and including nerve damage, permanent blindness and kidney failure. Thus it is necessary to detect the methanol concentration to avoid above discussed problems. Therefore it is better to develop a gas sensor which could detect methanol.

Need for toluene sensing

Toluene ($C_6H_5CH_3$) is a colorless, non-corrosive, flammable liquid with an aromatic odor similar to that of benzene. The odor threshold for toluene ranges between 2.5 and 8 ppm, and is irritating at 750 ppm. Toluene is a leading petrochemical building block and is also used as a solvent and an octane enhancer in gasoline. Toluene is a central nervous system (CNS) depressant, and a skin and mucous membrane irritant – severe dermatitis may result from its drying and defatting action. Other effects observed in humans after accidental or intentional inhalation (abuse situations) include renal (kidney) toxicity, cardiac arrhythmias, and blood dyscrasias, enlargement of the liver and developmental abnormalities. Therefore it is necessary to develop a gas sensor for toluene detection [2].

Need for Ammonia (NH3) sensing

Ammonia is most commonly produced chemical in industrial processes. It is also exist naturally in environment and in human breathing. It is also beneficial for agriculture and fertilizers. In the environment ammonia is a part of nitrogen cycle and is basically produced in soil from the bacterial processes.   Anhydrous ammonia gas is lighter than air that is why it may rises, so that generally dissipates and does not settle in low -laying areas.   But in the presence of moisture the liquefied   anhydrous ammonia gas converted into vapors which are heavier than air. Exposure to high concentrations of ammonia is air generally causes burning of nose, throat and respiratory zone. This may results in bronchiolar and alveolar edema and airpath destruction which in turn damages the respiratory. Its odor provides adequate early warning of its presence but it may damages the olfactory, reducing awareness of one's olfactory fatigue or adaptation, reducing awareness of one's long term exposure at low concentrations. Rapid skin or eye irritation is occurs at its low concentration exposure while it high concentration exposure may results in severe injury and burns. Thus it is important to develop gas sensors for ammonia detection.

Flammability limits or an explosive limit gives the amount of combustible gases in a mixture, between which limits this mixture is flammable. Gas mixtures consisting of combustible, oxidizing, and inert gases are only flammable under certain conditions. The lower explosive limit (LEL) describes the leanest mixture that is still flammable, i.e. the mixture with the smallest fraction of combustible gas, while the upper explosive limit (UEL) gives the richest flammable mixture.

Lower Explosive Limit (LEL)

The explosive limit of a gas or a vapor is the limiting concentration (in air) that is needed for the gas to ignite and burst out. LEL is the lowest concentration of a gas or a vapor in air capable of producing a flash of fire in presence of an ignition source (arc, flame, heat). At concentration in air below the LEL there is no fuel to continue an explosion. Gas concentrations lower than LEL are "too lean" to burn.

Upper Explosive Limit (UEL)

Highest concentration of a gas or a vapor in air able of producing a flash of fire in presence of an ignition source. Levels of concentration higher than UEL are much higher to burn. The Occupational Safety and Health Administration (OSHO) have a set of upper concentration limit in work for the workers safety and welfare. In table 5.1 the UEL, LEL and cut off exposure limits recommended by OSHO for test gases are listed.

Table 5.1: OSHA specified standards for chemical hazards [1, 2]

Test gas	Exposure limit by OSHO(ppm)	Lower explosive limit (LEL)(ppm)	Upper Explosive limit (UEL) (ppm)
Ammonia	50	150000	280000
Acetone	1000	26000	128000
Ethanol	1000	33000	190000
Methanol	1000	67000	380000
Toluene	200	12000	710000

5.1.2 Coating of chemical interface

PANI powders were dissolved in *N*-methyl pyrrolidone (NMP) solvent at a weight ratio of 0.1. The mixed solution was agitated for 24 hours continuously, and then filtered. Prior to the application of the coating layer, the surface of the IDT was cleaned in acetone, ethanol and de-ionized (DI) water and dried under IR radiations using IR lamp for 10 minutes. Its resistance was measured on Keithley's electrometer - 614. It showed infinity resistance. On LCR meter (Agilent 4284A) the resistance measured at 1 KHz frequency was 2.21MΩ. The other parameters are also measured and are reported in appendix C. Then, a PANI layer was drop casted and spread it over the IDT surface uniformly. The thickness of the PANI was approximately 2 μm, as measured by gravimetric method. The IDT was kept in desiccators for 24 hours at room temperature (~28 ^{0}C). Figure 5.1 shows the IDT structure used for experimentation. .

Fig. 5.1 Interdigital transducer (IDT) used for gas sensing.

5.1.3 Gas sensing Set-up

Figure 5.2 shows the set-up used for testing the PANI responses to ammonia using chemiresistors (IDT). The glass chamber of 500cc was used as test chamber with inlet valve to insert the amount of gas using syringe. This is a static measurement system.
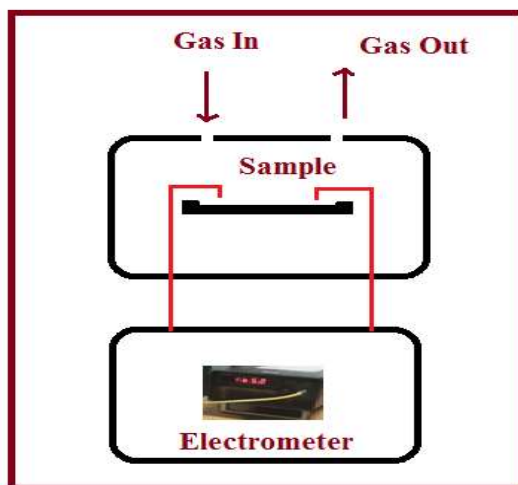
Fig.5.2. Gas sensor (Chemiresistor) characterization system

The electrometer (Keithley -614) was connected outside the chamber to measure the change in resistance of the sensor. All the measurements for chemiresistor were carried out using electrometer). The senor (Sample S10-3) was tested for ammonia for different concentrations (25-100 & 200 ppm).

5.1.4 PANI film coated Chemiresistor (IDT) based ammonia sensor

The performance of PANI deposited sensor was tested for different concentrations of ammonia at room temperature using the above explained labmade characterization system. For the PANI film sensor having metallic contacts were kept in the test chamber of known volume with electrical leads taken out for measurements. A fixed amount of (25 ppm) of ammonia gas was injected into the test chamber, the film resistance measured with respect to time (for every 30 seconds interval), until it reached a steady value. This procedure was followed once again after removing ammonia and exposing the test chamber to clean air. These steps were repeated for different concentrations of ammonia (25-100 & 200 ppm). The results of the measurements are reported in following section.

5.1.3 Results and discussions for PANI ammonia sensor
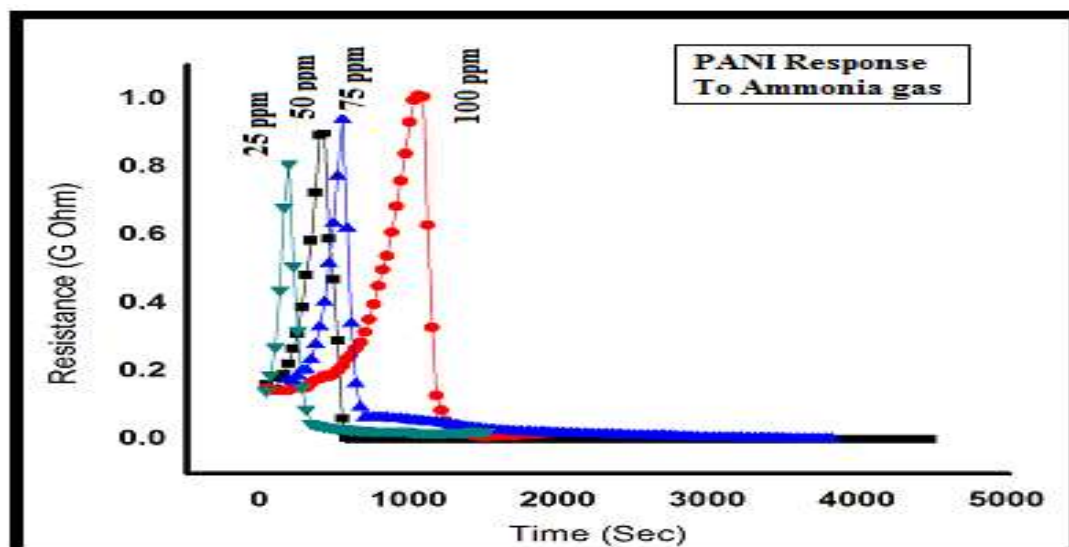
(a)
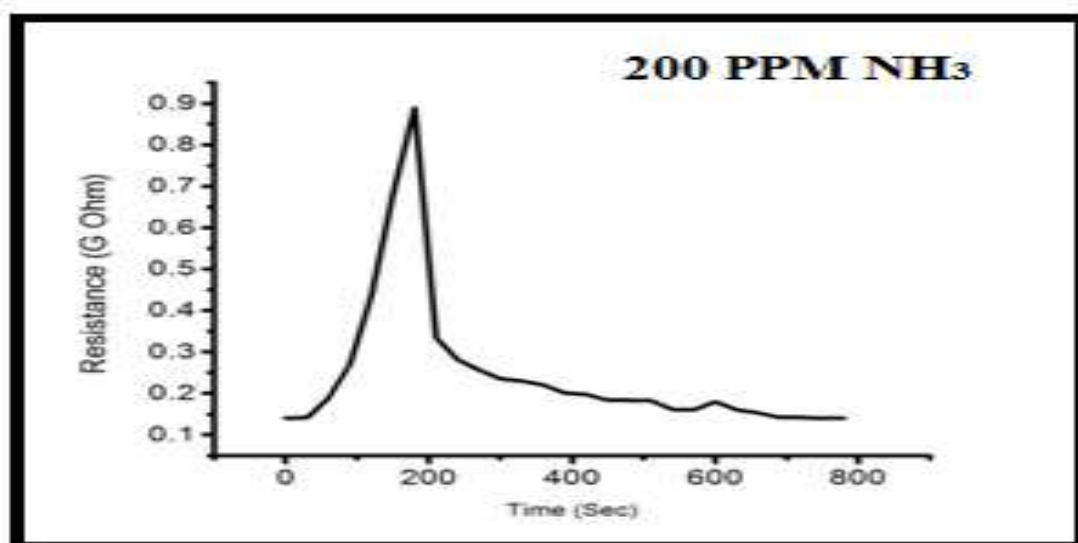
(b)
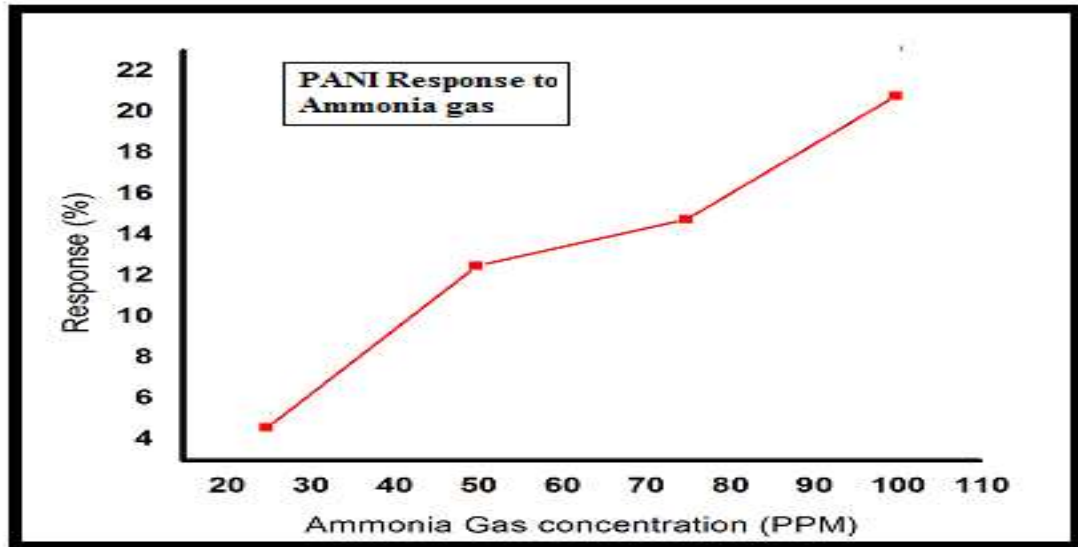
(c)
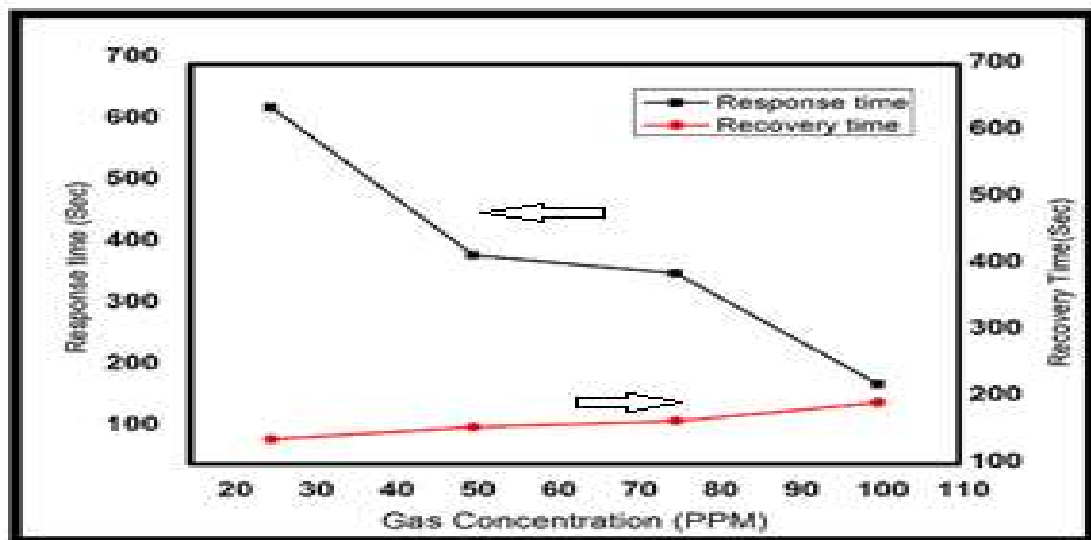
(d)

Fig. 5.3 (a) PANI Chronometric Response to Ammonia for (25-100) ppm
(b) at 200 ppm (c) PANI response to different concetrations of ammonia
(d) Response -recovery times for different concentrations of ammonia.

Figure 5.3(a) shows the polyaniline response to different concentrations of ammonia gas. The graphs shows the change in resistance, on the exposure of ammonia to polyaniline deposited IDT sensor. The resistance increase upto its

saturation value. As the natural air is purged to the sensor the desorption of ammonia takes place and its resistance falls dramitacally . The time required for desorption is less than for absorption this could be attributed to the large surface area of the sensor and less number of gas molecules.They may have less binding with the sensing layer.Figure 5.3(b) also shows the polyaniline response to ammonia at 200 ppm. It follows the same nature as reported in figure 5.3(a). The observed response is faster than the lower concentrations of ammonia. This fast response could be attributed to the large number of molecules available for surface reactions to take place.

Figure 5.3(c) shows the PANI reponse to different concentrations(25-100 ppm) of ammonia. It shoes that as the concentration of ammonia increases the response and ulitimately the relative sensitivity also increases. For small concentrations of ammonia, there is a lower surface reaction took place due to lower coverage of ammonia molecules on the grain surface. As increase in ammonia concentration, the number of the surface reactions and sensitivity also increases.

Gas response (S) is defined as the ratio of the change in resistance of the sensor after the exposure to the target gas to the original resistance in air. It is expressed as [1, 4]:

$$S = \frac{R_g - R_a}{R_a} \tag{1}$$

Where, R_a and R_g are the resistance of sensing materials in air and in a target gas medium respectively.

Figure 5.3(d) shows the relation between the response/recovery times and gas concentration. The response time (t_{res}) is the time required for the sensor to respond to a step concentration change from zero to a   certain concentration value(90%) . Recovery time (t_{rec}) is the time it takes for the sensor signal to return to its initial value after a step concentration change from a certain value (90%) to zero. It shows that as the gas concentration increases the response time decreases and recovery time increases. The decrease in response time is basically due to large number of molecules are available for the surface reaction

to takes place. At higher concentrations the adsorbed /absorbed molecules takes longer time to get desorbed and hence the recovery time increases with increase in gas concentrations. Table 5.2 below shows the response /recovery times and relative sensitivity of PANI with the sample S10-3 for the different concentrations of ammonia.

Table 5.2: Response/recovery times and sensitivity of PANI to ammonia

Gas Concentrations (ppm)	Response time(s)	Recovery time(s)	Relative Sensitivity (%)
25	630	90	4.6
50	390	110	12.5
75	360	120	14.77
100	180	150	20.8

5.1.4 Gas Sensing Mechanism

As shown in figure 5.3(a) The resistance of the PANI increases on exposure of ammonia. When the gas is released the resistance decreases and reaches to its initial value. Polyaniline is a p-type material and when it iteracts with ammonia(NH_3) there is reduction in charge carrier density. Since the majority carriers (holes) density gets decreased due to electron donating nature of NH_3 gas. This results in decreasing the conductivity of material and film resistance increases[1,3,4]. The following paragraph explains the same mechanism with the help of chemical reactions .

It is well known that during synthesis of PANI with HCl acid, the protonation reaction takes place as given below.

$$PA + HCl \longrightarrow PAH^+ + A^- \qquad (2)$$
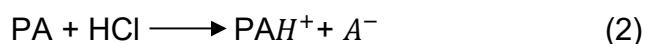
Where, PA- and PAH^+ are undoped and doped repeated block of PANI, respectively. As a result of the above equation 2, a neutral PANI molecule takes

proton and result in forming energetically favorable N^+-H chemical bonds. Therefore positively charged local centers placed at nitrogen are formed which in turn permits the hoping of valence electron from one such center to another , results in to rise of P- type conduction[2].When PANI reacts with ammonia, the following reversible reaction take place.

$$PAH^+ + NH_3 \longleftrightarrow PA + NH_4^+ \tag{3}$$
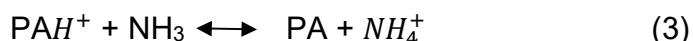
In the presence of ammonia, the above reaction goes predominantly toward right side: ammonia molecule gain proton from PANI thus forming energetically more favorable ammonium (PANI doping reaction). If it is exposed to natural air (no ammonia), the reaction (3) begins to go towards the left. Ammonium decomposes into ammonia and protons which being added to PANI molecule restore to initial level of doping [1, 3].

5.1.5 Chemiresistor (IDT) based VOCs sensor

The performance of PANI deposited sensor was tested for different concentrations of VOCs (ethanol .methanol acetone and toluene) at room temperature using the above explained labmade characterization system. For this PANI film sensor having metallic contacts were kept in the test chamber of known volume with electrical leads taken out for electrical measurements. A fixed amount of (200 ppm) of each VOC gas was injected into the test chamber, the film resistance measured with respect to time (for every 30 seconds interval), until it reached a steady value. This procedure was followed once again after removing VOCs and exposing the test chamber to clean air. These steps were repeated for different concentrations of VOCs (200-1000). The results of the measurements are reported in following section.

5.1.6 Results and Discussions

a) For Ethanol
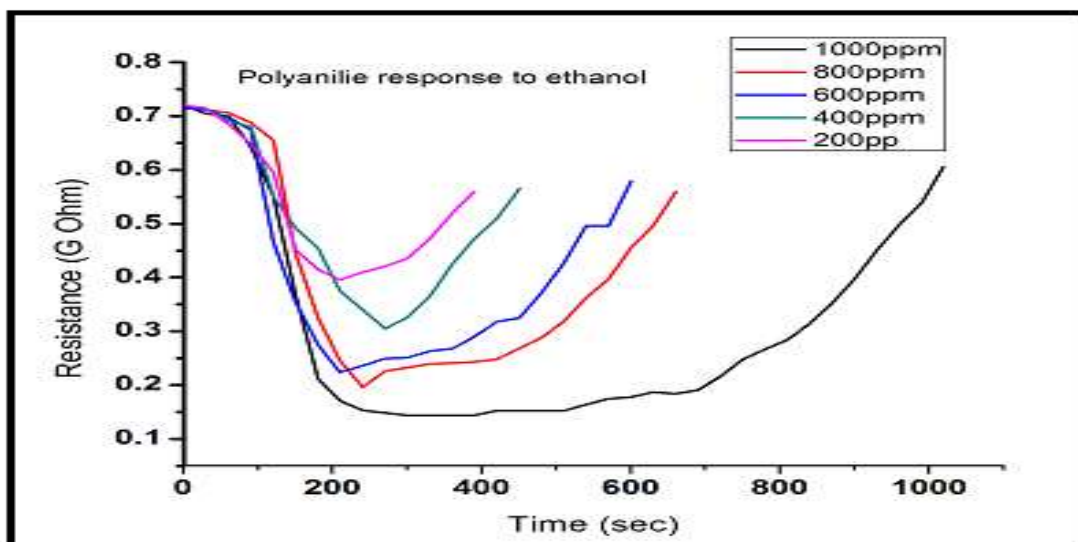
(a)
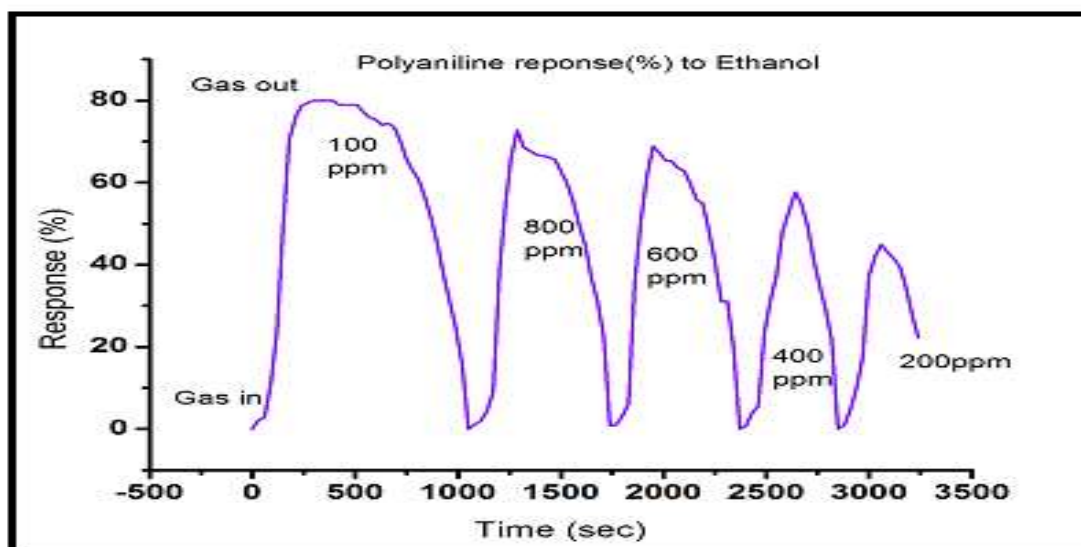
(b)
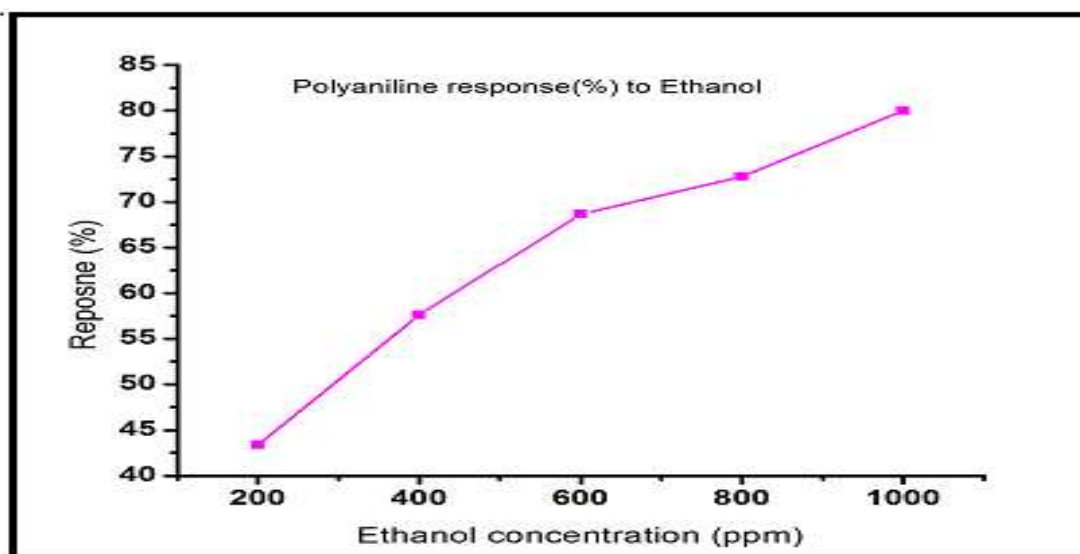
(c)
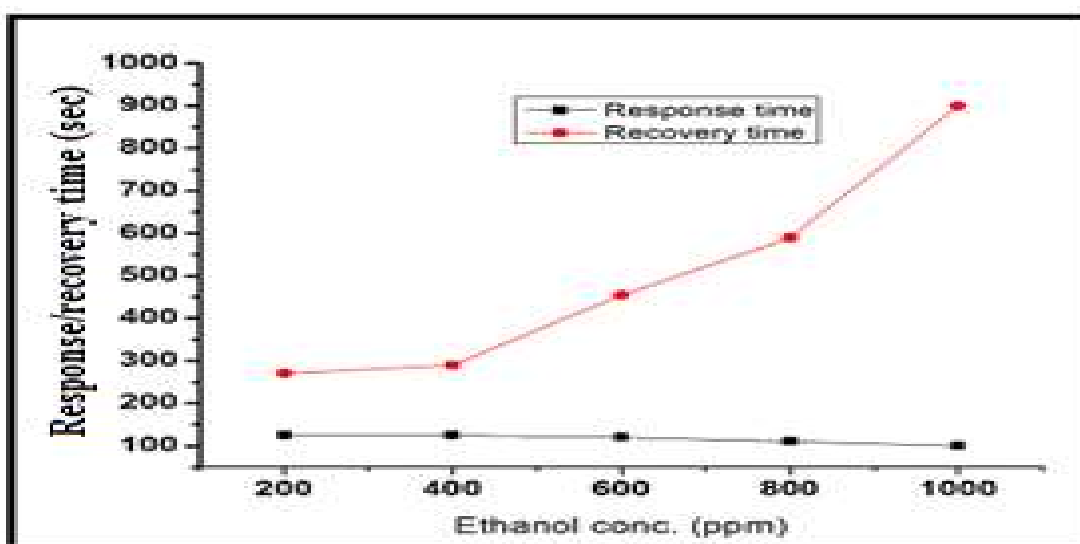
(d)

Fig.5.4 (a) PANI sensor resistances change with time (b) PANI sensor chronometric response to ethanol at different concentrations (c) PANI response vs. ethanol concentrations. (d) Response -recovery times vs. gas concentration.

Figure 5.4(a) shows the change in resistance of PANI coated sensor, which shows that the on the exposure of gas, resistance decreases with time. Initially the change

is large, after certain concentration, adsorption of ethanol becomes small and the change in resistance also becomes low. Figure 5.4(b) shows the PANI sensor chronometric response to different concentrations of ethanol (200-1000 ppm), which shows that on exposure higher concentrations of ethanol to the PANI deposited sensor the resistance of the sensor decreases very rapidly. The rapid change in resistance of the sensor could be attributed to the large number of gas molecules were available for surface reactions to take place. As we expose the senor to the natural air, the desorption of the gas molecules takes place and the resistance starts to regain its original value. The recovery process was quite slow, which could be attributed to the low rate of dissociation of gas molecules from the sensor surface as well as the large number of molecules need more time to disperse at hr ambient conditions.

Figure 5.4 (c) shows the relation between the gas concentrations and the sensors relative response with these concentrations. It is observed that as the ethanol concentration increases the sensors relative response and the sensitivity increases. There was no saturation in response observed it indicates that the sensor responds very well for this concentration range.

Figure5.4 (d) shows the relation between the gas concentration and response-recovery times. It shows that the response time decreases with increase in gas concentrations while the recovery times increase with increase in gas concentrations. This could be attributed as explained above that there exist large number of gas molecules for surface reaction to take place which occurs very rapidly; while the more time is required to liberate these gas molecules from the sensor surface.

b) For Methanol and Acetone
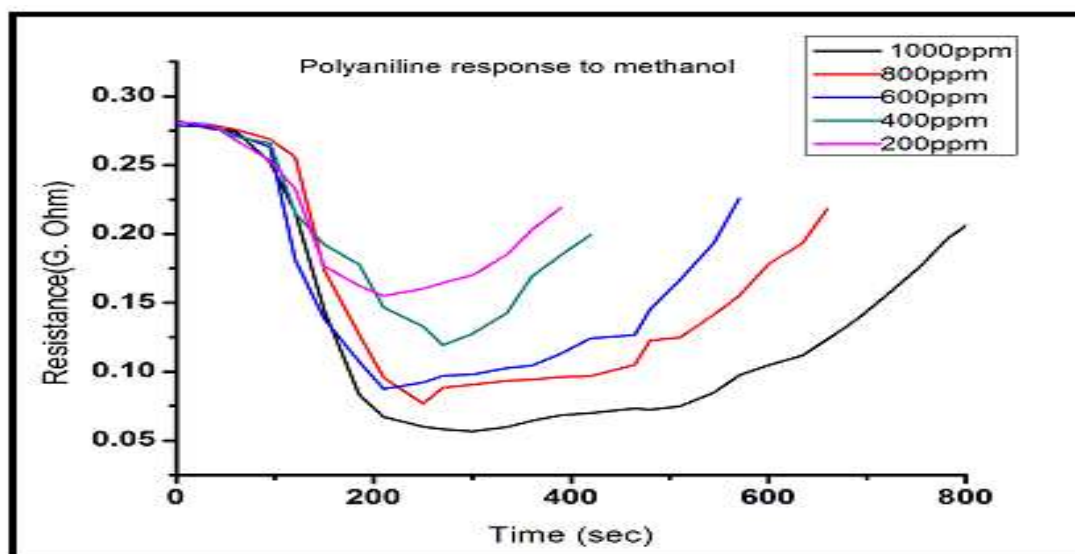
(a)
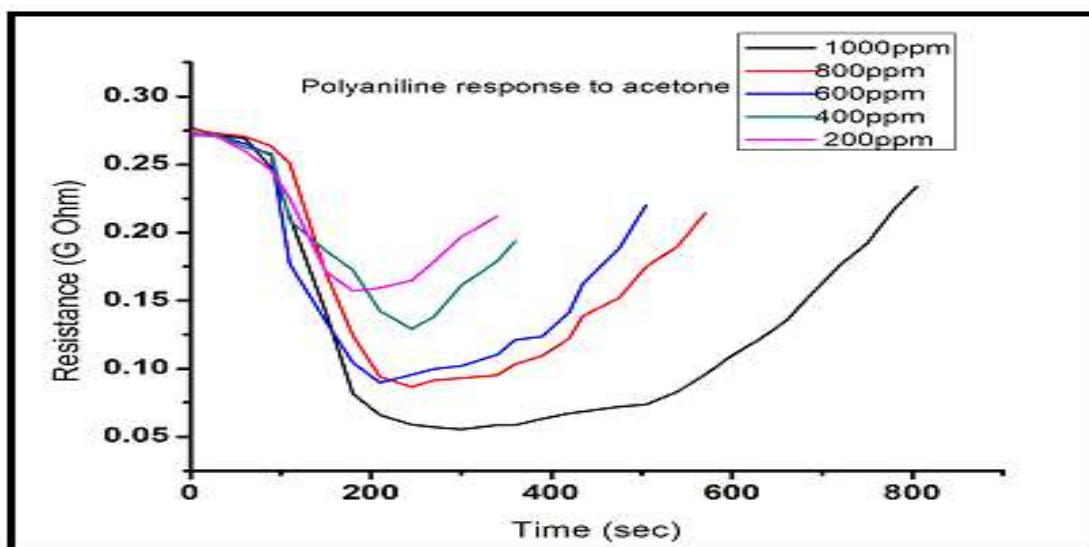
(b)
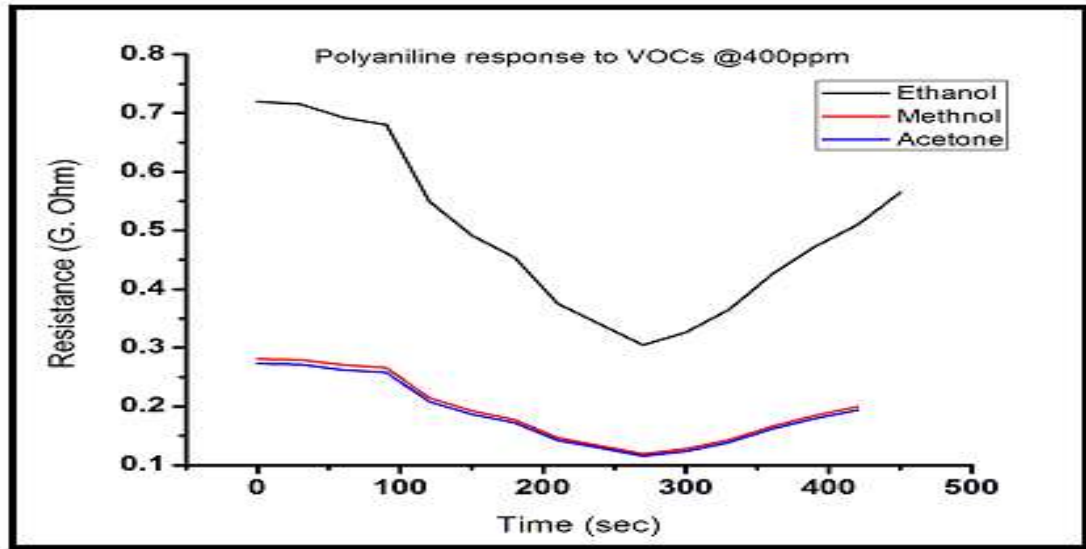
(d)

Figure 5.5 Chronometric response of PANI to (a) methanol (b) acetone and (c) relative response of PANI to ethanol, methano and acetone.

Figure 5.5(a) and (b) show the chronometric response of PANI to methnol and acetone for 200-1000 ppm concetrations. It is observed from the figures that the nature of resposnes is same that for ethanol . But the realtive change in resistance of the sensor is quite lower for methnol and acetone as compared ethanol.This is also manifested in figure 5.5(c). The response of the sensor to methnol and acetone is similar. The response to methnol is slightly higher than the reposne for acetone. Frome these curves, it is observed that the sensor is more senitive to ethanol than methnol and acetone for the proposed range of gas concetrations. The variation in response for these VOCs may be related to their molecular weights[13].

The observed response and recovery times for ethanol, methanol, acetone are in the same order 80-110 sec and 260-900sec respectively.

c) For Toluene
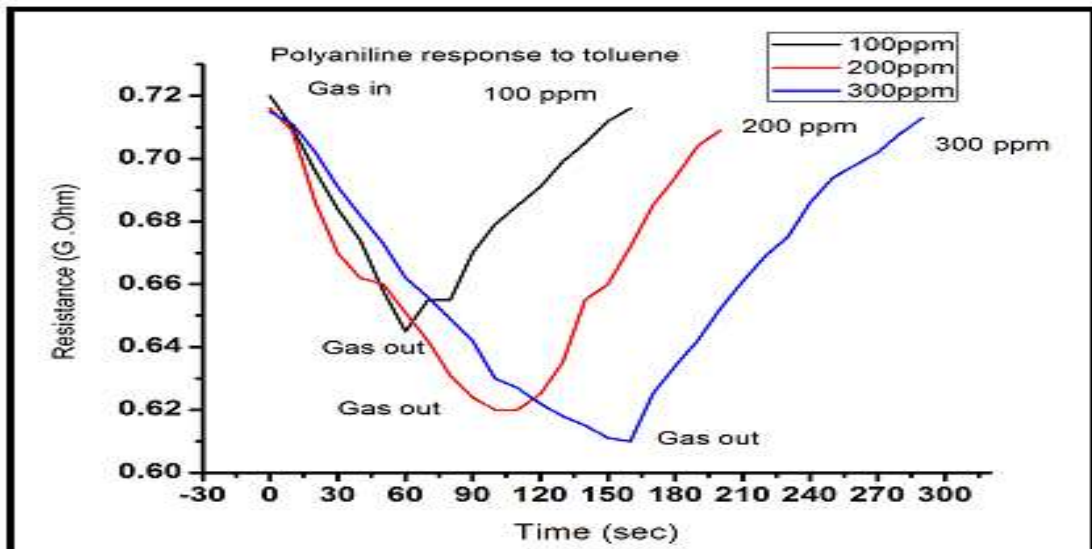
(a)
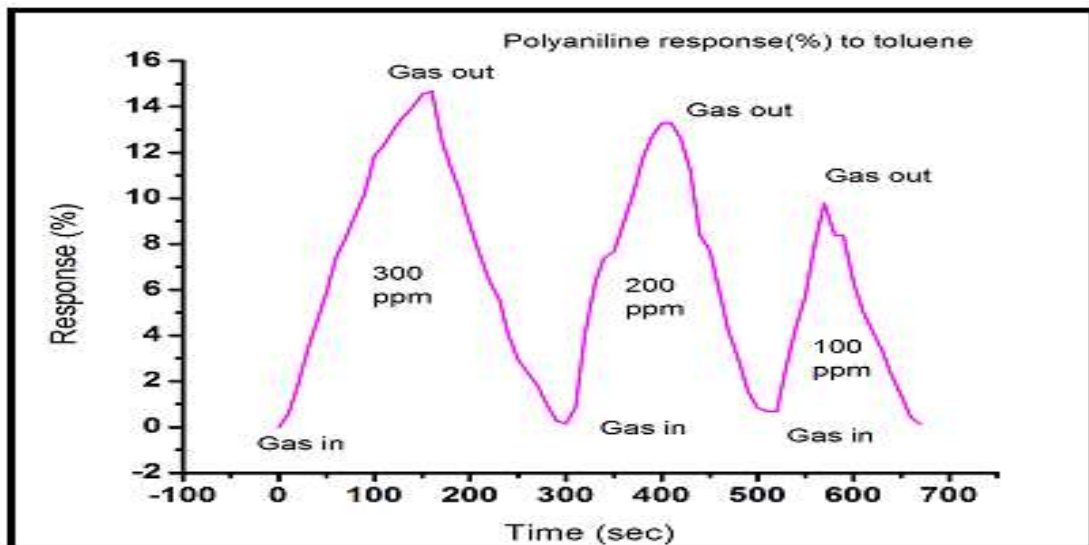
(b)
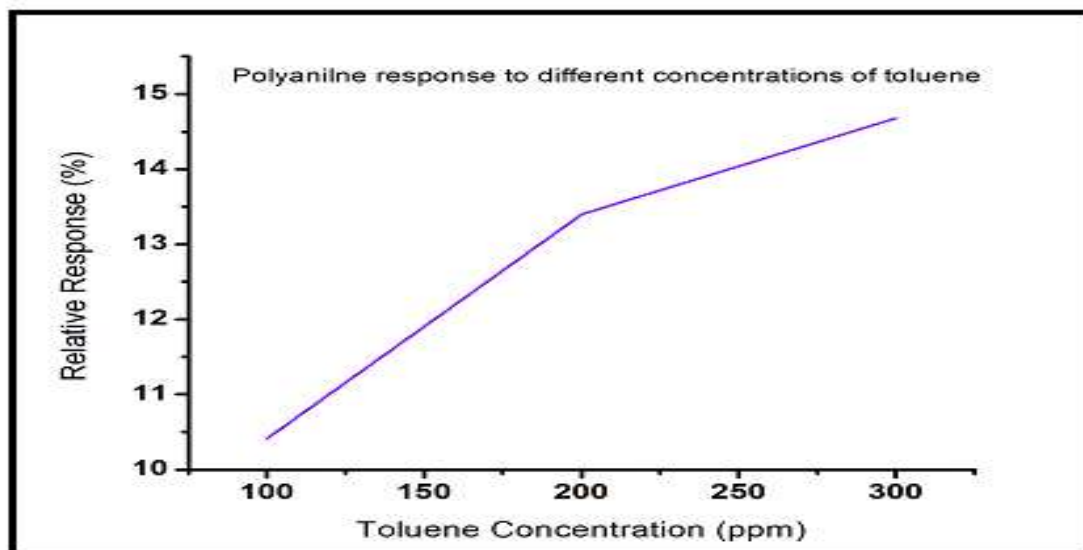
(c)

Figure 5.6(a) PANI chronometric responses to toluene (b) Relative response of PANI to different conc. of toluene. (c) relative response vs. gas concentrations.

Figure 5.6(a) shows the chronometric response of PANI to different concentrations (100-300 ppm) of toluene. It also show the same nature as that for other VOCs discussed here. The toluene concentration range selected here is different than other VOCs because the safe limit for toluene in air is 200ppm as recommended by OSHO. The response also shows that the percentage change in resistance is less here. The response times observed are less than the recovery time this could also be attributed to the number of molecules were sufficient for the reaction to take place. The large recovery time may also be related to the low desorption rate of toluene molecules at the ambient conditions.. Figure 5.6(b) shows the percentage response of PANI to different concentrations. It shows that the response is less for lower concentrations of toluene. Figure 5.6(c) also supports this observation. Thus polyaniline shows less sensitivity to toluene as compared to ethanol. The response and recovery times of PANI sensor to toluene are listed in table 5.3.

Table 5.3: Response -recovery time of polyaniline for toluene

Time	100 ppm	200 ppm	300 ppm
Response (t_{res})	65sec	80sec	100sec
Recovery(t_{rec})	80 sec	90sec	130 sec

5.2 PANI -SnO$_2$ Nanocomposite Based Chemiresistor (IDT) Gas Sensors

The main requirement from any sensor is that it should follow the 3BS criteria: best sensitivity, best selectivity, and better stability. As discussed above the PANI based ammonia sensor, the sensitivity obtained needs to improve. It is difficult to obtain the higher sensitivity with PANI alone. The sensitivity can be improved with the nanostructure [11] of the PANI and using better synthesis method of PANI. Another way to increase the sensitivity, selectivity and to improve the response/recovery times is to use suitable nanocomposite made up of metal or metal oxide nanoparticles with polymers [12]. After the rigorous literature review we planned to use PANI- SnO$_2$ nanocomposite as the sensing material for ammonia and VOCs detection. The synthesis of PANI - SnO$_2$ nanocomposite along with SnO$_2$ nanoparticles and their characterization is presented in chap. 4.

5.2.1 PANI- SnO$_2$ Nanocomposite Material Interface for Gas Sensor and its Testing

As discussed in above section 5.1, the same procedure is followed to prepare the PANI -SnO$_2$ nanocomposite solution and forming the film of it on the IDT structure. The sensor was initially tested using digital multimeter, Keithley's multimeter, LCR meter and electrometer. But for further characterization Keithley's electrometer-614 was used.

The performance of PANI-SnO$_2$ nanocomposite film deposited (drop casted) sensor was tested for different concentrations of ammonia at room temperature using the above explained labmade characterization system (fig.5.2). For this PANI-SnO$_2$ nanocomposite film sensor having metallic contacts were kept in the

test chamber of known volume with electrical leads taken out for electrical measurements. A fixed amount of (25 ppm) of ammonia gas was injected into the test chamber, the film resistance measured with respect to time (for every 30 seconds interval), until it reached a steady value. This procedure was followed once again after removing ammonia and exposing the test chamber to clean air. These steps were repeated for different concentrations of ammonia (25-100 & 200 ppm). The results of the measurements are reported in following section.

5.2.3 Results and Discussion of PANI- SnO$_2$ Nanocomposite response to Ammonia
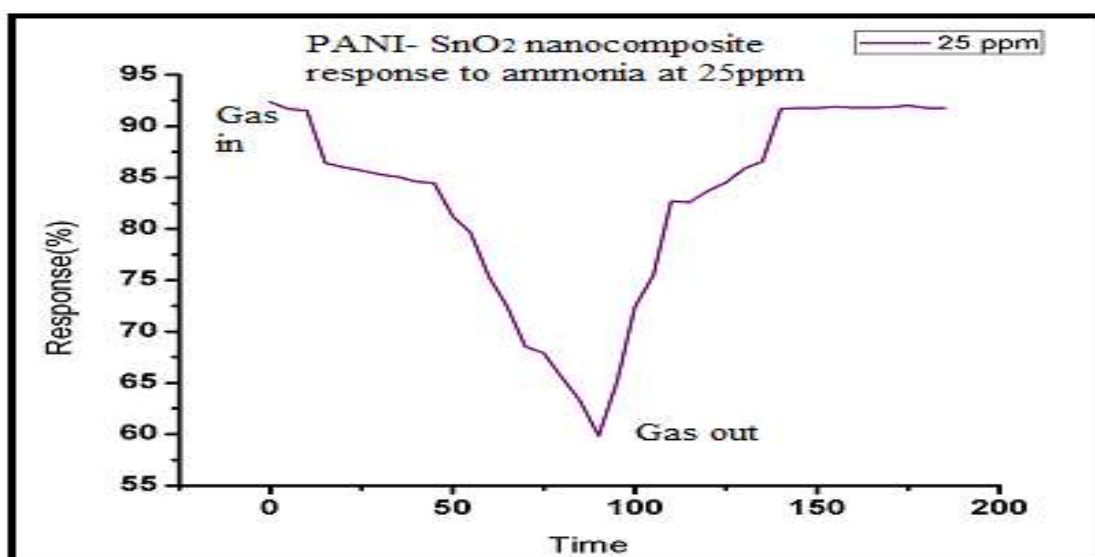
Fig 5.7 PANI - SnO$_2$ Nano composite for 25 ppm ammonia
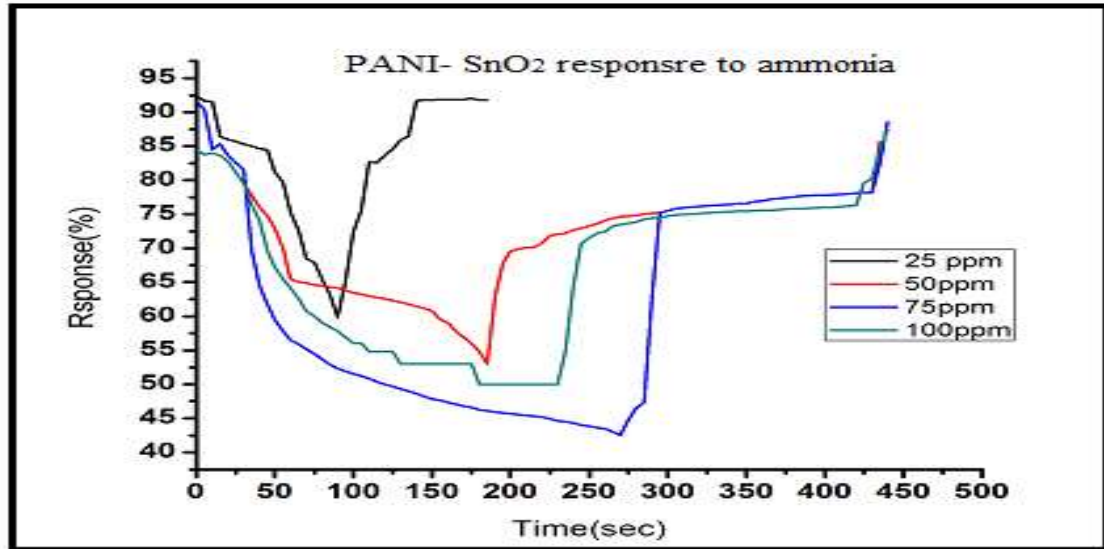
Fig 5.8 PANI – SnO$_2$ Ammonia for 25 - 100 ppm nanocomposite response
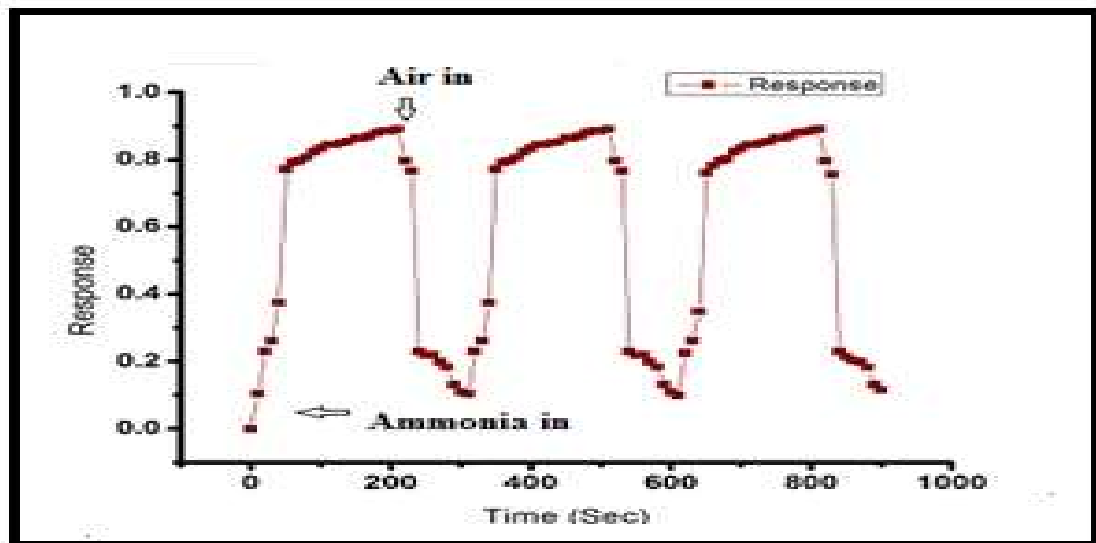
Fig.5.9. Repeatability of sensor to ammonia at 50ppm

Figure 5.7 shows the response of PANI -SnO$_2$ nanocomposite for 25 ppm of ammonia. The resistance of the sensor decreases when exposed to ammonia gas and it recovers the resistance when purged to natural air. For this case the response time and recovery times are in the same order. The recovery of gas is faster since the gas concentration is low. Figure 5.8 shows the composite response to different concentrations (25-100 ppm). From the figure 5.8, it is observed that

the response increases with increase in gas concentrations. The change in resistance increases for higher concentrations. The recovery times are less than the response time because the less time is required for gas desorption at the ambient conditions. The reason for high response time is due to inability of sensor to reach saturation in the resistance change and it can be attributed to large active surface area for the sensor (10mm x 20mm) Figure 5.9 shows the repeatability curves at 50 ppm, which shows that the sensor has good repeatability and reversibility.

5.2.3 PANI -SnO$_2$ Sensing Mechanism for Ammonia

The electrical resistance of PANI-SnO$_2$ nanocomposites shows a remarkable change when exposed to different concentrations (25-100 and 200 ppm) of ammonia. The sensing mechanism is governed by the protonation / deprotonation phenomena. It shows that resistance of the material decrease when it is exposed to increasing concentrations (25-200 ppm) of ammonia. This is mainly due to SnO$_2$ nanoparticles, which may act as a percolated high mobility path for electrons. PANI incorporation into oxide matrix creates an imbalance and a charge separation occurs at a polymer - nanoparticles interface. Thus, PANI-SnO$_2$ nanocomposite forms large number of p-n heterojunctions throughout the surface, giving rise to very high resistance at room temperature. When PANI-SnO$_2$ comes in contact with ammonia (NH$_{3)}$, this charge separation is released by NH$_3$ rupturing the hetero-junctions and the resistance decreased. The depletion region that was created at the interface because of difference in motilities of semiconductor and polymer is broken and inter-particle electron migration occurs through SnO$_2$ [11].

5.2.4 PANI -SnO$_2$ Nanocomposite Film coated Chemiresitor VOCs Sensor

The response of PANI -SnO$_2$ nanocomposite is tested for ethanol, methanol and acetone for the concentration range of 200-1000ppm using chemiresistor (IDT) as a sensor. Figure 5.7(a) shows the sensor chronometricresponse for ethanol. In this measurement the sensor response as function of time was measured for different concentrations of ethanol (200- 1000 ppm). It is observed that as we

increase the concentration value the response of the sensor also increases. This could be attributed to the increase of surface reactions with large number of available molecules of ethanol. The response of the sensor also depends on the type of synthesis method used and the porosity of the sensing material. If the material is more porous then the number of gas molecules get absorbed may be increased, resulting more change in its resistivity and hence change in resistance.

The response time varies with gas concentrations. At higher concentrations the response time is decreased, while the recovery time increases. This could be attributed to the time required for desorption of gas is more due to large number of molecules. The recovery of the resistance after removal of VOCs was determined by both oxygen re-adsorption from the ambient at the surface and re-oxidation of the oxide [10]. Figure 5.7(b) shows the relation between the relative sensitivity (% response) and the gas concentration. The relative sensitivity increases with increase in gas concentrations. At higher concentrations (above 800 ppm) there is less increase in sensitivity. This could attribute to the saturation in sensor response.

Figure 5.10 (a) shows the chronometric response of the sensor to ethanol. The nature of the response is similar to ethanol but the percentage response is less than the ethanol. This is more clearly shown in the figure 5.10 (b). Figure 5.11 (a) shows the chronometric response of the same sensor to acetone for the same concentrations. This also shows the same nature as that for ethanol and methanol but the percentage response are less as compared to that of ethanol and methanol with the exception that at higher concentration (above 800 ppm) the response of the sensor increases rapidly. Figure 5.9(b) supports to this observation. This could be attributed to increased surface reactions at this concentration. Figure 5.10 represents the sensitivity comparisons for ethanol, methanol and acetone. This clearly indicates that the sensor response is higher to ethanol than methanol and acetone. Thus the sensor is more selective to ethanol than methanol and acetone

for the concentration range of 200- 1000ppm. Table 5.4 lists the response and recovery times of the sensor for ethanol, methanol and acetone gas. The table 5.4 shows that the sensor responds to acetone faster than ethanol and methanol. This could be attributed to the surface reactivity can be significantly different depending on the functional groups involved [20].
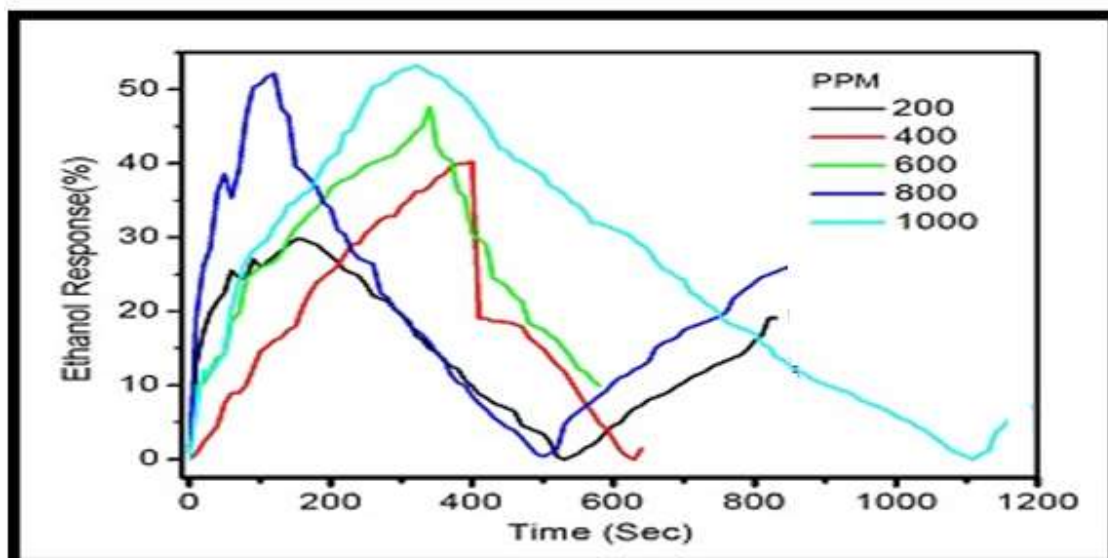
(a)
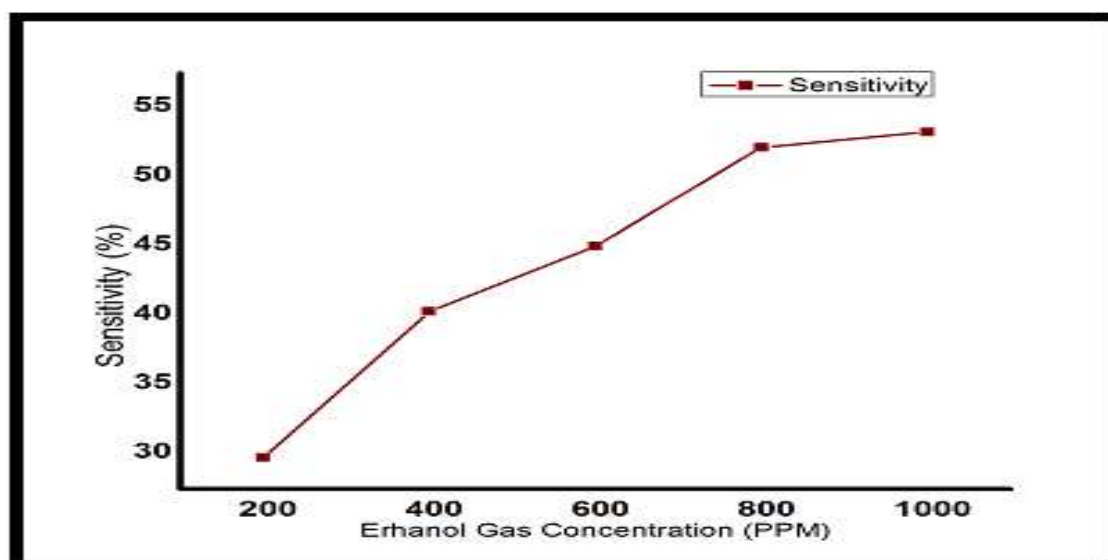
(b)

Fig. 5.10 (a) PANI -SnO$_2$nanocomposite (sample 2) chronometric response to ethanol (b) relative sensitivity of PANI- SnO$_2$ nanocomposite (sample 2) for different concentrations of ethanol
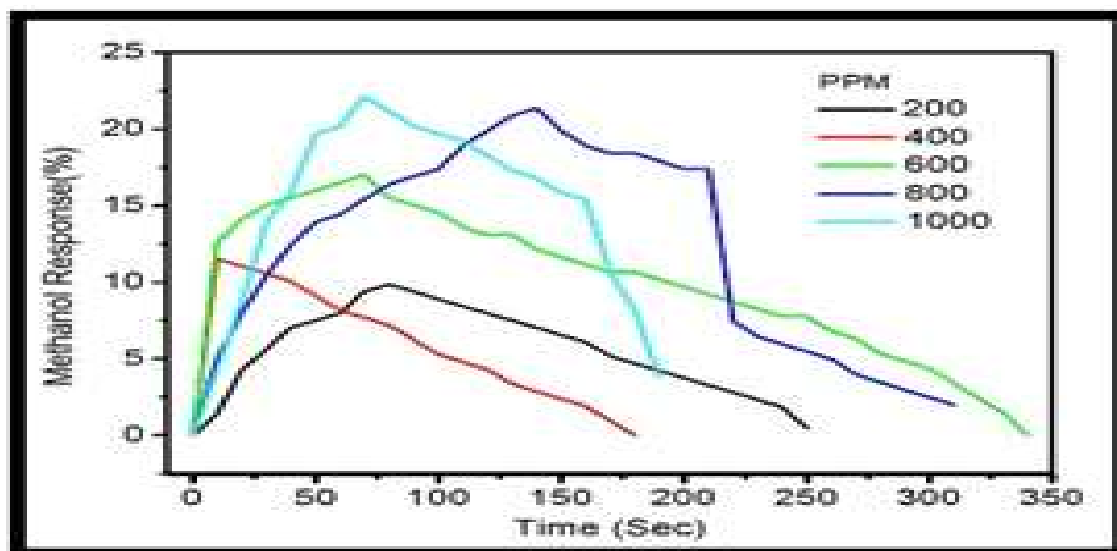
(a)
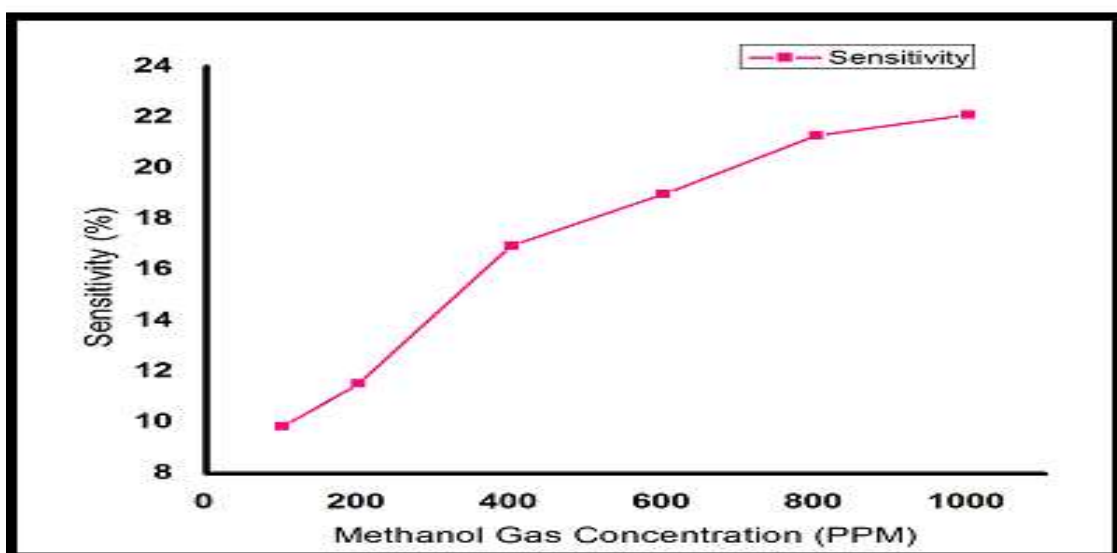
(b)

Fig.5.11 (a) PANI -SnO₂nanocomposite(sample 2) chronometric response to methanol (b) relative sensitivity of PANI- SnO₂ nanocomposite for different concentrations of methanol
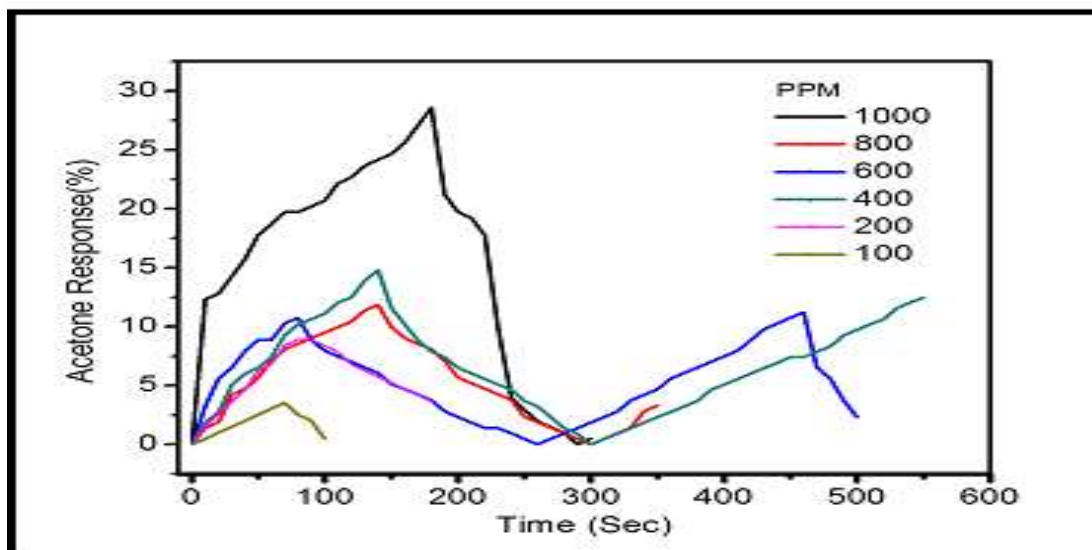
(a)
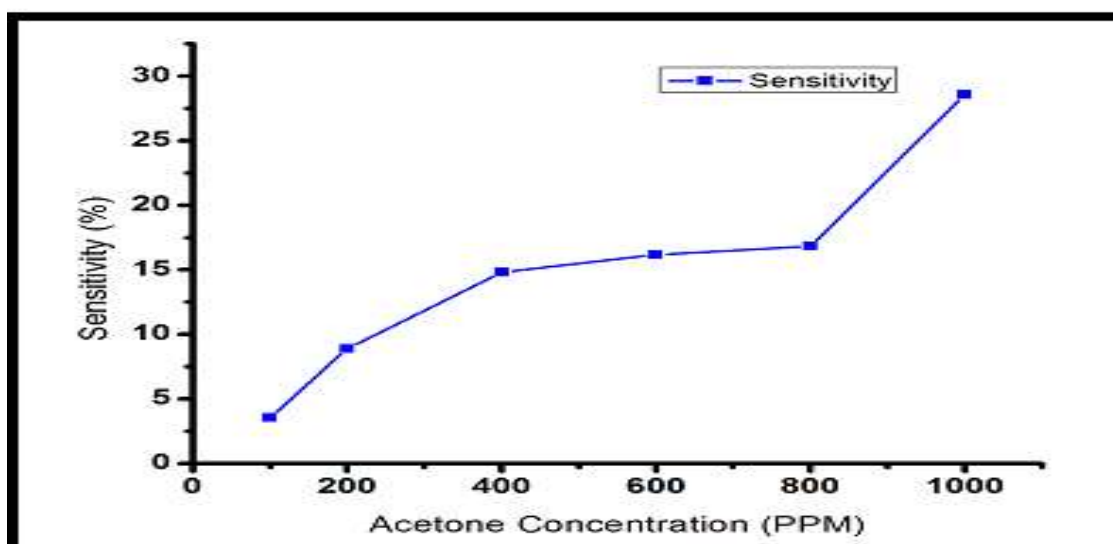
(b)

Fig.5.12 (a) PANI-SnO$_2$ nanocomposite chronometric response to acetone (b) . PANI-SnO$_2$ nanocomposite relative sensitivity too different concentrations of acetone
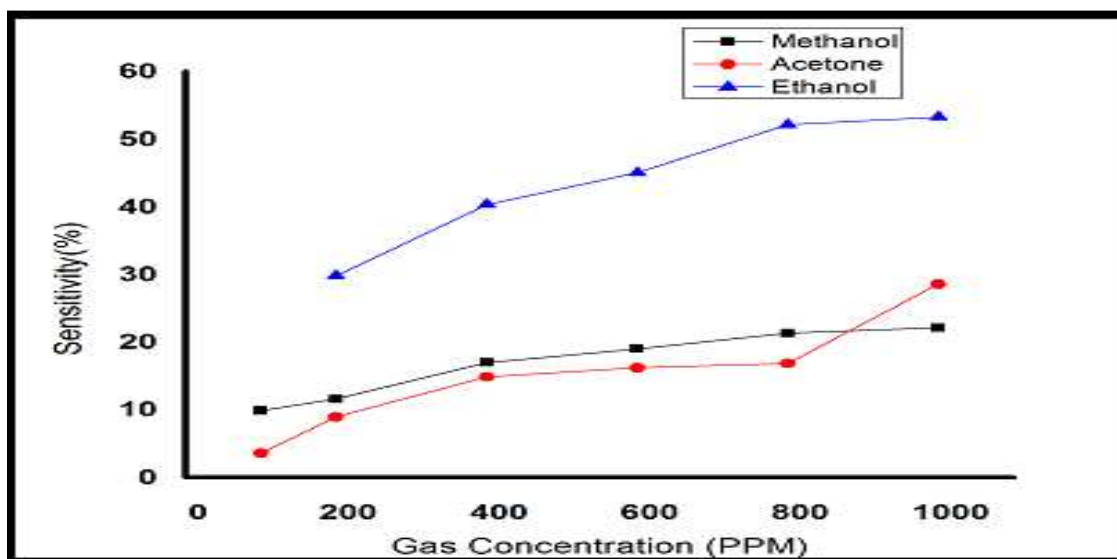
Figure 5.13 Comparison of sensitivities of PANI -SnO$_2$ nanocomposite sensor to VOCs.

Table 5.4 Response -recovery times of PANI- SnO$_2$ nanocomposite sensor to ethanol, methanol and acetone

Time	Ethanol	Methanol	Acetone
Response time (t$_{res.}$) sec	20-150	10-90	10-60
Recovery time (t$_{rec.}$) sec	140-390	100-280	60-220

5.2.5 PANI -SnO$_2$ Nanocomposite Response to Toluene Gas

Figure 5.14(a) shows the chronometric response of PANI- SnO$_2$ nanocomposite response to the toluene for 100-300 ppm concentration. It is observed that as the concentration of toluene gas exposure increases the sensor response also increases. With a small concentration of gas, exposed on a fixed surface are of a sample, there was a lower coverage of vapor molecule on the surface and hence less surface reaction occurred. As vapor concentration increases the surface reaction increases due to large surface coverage. The response time observed was large for higher concentration of gas while the recovery times were small. Figure 5.14(b) shows the relation between the toluene concentration and corresponding sensor response. This shows that within the proposed concentration range the response is linear and increases with increase in gas concentration.

(a)
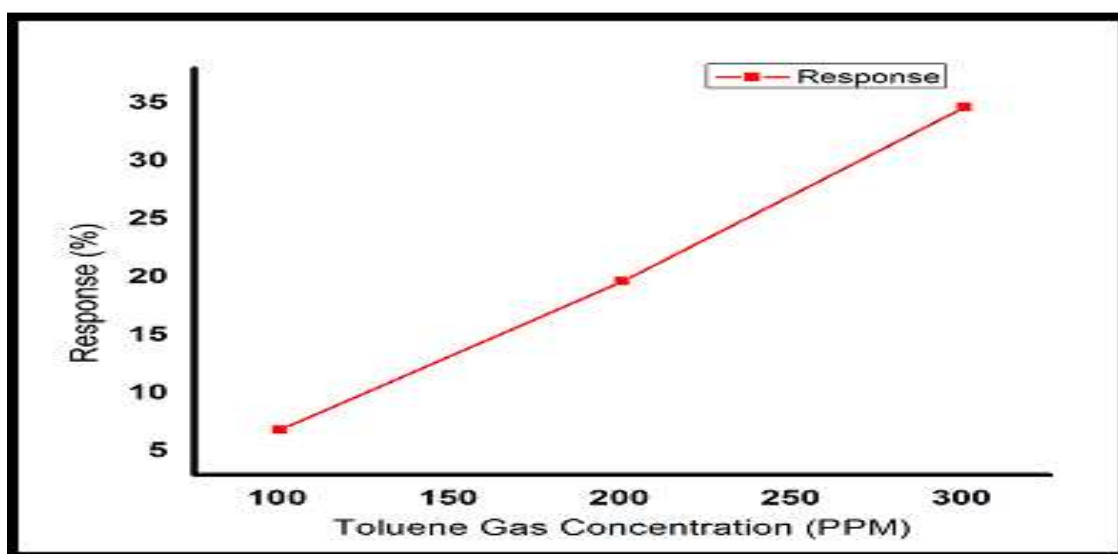
(b)

Fig.5.14 (a) PANI-SnO$_2$ nanocomposite chronometric response to toluene (b) . PANI-SnO$_2$ nanocomposite sensitivity to different concentrations of toluene.
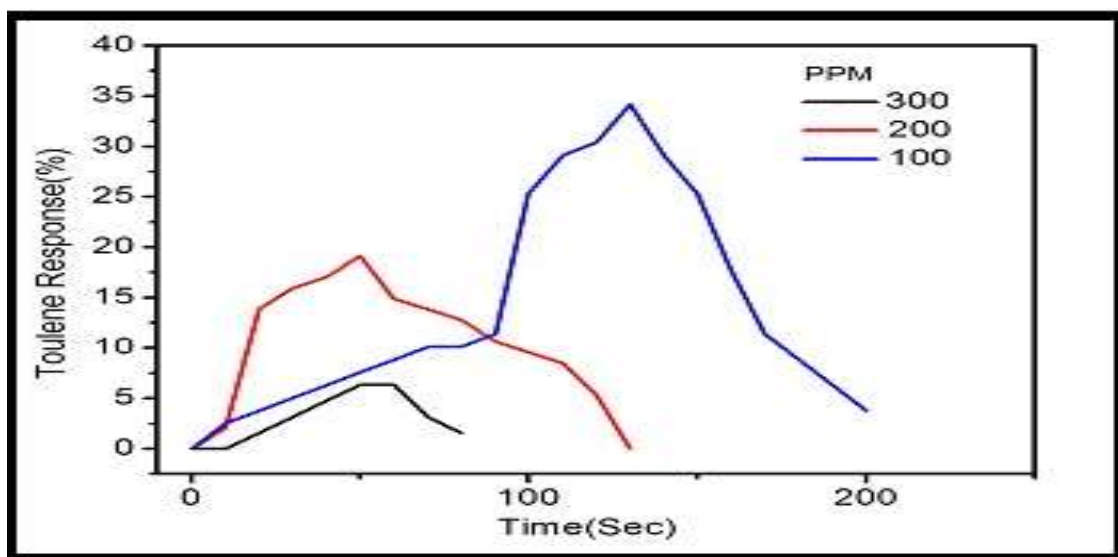
5.2.6 Conclusion

In this study, a chemiresistor sensor coated with PANI and PANI- SnO_2 nanocomposite film was investigated. It exhibited the responses to ammonia and VOCs. The developed sensor detects ammonia with concentrations 25-100 ppm with good sensitivity and ethanol, methanol, acetone for 200-1000 ppm and toluene for 100- 300 ppm, From the results obtained it is observed that the both the material are sensitive to ammonia and VOCs. But the relative responses observed are less for pure PANI coated sensors to these gases. For ammonia the response time values are higher than the recovery time but as concentration of ammonia increases the response time decreases and recovery time increases. The relative percent response of PANI to ethanol is higher than methanol, acetone and toluene. This shows that the PANI is selective ethanol. In case of PANI -SnO_2 nanocomposite film coated chemiresistor gas sensors the relative response /sensitivities are more than that of pure PANI, which could be attributed to the increased surface to volume ratio due to the porosity of the nanocomposite material. The response and recovery times of PANI -SnO_2 nanocomposite coated sensor are also improved. It shows higher response to ammonia than VOCs. Among VOCs it shows better response to ethanol than methanol, acetone and toluene. This indicates the feasibility of PANI -SnO_2 nanocomposite coated sensor in terms of a specific application of environmental ammonia and ethanol analysis.

5.3 Gas Sensing Studies using SAW Devices

To increase sensitivity and overall performance of gas sensor further we can use the well known device, known as surface acoustic wave (SAW) sensor. The SAW gas sensors are famous because of their remarkable sensitivity which is due to changes in the boundary conditions for the propagating wave, introduced by the interaction of active material with specific gas molecules [15,16,]. This unusual sensitivity results from the simple fact that most of the wave energy is concentrated near the crystal surface within one or two wavelengths. As a result, the surface wave is in its first approximation highly sensitive to any changes of the physical or

chemical properties of the thin layer placed on the crystal surface, as long as the thickness of the sensor material is significantly less than the surface wave wavelength. The presence of an entity in the propagation path of the surface waves causes a change in the phase velocity and amplitude of the waves [17]. For chemical sensing, these changes are induced by variation in properties of a coated sensing layer on the piezoelectric transducer upon exposure to target analytes. By detecting these changes at the output IDT via converted electric signal, one can obtain quantitative information about the analytes [15]. We used here the lab developed SAW sensor for ammonia and VOC detection. As a comparison we also used the readymade SAW IC for gas sensing having higher operating frequency (211 MHz) than our device. The following section briefly explains the setup used for SAW gas sensor characterization.

5.4 SAW Characterization Setup
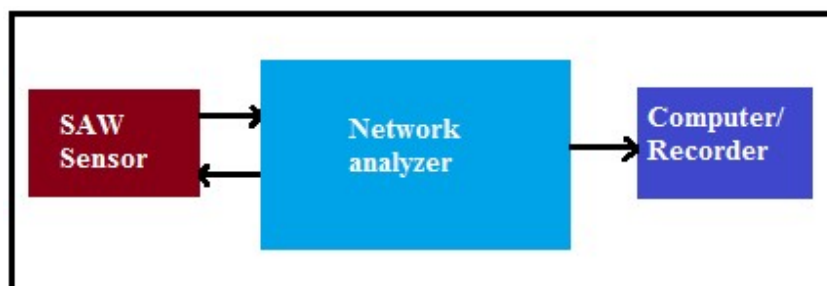
Fig. 5.15 Block diagram of SAW characterization system

Figure 5.15 shows the block diagram of SAW device characterization setup. In this setup the SAW sensor was mounted inside the glass chamber which is tight sealed. The target gases were introduced using micro syringes. The SAW device is connected to network analyzer using 50 ohm SMA connector and low loss coaxial cable. The frequency and attenuation changes are recorded on exposure of selected gas/vapors. After every cycle of gas exposure the chamber is purged with clean air and also cleaned by using lint free tissue paper. The responses of the sensors were tested for 25-100 ppm of ammonia gas and 200-1000 ppm of

VOCs. The toluene gas concentration was selected to 100-300ppm according to its safe limit in air.

5.5. PANI and PANI- SnO$_2$ nanocomposite Based SAW Ammonia Sensor

5.5.1 Coating the Sensing interface to SAW device

PANI and PANI SnO$_2$ nanocomposite powder was dissolved in *N*-methyl pyrrolidone (NMP) solvent at a weight ratio of 0.1 separately. The mixed solution was each agitated for 24 hours continuously, and then filtered. Prior to the application of the coating layer, the delay line surface of the sensor was cleaned using acetone. The sensors input and output IDTs were checked by multimeter on continuity mode to check any short between the finger electrodes. The S_{12} and S_{11} parameters of the SAW sensors are verified using network analyzer. After this a thin uniform layer of the prepared sensing layer was form on delay line area of the sensor fort both materials. While coating the layer the precaution were taken to protect any short between the input and output IDTs. Then the sensor was kept in desiccators for 6 hours to dry the sensing layer. The change in weight of the devices was recorded for further analysis. Again the devices was inspected for short between input and output IDTs. The change in frequency and attenuation was recorded.

5.5.2 Ammonia sensing using PANI and PANI- SnO2 Nanocomposite film coated SAW Sensor

The SAW sensor was mounted inside the chamber and coroneted to network analyzer.The performance of PANI and PANI -SnO$_2$ nanocomposite deposited sensor was tested for different concentrations of ammonia at room temperature using the above explained labmade characterization system. A fixed amount of (25 ppm) of ammonia gas was injected into the test chamber, the change in frequency ,attenuation change (insertion loss -S_{12}) of the SAW device was measured with respect to time (for every 20 seconds interval), until it reached a steady value. This procedure was followed once again after removing ammonia and exposing the test

chamber to clean air. These steps were repeated for different concentrations of ammonia (25-100 & 200 ppm). The results of the measurements are reported in following section.

5.5.3 Results and Discussion for PANI and PANI- SnO2 Nanocomposite film coated SAW Ammonia Sensor
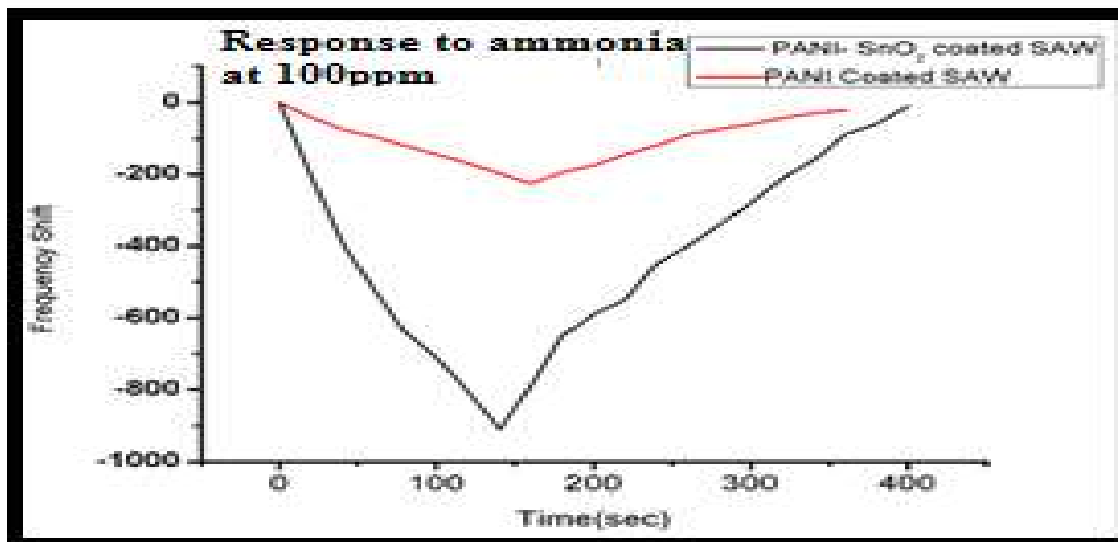
(a)
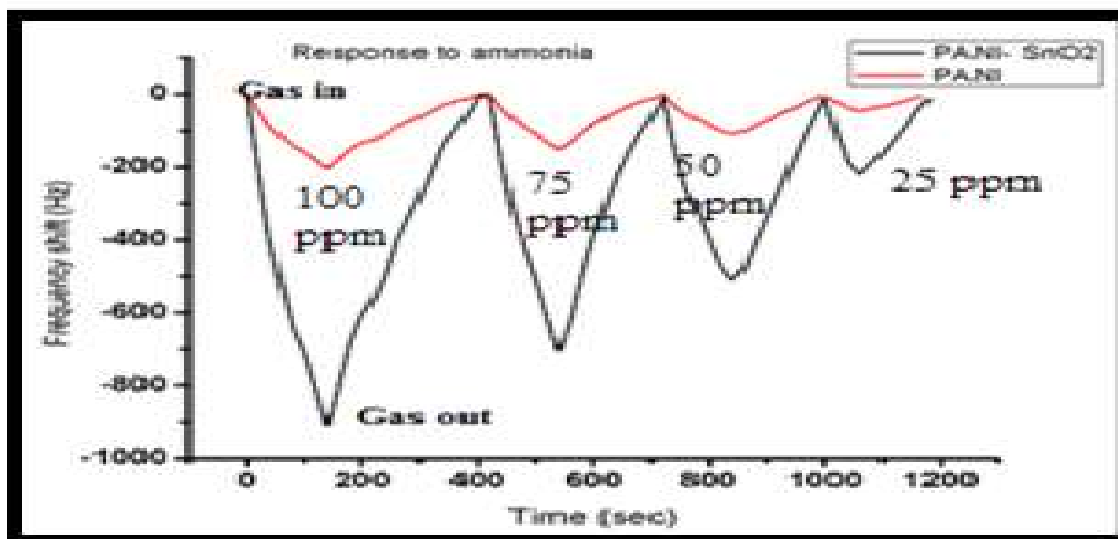
(b)
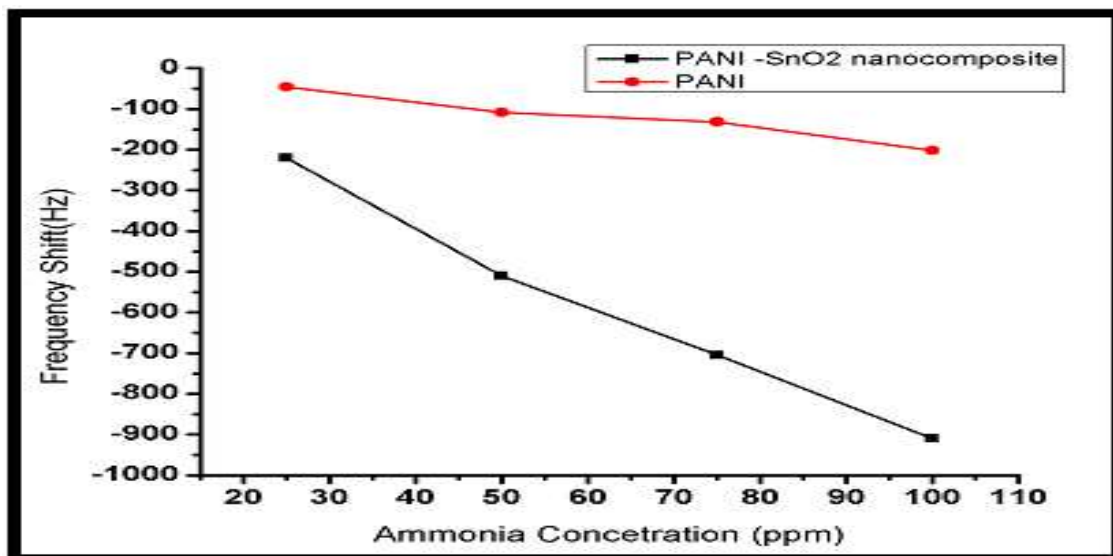
(c)
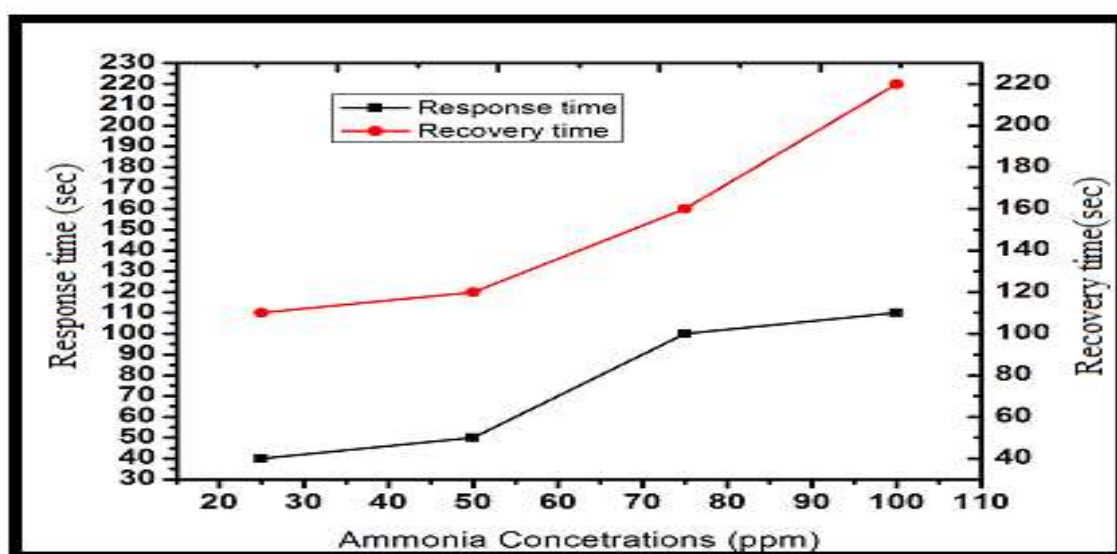
(d)

Fig. 5.16 (a) Chronometric response of PANI and PANI -SnO₂ coated SAW sensor for ethanol at 100ppm (b) Chronometric response of SAW sensor for different concentrations of ammonia (c)) Comparative frequency shift vs. ammonia concentration response of SAW sensor (d) Response -recovery time vs. ammonia concentrations

Figure 5.16(a) shows the chronometric response of PANI and PANI -SnO$_2$ nanocomposite coated SAW sensor for 100ppm ammonia gas. It is observed that after exposure of ammonia in the chamber the frequency of the SAW device decreases with time. This is attributed to the mass loading effect of the SAW sensor. As the gas molecules interact with the sensing layer coated on the delay line area of the device, they get sorbed on the sensing layer which results in change in mass of the sensing layer. Due to this the phase velocity as well as the attenuation of the device gets modulated. On the network analyzer, we observed the change in frequency and insertion loss (S$_{12}$). After reaching the steady value of frequency, the pure air was exposed to the chamber. With this the gas molecules get desorbed from the sensor surface and hence the mass get reduced therefore the frequency increases to its initial value and the insertion loss also decrease (regains) to its initial value. Figure 5.17(b) represents the chronometric responses of the same sensors for different concentrations of ammonia at room temperature. It is also observed that for low concentrations of ammonia the response and recovery times were reduced

From the curves (fig 5.16(a)-(b), it is observed that the PANI -SnO$_2$ nanocomposite film coated sensor shows better response to ammonia than the pure PANI film coated sensor. This could be attributing to the porous nature of the PANI -SnO$_2$ nanocomposite film, which adsorbs more molecules of ethanol and the mass loading increases and the frequency shift increases.

The change in SAW velocity (Δv) is given by [16]:

$$\frac{\Delta v}{v_0} = -\frac{K^2}{2}\frac{\sigma^2}{\sigma_s^2 + v_0^2 C_s^2} \qquad (4)$$

Where C$_s$is the surface capacity, σ_s is the sheer conductivity , K is the electromechancial coupling coefficient , v$_0$ is the unperturbed velocity. From the equation (4) the conductivity of the sensing layer σ_s varies inversely with SAW velocity i.e. resonant frequency.

When PANI- SnO_2 coated film exposed to the ammonia, the reaction of ammonia molecules with the initially absorbed oxygen molecules in the PANI -SnO_2 nanocomposite film led to a recombination of electrons and holes, increasing the conductivity of the sensing layer. The PANI -SnO_2 nanocomposite film coated have larger specific surface area than that of pure PANI coated film , therefore , the PANI -SnO_2 nanocomposite film can absorb more oxygen species and react with more ammonia molecules than pure PANI film under the same concentration of ammonia. Therefore, the device with PANI -SnO_2 nanocomposite film has a larger surface conductivity and frequency shift [16].

Figure 5.17(c) represents the relation between the ammonia gas concentration and corresponding frequency shift of the SAW device for PANI and PANI - SnO_2 nanocomposite. This shows that with the increase in gas concentration there is corresponding increased shift in frequency. The frequency shift is basically attributed to mass loading effect, but there could be some contributions of film conductivity change and film stiffness change. These are not taken in account because there is no positive shift in frequency observed [16, 18].

Figure 5.17(d) shows relation between gas concentration and response and recovery times for PANI -SnO_2 nanocmoposite film coated SAW sensor. The response time ($t_{res.}$) and recovery time ($t_{rec.}$) were measured and found to be 140sec (PANI)110sec,(PANI- SnO_2 nanocomposite) and 150sec(PANI) , 220(PANI- SnO_2 nanocomposite) respectively for 100 ppm ammonia concentration. This is surely good response time of the device as compared to the reported values in literature [14] for this range of SAW resonance frequency. This also shows that response and recovery times for PANI - SnO_2 nanocomposite coated sensor are improved than PANI coated SAW sensor.

5.5.4 Volatile Organic Compounds (VOCs) sensing using PANI- SnO₂ Nanocomposite film coated SAW Sensor

The performance of PANI -SnO₂ nanocomposite deposited sensor was tested for different concentrations of VOCs (Ethanol, methanol, acetone (200-1000ppm) and toluene (100-300ppm)) at room temperature using the above explained labmade characterization system. A fixed amount of (200 ppm) of each VOC gas was injected into the test chamber, the change in frequency ,attenuation change (insertion loss -S12) of the SAW device was measured with respect to time (for every 30 seconds interval), until it reached a steady value. This procedure was followed once again after removing each VOC and exposing the test chamber to clean air. These steps were repeated for different concentrations of each VOC (200-1000 ppm). The results of the measurements are reported in following section.

5.5.5 VOC sensing mechanism for PANI- SnO₂ Nanocomposite film coated SAW Sensor

The simple sensing mechanism is that volatile organic compounds adsorb on the substrate surface and the mass loading made frequency shift. The surface mass loading is responsible for frequency shift of SAW sensor as following equation [18]:

$$\frac{\Delta v}{v_0} = -\frac{w v_0 \rho_s}{4} \left(\frac{v_{x0}^2 + v_{y0}^2 + v_{z0}^2}{wP} \right) \qquad (5)$$

Where ρ_s is the surface mass density and v_{x0} , v_{y0} and v_{z0} are the SAW velocity at the surface. Grouping all the substrate-dependent constants together the results in the formula for the mass-induced change in SAW propagation velocity:

$$\frac{\Delta v}{v_0} = -C_m f_0\, \rho_s \qquad (6)$$

Where the mass sensitivity factor C_m is

$$C_m = \frac{\pi v_0}{2} \left(\frac{v_{x0}^2}{wP} + \frac{v_{y0}^2}{wP} + \frac{v_{z0}^2}{wP} \right) \qquad (7)$$

From equation (6), the frequency dependence of the SAW mass sensitivity: the velocities change $\frac{\Delta v}{v_0}$ various with the operating frequency f_0 and the surface mass density.

5.5.6 Results and Discussion for PANI and PANI- SnO₂ Nanocomposite film coated SAW Sensor

a) For Ethanol
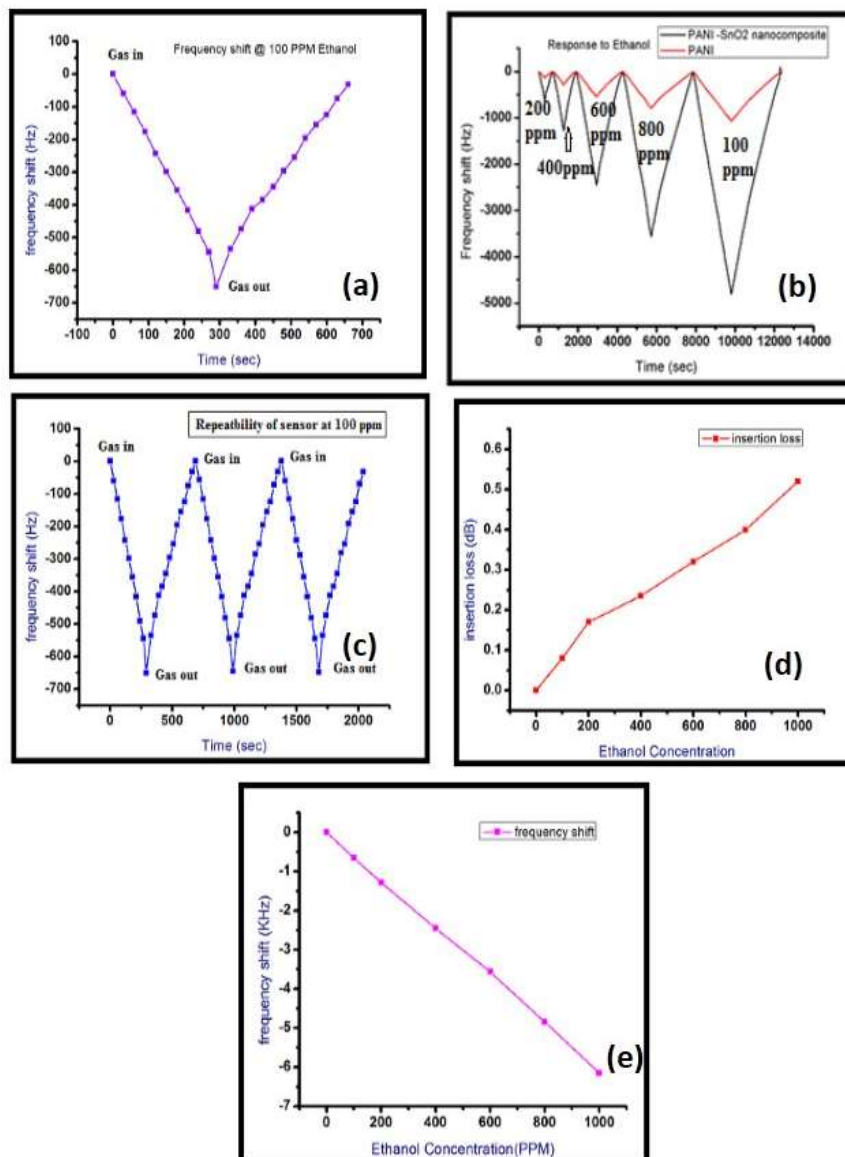
Fig. 5.17 (a) PANI -SnO$_2$ Chronometric response to ethanol (b) PANI and PANI- SnO$_2$ chronometric response to ethanol for 100-1000 ppm concentration. (c) Ethanol repeatability at 100 ppm (d) insertion loss vs. ethanol concentration (e) frequency shift Vs. Ethanol concentration.

Figure 5.17(a) shows the chronometric response of PANI- SnO$_2$ nanocomposite to ethanol for 100 ppm concentration. It shows that on exposure of ethanol gas to the frequency of the SAW sensor decreases linearly with time. This decrease in frequency could be attributed to the mass loading effect of SAW. On adsorption of the ethanol molecules on the surface of SAW sensor increase the mass value. The observed frequency shift is negative this is due to only mass loading effect. There is no positive frequency shift therefore the change in elastic modulus effect is negligible [14, 18]. The maximum change in frequency for 100 ppm ethanol is 655 Hz. After the fresh air is purged to the chamber the frequency increases toward its initial value. Figure 5.17(b) shows the PANI and PANI- SnO$_2$ nanocomposite coated SAW chronometric response to all the measured concentrations of ethanol (100-100ppm). It shows the frequency shift for the different concentrations of ethanol with respect to time executing mass loading effect. It is observed that the relative change in frequency for PANI- SnO$_2$ nanocomposite coated SAW is greater than the PANI coated SAW. This attribute to the large surface area available for ethanol molecules to get absorbed in for PANI- SnO$_2$ nanocomposite coated SAW due to porous nature of the sensing material therefore more increase in mass density and results in increase in mass loading takes place and hence shift in phase velocity of SAW (equation 6) which results corresponding shift in frequency. In case of PANI coated SAW sensor the surface area available for ethanol molecules to get absorbed is less. Figure 5.18(c) shows the PANI- SnO2 nanocomposite coated SAW sensor repeatability at 100 ppm of ethanol. This could be attributed to the stable response of the deposited film on the delay line of the SAW. Figure 5.17(d) shows the change in attenuation (insertion loss) with respect

to gas concentration. As the gas concentration increases the attenuation also increases, which also supports the mass loading effect of SAW sensor. With higher concentration the diffusion of the gas particles in the film is increased hence the insertion loss is increased. The response and recovery times are also prolonged due to gas molecules diffusing in and out of the film. Figure 5.17(e) shows the relation between the ethanol concentration and frequency shift. The negative shift in frequency increases with the increase in ethanol concentration; this is quite linear relation between the measurand and the sensor output.

The same principle is applicable for methanol, acetone and toluene. But according to their reaction with the sensing material the mass sensitivity and conductivity change is different and the response σ_s are different.

The sensitivity of the sensor with PANI -SnO$_2$ film is 655Hz/100ppm=~ 6.55Hz/ppm for ethanol and ~ 2Hz/ppm for PANI coated sensor. The is quite good as compared to reported by Timothy J. Giffiney et al [21].

b) For Methanol and acetone and toluene
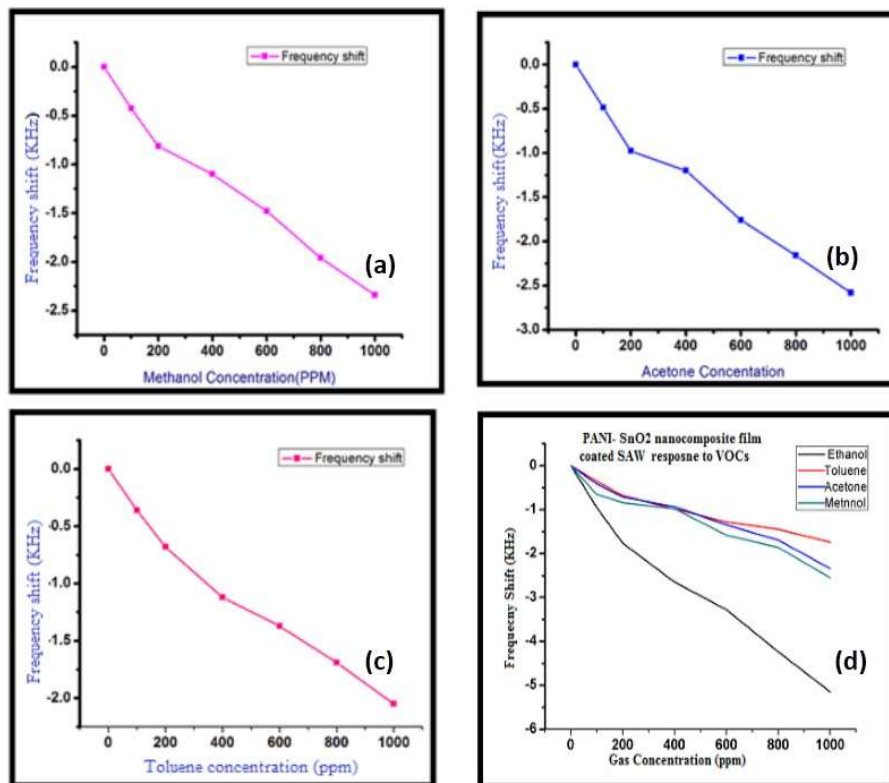
Figure 5.18 (a) frequency shif vs. methnol concentration (b) frequency shif vs. acetone concentration (c) frequency shif vs. toluen concentration (d) Frequency vs. VOCs concetration

Figure 5.18 (a)-(c) describes the PANI -SnO$_2$ response to the different concentrations of methanol, acetone, toluene respectively. For these VOCs there is also increase in negative shift of sensor frequency, it shows that the sensor exhibits mass loading effect. But the frequency shift is less than the shift due to ethanol sensing.

In case of VOCs sensing based on PANI material and its composite the sensing also depends on the boiling temperature, it is known that at lower boiling temperature, the enrichment of the gas in the polymer is lower and then the extent of physisorption is minor, so the response is greater when the boiling temperature is higher[13]. According to this principle the ethanol has higher boiling point (78.37 ^{0}C) than methanol (64.7 ^{0}C) and acetone (56 ^{0}C) and therefore may have higher sensing response to ethanol. But this is conflict to toluene. The sensors response to the VOCs can be expressed as:

<p style="text-align:center">S(ethanol) > S(methanol) > S(acetone) > S(toluene).</p>

Figure 5.18(d) shows the response of PANI -SnO$_2$ nanocomposite to ethanol, methanol, acetone and toluene. This follows the above expressed sensor response relation.

c) PANI - SnO$_2$ nanocomposite based SAW IC Response to VOCs and Ammonia
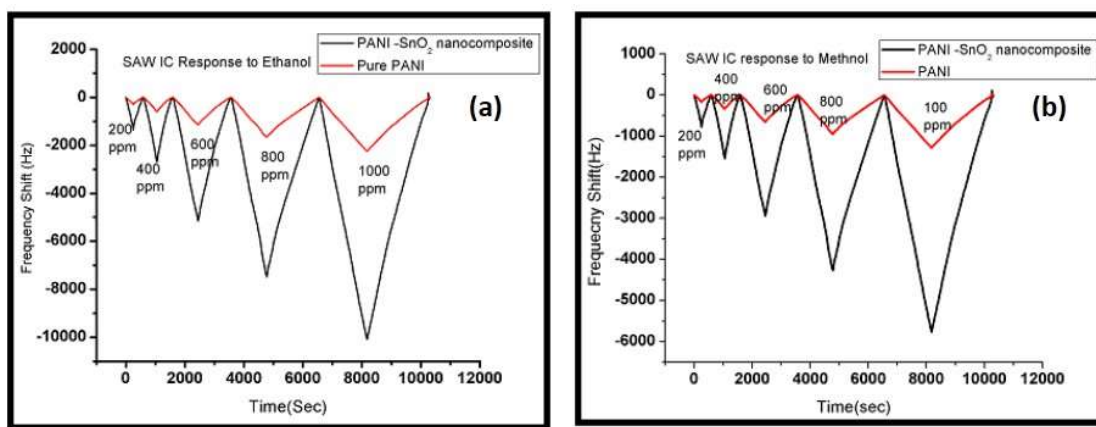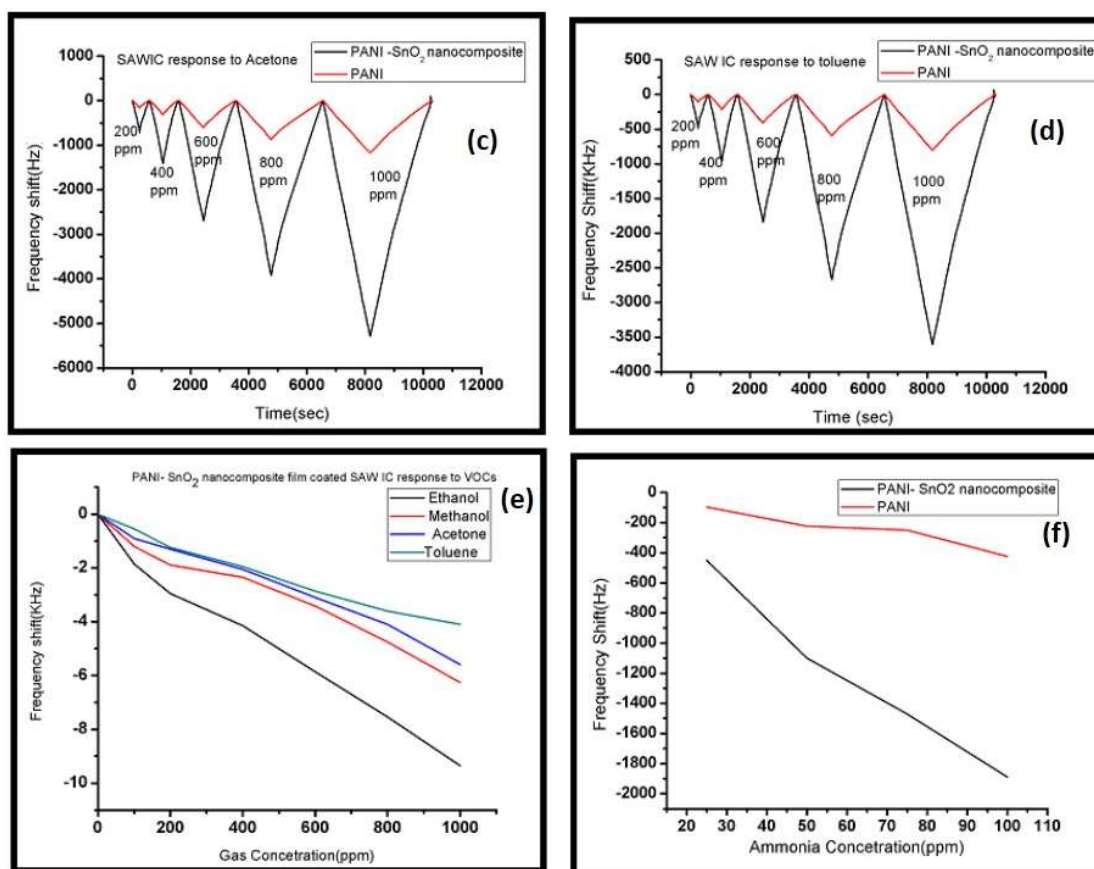
Fig.5.19, Comparative response of PANI and PANI- SnO$_2$ nanocomposite film coated to (a) Ethanol (b) methanol(c) acetone (d) toluene and (e) Frequency shift vs. gas concentrations for VOCs.(for PANI- SnO$_2$ nanocomposite). (f) frequency shift vs. gas concentrations for ammonia.(for PANI- SnO$_2$ nanocomposite).

Figure 5.19 (a) - (d) explains the response of PANI and PANI - SnO$_2$ nanocomposite film coated SAW IC (SIPAT LB 211 DS 01) to the ethanol, methanol, acetone and toluene respectively. The nature of the response is similar to the response of developed SAW sensor with higher frequency shift. The frequency shift observed here was higher than the frequency shift of developed SAW device, which could be attributed to the higher operating frequency (211 MHz) of the SAW IC sensor as compared to developed SAW sensor operating

frequency (97.27MHz -Harmonic frequency). Another possible cause could be the exact matching network for SAW IC sensor were available, while for developed SAW sensor the matching is only through the externally connected inductor , which were designed by the formula.

$$L_{eff} = \frac{1}{w_0^2 C_s} \tag{8}$$

$$\omega_0 = 2\pi f_0 \tag{9}$$

Where L_{eff} is the$_{inductance}$ of inductor, f_0 resonant frequency of SAW, C_s is the capacitance of finger pairs.

Figure 5.19 (e) shows the response of PANI -SnO$_2$ nanocomposite coated SAW IC Sensor for ethanol, methanol, acetone and toluene. It shows that the frequency shift is more for ethanol than methanol, acetone and toluene. Thus the sensor is selective to ethanol than methanol, acetone and toluene. Figure 5.19 (f) shows the response of PANI and PANI -SnO$_2$ nanocomposite film coated SAW IC sensor to ammonia gas for the concentration range of 25-100ppm. The shift in frequency for PANI- SnO$_2$ nanocomposite coated sensor is more than that of PANI film coated sensor, which is due to the more gas particles get adsorbed on the PANI -SnO$_2$ film due to the recombination of ammonia molecules with the surface adsorbed oxygen (O$^-_{ads}$ or O$^{2-}_{ads}$) on the SnO$_2$ surface of the composite. The shift is five times more for PANI -SnO$_2$ nanocmoposite.

5.5.7 Evaporation and mass loading effect Studies of VOCs Using Surface Acoustic Wave (SAW) Devices

Using developed SAW devices and SAW SIPAT IC we have studied both the mass loading [23] and evaporation studies of VOCs [22]. By loading the different amount of ethyl alcohol on the device surface its response is studied. It showed a very quick response to this mass load and also the changing mass of ethyl alcohol.

Transient Response of SAW Device for ethyl alcohol is shown in figure 5.20. It is observed that addition of ethyl alcohol on the delay line area of the SAW device, the frequency and insertion loss gets changed. The frequency decreases initially and after some time it regains its original value. The frequency gets changed due

to the increase in mass on delay line [23]. But as ethyl alcohol evaporates the mass reduces and the frequency increases towards its initial value. Figure 5.20 shows plots for five different cycles of same volume of ethyl alcohol. Here the time taken for each cycle is different. The possible reasons to the different time taken to regain its original value could be- change in evaporation rate of ethyl alcohol due to room temperature variation, reaction of ethyl alcohol with the film on the delay line[22,23][. But the change in frequency is constant ~75KHz /μl with maximum insertion loss of -27dB. [22].
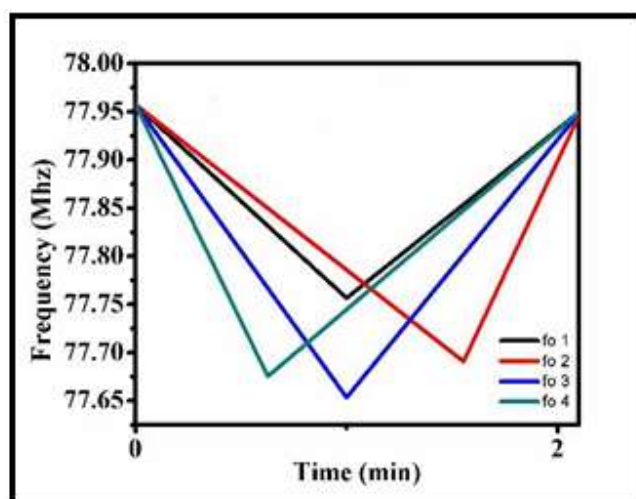
Fig.5.20. Transient response of SAW delay line device[23].

5.5.8 Conclusion

In this study, a SAW delay line sensor coated with a PANI and PANI-SnO$_2$ nanocomposite film was investigated. It exhibited a response to ammonia as well as the VOCs. The response occurred repeatedly and was recovered by fresh air. The developed sensor could detect ammonia concentrations of 25–100 ppm and had a response time of less than 40s. The Sensor also responds to ethanol, methanol, acetone and toluene concentrations from 200-1000ppm and had a highest relative sensitivity to ethanol compared with methanol, acetone and toluene, with response time of 220s.

We also used SAW IC (SIPAT Lb 211 DS 01) as senor for the ammonia and VOCs using PANI and PANI -SnO$_2$ nanocomposite as sensing layer. This SAW IC sensor shows response to both ammonia and VOCs, but the relative sensitivity to ammonia is more than that of VOCs. This indicates the feasibility of this SAW sensor in terms of a specific application of environmental ammonia and VOCs analysis. However, the sensing properties of the developed SAW delay line sensor in this study, including sensitivity and selectivity, are not good enough. In the future, we will attempt to improve the sensitivity, selectivity and sensor stability. The mass loading effect and evaporation studies of VOCs also studied using SAW device .It shows that as the mass on the surface of SAW device changes its frequency and insertion loss are get modulated. This proves device mass sensitivity.

The study of SAW device as a gas sensor using PANI and PANI-SnO$_2$ nanocomposite as s sensing layer has been completed here. The summary and conclusions of completed work are discussed in the next chapter.

References

[1] Anil G. Sonkusare , Sachin Tyagi ,Ranjan Kumar, Sunita Mishra," Room temperature ammonia gas sensing using polyaniline nanoparticles based sensor", International journal of materials science, ISSN 097-4589 Volume 12,Number 2(2017),pp. 283-291.

[2] Syed A. A. ,Dinesan M.K.," Review : Polyaniline - a novel polymeric material , Talanta ,38(8),815-837,1991 [cross reference].

[3] Kukla A. L.,Shrishov Y .M., Piletsky S. A. ,"Ammonia sensors based on sensitive polyaniline films", Sensors and Actuators B: Chemical, 37(3),1135-140, 1996.

[4] S. G. Pawar, S. L. Patil A.T. Mane, B. T.Raut, V. B. Patil," Growth, characterization and gas sensing properties of polyaniline thin films", Scholars Research library, Achieves of applied science research ,2009, 1(2) 109-114.

[5]Jin. Z., Su.Y. X., Duan, Y. X. Sensors and Actuators B 2001, 72(1) 75.[cross reference]

[6] Nicho M. F. , Trejo. M., Garcia-Valenzuela, A: Saniger,J. M.: Palacios, J,: Hu. H. Sensors and Actuators B 2001,76(1-3),18.[cross reference].

[7] Geng Li-na, "Gas sensitivty of polyaniline/SnO_2 hybrids to volatile organic compounds", Trans. Nonferrous Material Soc. China 19(2009) s678-s683.

[8]. Http://www.figaro.co.jp/en.

[9] Ulrich Hoefer, Joachim Frank, Maximilian Fleischher, High temperature Ga_2O_3 gas sensor and sno2 gas sensor : A comparison - Sensor and Actuator,2001,B 78: 6-11.

[10] P.A. Murade, V.S. Sangawar, G.N. Chaudhari, V.D. Kapse A.U. Bajpeyee, Curr. Appl. Phy. 11 (2010) 451.

[11] Sadanand Pandey," Highly sensitive and selective chemiresistor gas/vapor sensor based on polyaniline nanocomposite : A comprehensive review", hournal of science : Advanced Materials and Devices 1(2016)431-453.

[12] N.G. Deshpande , Y.G. Gudage , Ramphal Sharma , J.C. Vyas , J.B. Kim, Y.P. Lee ,"Studies on tin oxide-intercalated polyaniline nanocomposite for ammonia gas "Sensors and Actuators B 138 (2009) 76–84.

[13] M.C. Horrilloa,, M.J. Ferna´ndeza, J.L. Fontechaa, I. Sayagoa, M. Garcı´aa, M. Aleixandrea,J.P. Santosa, L. Are´sa, J. Gutie´rreza, I. Gra`ciab, C. Cane´ b ," Detection of volatile organic compounds using surface acoustic wave sensors with different polymer coatings" Thin Solid Films 467 (2004) 234– 238 .

[14] Chi-Yen Shen , Shih-Yuan Liou," Surface acoustic wave gas monitor for ppm ammonia detection" Sensors and Actuators B 131 (2008) 673–679.

[15] Jagannath Devkota, Paul R . Ohodnicki, David W. Greve," SAW Sensors for Chemical Vapors and Gases", Sensors 2017,17 ,801.

[16] Wei Li, Yuanjun Guo. Youngling Tang,Xiaotao Zu, Jinyi Ma, Lu Wang , Yong Qing Fu, "Room-temperature ammonia sensor based in ZnO nanorods deposited on ST-cut Quartz surface acoustic wave device", Sensors 2017,17,1142.

[17] Wiesaw P. Jakubik ,"Surface acoustic wave -based gas senosr",Thin solis films 520(2011),930-993.

[18] Yi- Tian Li, Hsu- Chao Hao, Mei-Ching Chen, Tai-Hsuan Lin, Pei- Hsin Ku, Chia- Min Yang,"Polymer -Coated Surface Acoustic Wave Sensor Array for Low concentration Detection", February 20-23, 2011, Kaohsung Taiwan.

[19] V. Bhasker Raj, A.T. Nirmal , Monika Tomar, M.U. Sharma, and Vinay Gupta," Efficient detection of ammonia using SAW devices coated with oxide sensing layers", ICS 2012.

[20] H. Gong,Y. G. Wang, S.C. Teo, L. Huang,"Interaction betwwen thin -film tin oxide sensor and five organic vaporas", Sensors and Acutators B 54(1999) 232-235.

[21] Timothy J. Giffney, Y. H. Ng, K.C. Aw, "A Surface Acoustic Wave Ethanol Sensor with Zinc Oxide Nanorods",Smart Material Research, Vol.2012, Article ID 210746.

[22]P.S.Varade*, A.D. Shaligram, *"Evaporation studies of volatile organic compounds using SAW devices",* American Institute Physics, **(Accepted)** ETMN 2017 AIP online conference series

[23] P. S. Varade, A.D. Shaligram*," Study on Mass loading and Acoustoelectric Effects in Surface Acoustic Wave Devices,"* International Journal of Innovative Knowledge Concepts, 6(3) March, 2018.

CHAPTER 6

SUMMARY/
CONCLUSIONS/FUTURE SCOPE

6.1 Introduction

The research contribution is summarized in this chapter of the thesis and the conclusions from the research work are stated. The aim and objectives stated in the thesis are analyzed and their results are described. The future scope of the research is also discussed at the end.

6.2 Summary and conclusions

The major contributions of the thesis are briefly summarized as follows.

1. Literature survey on Surface Acoustic Wave (SAW) device working principle, its design, simulation and applications as well as the gas sensing material synthesis and characterization.
2. Design of SAW delay line device for gas sensor application.
3. Model simulation of SAW devices using MATLAB and COMSOL multiphysics and presented paper in national conference and published in Journal 'Bionano frontier'
4. Fabrication of SAW delay line device using conventional photolithography technique.
5. Studied the mass loading effect using the developed SAW device and published a paper in the international journal IJIKC.
6. Evaporation studies of VOCs were carried out using the developed SAW device and presented the paper in international conference 'ETMN 2017'.
7. Synthesis and characterization of PANI and PANI- SnO_2 nanocomposite for gas sensing applications.
8. Testing of developed SAW delay line devices and chemiresitor as gas sensor for target gases using PANI and PANI -SnO_2 nanocomposites (ammonia and VOCs) and published a paper in international journal IJRSE.
9. Testing of SAW filter IC as gas sensor for the target gases.
10. Study and analysis of the developed gas sensor for its sensitivity, selectivity and response time.

This research work began with a study on the different gas sensors and their merits and demerits. Working principle of surface acoustic wave (SAW) devices, the main features of SAW device and its use as gas sensor, materials suitable for different gases and their synthesis, were studied as a part of literature review. Various gas sensors are available in market; most of them are metal, metal oxide based. These sensors need to be operated at elevated temperatures. The important factor of concern for gas sensor was to develop a high sensitivity, low response-recovery times and with better selectivity room temperature operated sensors. The main features of SAW devices are high sensitivity, cost effective, tiny structure, remotely operated and room temperature operation. They are widely used as filters in television, mobiles and sensors. Due to their high sensitivity SAW sensors became popular mainly in chemical and biosensing applications.

Initially a SAW delay line device was designed with different resonant frequencies starting from 10 MHz to 20 MHz. This range of frequency was selected by taking in account the lithography constraints at our laboratory. Out of available piezoelectric substrates, the author selected $128\,^0$ YX cut $LiNbO_3$ as piezoelectric substrate, since this substrate offers an excellent electromechancial coupling coefficient (K^2 =5.6 %) and high acoustic velocity (Vp =3992 m/s) as compared to commonly available piezoelectric substrates which helps in improving sensor performance. Though it has 75 ppm as a TCF but it does not causes any impact on the device performance, since the device is designed for room temperature operation. While designing the device the important physical parameters: finger width and finger gap which ultimately decides the resonant frequency are selected according to the lithography limitations at our working place. The aperture width also selected in manner to decrease the losses due to beam steering. The IDT gap (delay line) is selected for minimum insertion loss and appropriate for deposition of gas sensing material film. The connecting pad area is also selected in a way that the contacts can be easily formed by using copper wire (200 µm in diameter) and silver paste.

The modeling of the device is carried out based on the equivalent circuit theory and transmission matrix model using the MATLAB. The radiation conductance (G), acoustic susceptance (B), insertion loss and frequency response of the device were studied using equivalent circuit theory. No second order effects were considered in this simulation. In case of transmission matrix method the detailed study of SAW delay line is carried out. The effect of varying number of fingers in input and output IDTs on frequency and phase characteristics of SAW delay line were studied. It showed the changes in bandwidth of the device, since bandwidth depends (BW = 2 f_0 / N_p, where N_p is the number of finger pairs) on number of fingers in the IDT. The ripples in the frequency response can be attributed to the reflection between fingers and also impedance mismatch with the 50 Ω source and load impedance used in the simulations. In addition, triple transit interference (TTI) and Electromagnetic interference (EMI) causes additional ripples in the pass band. Also, the increased side lobe levels are due to the fact that neither of the transducers were apodized to provide better side lobe suppression. Same SAW device were modeled and simulated using COMSOL multiphysics (ver. 5). This is finite element method based software. The change in frequency due to mass loading effect is studied for the proposed device. The change in frequency is calculated after simulations by taking the difference in frequencies observed for switch 0(without mass loading) and switch 1(with mass loading). It is observed that the errors are possible if the material parameters provided are not exact. The main drawback of this software is, it needs larger memory space. The simulated results are not matched with the experimental values due to variation in practical conditions and the parasitic effects are not considered for simulations.

To fabricate the designed SAW device, first the mask layout of the device was prepared using the software CorelDraw and AutoCAD. The masks were prepared/printed on transparency paper. Both the positive and negative masks were prepared for the same design. The dimensions of the device pattern on mask

are same as that of designed value with a maximum offset of ~ ± 5µm. According to mask size and suitable for handling, the 3" wafer of LiNbO$_3$ were diced into a square shape pieces of 2.4 cm x 2.4 cm. Since the thickness of the IDT patterns is also important parameters as far as the impedance of the IDT is concern. By using thermal evaporation technique aluminum films are formed on the neatly cleaned LiNbO$_3$ substrates. The thickness of the aluminum films were measured using tally-step method. The measured thickness was ~ 300 nm. There are different conducting materials available for patterning the IDTs on the piezoelectric substrates. In present work aluminum was used for IDT patterning. Metals other than aluminum can result in greater reflectivity per electrode. The aluminum was chosen because it is simple to process, cost effective and offers better adhesion on LiNbO$_3$ substrate. Gold has better acoustic reflectivity than aluminum, which could help to reduce the undesired spike in impedance. But the gold deposition needs an additional layer of chromium for better adhesion. Using standard photolithography procedure the IDT patterns were formed on the substrates. The substrates were inspected under digital microscope for pinholes. In few samples the pinholes were observed, this could be due to some dust particles deposited on the substrate before aluminum film deposition. It is necessary to control all the parameters of lithography for better patterns; all the parameters of lithography are precisely set. The baking temperature is also one of the important parameters which affect the adhesion of photoresist on the substrate. The concentration of etching solution, UV exposure intensity and time are also of much importance, which may cause under-cuts in the IDT patterns if not well controlled. The edges of the developed patterns in some samples were not sharp, which causes the minute variation in finger width and finger gaps which results in variation in resonant frequency. There was ± 10 µm variation in finger width due to this the resonant frequency varies by ± 1MHz. The final improvements to be made are in the fabrication techniques. To decrease the misalignment, a tool with an automatic wafer aligner should be used. The substrate allows for acoustic wavefronts traveling in a single direction, but a misalignment leads to a dampened response

caused by a phenomenon known as "walk-off". Walk-off occurs when an acoustic wave propagate along a direction other than one of the principal crystallographic axes. In this case, the wavefronts of the acoustic wave propagate in a different direction than the power flow (i.e., the Poynting vector).using the tool with consistent performance will reduce the effect of misalignment. The contact leads were formed by using copper wire of 200 μm diameter and silver paste. The devices were mounted on PCB with SMA connectors on both the ports forfurther connections to test the device using measuring instrument such as network analyzer. Most of the measurements were performed using network analyzer (E5065A).It is also observed that there is deviation in insertion loss due to lower quality of SMA connector as well as the additional mass of the silver paste on the device. It is difficult to use same amount of silver paste for connections therefore the insertion loss variation differs in different devices.

The device characterization is carried out using function generator, digital storage oscilloscope (DSO) and network analyzer. Using function generator and DSO there was limitation for characterization due to limit of frequency on arbitrary function generator (20MHz). Another problem the signal attenuation due to impedance mismatch and long cables. Using network analyzer the devices were tested for 'S' parameters. The value of S_{21} and S_{11} are slightly varied from the expected values due to poor impedance matching. The device also showed the better characteristics at higher frequencies around 99 MHz. This could be the harmonic frequencies of the SAW. As reported by other researchers [Sridevi Krishnamurti et.al.] one can use the SAW device as sensor for harmonic frequencies which is advantageous as far as the device dimensions constraints are concern due to lithography limitations. Here the author also operated the device at the harmonic frequencies. This showed the improvement in the device sensitivity.

The author also used the SAW IC (SIPAT LB 211DS 01) whose resonance frequency is 211 MHz. It is cut opened and assembled with its matching network on the printed circuit board (PCB). Its S parameters (S_{11}, S_{12}, S_{21}, and S_{22}) measured on network analyzer and were found to be very close to the standard values.

After the development of SAW device, the preparation of gas sensing material is carried out. Thorough literature survey of gas sensors based on polyaniline and polyaniline -nanocomposite films were carried out. Different researchers have used different deposition techniques like electrochemical method, Langmuir - Blodgett, chemical method, sol-gel method, and method like drop-casting, spin - coating and mechanical mixing for making composites. The characteristic features of materials were measured using various characterization techniques such as XRD, FTIR, SEM, FE- SEM, TGA, UV-Vis are reported. Gas sensing characteristics of these materials for various oxidizing and reducing gases were reported and some of them discussed possible sensing mechanism. The data collected from the literature was used during interpretation and for results obtained in the present work.

In the present work the author proposed the study of polyaniline and polyaniline - SnO_2 nanocomposite for VOCs and ammonia sensing study. The polyaniline (PANI) is obtained in powder form by aniline synthesis using chemical method. The filtered powder used for making films for gas sensing. The characterization of PANI was carried out using FTIR, XRD, TGA-DTA and SEM. FTIR results indicated peaks corresponding to characteristics bands present in the PANI ring which was confirmed by comparing results with reported FTIR results for PANI. XRD showed the non-crystalline nature of the obtained powder of the PANI. TGA-DTA showed the change in weight with two step thermal cycle. The first step loss of weight could be due to the loss of moisture and the second step of loss is for bound water of these polymers. To check gas sensitivity, thin films were prepared

on glass and interdigital transducer pattern by dissolving PANI powder in organic solvent (N-methylpyrroldyne). Initial base resistance values of these films were high due to weak adhesion of films to substrates. Analysis of gas sensing results showed moderate and less reproducible sensitivity, slow response, and particularly the partial recovery.

Polyaniline (PANI) alone is not much sensitive for gas sensing application. To improve the gas sensing performance of PANI, nanostructured particles of SnO_2 were added and formed the composite. Work on synthesis and characterization of PANI- SnO_2 nanocomposite was carried out. The polymerization is done by two different methods. First, SnO_2 nanostructure was synthesized using sol-gel method and then in-situ polymerization of aniline is carried out using SnO_2 nanoparticles. The second method followed was solution route technique. The obtained structure was slightly non-uniform with rod shape. The characterization of this composite is done using XRD, FTIR, and FE- SEM. The XRD spectrum peaks are close to the standard XRD of SnO_2. However, these peaks show a small shift (0.20 to 0.50 degree) from their respective standard positions which may be due to polyaniline matrix. In addition, the author observed relatively larger peak broadening; compared with XRD of pure SnO_2. This suggests that tin oxide was present in the polyaniline matrix, and presence of polyaniline has influenced the preferred orientation of tin oxide grains in the composite to some extent. The FTIR shows the characteristics peaks of both PANI and SnO_2 this confirms the composite is of PANI- SnO_2. The FE-SEM study shows the particle structure like nano rods with their length varying from ~450 - 700nm with their diameter less than 100 nm. Gas sensing characteristics were studied at room temperature by preparing thin films on IDT and delay line area of SAW sensor. The responses of the films were tested for ammonia and VOCs (acetone, ethanol, methanol and toluene) for different concentrations. Among the VOCs, it showed highest sensitivity to ethanol at 200 ppm. But with larger response and recovery times for VOCs as compared to ammonia.

The results of present work indicate that the PANI- SnO_2 material with SAW device can be used as high sensitivity sensor for ethanol and also for the ammonia. In general SAW delay line device with suitable sensing material can be used as a high sensitivity gas sensor at room temperature. But this is not the final achievement of the proposed work, this is just achieved the baseline development of SAW delay line device for gas sensing application. There is scope to develop a SAW device with structural improvement and miniaturization. This will further increase the device sensitivity, increase the number of devices per wafer and ultimately reduce the cost. Again the there is lot of scope in synthesizing most sensitive sensing materials for the target gases.

Based on results delivered in this thesis the author has clearly demonstrated that the aim and objectives stated in chapter 1 section 1.2 have been satisfied. Major finding and outcomes derived from this research can be summarized as follows.

- The modeling of the SAW device shows that the sensitivity of SAW depends on its coupling coefficient, finger width and finger spacing. Lesser the dimension higher is the sensitivity.
- The development of SAW delay line device for gas sensing application at room temperature was successfully undertaken by the author.
- The preparation of polyaniline and polyaniline - SnO_2 nanocomposite material for ammonia and VOCs sensing was successfully achieved by the author.
- The gas sensing results provide strong evidence that high sensitivity can be achieved utilizing a PANI- SnO_2 nano- composite based SAW gas sensor for ethanol and ammonia.
- The sensor response and recovery times were found to be influenced by the concentration of analyte gas. Higher gas concentrations, found to result in faster dynamic response.

- One can operate the SAW devices at their harmonic frequencies which are definitely greater than fundamental frequencies and contribute to improve the sensitivity.

- The sensor was also studied for its repeatability. At room temperature the sensor has good repeatability

6.3 Future Scope

Stability is always an issue in case of most of the gas sensor. The stability of film conductivity over long duration along with stable sensitivity is of main concern and it may be achieved by passivation of the surface with another material layer retaining the sensor characteristics. Since SAW made of 128^0 YX cut is one of the stable device but the PANI- SnO_2 film may need to improve to its stability by adopting the technique as mentioned above. To improve the material sensitivity the layered structure strategy could be followed with appropriate layer material, their composition and thickness. There is also scope for the investigation of layered SAW resonators and different IDT structures for gas sensing applications.

To include sensitive layer material parameters, this would enable better matching of the velocity-permittivity product of the SAW device to the sheet conductivity of a given sensitive layer. Further there may be scope for other nanostructures of SnO_2 which may improve the gas sensing performance and sensor stability.

In case of simulation –

1. To develop acoustic absorber for transmission matrix method and COMSOL multiphysics to enable reduced model size and computation time.

2. To include mass loading effect caused by IDT metallization layer. Also the COMSOL multiphysics based 3D simulations which will take in account the parasitic effects on sensor performance can be developed.

Appendix

A. Important Substrate Materials Used in SAW Sensor Applications

The different substrate materials with their important characteristics used in saw sensor applications are listed in table A.1 [1, 2].

Table A. 1 Different Substrate material used in SAW sensors

Substrate	Propagation	K^2(%)	Acoustic Velocity (m/s)
ST -quartz	X	1.89	3158
Y- quartz	X	1.1	3159
Y- LiNbO$_3$	Z	4.5	3488
Y-128^0 LiNbO$_3$	X	5.6	3992
77.5^0 Y- LiTaO$_3$	X	1.6	3379
36^0 Y- LiTaO$_3$	X	5	4160
Langasite	-	3.2	2742
100-011 GaAs	-	0.7	2864
Y-60^0 Cds	-	-	1702
ZnO	-	-	2639

B. Material Constants of Lithium Niobate

Material constants of Lithium niobates used in this thesis are taken from [3,4]. The constants for YX- cut LiNbO$_3$ are given below.

Density (ρ)=4675 Kg/m^3

$$\text{Stiffness }, C^E = \begin{bmatrix} 20.3 & 5.3 & 7.5 & 0.9 & 0 & 0 \\ 5.3 & 20.3 & 7.5 & -0.9 & 0 & 0 \\ 7.5 & 7.5 & 24.5 & 0 & 0 & 0 \\ 0.9 & -0.9 & 0 & 6.0 & 0 & 0 \\ 0 & 0 & 0 & 0 & 6.0 & 0.9 \\ 0 & 0 & 0 & 0 & 0.9 & 7.5 \end{bmatrix} \times 10^{19} \text{ N/m}^2$$

$$\text{Piezoelectric constant}, e = \begin{bmatrix} 0.0 & 0.0 & 0.0 & 0.0 & 3.7 & -2.5 \\ -2.5 & 2.5 & 0.0 & 3.7 & 0.0 & 0.0 \\ 0.2 & 0.2 & 1.3 & 0.0 & 0.0 & 0.0 \end{bmatrix} \text{C /m}^2$$

$$\text{Permittivity}, E = \begin{bmatrix} 44 & 0 & 0 \\ 0 & 44 & 0 \\ 0 & 0 & 29 \end{bmatrix}$$

C. Absorbing Boundary Conditions

In order to avoid reflections of waves from the boundaries or edges of the SAW devices, absorbing boundary conditions are applied in the FEM simulations. The influence of wave reflections from boundaries can be assuming critical damping along the boundaries [5]. This can be achieved by employing suitable values for Rayleigh damping coefficients in the COMSOL Multiphysics software. In Rayleigh damping model, The Rayleigh damping matrix Z is a linear combinations of mass and stiffness matrix as given below.

$$\xi = A_{dm} M + B_{dk} k$$

Where the mass proportional damping parameter (A_{dm}) and stiffness prportional damping parameter (B_{dk}) are damping coefficients and they are related to damping ratio (ξ) as

$$\xi = \frac{A_{dm} + B_{dk}\omega^2}{2\omega}$$

Absorbing boundary can be achieved by asuming critical damping $\xi = 1$ and $A_{dm} = 0$ then $B_{dk} = \frac{1}{\pi f}$.

References

[1] M. Thompson and D. C. Stone ,"In Surface -Launched Acoustic wave Sensors-chemical Sensing and Thin film characterization , New York: Wiley & sons,1997 [cross reference].

[2] Piezoelectric Materials and Devices, "http://www.newpiezo.com/product.html [cross reference].

[3]A.W. Warner , M.Onoe, G. A. Coquin ," Determination of elastic and piezoelectric constants for crystals in class (3M)", The journal of the acoustical society of America , Vol. 42,pp.1223-1231,1968[cross reference].

[4] Hercules G du plessisi and Willem J Perold," Simulation of ZnO Enhanced SAW Gas Sensor", proceeding of the 2013 COMSOL conference in Rotterdam.

[5] Thesis of N. Ramakrishanan," Mass loading Effect of Resonant Structures in Surface Acoustic Wave Devices for Sensing Applicatios",TH-967_05615302.

List of Publications

International Journals:

[1] **Varade PS**, Gangal SA, Shaligram AD, "*Synthesis, characterization of polyaniline –SnO$_2$ for volatile organic compounds*" December 2017, IJRSE.

[2] **P.S. Varade**, A.D. Shaligram, *"Evaporation studies of volatile organic compounds using SAW devices",* American Institute Physics, **(Accepted)** ETMN 2017 AIP online conference series.

[3] **P. S. Varade**, S. A. Gangal, A.D. Shaligram,"*Simulation of SAW Delay line Sensor using MATLAB",* Bionano Frontier, Vol. 10 Issue-2.July 2017.

[4] **P.S. Varade**, A.D. Shaligram*," Study on Mass loading and Acoustoelectric Effects in Surface Acoustic Wave Devices,"* International Journal of Innovative Knowledge Concepts, 6(3) March, 2018.

National Conferences:

[5**] P. S. Varade**, S. A. Gangal ,Umesh Yadav, "*Simulation of SAW devices using Matlab*" in **National Conference on Emerging Trends in Physical Sciences,** 23rd - 24th January 2015, Department of Physics, N. B. Mehata (Valwada) Science College, Bordi , Dist. Palghar.

[6] **P. S. Varade**, A. D. Shaligram, "*Evaporation Studies of VOCs Using Surface Acoustic Wave (SAW) Devices"* In the **International Conference "ETMN 2017**, 06th- 07th October 2017, Solapur University, Solapur.

[7] **Varade PS,** Gangal SA, Shaligram AD,"*Synthesis, characterization of polyaniline –SnO_2 for volatile organic compounds*" in **the International conference" ICANN 2017",** 7th- 9th December 2017.T. C. college, Baramati, ,Pune.

[8] **P. S. Varade**, S. A. Gangal, A. D. Shaligram, *"Simulation of Saw Delay Line Sensor Using Matlab"* in the national conference organized by Indira College, Pune on 22nd - 23rd December 2017.

.